

Sheffield Hallam University

Studies of the modification of ion and water movement through clays and shales.

CRASTER, Bernadette.

Available from the Sheffield Hallam University Research Archive (SHURA) at:

<http://shura.shu.ac.uk/19509/>

A Sheffield Hallam University thesis

This thesis is protected by copyright which belongs to the author.

The content must not be changed in any way or sold commercially in any format or medium without the formal permission of the author.

When referring to this work, full bibliographic details including the author, title, awarding institution and date of the thesis must be given.

Please visit <http://shura.shu.ac.uk/19509/> and <http://shura.shu.ac.uk/information.html> for further details about copyright and re-use permissions.

CITY CAMPUS, HOWARD STREET
SHEFFIELD S1 1WB

101 687 817 6



SHEFFIELD HALLAM UNIVERSITY
LEARNING CENTRE
CITY CAMPUS, HOWARD STREET
SHEFFIELD S1 1WB

REFERENCE

ProQuest Number: 10694390

All rights reserved

INFORMATION TO ALL USERS

The quality of this reproduction is dependent upon the quality of the copy submitted.

In the unlikely event that the author did not send a complete manuscript and there are missing pages, these will be noted. Also, if material had to be removed, a note will indicate the deletion.



ProQuest 10694390

Published by ProQuest LLC (2017). Copyright of the Dissertation is held by the Author.

All rights reserved.

This work is protected against unauthorized copying under Title 17, United States Code
Microform Edition © ProQuest LLC.

ProQuest LLC.
789 East Eisenhower Parkway
P.O. Box 1346
Ann Arbor, MI 48106 – 1346

**Studies of the Modification of Ion and Water Movement through
Clays and Shales**

Bernadette Craster

A thesis submitted in partial fulfilment of the requirements of
Sheffield Hallam University
for the degree of Doctor of Philosophy

June 1999

Collaborating Organisation: Schlumberger Cambridge Research



Acknowledgments

I am very grateful to the Schlumberger Cambridge Research management team (past and present) for giving me the opportunity to undertake this program of study. I would like to thank Dr Chris Breen, Sheffield Hallam University for his advice during the research period and the writing up phase. Also to be acknowledged for support and guidance are Dr's John Cook, Chris Hall, Paul Howard, Tim Jones, Geoff Maitland, Gerry Meeten, Paul Reid and John Sherwood from Schlumberger Cambridge Research. I would like to thank Terry Bailey from the engineering workshop and Pauline Mockler from the library for their continued willingness to help.

Abstract

The movement of water and ions through compacted clays is monitored under different conditions. Firstly clay mixtures are subjected to compaction pressures in the range of 10 to 600 bar during which time the change in porosity is monitored and the conductivity of the compacting slurry measured. In the second instance thin films of montmorillonite are prepared and placed in a newly designed Clay Membrane Cell. The movement of ions and water across the montmorillonite film is detected in the presence and absence of newly designed polyglycols. These polyglycols were found to be efficient in preventing the swelling of montmorillonite clay and consequently shale samples.

The compaction profiles for kaolinite, illite, Ca greenbond and Fullers Earth were not affected by the presence of electrolyte in the pressure range investigated. However the relative porosities could be explained in terms of the different microstructures of the compacts imaged using scanning electron microscopy. Ca greenbond formed well orientated structures and had a higher porosity than Fullers Earth which formed domain like compacts. Application of the model of Waxman and Smits to the conductivity *versus* porosity profiles of Ca Greenbond and Fullers Earth slurried in calcium chloride allowed the cementation factor (m) to be determined. Values of 4.4 and 1.8 were determined respectively for Ca greenbond and Fullers Earth reflecting the difference in the aspect ratios of the clay domains. The activation energy for conduction in Fullers Earth slurried in 0.5 or 0.05 M calcium chloride was found to increase from 21 to 25 kJ mol⁻¹ as the porosity was reduced from 60 to 40 percent. This finding indicated the switch from bulk conduction processes towards surface conduction.

The intercalation of polyethylene glycol and polyalkylene glycol molecules from water and 1M potassium chloride, sodium chloride or calcium chloride solutions into self supporting films of SWy-1 montmorillonite was studied. The basal spacings of the wet glycol complexes were in keeping with those obtained for the relevant pastes without glycol added. This showed that the polyglycol molecules displaced some of the water from the montmorillonite surface. Once in place a bilayer of a polyalkylene glycol prevented the swelling of the calcium or sodium exchanged SWy-1 further on the addition of water. A hydrophilic glycol such as polyethylene glycol did not prevent the osmotic swelling of the clay. In the case of the potassium exchanged montmorillonite the insertion of a single layer of any polyglycol into an SWy-1 film prevented swelling when water was added. These findings were used to help in the design of more inhibitive additives for water based muds. The recovery levels of Oxford shale cuttings from dispersion tests where polyethylene glycol, polyalkylene glycol and sorbitol-po were added to water was 10, 56, and 87 wt% respectively.

A new cell to allow the movement of water and ions through a 120 µm thick film of SWy-1 and ballotini was designed. This new Clay Membrane Cell was validated by detecting the development of osmotic barriers setup by sodium and potassium silicate systems and lacking in the case of glycolated films. Further modification of the clamping procedure of the SWy-1 composite film allowed the transport of water and ions through the film to be monitored. The permeability of the film to water was detected as of the order of 10×10^{-20} m² and the permeability could be altered with the addition of different additives. Full analysis of the changes in permeability could be performed after a test time of one week compared with a test time of several months in a shale core experiment using the Hassler cell.

Thesis contents

Chapter 1: Introduction

Chapter 2: Basic theory of clays and silicates

1. Introduction	4
2. Clay minerals.....	4
2.1 Terminology.....	4
2.2 Clay structure	4
2.3 Uses of clays.....	6
3. Clay chemistry.....	7
3.1 Charged nature of clays.....	7
3.2 Hydration of clays.....	8
3.3 Double layer formation	10
3.4 Surface diffusion of ions	11
3.5 Flocculation and tactoid formation	12
4. Interaction of organic matter with clays.	14
4.1 Charged organics.....	15
4.2 Adsorption of uncharged polymers.....	15
5. Clays in sedimentary rocks	19
6. Ion and water movement through shales and clays	23
7. Silicates.....	26
8. References	27

Chapter 3: Characterisation of synthetic shales

1. Introduction	34
2. Specific background theories	35
2.1 Resistivity models for clay bearing rocks	35
2.2 Arrhenius rate law	37
2.3 Clay phase porosity	38
3. Experimental	39
3.1 The clays and quartz	39
3.2 Preparation of Shale and Sandstone samples for resistivity measurements	40
3.3 Compact preparation	41
3.3.1 <i>Compaction apparatus</i>	41
3.3.2 <i>Heating instrumentation</i>	43
3.3.3 <i>Slurry preparation and compaction procedures</i>	43
3.3.4 <i>Compaction and temperature equilibration times</i>	44
3.4 The resistivity measurements	45
3.4.1 <i>The electrodes</i>	45
3.4.2 <i>Electrode evaluation</i>	45
3.4.3 <i>Experiments with pure electrolytes</i>	46
3.5 Compact porosity and microstructural determination	47
3.5.1 <i>Scanning electron microscopy (SEM)</i>	47

3.5.2 Porosity determination	47
4. Results and Discussions	48
4.1 Compaction behaviour of clays.....	48
4.1.1 Contribution of clay chemistry to compaction profiles	48
4.1.2 Effect of added electrolyte on the compaction profiles	56
4.1.3 The porosity of mixed-clay compacts	58
4.1.4 The porosity of compacts with quartz added.....	63
4.1.5 Summary.....	64
4.2 Conductivity measurements-methods and results.....	65
4.2.1 Electrode evaluation	65
4.2.2 Comparison of platen electrodes with liquid electrodes.....	67
4.2.3 Electrode end effects	68
4.2.4 Summary.....	70
4.3 Conductivity of clay compacts.....	71
4.3.1 Temperature effects.....	78
5. Conclusions	80
6. Future work	80
7. References	81

Chapter 4: Designing polyglycols for shale stabilisation

1. Introduction	84
2. Background	85
2.1 X-ray diffraction.....	85
2.2 Infrared spectroscopy.....	87
3. Experimental	87
3.1 Materials.....	87
3.1.1 Glycols.....	87
3.1.2 Polyglycol solutions.....	88
3.1.3 Mud preparation.....	88
3.1.4 Clay	89
3.1.5 Ion Exchange	89
3.1.6 Shale.....	90
3.1.7 Clay-polyglycol complexes	91
3.2 Adsorption studies.....	91
3.2.1 Glassware.....	91
3.2.2 Adsorption isotherms	91
3.2.3 GPC analysis.....	92
3.2.4 Infrared spectroscopy	93
3.2.5 X-ray diffraction.....	94
3.3 Molecular simulations.....	95
3.4 Shale dispersion tests	95
3.4.1 Closed-bottle test method for mechanistic studies	96
3.4.2 Slake Durability (Vole cage) tests.	96
3.5 Bulk hardness tests.....	96
4. Results and discussion	97
4.1 Stabilisation of montmorillonite-glycol-water complexes.....	97
4.2 Adsorption Isotherms	100
4.3 Stabilisation of montmorillonite-glycol-salt complexes	108
4.3.1 Interactions with potassium exchanged clay.....	108
4.3.2 The addition of potassium chloride	109

4.3.3 The addition of calcium and sodium chloride	112
4.4 Summary	114
5. Testing the mechanism on shale	115
5.1 Cuttings dispersion tests with freshwater	116
5.2 Cuttings dispersion tests with salt added	119
5.3 Designing a new shale dispersion inhibitor	121
6. Conclusions	122
7. Future work	122
8. References	124

Chapter 5: Design and recommended use of a clay membrane cell to investigate barrier formation by polymers

1. Introduction	127
2. Background theories.....	127
2.1 Pertinent literature.....	127
2.2 Diffusion, Osmosis and Permeability	129
2.3 Model for ion and water movement through films	132
3. Designing the Clay Membrane Cell.....	136
4. Experimental	142
4.1 Clay Membrane Cell	142
4.2 Clay film preparation	144
4.3 Mounting the film in the cell.....	144
4.4 Solution preparation.....	145
4.5 Ion transfer analysis	145
4.6 Cuttings dispersion tests.....	146
4.7 Synchrotron radiation experiments	146
5. Results and discussion	146
5.1 Clay films supported by coarse discs.....	147
5.1.1 Comparing silicates with glycols.....	147
5.1.2 Silicates	150
5.1.3 Summary.....	153
5.2 Clay films supported by fine discs	154
5.2.1 Osmotic tests	154
5.2.2 Clay film examination through synchrotron experiments.....	157
5.2.3 Pathways for diffusion	160
5.2.4 Application of the Sherwood model.....	164
5.2.5 Hydrostatic tests.....	169
6. Conclusions	173
7. Future work	174
8. References	175

Chapter 6: Summary and Conclusions

1. Introduction

Schlumberger is a service company for the oil industry, supplying well logging expertise and drilling fluids amongst other things. Schlumberger Cambridge Research (SCR) is one of the research centres where projects are run to help interpret drilling logs and also to design better quality drilling fluids. The author of this thesis is employed at this research laboratory and the “The modification of ion and water movement through clays and shales” is of interest to Schlumberger. The reasons why Schlumberger is interested in this subject will be outlined in this chapter, along with the areas of research presented in this thesis.

In the search for oil and gas, wells are often drilled several thousands of metres deep with bottom hole diameters sometimes as small as 6 inches. Drilling assemblies are expensive as is drilling rig time; sometimes tens of thousands of dollars per day. Therefore lost time during the drilling process is to be avoided. Since approximately 70 % of the footage drilled in the world is through clay bearing sedimentary rocks called shales, it is obvious that these systems need to be studied. The need for research in this formation type is intensified when one considers that shales containing swelling clays are a problem formation. These tend to swell when in contact with water from the drilling fluid, often caving in and causing the drill string to become stuck. Logging While Drilling (LWD) tools can be used to follow the bit and detect clay bearing rocks from gamma ray logs or resistivity logs. However the interpretation of the in depth profiles to give the chemistry of the clay present and the exact porefluid content is not yet possible.

Drilling these sections with oil based muds (OBM) (which are really emulsions) gives fewer shale problems and better wellbore stability. Recently environmental legislation has restricted the use of OBM. In fact drilling with such muds is either banned or special disposal of the oil-contaminated shale cuttings from behind the bit in landfill sites is stipulated. The key to designing water based muds that perform as OBM is to understand the interaction of water with shale in the presence and absence of salt and then to understand how better wellbores are drilled with emulsion systems.

Research into the interaction of water with clays in the presence and absence of electrolyte is extensive and a few are mentioned here [1-3]. This work has shown the following factors to be important;

- the ability of clays of different chemistry to swell to different extents,

- the internal structure or effective surface area of the compacted clay,
- applied pressure or allowed developed swelling pressure,
- strength and nature of the electrolyte
- the addition of adsorbed polymer.

Some fundamental work has also been carried out on shale in research on their interaction with water based muds [4-6] and oil based mud systems [7]. This work has shown that osmotic barriers are set up on the shale surface. These membranes allow for the movement of water but not of salt. Therefore the shale can be forced to shrink rather than swell if the water activity of the drilling mud is lower than that of the porefluid. If the structure and clay-chemistry of shales could be determined from resistivity logs, and waterbased mud additives that gave good shale stability with oil based mud performance could be designed, then wellbore stability problems in swelling shale sections would be solved.

One of the approaches in this thesis has been to carry out experiments on research standard clay samples and where time allowed compare these results with those obtained for similar experiments on shale samples. The thesis is divided into three main sections and each chapter is presented as an independent entity in terms of relevant theories, experimental work and results. Chapter 2 gives basic background theory of clays and shales and Chapter 6 provides a combined summary and conclusions. The chapters with a summary of their content are listed below.

Chapter 3; “Characterisation of synthetic shales”.

The porosity of single clay and clay mixtures at compaction pressures relevant to wellbore conditions are investigated. Experimental systems were designed for the resistivity measurement of such clay compacts. The dependence of measured resistivity on clay chemistry and added electrolyte is examined.

Chapter 4; “Designing polyglycols for shale stabilisation”.

The mechanism of montmorillonite stabilisation by polyglycols is reviewed and expanded on. The mechanism is verified for a number of different polyglycol chemistries and the hydration of shale in the presence of these waterbased additives is examined.

Chapter 5; “Design and recommended use of a Clay Membrane Cell to investigate barrier formation by polymers”

The design path of an osmotic cell containing a 120 μm thick montmorillonite film with glass bead inclusions will be described. Use of the cell to detect osmotic barrier

formation will be outlined. The application of a transport model previously developed by Sherwood SCR [8] to determine the permeability of the mineral film to water and , the diffusivity of the salt through the membrane.

2. References

- [1] Slade P.G, Quirk J.P. and Norrish, K. Crystalline swelling of smectite samples in concentrated NaCl solutions in relation to layer charge, *Clays and Clay minerals*, **39**, 234-238, 1991.
- [2] Maio, C.D. Exposure of bentonite to salt solution: osmotic and mechanical effects, *Geotechnique*, **46**, 695-707, 1996.
- [3] Fritz, S. Ideality of clay membranes in osmotic processes: A review, *Clays and Clay Minerals*, **34**, 214-223, 1986.
- [4] van Oort, E., Hale A.H., Moody F.K. and Roy S. Critical parameters in modelling the chemical aspects of borehole stability in shales and in designing improved water-based shale drilling fluids, SPE 28309, 171-186, 1994.
- [5] van Oort E. Physico-chemical stabilisation of shales, SPE 37263, 1-16, 1997.
- [6] Reid P.I, Elliott G.P, Minton R.C, Chambers, B.D, and Burt D.A. Reduced environmental impact and improved drilling performance with water-based muds containing glycols, SPE 25989, 253-263, 1993.
- [7] Bailey L., Denis J.H., Goldsmith, G., Hall P.L and Sherwood, J.D. A wellbore simulator for mud-shale interaction studies, *Journal of Petroleum Science and Engineering*, **11**, 195-211, 1994.
- [8] Sherwood J. D. A model of hindered solute transport in a poroelastic shale,., *Proceedings Royal Society of London, A* **445**, 679-692, 1994.

1. Introduction	4
2. Clay minerals.....	4
2.1 Terminology	4
2.2 Clay structure	4
2.3 Uses of clays.....	6
3. Clay chemistry.....	7
3.1 Charged nature of clays.....	7
3.2 Hydration of clays	8
3.3 Double layer formation	10
3.4 Surface diffusion of ions	11
3.5 Flocculation and tactoid formation	12
4. Interaction of organic matter with clays	14
4.1 Charged organics.....	15
4.2 Adsorption of uncharged polymers.....	15
5. Clays in sedimentary rocks.....	19
6. Ion and water movement through shales and clays	23
7. Silicates	26
8. References	27

1. Introduction

Since the research work carried out in this thesis deals with swelling and non swelling clays it was thought appropriate to supply some background information on clays in general. The aim of this Chapter is to inform the reader of the origins, chemistry and uses of clays, but more importantly to define more closely what they are and highlight the characteristics that are most pertinent in this study.

2. Clay minerals

2.1 Terminology

The word “clay” is frequently used as a size classification for components of soils and sediments [1]. Hence, clays describe a chemically heterogenous and structurally complex group of colloidal particles, having mean diameters ranging from a few tens of nanometers to a few microns [2]. Chemically this group consists of some hydrous aluminium silicates, with small amounts of finely divided quartz, feldspars, carbonates, oxides and hydroxides and some organic matter. “Clay minerals” refer solely to the fine grained hydrous silicates of aluminium, magnesium or iron [3]. Although the basic building blocks for clay minerals are similar, their appearance and behaviour can differ greatly.

2.2 Clay structure

Clay minerals consist of two main building blocks. A sheet of silicate tetrahedra, consisting of two layers of oxygen atoms containing silicon in four-fold (tetrahedral coordination) as shown in Figure 1.

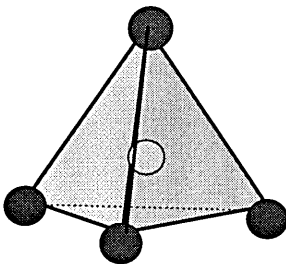


Figure 1: A schematic of a single silica tetrahedron. Here the silicon ion is represented by light grey and the oxygen ions by dark grey.

An octahedral sheet, consisting of two layers of oxygen ions or hydroxyl groups between which aluminum, magnesium or iron are bonded in six-fold coordination. If the layer

consists principally of trivalent aluminum ions occupying two-thirds of the available octahedral interstices, this is known as a gibbsite-type or a dioctahedral layer. Conversely if magnesium is mainly present the layer is called a brucite or a trioctahedral layer.

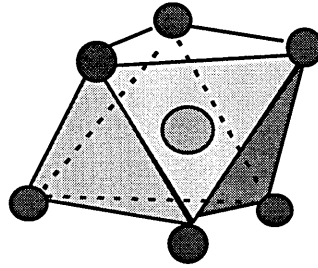


Figure 2: A schematic of a single octahedral unit. The aluminium atom is positioned in the centre.

The structural unit of clays (sometimes called unit layers) consist of different arrangements of tetrahedral and octahedral sheets. In the kaolinite group of clay minerals an octahedral sheet is coupled with a tetrahedral sheet while for smectites and illites one octahedral sheet is sandwiched between two tetrahedral sheets. The structural arrangement of montmorillonite is given in Figure 3.

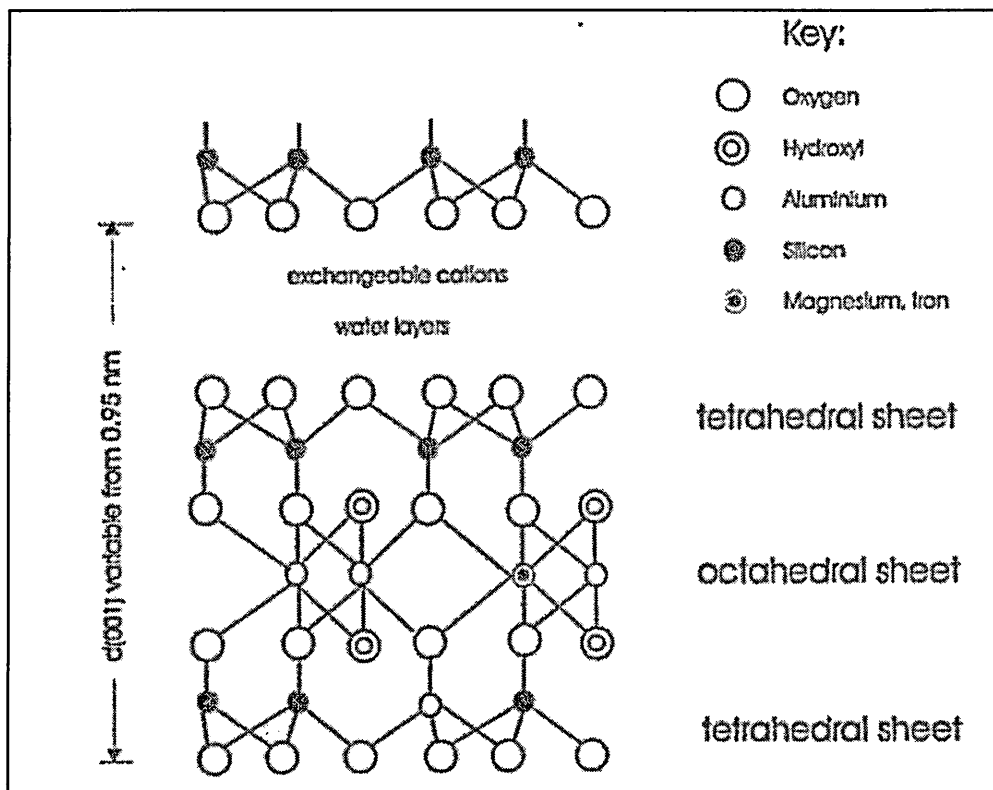


Figure 3. :The layered structure of montmorillonite [4].

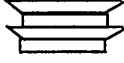
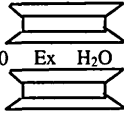
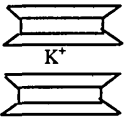
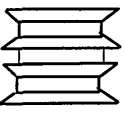
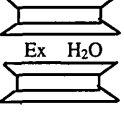
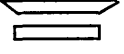
MINERAL	STRUCTURE	COMPOSITION (IDEALISED)	CATION EXCH CAP ¹ meq/100g
Kaolinite		$Al_2Si_2O_5(OH)_4$	1-10
Montmorillonite		$Ex_x[Al_{2-x}Mg_x]<Si_4>O_{10}(OH)_2$	80-140
Illite		$K_{1-x}[Al_2]<Al_{1-x}Si_{3+x}>O_{10}(OH)_2$	10-40
Chlorite		$[Mg,Al]_3(OH)_6[Mg,Al]_3<Si,Al>_4O_{10}(OH)_2$	5-30
Vermiculite		$Ex_x[Mg_3]<Al_xSi_{4-x}>O_{10}(OH)_2$	100-180
		Tetrahedral layer Octahedral layer	

Figure 4: Structural arrangement of different type of clay showing the potential for water adsorption in the interlamellar region of montmorillonite. Ex represents the exchange cations (see Section 3.1) [5]. ¹The cation exchange capacity is the concentration of exchangeable cations on the clay surface expressed in milli equivalents per unit weight of clay.

In the clay structure, silica tetrahedra and alumina octahedra are interconnected ionically by sharing of O^{2-} at polyhedral corners and edges [5].

2.3 Uses of clays

Kaolinite is used in pottery and porcelain manufacture, while the other clay minerals are commonly used as extenders in paints and plastics and rubbers. Smectites are frequently used as binding agents in the preparation of ceramics [6] and in oilwell drilling fluids, either in the form of Na montmorillonite (in aqueous fluids) or as an organophilic clay (in water-in-oil emulsion based fluids) [7]. In civil engineering they are used to alter the movement of water or chemical wastes, for lubrication of cables or pipes and as a waterproofing agent [8]. Smectites are also used as an absorbent, in industry for removal of oil and grease from floors and in pet litter trays. Clays can be used for decolourising vegetable oils, clarifying wine and in water filtration and purification [9], [10].

3. Clay chemistry

3.1 Charged nature of clays

One of the important properties of clays is that their unit layers are electrically charged. The origin of this negative electrical charge of clay particles is isomorphous substitution of cations existing in the lattice by cations of lower charge, e.g. the substitution of aluminum for silicon in the tetrahedral sheet or magnesium or iron for aluminum in the octahedral layers. Clays will adsorb cations and anions to neutralize the layer charge and these ions are readily exchanged when the clay comes into contact with electrolyte [11]. The clay is then said to have a certain cation exchange capacity (CEC) usually quoted as the number of chemical equivalents per unit weight of dry clay. Montmorillonites contain extensive isomorphous substitution of this kind, and frequently have CEC values in excess of 100 milliequivalents/100g (refer to Figure 4). The exchange cations are held between the adjacent tetrahedral layers.

Depending on the relative humidity (or, when in contact with liquid, the ionic concentration) smectites may adsorb water and hydrate during which the crystal lattice swells in a direction perpendicular to the plane of the surface oxygens. However the amount of isomorphous substitution does not guarantee the CEC or the degree of swelling. For example, at high levels of substitution of silicon by aluminum, potassium ions can be strongly ionically bonded in the interlayer region in a non swelling and non exchangeable state, as in illite, which is essentially a fine grained mica. It is then interesting to note that illites which have a higher negative layer charge than smectites (montmorillonite), have lower cation exchange capacities.

The negatively charged clay surfaces do not have an equal affinity for all cations, but in fact exhibits selectivity which depends on such factors as ionic charge, size and state of hydration of the cations. Generally cation exchange selectivity increases with cation charge and (for a given charge) increases with ionic radius. Thus the order of increased affinity for the alkali metal ions is $\text{Li} < \text{Na} < \text{K} < \text{Rb} < \text{Cs}$ and for the alkaline earth ions is $\text{Mg} < \text{Ca} < \text{Sr} < \text{Ba}$. In both of these series increasing adsorption selectivity corresponds to decreasing polarizability and energy of hydration in aqueous solution, i.e. the cation which holds on to their hydration shells most strongly are least strongly adsorbed by clays. In general cations which are least preferred by the surface (such as sodium) are associated with limited particle

aggregation and extensive swelling, while strongly bound ions (such as potassium) promote extensive aggregation and limited swelling.

3.2 Hydration of clays

The behaviour of clays in the presence of water is complex, important, and often dramatic. Research has been carried out over the years on the structure of water immediately adsorbed at the clay surface [12]. In particular it has not been clear to what extent its density and structure resemble or differ from that of bulk water or ice. There is also some controversy as to what distance the effect of the clay surface modifies its properties. Clay hydration from the dry state is an exothermic process and under standard laboratory conditions the clays usually contain 5 wt% of free and bound water. The adsorption of water by clays can occur either by hydration of the crystal surfaces or hydration of the exchange cations. Some values for the cations naturally found in wellbore shales are given in Table 1.

Ion	Dehydrated ion diameter (Å)	Charge density (charge/Å ²)	Hydrated ion diameter (Å)
Sodium (Na ⁺)	1.90	0.088	11.2
Potassium (K ⁺)	2.66	0.045	7.6
Magnesium (Mg ²⁺)	1.30	0.376	21.6
Calcium (Ca ²⁺)	1.90	0.176	19.0

Table 1: Characteristic sizes of cations commonly found on montmorillonite surfaces [13].

It is interesting to note that the potassium ion tends to swell the least due to the low charge density.

When the siloxane surfaces hydrate, hydrogen bonds are set up between the water proton and a surface oxygen. Hydration of the exchange cations amounts to the formation of a coordinated complex. In kaolinite water can be adsorbed only on the external surfaces of which there are two types, alumina and siloxane. On the alumina surface the proton on the hydroxyl group bonds to the oxygen in the water molecule. In smectites water may also be held in the interlayers between the individual structural units. Removal of this water requires more energy (heating above 100 °C) than in the case of kaolinite where the enthalpy of adsorption is small.

In montmorillonite at low humidities the interlayer cations are unhydrated and embedded in the hexagonal cavities (see Figure 5) between adjacent siloxane surfaces so that initial adsorption occurs at the external surfaces.

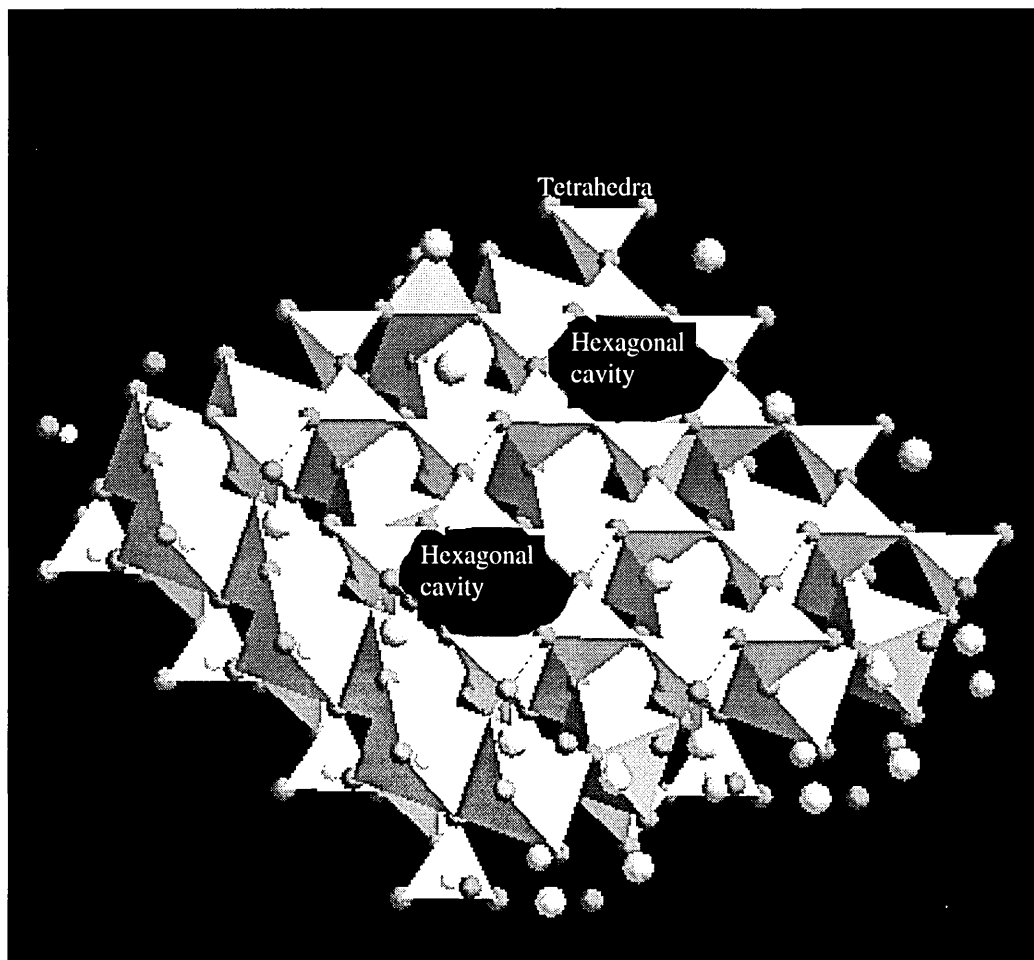


Figure 5: The top of the silicate sheets showing the hexagonal cavities.

As the relative humidity is increased the interlayer cations become hydrated, causing a stepwise expansion of the interlayer spacing. Further adsorption of water finally results in multilayer adsorption. However monovalent and bivalent exchange forms behave rather differently. X-ray diffraction studies indicate that the Na^+ exchanged clay exhibits a series of hydration states one, two, three or more molecular sheets of interlayer water, the number of sheets increasing with increased relative humidity. Also on complete immersion in water calcium montmorillonite does not expand beyond three or possibly four interlayer water sheets whereas sodium undergoes essentially unlimited osmotic swelling to larger interlayer spacings. Osmotic swelling is exhibited only by lithium and sodium clays. Exchange cations of higher charge as well as larger

monovalent cations e.g. potassium permit only limited swelling of smectites up to a few water layers.

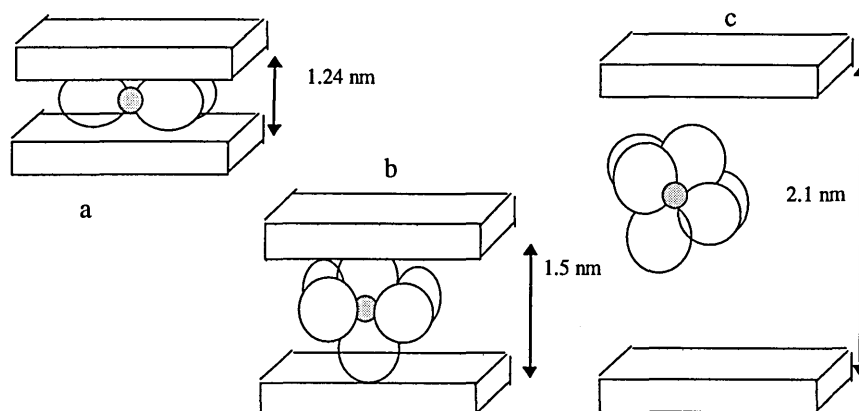


Figure 6: The position of the calcium ion in the centre of the interlamellar region on hydration [14].

As the calcium exchanged clays hydrate the solvated calcium ion remains in the centre of the interlamellar region as shown in Figure 6. Using molecular simulations Boek *et al.* [15] have shown that the potassium ion for instance would remain close to the clay surface on hydration.

It is clear that energy barriers to extensive layer separation exist which cannot be overcome if the ion/surface Coulomb attractions are strong, or if the hydration energy of the cation is low. Neutron scattering studies indicate that beyond 10 Å from the siloxane surfaces the adsorbed water is dynamically similar to bulk water [16].

3.3 Double layer formation

The osmotic swelling to relatively large interplatelet spacings exhibited by Na^+ and Li^+ exchanged forms of montmorillonite can be explained on the basis of electrical double layer theory [11], [17]. Basically the negatively charged clay platelets cause a net attraction of cations and a net repulsion of anions, causing the region near each platelet to have a positive electrostatic charge which tends to repel adjacent platelets. These are counteracted by attractive van der Waals forces operating at short distances [18], the resultant of which creates an energy minimum at each interplatelet separation which is a function of electrolyte concentration. The characteristic double layer thickness can be shown to vary as the square root of the ionic concentration.

At high salt concentrations, the double layers are still further compressed and the repulsive forces again become weaker than the attractive forces. In the fluid part of the

electrical double layer opposite a negatively charged surface there is an excess of positive ionic charge, or, stated precisely, an excess of cations and a shortage of anions as compared with the ionic concentrations far from the surface in the bulk of the electrolyte solution. By definition the difference between the conductance in the range of the double layer and that in the bulk fluid is equal to the surface conductance. The ions located in spaces between the electrokinetic “plane of shear” and the surface (which includes the Stern part of the double layer) are usually considered immobile (see Figure 7). The charge of the clay double layer on the other hand is entirely determined by imperfections within the clay lattice. In order to retain electrical neutrality this negative lattice charge is compensated for by cations. These cations stay with the clay during drying and resuspension. The addition of electrolyte does not change the double layer charge. However the addition of electrolyte will compress the double layer (Table 2).

Molarity	Double layer thickness (nm)
10^{-1}	1
10^{-3}	10

Table 2: Dependence of diffuse double layer thickness on concentration for a 1:1 electrolyte [19].

There will be a shift of counter ions to the space between the plane of shear and the clay surface. If this shift indeed reduces the average mobility of the counter ions a decrease in specific surface conductance would be expected.

3.4 Surface diffusion of ions

The value of the zeta potential (ξ) can be determined by measuring the mobility of a charged colloidal particle in an applied electric field or by determining the surface conductivity. Many researchers have carried out such studies in the past both for clays [11] , [20] and polymer particles such as polystyrene latex [21-24]. However some discrepancies between the values calculated from the electrophoretic mobility and those determined from surface conductivity were found. This discrepancy is due to the approach taken to the mobility of ions in the Stern layer and indeed the position of the Stern layer

itself. If the ions in the Stern layer are indeed mobile then the electrophoretic mobility is reduced and the surface conductivity increased.

As long ago as 1947, Grahame [25] suggested that two types of ions existed in the Stern layer, those which were not separated from the surface by a hydration shell and those that were. The extent of this so called ion pair formation depended on the salt concentration and on the charge density of the cation (increases as the ion hydration decreases). Gan and Low [26] agreed with the conclusions of Grahame stating that the ions are tightly held by electrostatic forces when the clay is dry but on hydration some of the exchangeable cations dissociate from the surface and some remain undissociated. They used infrared spectroscopy to monitor the Si-O vibrations which depended on the proximity of adsorbed cations. They examined changes in these frequencies with different cations and salt concentrations and concluded that increasing the salinity around the clay encourages a net flux of cations into this region but not anions. Since the measured charge density on the shear plane is indirectly known to increase with increasing salinity they concluded that the plane of shear was moved towards the clay surface with increased salinity. This suggest that the Stern layer is in fact wider than expected in fact in line with Israelachvili and Adams [27] who found that the plane of shear could be as far as 2.5 nm from the surface of mica.

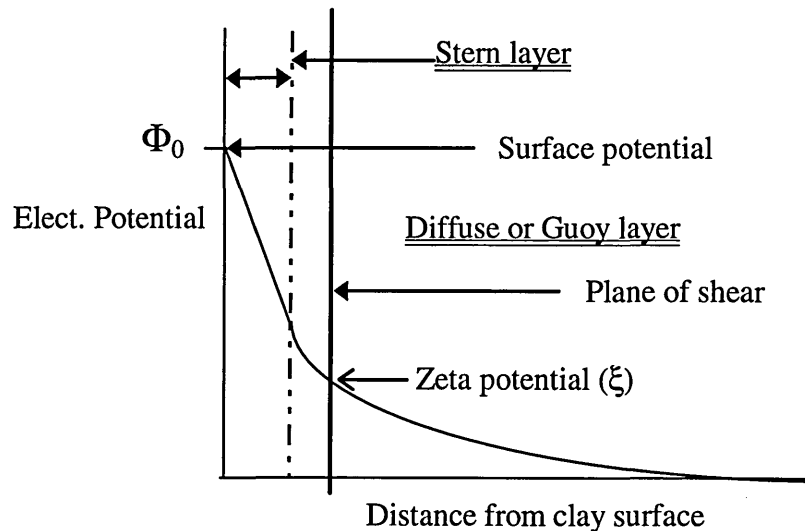


Figure 6: Model of the double layer out from a clay particle (first line on the left). Based on a schematic representation by Gan and Low. [26].

3.5 Flocculation and tactoid formation

The use of thin self supporting clay films as substitutes for shale samples in transport experiments will be evident in this thesis in Chapters 4 and 5. It is difficult to determine the exact structure of these films as preparation for subsequent imaging using electron

microscopy can often cause shrinkage or expansion. It is possible to postulate on the arrangement of clay particles in a compacted layer if information is available on the arrangements of these layers in suspension.

Clay layers can be grouped together in dispersions in the form of tactoids. In these regions the particle concentration is higher than in the rest of the dispersion. In these tactoids the clay layers are orientated at distances of the order of less than 100 Å from each other in a face-to-face orientation. One explanation for this structuring is that the layers lie in the regime of van der Waals attractive forces and are held together in a “potential well”

Support for such tactoid formation has come from electron microscopy, neutron and X-ray scattering, viscosity, and light scattering, [28], [11]. From such studies it is apparent that different ion exchange forms of clay have specific numbers of clay layers in the tactoids and that during the ion exchange process the tactoid size tends to change regularly with the degree of ion exchange.

Montmorillonite	n/n_{Li}
Li	1.0
Na	1.7
K	2.7
Cs	3.0
Ca	7.0

Table 3: Alteration in the number of montmorillonite layers in a tactoid (n) with the predominant cation relative to values for lithium exchanged clay. Data taken from [28]. Collected from light transmission measurements on a 0.2 % suspension.

Hysteresis in gel compaction has been attributed to the reordering of floc structures as pressure is exerted on the gel where the maximum pressure used was 8 bar [29].

Cases *et al.* [30] have carried out similar studies and their interpretation of the structure of a montmorillonite gel is given in Figure 7.

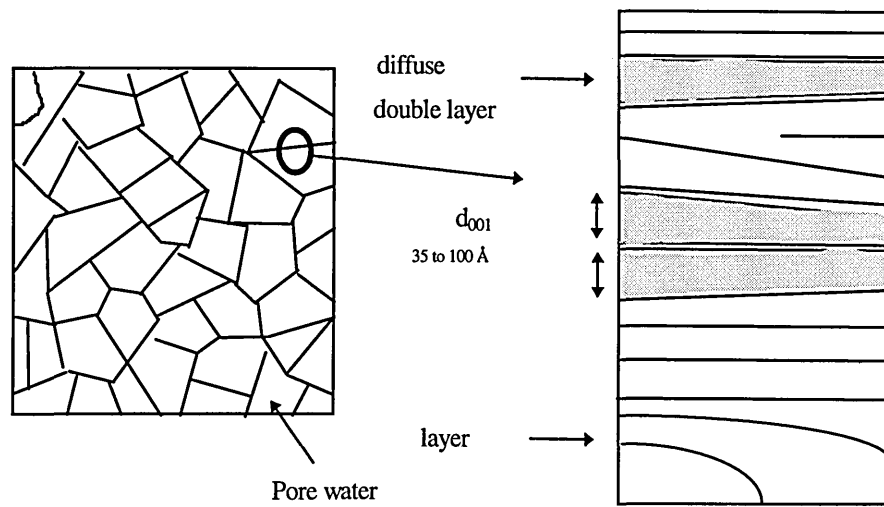


Figure 7: Schematic representation of the structure of a Na-montmorillonite gel. Na-montmorillonite dispersed in 10^{-3} M NaCl and subject to 0.032 bar. Taken directly from [30].

Here the compaction pressure was low (0.032) bar. One would imagine that the gel network is broken down at higher pressures but that the clay layers may not be perfectly aligned.

4. Interaction of organic matter with clays.

Many organic molecules can be readily adsorbed by clay minerals. The fact that clays adsorb these species is put to use in cosmetics, food purification and when altering the rheology of a drilling fluid [31].

In some cases, particularly for non-polar organic molecules, the interaction forces are relatively weak, corresponding to physical adsorption only. However polar or ionic organic species can enter into a wide variety of chemical reactions to form complexes with clay minerals. Kaolinite and smectite group minerals can be expanded by penetration of such molecules between the unit layers to form an intercalation complex. Depending on the nature of the organic species the bonding in the organo-clay complexes can occur *via*

- Hydrogen bonding
- Ion dipole forces, including formation of coordination complexes to exchangeable cations
- Bonding via “water bridges” between organic molecules and hydrated cations.

- Cation exchange
- d- π bonding between adsorbed arenes and transition metal exchange ions.

4.1 Charged organics

The adsorption of organic cations on the clay surface or in the interlamellar region is often exploited. Firstly it can be useful in determining the cation exchange capacity of the clays when the alkylammonium ion displaces the metal cation on the clay surface. Mortland and Barake [32] were the first to demonstrate that in systems where both organic and inorganic cations are present on the clay surface the ions are not well mixed. Also the ions will replace the remaining metal cations in a layer before inserting themselves into a new layer. This order of adsorption is of interest today to researchers investigating the properties of nanocomposites [33]. They claim to control the polymerisation rate of epoxide in the clay interlayer spacing by temperature and cation acidity. Both the acidity and the initial interlayer spacing are varied by exchanging the inorganic cation for an onium ion e.g $\text{CH}_3(\text{CH}_2)\text{NH}_3^+\text{Cl}^-$.

The adsorption of organic cations on clays is also used in herbicides [34], photostabilization of pesticide-clay complexes [35] and the hydrophobic modification of clay surfaces [36], [37]. The use of the cationic dye molecules such as methylene blue to probe the surface charge on the clay is used on location to determine the concentration of swelling clay in the mud samples from the wellbore by UV analysis of the un adsorbed dye. Recently the UV and adsorption characteristics of dyes have been manipulated to examine the interaction of the dye with the clay surface. For example methylene blue has been used as a molecular probe and has been used in this way on dispersions of several clays [38].

4.2 Adsorption of uncharged polymers

In Chapter 4 the interaction of glycols such as polyethylene and polypropylene glycol with the surface of montmorillonite is examined. Observations from this are used in the development of mud additives for the stabilisation of swelling clays downhole. In this section a description of the relevant literature on this subject will be presented. Examples of neutral polymers that are frequently adsorbed on clay surfaces are classes of ethylamines, glycols and alcohols. When the adsorbing polymer contains OH, NH_2 , or NH_3 groups then the interaction is direct with the clay surface or the hydration shell of the cation *via* hydrogen bonding [39].

Neutral but polar organic molecules which are miscible with water such as alcohols can replace water in the interlamellar space of montmorillonite, being coordinated to the exchange cations or held more closely between cation solvation sheaths. Many studies have been carried out on the intercalation of low molecular weight nonionics ($< 1,000 \text{ g mol}^{-1}$) particularly polyglycols into kaolinite illite, and montmorillonite [40-49]. These intercalation complexes can be prepared by reacting air-dried or dispersed montmorillonite with the polyglycol in either liquid or vapour form, or in solution. In most cases the complexes form well ordered structures which can be studied using X-ray or neutron diffraction, or Fourier Transform Infrared spectroscopy.

The adsorption of these polymers on the clay surface was proposed by Parfitt and Greenland [43] to be mainly driven by the gain in entropy when water molecules were displaced from the clay surface. This was proposed since the measured enthalpy of adsorption were small tending to zero for polyethylene glycols (peg) with a molecular weight of 600 g mol^{-1} ; the polymers are held at the clay surface by van der Waal forces [50]. Adsorption studies on calcium montmorillonite showed that the calculated entropy increased from +2.0 to +11.1 when changing from polyethylene glycols with molecular weights of 300 and 600 g mol^{-1} . It was proposed that the entropy change was composed of a conformational term and a hydration term. The hydration term dominates and depends on the loss of water from the polymer, the clay surface and the addition of these water molecules to the external solution. The higher molecular weight polyglycols exist as coils in solution and the extent of the coiling depends on the solvent [50]. On adsorption the conformation of the polymer changes to something comparable to a periodic waveform with segments touching the mineral surface (trains) and some in solution (loops). Even when the segment interaction energy is of the order of kT the cumulative energy can be high since *ca.* 40 % of the polymer is in contact with the mineral surface [51]. Therefore one would expect the higher molecular weight species to give high affinity type adsorption isotherms (H type) where the initial uptake of polyglycol is impossible to monitor. The probability of desorption of the adsorbed species by washing with solvent also decreases with increasing molecular weight [43]. Ash *et al.* [52] proposed the parallel-layer model for adsorbates for oligomers ($< 4,000 \text{ g mol}^{-1}$) which lie flat on the clay surface. This model accounts for every possible conformation of the adsorbed oligomer. It was used by Burchill *et al.* [41] to determine

the configurational energy and the equilibrium constant for the adsorption of polyglycols below $4,000 \text{ g mol}^{-1}$.

The formation of a 17.8 \AA montmorillonite-glycol complex was first shown by Bradley [53] to represent a bilayer of ethylene glycol ($\approx 8 \text{ \AA}$) in the interlamellar region; this is generally now an accepted view. However Aranda and Hitzky [54] studied the adsorption of polyethylene oxides (peo) (600 to $4,000 \text{ g mol}^{-1}$) onto sodium montmorillonite from acetonitrile solutions. Tentative evidence for the intercalation of the ethylene oxides in helical conformation with the clay counterions in the mid plane between the two silicate layers was gathered using Infrared and Nuclear Magnetic Resonance spectroscopy and X-ray diffraction techniques. They also assumed that the polymer maintains the close coiled structures found around the ions in the salt solutions and slots into the interlamellar region. Wu and Lerner [55] recently suggested that peo $1,000 \text{ g mol}^{-1}$ intercalated as a bilayer into sodium montmorillonite. Since adsorbing poly[oxymethylene oligo(oxyethylene)] (pem) on the clay gave the same thickness of polymer in the interlayer region they concluded that both polymers adsorbed in the “traditional conformation”. The helical conformations of peo and pem would be different due to the irregular placement of methylene linkages in the latter.

Eltantawy and Arnold [56] studied the adsorption of 2-ethoxyethanol (ethylene glycol monoethyl ether) (egme) on montmorillonite in the presence of calcium chloride-egme mixtures and they concluded from XRD measurements that a layer of egme was associated with each clay surface. One such well-known complex is formed when methylene glycol replaces water in the interlamellar space of montmorillonite. It forms a bilayer complex with a basal spacing of *ca.* 17 \AA in which the O-C-C-O chains lie parallel to the surface oxygens of the sheet but with the zig-zag of the chains perpendicular to this plane, in such a manner that the methylene groups are able to key into the ditrigonal cavities of the siloxane surfaces.

These findings have since been contested by Nguyen *et al.* [44] who used polarized attenuated total reflectance spectra to deduce the orientation of egme between the surfaces of calcium montmorillonite adsorbed from egme-calcium chloride mixtures. Nguyen *et al.* concluded that a single layer of molecules were orientated at 44 degrees to the clay surfaces with the calcium ions held in the centre. However Kellomäki *et al.* [47] contested these findings claiming that Nguyen *et al.* [44] could have been analysing the egme adsorbed on the external surfaces.

The position of the cations in the interlamellar complex of aliphatic chain compounds may either be central or adjacent to the surface depending on the extent of the ion/adsorbate interaction. One could suggest that the ease with which a counter ion might be exchanged from the clay surface in the presence of adsorbed glycol and water would depend on the location of the ion and the nature of the interaction with the surrounding species. No conclusive study could be found in the literature on the ease of exchange of the counterion in the presence of these adsorbed species. The adsorbed amount of polymer commonly called Q_{\max} has been shown to vary with the exchange cation on the clay surface. Breen *et al.* [40] studied the adsorption of a polyalkylene glycol (pag) from water onto a Texas montmorillonite. The clay had been pre-exchanged to the Cs, K, Na and Mn forms. Q_{\max} values for the corresponding clays were, 48 mg g⁻¹ for Cs, 84 mg g⁻¹ for K, 103 mg g⁻¹ for Na and 129 mg g⁻¹ for Mn. Breen *et al.* [40] proposed that the exchange ion determined the effective surface area of the montmorillonite available to the pag for adsorption.

Parfitt and Greenland [43] show that the interaction of peg 300 becomes energetically more favourable as the exchange ion on montmorillonite reduces in polarising power changing from Al to Ca to Na and to Cs. This data is in agreement with the hypothesis of Burchill *et al.* [41] that the glycol does not interact directly with the cation but with the hydration shell.

Neutron scattering studies were carried out by Burchill *et al.* [41] to scope the dynamics of the water near the surface of sodium montmorillonite in the presence of adsorbed peo. From their study they concluded that the those polymers having molecular weights from 800 to 4,000 g mol⁻¹ adsorbed in flattened conformation on the clay surface displacing the non-coordinated water and binding to the silicate surface and hydrated cations *via* a water bridge. However *ca.* 15 mm thick clay beds were required for the experiments which gives some uncertainty as to the clay surface being examined; i.e. internal or external. Using XRD and Infrared spectroscopy Parfitt and Greenland [57] studied the adsorption of water onto calcium and sodium montmorillonites containing peg 300 and peg 20,000. They concluded that the adsorption of water after the intercalation of peg followed the same trends as for non-glycolated montmorillonite; calcium clay-glycol showed stepwise expansion compared with extensive swelling of the sodium analog.

Polyethylene glycols 300 to 5,000 in molecular weight and polypropylene glycols of weights of 750 and 400 were tested for their effect on the water activity of the glycol solutions [58]. It was found that with a weight fraction of 0.3 the water activity was still 0.96 or higher. Considering that these polymers are added at 0.05 wt fraction to drilling fluids it is considered that they have no effect on the osmotic pressure differential between the drilling fluid and the porefluid in the rock matrix.

5. Clays in sedimentary rocks

Sedimentary rocks such as mudrocks are formed from ocean floor sediments by burial to depths of several kilometres, accompanied by the development of high pressures and moderately high temperatures [59]. Mudrocks can contain as much as 40 wt% of clays and may be classified as shales or mudstones respectively depending on whether the clay mineral microfabric is highly orientated, leading to bedding plane fissility or randomly orientated. Bands in shales range from 0.05 to 1.0 mm in thickness with the majority of bands in the range of 0.1 to 0.4 mm. There appears to be three kinds: alterations of coarse and fine particles, such as silt and clay; alterations of light and dark layers with different organic contents; and alternations of calcium carbonate and silt. This banding of various materials can be claimed to be the result of differential settling rates of the several components or differing rates of supply of these materials to the sea floor. The composition of sedimented clays and shales is varied, because these materials come from abrasion processes (mainly silt), weathering (residual clays), and chemical and biochemical additions. Some of these processes have been represented in Figure 9.

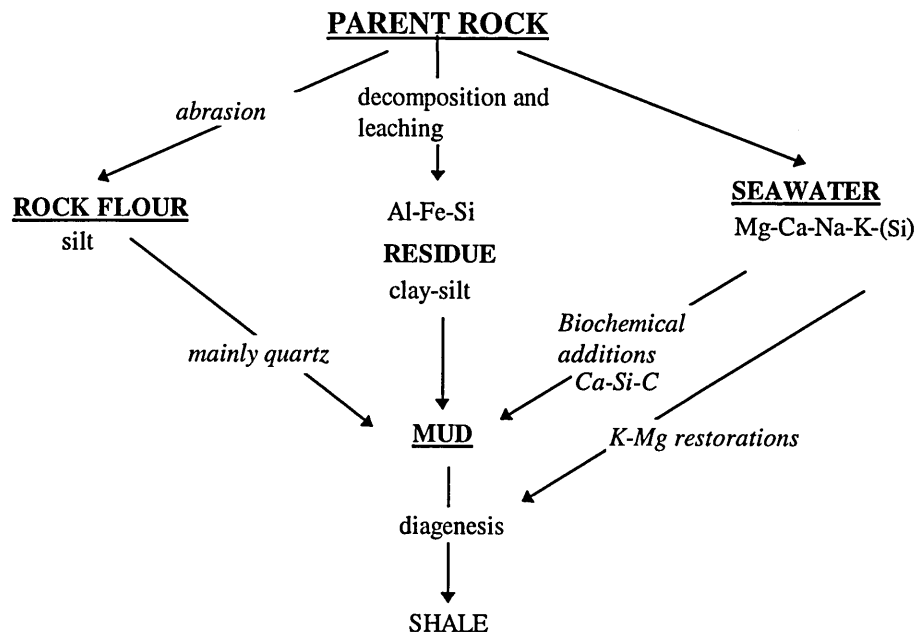


Figure 9: Processes occurring prior to the formation of shale [59].

These chemical additions are either materials precipitated from solutions and deposited concurrently with accumulating clays, such as calcium carbonate; or they are materials added by reaction or exchange with the surrounding medium (usually sea water), such as potassium or magnesium. The several varieties of shales are mainly dependent on the relative importance of the different contributing sources; hence both mineralogy and chemical composition fluctuate within wide limits. The average mineral composition of shale is quoted by Shaw and Weaver [60] as

Constituent	Weight percent
Quartz	33.8
Feldspar	4.0
Clay minerals	56.4
Iron oxides	< 0.5
Carbonates	2.6
Other minerals	< 2.0
Organic matter	1

Table 4: The average mineral composition of shale.

The data provided in Table 4 should really be taken as a guide to the minerals that need tracing during analysis of shales in general. Variations in the type of clay present in the shales can lead to changes in the mechanical behaviour.

Class	Texture	CEC meq/100	Water Cont. wt%	Clay Minerals	Clay wt%	Density gm/cc
A	Soft	20-40	25-70	Smectite + illite	20-30	1.2-1.5
B	Firm	10-20	15-25	Illite + mixed layer	20-30	1.5-2.2
C	Firm-hard	10-20	2-10	Illite + mixed layer	20-30	2.3-2.7
D	Hard	3-10	5-15	Illite + possible smectite	20-30	2.2-2.5
E	Brittle	0-3	2-5	Illite, kaolinite, chlorite	5-30	2.5-2.7

Table 4: Classification of shale according to the mineralogy from Weaver [2].

The clay mineral fraction may contain illite-smectite, illite-mica, mica-montmorillonite, kaolinite, montmorillonite, and chlorite [61]. A schematic of a mixed layer illite-montmorillonite is given in Figure 10.

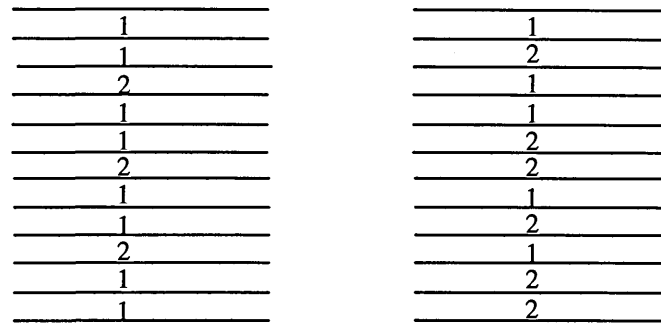


Figure 10: A schematic representation of a mixed layer illite (1) and smectite (2) [61].

Many “mixed-layer” clay minerals are also known. The structure of the group is the result of ordered or random stacking of the basic clay mineral units one upon the other on a fine scale in the *c* direction. Sometimes the ordered stacks are given new names such as rectorite for mica-montmorillonite but most often the random stacks such as illite-smectite remain unnamed. Clay mineral layers are strongly bound internally but weakly bound to each other allowing the different clay minerals to slot into different positions of a stack.

Shales undergo many post-depositional modifications, some physical and some chemical. The first includes compaction, with pore space reduction and improved clay mineral orientation; the second involves mineral transformation. The porosity of shale under an overburden of 1,800 m is typically only 9 or 10 percent. The decrease in porosity when going from a mud to a shale is largely the result of compaction. It has been clearly shown that the clay mineralogy of a sediment may be altered on burial. Montmorillonite and kaolinite tend to disappear with increasing depth and illite and chlorite materials take their place. A map of Great Britain showing the ages and distributions of shales is shown in Figure 11. Fullers Earth used in these studies comes from the Middle Jurassic and Lower Cretaceous bands in southern England [62]. The sample used in this study was taken from an outcrop in Redhill in Surrey. While Oxford Clay is a Jurassic shale quarried near Oxford, England.

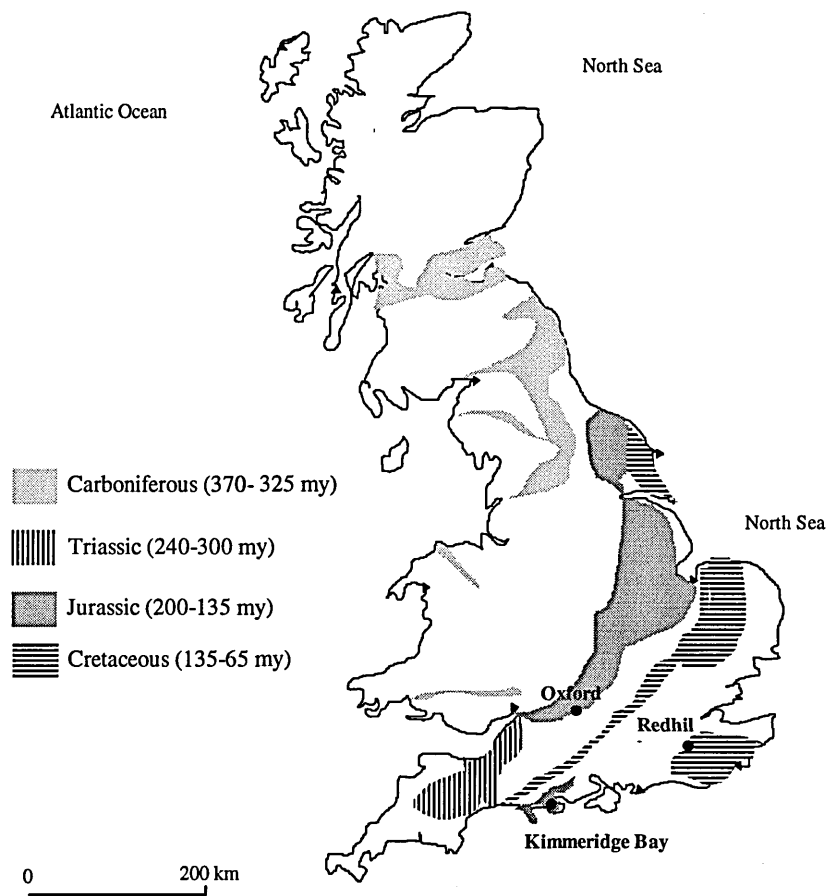


Figure 11: The distribution of shales in Great Britain. The ages of the shales are represented by millions of years (my).

The presence of excess pore water pressures in shales help in determining the extent of consolidation and effective pressure as a function of depth. High rates of fine grained sediment deposition added to very low permeabilities can result in the occurrence of excess pore pressure. The clay fabric and the particle-to particle arrangements determine the sizes of the pore spaces and their geometry, and ultimately control the permeability to water [63]. Meade [64], pointed out the important inverse relationship between particle size and porosity, particularly within the range of overburden stress up to 10 MPa. He recognised that the effect of particle size (comparing silt and clay) may be strong enough to obscure the expected decrease in porosity with increasing burial depth.

Pore dimensions decrease with burial depth as was found by Borst [65] from a large study on lots of shale samples. The decrease in maximum pore dimension with depth was typically $1\mu\text{m}$ at 100 m ($\approx 2\text{ MPa}$) to 4 nm at 10 km (200 MPa). Overburden pressures have been calculated assuming 2.2 MPa m^{-1} .

Engelhardt and Gaida [66] measured the final porosities of montmorillonites slurried in sodium chloride solutions ranging in concentrations from 0.6 to 4.6 mol L^{-1}

Their data shows that the concentration of the electrolyte had no effect on the final porosity at least in the pressure range of 3 to 320 MPa. Also Mesri and Olson [67] carried out a study on the compaction of Na Montmorillonite slurried in sodium chloride varying between 5×10^{-4} to 1×10^{-1} mol L⁻¹ in the pressure range up to 10 MPa. They agreed with Engelhardt and Gaida that at consolidation pressures of 5 MPa the porosities of all the compacted slurries were the same. However in both cases the time taken to reach an equilibrium compaction value (albeit fractions of hours) was higher at low salinities and the effect was more apparent when compacting montmorillonite than kaolinite.

6. Ion and water movement through shales and clays

In the wellbore the ingress of water and ions into the shale sections is of interest when trying to control the degree of swelling and prevent borehole instability. There is no doubt that water and ions can move into shale sections and clay rich beds, and some proof of this will be given in this section. However the trajectory of an ion or a water molecule through the compacted clay is still unknown, i.e do these species move through the interlamellar region close to the clay surface or through the macro pores; if these exist. A brief review of research in the general area of ion and water movements through shales and clay will be given here.

Neutron scattering studies on the movement of water through calcium exchanged montmorillonite clays have shown that there are two types of water in the clay matrix [68], [16]. The tightly bound fraction of 6 molecules or so per cation and the weakly bound molecules which diffuse more rapidly between the silicate surface and the exchange cations. However the less bound water also exhibits a long-range diffusion which is assigned to the movement of the water molecules between the interlamellar region and the micropores in the clay structures. These self-diffusion coefficients were 5 times smaller for the water molecules moving between micropores than the expected value for movement in bulk solution. When the water content of a calcium montmorillonite dispersion increased from 0.09 to 0.26 g water/ g of clay the measured diffusion coefficient increased from 0.2 to 4.0×10^{-10} m² s⁻¹. Evidence was also given for two types of water in the sodium montmorillonite dispersions.

In some studies radioactive tracers were used to track the movement of water and ions in shales [69]. Under zero applied pressure the movement of water and ions through the shale sample was diffusion controlled and with an applied pressure advection resulted and the transport rates of water and ions were increased. However the permeability of

shales and compacted clays are relatively low (10^{-24} to 10^{-18} m^2) which results in the movement of water by diffusion at high compaction pressures [70]. Some workers have proposed the existence of an charged barrier in shale leading to the blocking of ion movement and therefore the water can flow due to the developed osmotic pressures [71], [72], [70].

Anion exclusion prevents the movement of ions between two clay surfaces leading to the natural membrane properties of clays and shales [73]. Anions are repelled by the negative clay surface but diffusion from the equilibrium surface towards the clay layers counteracts the electric repulsion to some extent. However on compaction the clay platelets approach each other and the two adjoining layers will eventually overlap lowering the concentration of anions between the clay surfaces. In fact anion exclusion has been used to study the effective surface area of clays containing different exchange cations. Edwards and Quirk [74] were among the first to use anion exclusion measurements to demonstrate that the effective surface area of a calcium exchanged montmorillonite was less than that of a sodium exchanged clay in suspension; $85 \text{ m}^2 \text{ g}^{-1}$ versus $560 \text{ m}^2 \text{ g}^{-1}$.

The membrane properties of shales and compacted clays have been examined via potential measurements across films of the materials. These measurements can be used to calculate the transport coefficients of anions and cations in the matrix [75, 76, 77]. When sodium chloride is present and the membrane has no anion rejection properties the transport coefficient of the chloride ion is 1. That is the chloride ion diffuses faster than sodium ions. In studies on shales Cavaliere *et al.* [75] demonstrated that the cation transport coefficient approached 1 for shales sampled at burial depths of 3055 m. This suggests that the clay layers are so overlapped that the anions are unable to move through the shale matrix and that the charge is carried by the cation.

In radioactive tracer experiments there is usually an initial delay in the break through of the tracer cation and analysis can show that there are ion exchange processes occurring on the clay surface. These ion exchange processes have also been shown to occur in shales [78].

Calculation of the electrical ion dipole association energies of the different cations for water and inclusion of this term in the classic diffuse double layer theory indicated that a fraction of the adsorbed cations reside directly on the clay surface (within 1 \AA) and are not completely hydrated. It was also calculated that ions residing on the surface must attain a high activation energy to move from one exchange site to an other and therefore their

mobility is limited. Only the completely hydrated adsorbed cations (above 4 Å from the surface) should have mobilities near the mobilities of these ions in bulk solution [79].

From this study it is obvious that the process of ion exchange is controlled by the energetics at the clay surface. The invading cation also needs to gain access to the exchange site which can be hindered by the bedding of the clays.

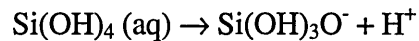
Using conductivity measurements Shainberg and Kemper [80] calculated the reduction in relative mobility of calcium ions on the outside of the clay tactoids compared with those in the centre of the tactoid. They found that as the fraction of calcium on the exchange sites increased from 0.2 to 0.8 mole fraction the mobility of the calcium ion relative to that of sodium decreased from 0.59 to 0.1. Interestingly at calcium loadings below 0.2 mole fraction the conductivity was unaffected by the replacement of sodium ions for calcium on the clay surface. It has been well established in various studies using X-ray diffraction [81], rheology, sedimentation [82] and light scattering [11] that calcium clays exist in tactoids averaging 4 to 7 clay layers each. Inside the tactoids where there are on average 1.5 molecular layers of water on each surface the concentration of the cations is very high, most of the water molecules there are under strong influence of the adsorbed cations and this water has a much higher viscosity than bulk water. The greater viscosity between platelets and the probability that interplatelet Ca is held in a more stable position by two exchange sites directly opposite each other on adjacent platelets may greatly reduce the mobility of the Ca within the tactoids compared with that on the surface.

Direct measurements on shales and compacted shale fragments have shown that the solutions eluted from compacting multi-ionic clay-water systems become more dilute in their electrolyte content as the compaction pressure increased. Shackelford and Daniel [83] describe the various experimental set ups used to measure diffusion coefficients in soils. They describe two types of measurements which lead to the effective and apparent diffusion coefficients. The effective coefficient takes account of the tortuosity of the matrix through which the ion is travelling but does not allow for ion surface interactions; whereas the apparent tortuosity factor includes both. Estimates of the effective diffusion coefficient through soils can be made using anions such as Cl or I to give the tortuosity factor allowing it to be used in calculating the cation diffusion coefficient in subsequent experiments. Oscarson *et al.* [84] determined the effective diffusion coefficient for iodide through compacted bentonite with a porosity of 50 wt% and found it to be $3 \times 10^{-12} \text{ m}^2 \text{ s}^{-1}$ compared with $2 \times 10^{-9} \text{ m}^2 \text{ s}^{-1}$ in solution.

7. Silicates

Silicates are sometimes added to drilling fluids and are found to contribute to wellbore stability. The development of osmotic barriers by silicate systems will be examined in Chapter 5 and hence an introduction to silicates will be given in this section.

Soluble silicates have been used in a wide range of industrial processes for many years and a large body of literature on their behaviour has been generated [85], [86]. Silicates are not to be confused with dispersed colloidal silica, as the silicates dissolve at pH 9 in the absence of divalent ions. The most weakly hydrolysed form of silica detectable in aqueous solution is orthosilicic acid, $\text{Si}(\text{OH})_4$ [87]. Above pH 7 further hydrolysis involves the deprotonation of silanol group to form an anionic species



Because $\text{Si}(\text{OH})_3\text{O}^-$ is a very weak acid, $\text{Si}(\text{OH})_2\text{O}_2^{2-}$ is observed in appreciable quantities only above pH 12. In fact $\text{Si}(\text{OH})_4$ may polymerise into siloxane chains then branch and crosslink. Iler [88] recognised three stages of polymerisation:

- (1) Polymerisation of monomers to form particles,
- (2) growth of particles,
- (3) linkage of particles into branched chain networks and then gels.

These stages have been represented in a chart in Figure 12.

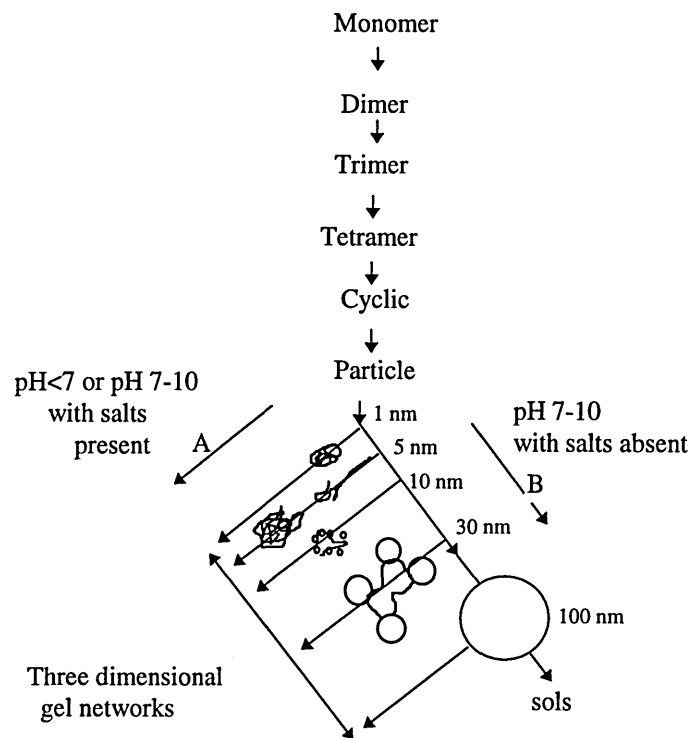


Figure 12: Polymerisation pathways of silicates. Chart reproduced from Iler [88].

8. References

- [1] van Olphen H., An introduction to clay colloid chemistry: for clay technologists, geologists and soil scientists: 2nd edition, John Wiley & Sons, 1977.
- [2] Weaver C.E.. Developments in sedimentology, 44, Clays, muds and shales, Elsevier, 1989
- [3] Bolt G.H. and Bruggenwert M.G.M., Composition of the soil:, Soil Chemistry A: basic elements, Elsevier, 1981.
- [4] Hofmann U., Endell K. and Wilm D. Zeitsch. Fur Kristall., **86**, 340-355,1933.
- [5] Berner R.A. Principles of chemical sedimentology, International series in the earth & planetary sciences, Mc Graw-Hill, 166, 1971.
- [6] Velde B. Introduction to clay minerals. Chemistry, origins, uses and environmental significance, Chapman & Hall, 164-175, 1992.
- [7] Gray G.R. and Darley H.C. Composition and properties of oil well drilling fluids, Gulf publishing, 138-181, 1980.
- [8] Hall P.L. Clays, their significance, properties origins and uses, In: A Handbook of Determinative Methods in Clay Mineralogy, Ed. M.J. Wilson, Blackie, 22, 1987.
- [9] Madsen M. and Schlundt J. Low technology water purification by bentonite clay flocculation as performed in Sudanese villages: bacteriological examinations, Water Research, **23**, 873-882, 1989.
- [10] Borja R., Martin A., Duran M.M and Luque Y.M. Kinetic study of the anaerobic purification of a cheese factory waste water, Rev. Esp. Cienc Tecnol. Ailment. **32**, 19-32, 1992.
- [11] Swartzen-Allen S. and Matijevic' E., Surface and colloid chemistry of clays, Chemical Reviews, **74**, 385-400, 1974.
- [12] Low P.F. The clay water interface. In Proceedings International Clay Conference, Denver, Colorado. Eds: L.G Schultz and H. van Olphen, 247-256, 1987.
- [13] Mitchell J.K. Fundamentals of soil behaviour, 2nd edition, John Wiley and Sons, 113-130, 1993.
- [14] Pinnavaia T.J., Advanced chemical methods for soil and clay minerals research, Ed. Stucki J.W and Banwart W.L., D. Reidel, Boston, Chapter 8, 1980.

- [15] Boek E.S., Coveney P.V. and Skipper N.T., Monte Carlo molecular modeling studies of hydrated Li, Na, and K smectites: Understanding the role of potassium as a clay swelling inhibitor, *Journal of the American Chemical Society*, **117**, 12608-12617, 1995.
- [16] Tuck J.J, Hall P.L., Hayes M.H.B., Ross D.K. and Hayter J., Quasi-elastic neutron scattering studies of the dynamics of intercalated molecules in charge-deficient layer silicates. 2. High resolution measurements of the diffusion of water in montmorillonite and vermiculite, *J. Chem. Soc. Faraday Trans. I*, **81**, 833-846, 1985.
- [17] Helmy A.K. The limited swelling of montmorillonite, *Journal of Colloid and Interface Science*, **207**, 128-129, 1998.
- [18] Barclay L. and Ottewill R., Measurement of forces between colloidal particles, *Discussions Faraday Society* 1 138-171, 1970.
- [19] Hunter R.J. *Foundations of colloid science*, **1**, Oxford Science Publications, 332, 1987.
- [20] Chan D.Y.C., Pashley R.M. and Quirk J.P., Surface potentials derived from co-ion exclusion measurements on homoionic montmorillonite and illite, *Clays and Clay Minerals*, **32**, 131-138, 1984.
- [21] Van der Put A.G. and Bijsterbosch B.H. Electrokinetic measurements on concentrated polystyrene dispersions and their theoretical interpretation, *Journal Colloid Interface Science*, **92**, 499, 1983.
- [22] O'Brien R.W. and Perrins W.T. The electrical-conductivity of a porous plug, *Journal Colloid Interface Science*, **99**, 20-31, 1984.
- [23] Zukoski C.F and Saville D.A. An experimental test of electrokinetic theory using measurements of electrophoretic mobility and electrical conductivity, *Journal of Colloid and Interface Science*, **107**, 322-333, 1985.
- [24] Zukoski C.F and Saville D.A. J. The interpretation of electrokinetic measurements using a dynamic model of the stern layer, *Journal of Colloid and Interface Science*, **114**, 32-53, 1986.
- [25] Grahame D. The electrical double layer and the theory of electrocapillarity, *Chemical Reviews*, **41**, 441-501, 1947.
- [26] Gan H. and Low P.F., Spectroscopic study of ionic adjustments in the electric double layer of montmorillonite, *Journal of Colloid and Interface Science*, **161**, 1-5, 1993
- [27] Israelachvili J.N., and Adams G.E., Measurement of forces between 2 mica surfaces in aqueous electrolyte solutions in range 0-100 nm. *J. Chem. Soc. Faraday. Trans.*, **74**, 975-985, 1978.

- [28] Schramm L. and Kwak J. Interactions in clay suspensions: the distribution of ions in suspension and the influence of tactoid formation, *Colloids and Surfaces*, **3**, 43-60, 1982.
- [29] Viani B., Low P. and Roth C. Direct measurement of the relation between interlayer force and interlayer distance in the swelling of montmorillonite, *Journal of Colloid and Interface Science*, **96**, 1, 229-244, 1983.
- [30] Cases J.M., Pons C.H., Berend I., Francois M., Hong Min J., Tchoubar D., Besson G., Thomas F., and Bottero J.Y., Fluid-swelling clays interaction, *Physical Chemistry of Colloids and Interfaces in Oil Production*, Ed. Toulhoat H., and Lecourtier J., Editions Technip, Paris, 27, 1992.
- [31] Gray G.R. and Darley H.C.H. Composition and properties of oil well drilling fluids. Gulf publishing company, Houston, 181-277, 1980.
- [32] Mortland M.M and Barake N., Interaction of ethylamine and metal ions on montmorillonite. *Trans.8th Int Congr. Soil Sci.* 3, 433-443, 1964.
- [33] Yun K. Y., Constantino V. R. L. and Pinnavaia T. J. Synthesis and Catalytic Properties of Silicate-Intercalated Layered Double Hydroxides Formed by Hydrolysis of Tetraethylorthosilicate, *Clays and Clay Minerals*, **43**, 503-510, 1995
- [34] Orgam A.V., Jessup R.E, Ou L.T. and Rao P.S.C. Effect of sorption on biological degradation rates of (2,4-dichlorophenoxy) acetic acid in soils: *Applied. Environmental. Microbiology.* **49**, 582-587, 1985.
- [35] Margulies L., Rozen H. and Cohen E. Photostabilization of a nitromethylene heterocycle on the surface of montmorillonite. *Clays and Clay Minerals*, **36**, 159-164, 1987.
- [36] Favre H. and Lagaly G. Organo-bentonites with quaternary alkylammonium ions. *Clay Minerals*, **26**, 19-32, 1991.
- [37] Jaynes W.F. and Boyd, S.A. Hydrophobicity of siloxane surfaces in smectites as revealed by aromatic hydrocarbon adsorption from water. *Clays and Clay Minerals* **39**, 428-436, 1991.
- [38] Cenens J. and Schoonheydt R.A. Visible spectroscopy of methylene blue on hectorite, laponite B , and Barasym in aqueous suspension. *Clays and Clay Minerals.* **36** 214-224, 1988.
- [39] Raussell J.A and Serratosa J.M. Reactions of clays with organic substances, In: *Chemistry of Clays and Clay Minerals*, 371-421, 1987.
- [40] Breen C., Rawson J.O, Mann B.E, and Aston M. In situ ¹³³Cs and ¹H solution-phase NMR, thermoanalytical and X-ray diffraction studies of the adsorption of

- polyalkyleneglycol on Texas bentonite, *Colloids and Surfaces A: Physiochemical and Engineering Aspects* **132**, 17-30, 1998.
- [41] Burchill S., Hall P.L., Harrison R., Hayes M., Langford J., Livingston W., Smedley R, Ross D. and Tuck, J. Smectite-polymer interactions in aqueous systems, *Clay Minerals*, **18**, 373-397, 1983.
- [42] Gu B. and Doner H. E. The interaction of polysaccharides with Silver Hill Illite, *Clays and Clay Minerals*, **40**, 2, 151-156, 1992.
- [43] Parfitt R.L and Greenland D. J. The adsorption of poly(ethylene glycols) on clay minerals, *Clay Minerals*, **8**, 305-317, 1970.
- [44] Nguyen T.T, Raupach M. and Janik L.J. Fourier transform infrared study of ethylene glycol monoethyl ether adsorbed on montmorillonite: implications for surface area measurements of clays, *Clays and Clay minerals* **35**, 60-67, 1987.
- [45] Billingham J., Breen C. and Yarwood J. Adsorption of polyamine, polyacrylic acid and polyethylene glycol on montmorillonite: an in situ study using ATR-FTIR, *Vibrational Spectroscopy* **14**, 19-34, 1997.
- [46] Zhao X., Urano K. and Ogasawara S. Adsorption of polyethylene glycol from aqueous solution on montmorillonite clays, *Colloid and Polymer Science*, **267**, 899-906, 1989.
- [47] Kellomäki A., Nieminen P., and Ritamaki L. Sorption of ethylene glycol monoethyl ether (egme) on homoionic montmorillonite, *Clay Minerals*, **22**, 297-303, 1987.
- [48] Platikanov D., Weiss A. and Lagaly G. Orientation of nonionic surfactants on solid surfaces: n-alkyl polyglycol ethers on montmorillonite, *Colloid and Polymer Science*, **255**, 907-915, 1977.
- [49] Tunney J. and Detellier C. Aluminosilicate nanocomposite materials. Poly(ethylene glycol)-kaolinite intercalates, *Chem. Mater.*, **8**, 927-935, 1996.
- [50] Fleer G.J, Stuart M.A., Scheutjens J. M. H. M., Cosgrove T. and Vincent B. *Polymers at interfaces*, Chapman and Hall, 234-255, 1993
- [51] Theng B.K. Clay-polymer interactions: summary and perspectives, *Clays and Clay Minerals*, **30**, 1-10, 1982.
- [52] Ash S.G., Everett D. H. and Findenegg G.H. Multilayer theory of adsorption of n-mers and its application to flexible tetramers and trimers, *Trans. Faraday Soc.* **66** 708-722, 1970.

- [53] Bradley W.F. Molecular associations between montmorillonite and some polyfunctional organic liquids, *Journal of the American Chemical Society*, **67**, 975-981, 1945
- [54] Aranda P. and Ruiz-Hitzky E. Poly(ethylene oxide)-silicate intercalation materials, *Chem. Mater.* **4**, 1395-1403, 1992.
- [55] Wu J., and Lerner M., Structural, thermal and electrical characterization of layered nanocomposites derived from Na-Montmorillonite and polyethers, *Chem. Material*, **5**, 835-838, 1993.
- [56] Eltantawy I.M. and Arnold P.W. Ethylene glycol sorption by homoionic montmorillonites, *J. Soil Sci.* **25**, 99-110, 1974.
- [57] Parfitt R.L and Greenland D. J. Adsorption of water by montmorillonite-poly(ethylene glycol) adsorption products, *Clay Minerals*, **8**, 317-327, 1970.
- [58] Malcolm G.N and Rowlinson J.S. The thermodynamic properties of aqueous solutions of polyethylene glycol, polypropylene glycol and dioxane, *Transactions of the Faraday Society*, **53**, 921-931, 1957.
- [59] Pettijohn F.J. *Sedimentary rocks* 260-299, Harper and Row, New York, 1975.
- [60] Shaw, D.B., and Weaver C.E., The mineralogical composition of shales: *Journal. Sediment Petrology*, **35**, 213-222, 1965
- [61] O'Brien N.R. and Slatt R.M. *Argillaceous rock atlas*. Springer-Verlag, New York, 123-128, 1990.
- [62] Jeans C.V., Merriman R.J., and Mitchell J.G. Origin of middle Jurassic and lower cretaceous Fullers Earths in England., *Clay Minerals*, **12**, 11-44, 1977.
- [63] Bennett R.H., Burns J.T., Clarke T.L., Faris J.R, Forde E.B, and Richards A.F. Piezometer probes for assessing effective stress and stability in submarine sediments, In *Marine slides and other mass movements*: Ed S. Saxon and J.K. Nieuwenhuis, New York, Plenum 129-161, 1982.
- [64] Meade, R.H., Factors influencing the early stages of the compaction of clays and sands: Review: *Journal of Sedimentary petrology*, **36**, 1085-1011.
- [65] Borst R.L. Some effects of compaction and geological time on the pore parameters of argillaceous rocks, *Sedimentology*, **29**, 291-298, 1982.
- [66] Engelhardt W. Von and Gaida K.H. Concentration changes of pore solutions during the compaction of clay sediments, *Journal Sedimentary Petrology* **33**, 919-930, 1963.
- [67] Mesri G. and Olson R.E. Consolidation characteristics of montmorillonite, *Geotechnique*, **21**, 341-352, 1971.

- [68] Tuck J.J, Hall P.L., Hayes M.H.B., Ross D.K. and Poinsignon C. Quasi-elastic neutron scattering studies of the dynamics of intercalated molecules in charge-deficient layer silicates. 1. Temperature dependence of the scattering from water in Ca-montmorillonite and vermiculite, *J. Chem. Soc. Faraday Trans. I*, **80**, 309-324, 1984.
- [69] Ballard T.J, Beare S.P. and Lawless T.A. Fundamentals of shale stabilisation: Water transport through shales, SPE 24974, 1992.
- [70] van Oort E. Critical parameters in modelling the chemical aspects of borehole stability in shales and in designing improved water-based shale drilling fluids, SPE 28309, 1994.
- [71] Fritz S.J. Ideality of clay membranes in osmotic processes: A review, *Clays and Clay Minerals*, **34**, 214-223, 1986.
- [72] Bailey, L., Denis J.H. and Maitland G.C. Drilling fluids and wellbore stability-current performance and future challenges, *Chemicals in the Oil Industry Symposium*, Imperial College, London, 1991.
- [73] Kharaka Y.K. and Berry F.A. Simultaneous flow of water and solutes through geological membranes I. Experimental investigation, *Geochimica et Cosmochimica Acta*, **37**, 2577-2602, 1973.
- [74] Edwards D.G. and Quirk J.P. Repulsion of chloride by montmorillonite, *Journal of Colloid Science*, **17**, 872-882, 1962.
- [75] Cavaliere R., Longhi P., Mussini T., and Neglia S. Electrochemical phenomena in shale membranes: Membrane potentials and related transport parameters. *Gazzetta Chimica Italiana*, **109**, 399-407, 1979.
- [76] Wyllie M.R.J. Some electrochemical properties of shales, *Science*, **108**, 684-685, 1948.
- [77] Helmy A.K., Nartale I.M., and Grazdn A.M. Electric potentials of bi-zonal clay film membranes, *Colloid and Polymer Science*, **254**, 50-54, 1976.
- [78] Sherwood J. D. and Bailey L. Swelling of shale around a cylindrical wellbore, *Proceedings of the Royal Society of London*, **A444**, 161-184, 1994.
- [79] Shainberg I. and Kemper W.D. Hydration status of adsorbed ions, *Soil Science Society of America Proceedings*, **30**, 700-725, 1966.
- [80] Shainberg I. And Kemper W.D. Electrostatic forces between clay and cations as calculated and inferred from electrical conductivity, 14th International Conference on Clays and Clay Minerals, 117-133, 1966

- [81] Norrish K. and Quirk J.P. Crystalline swelling of montmorillonite, *Nature*, **173**, 255-257, 1954.
- [82] Blackmore A.V. and Miller R.D. Tactoid size and osmotic swelling in calcium montmorillonite, *Proceedings Soil Science Society America*. **25**, 169-173, 1961.
- [83] Shackelford C.D. and Daniel D. E. Diffusion in saturated soil 1 and 2, *Journal of Geotechnical Engineering*, **117**, 467-507, 1991.
- [84] Oscarson D.W., Hume H.B., Sawatsky N.G. and Cheung S.C.H. Diffusion of iodide in compacted bentonite, *Soil Science American Journal*, **56**, 1400-1406, 1992.
- [85] Brinker C.J., Sol-Gel processing of silica, Chapter 18, 361-398, In: *The colloid chemistry of silica*, Ed. Horacio E. Bergna, *Advances in Chemistry Series 234*, American Chemical Society, DC, 1992.
- [86] Vail J.G., *Soluble silicates, their properties and uses*, American Chemical Society publications, New York, 1952.
- [87] Weldes H.H. and Lange K.R., *Properties of soluble silicates*, *Industrial and Engineering Chem.*, **61**, 1969.
- [88] Iler R.K, *The Chemistry of silica*; Wiley-Interscience, New York, 1978.

1. Introduction	34
2. Specific background theories	34
2.1 Resistivity models for clay bearing rocks	35
2.2 Arrhenius rate law	37
2.3 Clay phase porosity	38
3. Experimental	39
3.1 The clays and quartz	39
3.2 Preparation of Shale and Sandstone samples for resistivity measurements	40
3.3 Compact preparation	41
3.3.1 <i>Compaction apparatus</i>	41
3.3.2 <i>Heating instrumentation</i>	42
3.3.3 <i>Slurry preparation and compaction procedures</i>	43
3.3.4 <i>Compaction and temperature equilibration times</i>	44
3.4 The resistivity measurements	45
3.4.1 <i>The electrodes</i>	45
3.4.2 <i>Electrode evaluation</i>	45
3.4.3 <i>Experiments with pure electrolytes</i>	46
3.5 Compact porosity and microstructural determination	47
3.5.1 <i>Scanning electron microscopy (SEM)</i>	47
3.5.2 <i>Porosity determination</i>	47
4. Results and Discussions	48
4.1 Compaction behaviour of clays	48
4.1.1 <i>Contribution of clay chemistry to compaction profiles</i>	48
4.1.2 <i>Effect of added electrolyte on the compaction profiles</i>	56
4.1.3 <i>The porosity of mixed-clay compacts</i>	58
4.1.4 <i>The porosity of compacts with quartz added</i>	63
4.1.5 <i>Summary</i>	64
4.2 Conductivity measurements-methods and results	65
4.2.1 <i>Electrode evaluation</i>	65
4.2.2 <i>Comparison of platen electrodes with liquid electrodes</i>	67
4.2.3 <i>Electrode end effects</i>	68
4.2.4 <i>Summary</i>	70
4.3 Conductivity of clay compacts	71
4.3.1 <i>Temperature effects</i>	78
5. Conclusions	80
6. Future work	80
7. References	81

1. Introduction

Destabilisation of the wellbore during the drilling process is a major concern especially in the sections containing shale [1], [2], [3]. In shale it is likely that clays are present which can swell in contact with water, aiding the erosion of the wellbore wall. In some cases the shale sections have been isolated or uplifted over geological time and the pore fluid pressure is higher than expected for the burial depth. Wells are usually drilled with the mud pressure higher than the pore pressure to reduce gas influx and prevent wellbore collapse; sudden reversals in differential pressures can cause problems.

Recently, logging tools have been designed to measure the resistivity of the shale matrix at the drill bit in real time [4]. Data from these Resistivity At the Bit (RAB) measurements could be useful in determining the pore pressure, lithology and perhaps even the cation exchange capacities of the clay bearing formations [5]. Much of the research to date deals with the interpretation of resistivity measurements on sandstones, limestones and shaly sands. A model was needed to help interpret resistivity logs from shale sections.

The experimental study was made on clay silt compacts sometimes termed “synthetic shales” and also on real shale systems. The author worked on the design of electrodes for resistivity measurements and on the characteristics of the synthetic shales under the supervision of Dr John Cook.

It was initially intended that the conductivity of swelling clays under simulated down hole conditions be investigated, and that the boundary between a shaly sand and a sandy shale be defined by changing the silt fraction.

In this Chapter results from the following experiments will be presented and discussed;

- contribution of individual clays to the porosity of mixed clay systems and clay silt mixtures,
- design and evaluation of electrodes for shale resistivity measurements and,
- conductivity measurements on clay compacts and their interpretation using the model of Waxman and Smits [6].

2. Specific background theories

Theories discussed in this section are supplied for use in interpreting data. In cases where they draw on theoretical principles outlined in earlier chapters then the relevant section numbers are supplied for reference.

2.1 Resistivity models for clay bearing rocks

As long ago as 1924, Fricke was interested in the electrical conductivity of suspensions with ellipsoidal inclusions [7]. Others such as Lord Rayleigh, Schofield and Archie have carried out research in this particular area. It is Archie's empirical law from 1942 that allows the interpretation of resistivity measurements on clean electrolyte-saturated sandstones both in the laboratory and in the wellbore [8]. The law states that

$$F = \Phi^{-m} = \frac{\sigma_w}{\sigma_m} \quad (1)$$

where σ_m is rock conductivity, σ_w is the pore fluid conductivity, F is the formation factor, m is the cementation factor, and Φ is the volume porosity. The term m represents the tortuosity of the pore space and is called the cementation factor. This name arises due to the fact that the internal geometry of sandstones can be modified by the natural carbonate or siliceous cements, which bind touching sand grains. Changes in the dispersed state or aspect ratio of sand grains or compacted clays will manifest themselves in the cementation factor m ; giving higher values for more dispersed systems [9].

Rock resistance can be easily measured at ambient temperature and pressure using the four terminal liquid electrode method [10] and this method will be used in experiments here and described in Section 3.4.2 Chapter 3.

When dealing with sandstones containing clays one must allow for the contribution of the cations on the clay surface. Waxman and Smits [6] first proposed that the clay fractions may contribute to the overall transport of charge. They considered sand grains in contact with each other and coated with layers of clay. The movement of ions, and the distribution of ions, on the clay surface was described in Chapter 2, Section 3.4 and 6.0. Waxman and Smits [6] proposed that the pore fluid conductivity is the sum of the effects of the clay counterions and of ions added externally to the pore fluid. On this basis it was proposed that the conductivity of a matrix is given by

$$\sigma_{\text{clay}} = (BQ_v + \sigma_w) \Phi_{\text{clay}}^m \quad (2)$$

where Φ_{clay} is equal to the normal sample porosity of a pure clay mixture and B is the specific conductance of the counterions. Q_v is the concentration of counterions per unit volume of effective pore space and is given by

$$Q_v = Cd_g \left(\frac{1 - \Phi_{\text{clay}}}{\Phi_{\text{clay}}} \right) \quad (3)$$

where C is the cation exchange capacity of the clay, i.e., the number of equivalents of exchange sites per unit mass of the dry clay, and d_g is the grain density of the dry clay.

A simple model will be used to determine the term in brackets in Equation 2; σ_w will be given by the measured conductivity of the slurry liquid, and BQ_v (the conductivity from the clay surface) will be estimated from the experimental data. Assuming some fraction A of the counter ions contribute to the conduction, BQ_v is given by:

$$BQ_v = A\Lambda Cd_g \left(\frac{1 - \Phi_{\text{clay}}}{\Phi_{\text{clay}}} \right) \quad (4)$$

where Λ is the molar conductivity of the counterions. Using this in Equation 2 gives

$$\sigma_{\text{clay}} = \left(A\Lambda Cd_g \left(\frac{1 - \Phi_{\text{clay}}}{\Phi_{\text{clay}}} \right) + \sigma_w \right) \Phi_{\text{clay}}^m \quad (5)$$

This model assumes that the clay layers form tactoids in the compact and that conduction takes place around the outside of the tactoid rather than through the interlayer regions.

Hence both surface and bulk conduction are assumed to have the same formation factor.

Others have used similar models to account for the conductivity of shaly sands [11], [12], [13] but no systematic study on sandy shales can be found. Recently there has been a resurgence in this research area mainly by Revil *et al.* [14], who have advanced on the model of Waxman and Smits and allowed for the difference in contribution of anions and cations to conduction in the pore space as the electrolyte concentration changes.

However the most extensive set of data on the conductivity of clay gels remains that of Cremers [15]. In that study the model of Waxman and Smits was applied to the conductivity data obtained at 1 kHz for a calcium exchanged montmorillonite slurried in

calcium chloride. The porosity of the clay gels was not reduced below 0.6 in Cremers study as the maximum compaction pressure used was 15 bar compared to an expected several 100 bar pressures for clays in the wellbore. The data set will be extended in this Chapter to determine the effect of higher pressures, salinity and clay type on the values of A and m .

2.2 Arrhenius rate law

The electrical resistance of a cylinder R_{res} of radius r and length l , assuming axial flow, is given by

$$R_{res} = \frac{\rho l}{\pi r^2} \quad (6)$$

where ρ is the resistivity of the material [10]. The electrical conductivity (σ) of the material is the inverse of ρ , and it is given by

$$\sigma = \frac{l}{\pi r^2 R_{res}} \quad (7)$$

The SI units of σ and ρ are $S\ m^{-1}$ and $\Omega\ m$ respectively.

Conduction in a rock or a clay slurry is through the pore fluid, and so conductivity should increase with temperature. The temperature dependence can be described by the Arrhenius rate law which states that the rate of a process is proportional to

$$\exp\left(\frac{-E_a}{RT}\right) \quad (8)$$

where E_a is the activation energy of the process ($J\ mol^{-1}$), R is the ideal gas constant ($J\ K^{-1}\ mol^{-1}$) and T is the absolute temperature (K). Equation 9 shows how the dependency of the conductivity on temperature can be determined from experimental data.

$$\sigma = \sigma_0 \exp\left(\frac{-E_a}{RT}\right) \quad (9)$$

where σ is the conductivity at temperature T , σ_0 is the pre-exponential factor and is almost independent of temperature. Plotting $R \ln \sigma$ as a function of T^{-1} gives a straight line if E_a is independent of temperature. Measurements of the activation energy for conduction in shaly sands have shown that the activation energy actually varies over wide temperature ranges; values were halved by increasing the temperature from 36 °C to 100 °C [12]. The Arrhenius rate law has been applied to slurries of clays in various electrolytes [9] to determine the activation energy for conduction. Cremers [15], along with Weiler and Chaussidon [16] found values of 19 kJ mol⁻¹ for the activation energy for surface conduction in calcium montmorillonites compared with 14 kJ mol⁻¹ in the bulk solution.

2.3 Clay phase porosity

Two models exist for the porosity of a clay-silt mixture, one for a shaly sand (Figure 3.1a) and the other a sandy shale (Figure 3.1b), [17]. In a shaly sand, the clay is dispersed between load-bearing silt particles which allows the porosity of the clay to vary. In a sandy shale, silt particles in the clay pore space replace both porosity and load-bearing clay and the stress is shared by both the clay and silt. It has been verified [17], albeit for a limited sample ranges that shales with greater than 40% by volume of clay in their solids fraction would represent a sandy shale.

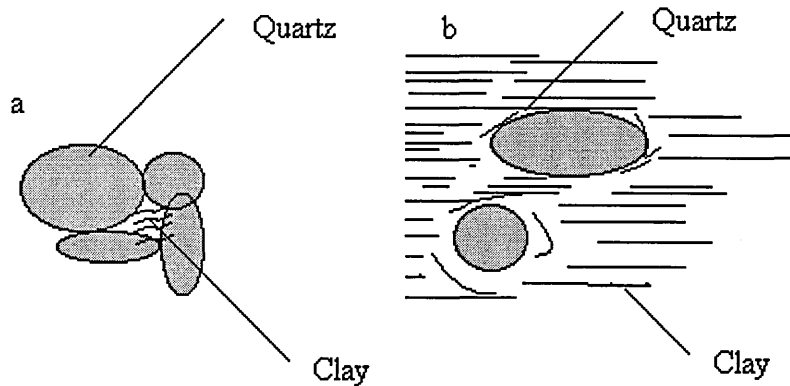


Figure 3.1: Schematic representations of (a) a shaly sand and (b) a sandy shale.

In this case of a sandy shale, the volume porosity of the clay phase is defined as

$$\Phi_{\text{clay}} = \frac{\Phi}{1 - V_s} \quad (10)$$

where Φ_{clay} is the volume porosity of the clay without quartz, Φ is the volume porosity of the shale and V_s is the volume fraction of silt in the saturated shale.

3. Experimental

In this section the materials used in the preparation of clay compacts will be described and the methods will also be outlined.

3.1 The clays and quartz

Due to the ease of contamination of clays the samples used in these studies were ordered specifically for the work outlined in this Chapter. Clay types were chosen for different experiments depending on their chemical nature in terms of cation exchange capacity and their likely abundance in shales found in wellbores. Illite was obtained from the Clay Minerals Society (Missouri) which has documented the origins and chemistry of the clays [18]. Natural greenbond, a pulverised Wyoming montmorillonite sold by Ashland Chemicals, was obtained from the Institute Français du Pétrole. Gelwhite, a white Texas montmorillonite, was obtained from English China Clays. Finally, Fullers Earth was obtained from Laporte Earths in Surrey.

All the clays were used as received in powdered form from the supplier except for Fullers Earth and Illite. These were ground from pieces several inches in diameter in a covered ball mill for 1 hour. The less than 125 μm solids were retained. Approximately 10 g of the clay was dispersed in each 100 ml of water and centrifuged at 9,000 rpm for 2 hours to remove the quartz fraction. The remaining gel was then collected and dried at 105 °C overnight after which it was reground to a fine powder using a pestle and mortar. The cation exchange capacity of each clay was determined following the method outlined in [19]. One gram of clay prepared as above was dispersed in 50 ml of 0.1 M tetramethyl ammonium bromide for 12 hours. The eluent was analysed for potassium, sodium, magnesium and calcium using atomic absorption spectroscopy. Results from this analysis are given in Table 3.1. All the data listed in Table 3.1 were for the naturally occurring samples, but for some studies it was necessary to change the cation on the clay surface. An example of two such experimental procedures is given below.

Natural greenbond, a mixed-ion clay, was exchanged to the calcium form (Ca greenbond) using calcium chloride. Forty grams of desilted clay was dispersed in 1000 ml of 1 M calcium chloride and stirred overnight. The suspension was placed in dialysis tubing and immersed in de-ionised water. The conductivity of the de-ionised water was

measured using a Howe conductivity meter. The water was changed daily until a conductivity of 2 S m^{-1} was obtained. This took approximately three days.

Clays	CEC	Na	Ca	K	Mg
	meq/100 g				
greenbond	83.7	54.8	20.7	2.6	5.7
Gelwhite	83.9	30.5	42.4	0.6	10.6
Fullers Earth	90.0	0.5	84.9	1.4	3.1
kaolinite	4.5				
illite	21.0

Table 3.1: The cation exchange capacity (CEC) and exchangeable quantity of each cation present in the clays used.

Fullers Earth was exchanged to the sodium form (Na Fullers Earth) as follows:

Approximately 50 g of the desilted clay was dispersed in 750 ml of de-ionised water for two hours. EDTA Na_2 (74.448 g) was added to 1000 ml of 1.2 M sodium hydroxide. The resulting EDTA $\text{Na}_{3.5}$ was added to the clay suspension which was stirred overnight. The clay was then purified as described above. Na Fullers Earth was exchanged to the calcium form (Ca Fullers Earth) using CaCl_2 as for greenbond. Silica flour, with a mean particle size of 10 microns, was purchased from Hepworth Minerals.

3.2 Preparation of Shale and Sandstone samples for resistivity measurements

Blocks of Clashach sandstone and Jurassic 2 shale were outcrop samples obtained by Schlumberger from an undisclosed location. Samples of these rocks were prepared for use in electrode evaluation experiments, in particular a comparison of the new platen electrodes *versus* the conventional liquid electrodes.

A sample of Clashach sandstone was cored with a diamond coring barrel (25.4 mm i.d) then the ends were ground flat and parallel on a diamond grinding wheel. The dimensions of the sample were such that the length to diameter ratio was at least 2. The core was dried at $105 \text{ }^\circ\text{C}$ for 12 hours and allowed to cool in a vacuum desiccator. Then the porosity of the Clashach sandstone core was measured using a Helium Expansion Pycnometer. The Clashach sandstone sample (Φ is 0.24) was vacuum-saturated with sodium brine ($0.69 \text{ } \Omega \text{ m}$).

Samples of Jurassic 2 shale were cored parallel and perpendicular to the bedding plane. Each end was ground flat to ± 10 micron on a diamond grinding wheel. A sample approximately 5 mm long was cut using a diamond saw and the end was reground and a thicker slice removed. This procedure was repeated until a sample set at approximately 5 mm length intervals had been obtained. The samples were then placed in a holder where the second end was ground flat and parallel on silicon carbide paper (Grit 1200 and 400). Final lengths were recorded to an accuracy of ± 0.1 mm using a vernier calipers. The samples were vacuum saturated with de-ionised water ($0.1 \text{ M}\Omega \text{ m}$).

In studies of surface conduction effects a shale core of different diameter was required. A Jurassic 2 shale sample was cored perpendicular to its bedding plane with a diamond coring barrel (150 mm internal diameter). One end of the core was ground flat ($\pm 10 \mu\text{m}$) with a diamond grinding wheel. The sample was trimmed to 43 mm and the other end ground flat and parallel on silicon carbide paper (1200 grit). The sample was vacuum saturated with de-ionised water to replace pore air. Measurements were made as outlined in Section 3.4.2 and subsequent cores taken from the original core until a 25.4 mm diameter core was obtained.

3.3 Compact preparation

3.3.1 Compaction apparatus

A schematic representation of a compaction cell is given in Figure 3.2. These cells were manufactured in house. Basically these cells consisted of a concentric cylinder of internal diameter 25.4 mm machined from steel. Modifications to the design of the basic cell were required to reduce the compaction time for montmorillonite slurries and prevent current flow through the cell body during electrical measurements. A ceramic liner was purchased from Fairey Industrial Ceramics and was glued into the cell using epoxy resin. Radial drainage from montmorillonite gels was then made possible through the porous liner to an outside line tapped in the cell wall. The ceramic liner was prone to fatigue and so the cell was replaced frequently. Kaolinite and illite slurries were compacted under radial drainage in the ceramic-cell for consistency as time did not permit a comprehensive comparison of the effect of radial drainage *versus* axial drainage on the compact microstructure.

The configuration of the top and bottom platens will be dealt with in Section 3.4.1 since these contained the resistivity sensors. The cells were positioned in rigid load frames and the top platens loaded using a hydraulic piston purchased from Enerpac which

was in turn powered by a Haskel pump. The change in sample length was detected by a potentiometer monitored by a data acquisition system consisting of a Dell 286 PC interfaced to a Microlink logger. The pore fluid lines in the ceramic lined cells were connected to reservoirs containing the slurring fluid to prevent the sample drying during compaction.

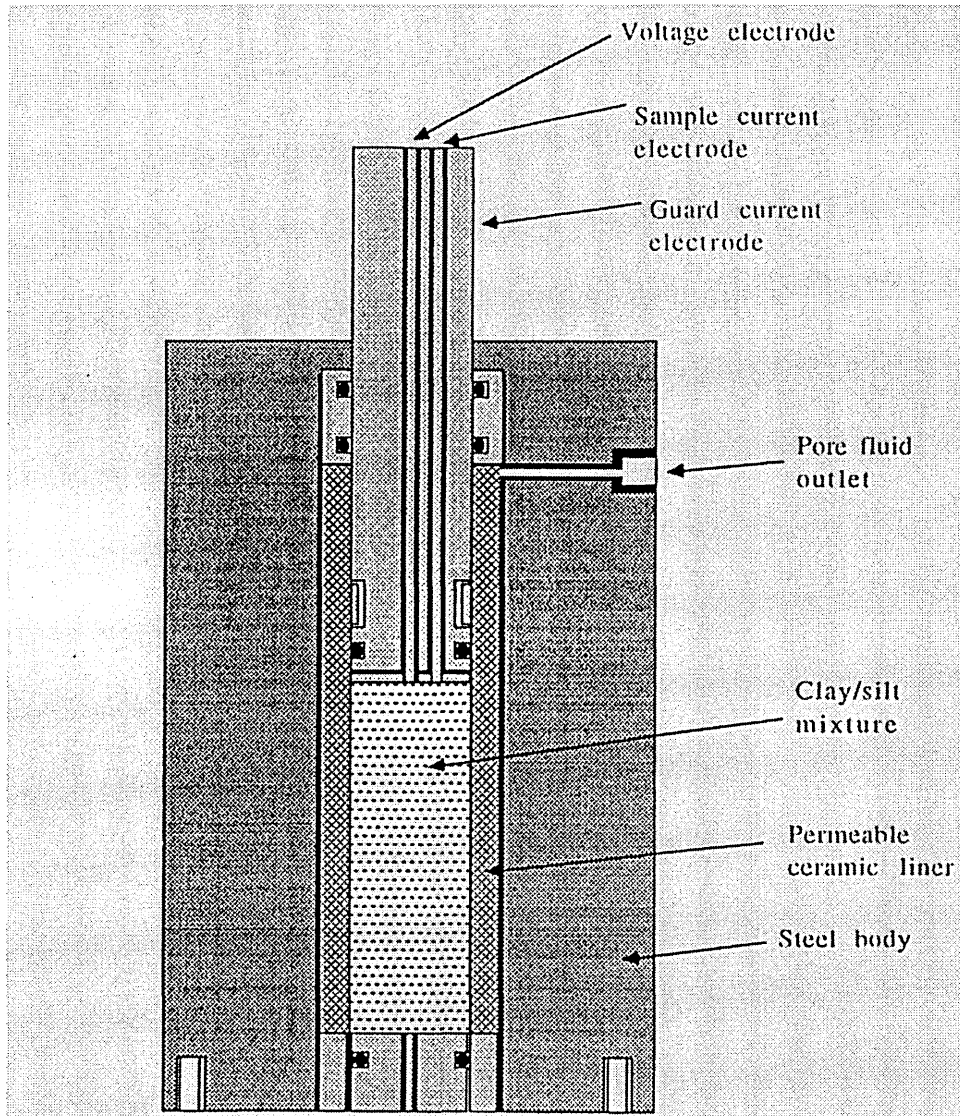


Figure 3.2: A schematic of a cell used in the compaction of smectite slurries by radial drainage. The cell height was 203 mm and the platen diameter was 25.4 mm.

3.3.2 Heating instrumentation

The compaction cells were wrapped in 1.5 m of 150 W m^{-1} heating tape leaving the pore lines and cell ends uncovered. Glass fibre tape with acrylic adhesive was used to mold the heating tape into a reusable shape. The temperature controller used was a Cal 9000

interfaced to a sheathed platinum resistance thermometer which was attached to the top of the pressure vessel using glass fibre tape.

A T type thermocouple was inserted into the current electrode of the top platen in the axial drainage cell and the bottom platen in the radial drainage cell (not shown in Figure 3.2) to detect the temperature of the cell contents. The potential from the thermocouple was amplified by Comark instrumentation and the analogue output connected to the Microlink data logger.

3.3.3 Slurry preparation and compaction procedures

Before preparing the mixed clay samples, illite and Gelwhite and other smectites were dried overnight at 200 °C to remove both free and bound water, while kaolinite was dried at this temperature for consistency. The clays were weighed while hot into dry lidded beakers and the powders were mixed by shaking the container vigorously for approximately one minute. The mass of illite added to kaolinite was varied, to determine the effect of the illite fraction on the porosity. Different masses of Gelwhite were added to a mixture containing equal amounts of kaolinite and illite, to investigate the effects of Gelwhite concentration.

The slurries for compaction were made sufficiently fluid to minimise air entrapment when the compaction cell was being charged. The volume of de-ionised water added to the clay mixture was varied for each clay combination, in order to prevent sedimentation and to provide a slurry sufficiently fluid for charging to the compaction cells. For example the weight ratio of water to solids for a kaolinite and illite mixture was approximately 1, and for a pure Gelwhite system approximately 0.3. The mixture was allowed to hydrate overnight and then stirred by hand until homogeneous.

Approximately 30 mls of slurry was poured into the cell. The top platen was inserted under a vacuum setup by the vacuum sleeve shown in Figure 3.3. This allowed for the air between the slurry and platen to be removed. The slurry was then loaded axially with a brass platen which sealed on the ceramic liner as it moved through the cell. The fluid from the slurry was pushed through the porous liner and collected in a pore line drilled through the cell wall. Each cell was loaded by an Enerpac hydraulic cylinder which was bolted to a load frame and pressurised by an air driven Haskel pump. The pressure was increased in steps of 50 bar to 400 bar, while the position of the top platen was monitored using a potentiometer interfaced to a data logger. After removal from the cell, the length of the compact (around 7 mm) was measured using Vernier calipers, and the change in length as a function of cell pressure was determined from the

logged data. At equilibrium compaction, the compact was pushed from the cell and fractured with a mallet to provide samples for porosity determination and homogeneity checks. Slurries of the pure clays were compacted at different pressures and their porosity was determined to check the accuracy of the pure clay compaction *versus* pressure graphs.

At equilibrium compaction, the Cal 9000 temperature controller was set to 30 °C and the cell resistivity monitored until a steady state was reached. The temperature was increased in steps of 20 °C to 70 °C, where the cell contents were allowed to cool to ambient temperature. The only limitation on the number of pressure and temperature steps up to 450 bar and 70 °C respectively was time. Above these limits the fatigue of the ceramic liner in this particular configuration was a concern.

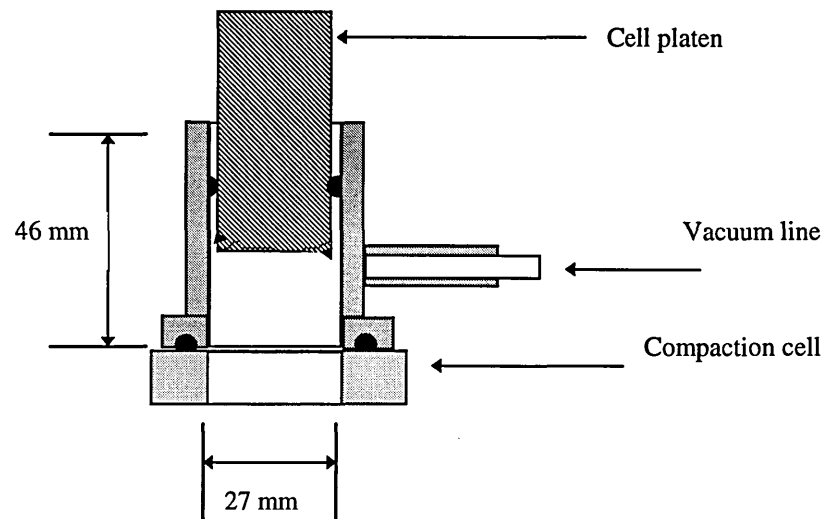


Figure 3.3: Adaptor to allow the compaction cells to be charged under partial vacuum.

3.3.4 Compaction and temperature equilibration times

Equilibrium compaction was taken to be reached when the stroke transducer changed by less than 0.03 mm in 5 minutes. For example a 35 mm compact of Fullers Earth and CaCl₂ was produced in 8 hours under radial drainage. The temperature of the cell contents reached a plateau value after heating for 30 minutes. The cell temperature was usually 3% less than that requested on the temperature controller. The conductivity of the clay slurry increased as the temperature increased, equilibrating at each temperature in less than five minutes.

3.4 The resistivity measurements

3.4.1 *The electrodes*

The basic design of the platens is of concentric current and voltage terminals, the former of much greater area than the latter, to minimise polarisation. Brass was chosen as the platen material because of its ease of machining, chemical resistance and mechanical properties. Epoxy resin (Ciba-Geigy Araldite) was used as the electrical insulator between the voltage and current terminals (Figure 3.2). The platen ends were machined flat to ± 10 microns in compliance with the core end specifications for compression testing. The rock sample was mounted between two such platens. To reduce polarisation of charged clay bearing shales and the electrolytic pore fluid, a constant amplitude alternating current (5 kHz) was applied to the shale sample via the current terminal. The current was also passed through a high stability carbon film resistor, to control current feedback. In an attempt to eliminate any contact potentials, the voltage measurements were made with a high input impedance circuit (100 M Ω). The voltage signals were passed through an AC to DC converter and the resultant digital signal monitored by a data acquisition system consisting of a Dell 286 interfaced to a Microlink logger. In the radial drainage cell, the fluid-saturated ceramic liner had a lower electrical resistance than the compact. There was some concern that the applied current would flow down the liner and not through the clay slurry. To prevent this current leakage happening, the voltage measured across the sample was applied to guard electrodes, one on the top platen and the other, a brass ring on the bottom of the ceramic liner. The ambient temperature in the laboratory was 18 ± 2 °C and no attempts were made to log the temperature with the conductivity.

3.4.2 *Electrode evaluation*

The results obtained with the new electrodes were compared with values measured using the liquid electrode setup referred to in Section 2.1. The Clashach sample was reheated to 105 °C and pushed into 150 mm of shrink-fit plastic (RS) (25.4 mm i.d). The shrink-fit was cut to the required length and the voltage terminal added. The system was vacuum saturated in brine with a resistivity of 0.82 Ω m. The platens (current electrodes) were placed in the shrink fit under the liquid level as shown in Figure 3.4. Checks were made for air bubbles and fluid leakage between the shrink fit and the sample surface. The resistance was measured, the core resaturated and the measurement repeated using the

brass electrodes. The formation and cementation factors for the core were determined using Archie's law. The resistance and length of each sample were measured.

A four terminal (5 kHz) resistance measurement was made 5 seconds after removal from the desiccator, using the silver foil electrodes. Successive cores of decreasing diameter were taken from the initial core, saturated and the measurement repeated.

The thermocouple was removed from the current electrodes in the top and bottom platens to investigate its affect on the measured resistance, and hence the activation energy. The resistance measured was slightly lower without the thermocouple; however, this had a negligible affect on the activation energy.

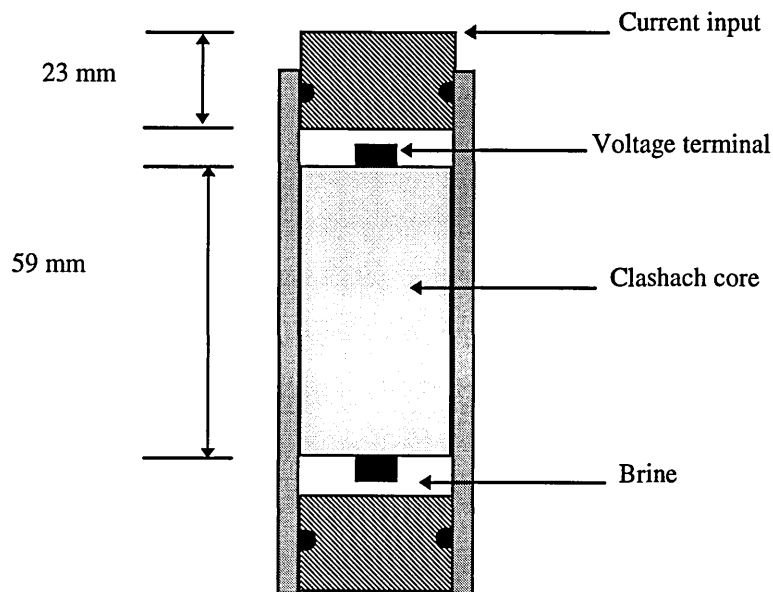


Figure 3.4: A schematic representation of the setup for a liquid electrode measurement.

3.4.3 Experiments with pure electrolytes

The conductivity of 0.1 M NaCl, 0.05 M CaCl₂ or 0.5 M CaCl₂ measured in the compaction cells was much higher than that specified in the literature, so the conductivity of the salt solutions was determined in a beaker using graphite ring electrodes connected to a Wayne Kerr Number 6425 component analyser. The solution could be heated using a hot plate. It was important to de-gas the de-ionised water before making the electrolyte solution, thus preventing air bubbles contacting the electrode. This bench method was also used to determine the activation energy of high porosity Fullers Earth and kaolinite slurries.

3.5 Compact porosity and micro-structural determination

3.5.1 Scanning electron microscopy (SEM)

To remove excess incident electrons from the surface of non-conducting SEM samples, it is normal to sputter-coat them with a conductive gold film. However, the clay compacts used here were imaged without a coating to minimise the sample manipulation. The compacts were fractured and glued to an aluminium sample holder using quick-set epoxy resin which was allowed to set before inserting the sample into the SEM. The acceleration voltage applied to the electron beam incident on the sample was increased from 5 kV in steps of 2 kV to 25 kV and the charging of the sample at each acceleration voltage was monitored to prevent sample damage while aiming for maximum resolution. Each sample was photographed at the same magnification using Polapan type 52 Polaroid film.

3.5.2 Porosity determination

The compacts were pushed from the cell using the load frame assembly. The compact length was measured and the mass fraction of pores (see Equation 11) was determined by drying the compact at 105 °C for 24 hours. The grain density of the dry clays were determined in a Helium expansion pycnometer. Three segments of the fractured compact were weighted to 4 decimal places on a Sartorius balance, and placed in a furnace at 200 °C overnight. The samples used varied in weight from 0.5 to 1.5 g, as outside this range some variation in the percentage mass loss was observed. The adequacy of a 12 hr drying time was verified by checking the weight loss of a compact for a drying period up to 24 hr. The samples were weighed while still hot and the weight porosity calculated from

$$W_{\phi} = \frac{W_w - W_d}{W_w} \quad (11)$$

where W_{ϕ} is the weight of water per gram of prepared compact, W_w is the wet weight of a compact segment, and W_d is the weight after drying at 200 °C. The weight porosity was converted to the volume porosity by dividing the weight of each clay type by its grain density (d_g).

Clay	d_g (g cm ⁻³)
Kaolinite	2.65
Illite	2.80
Fullers Earth	2.23 *
Gelwhite	2.70

Table 3.2: The grain densities used to convert weight porosity to volume porosity. These values exclude bound water for the illite and Gelwhite clay but include the bound water for Fullers Earth.

The change in the sample volume of a pure clay as a function of applied compaction pressure was converted to the corresponding change in porosity as follows:

$$\Phi_t = \frac{V_t - V_c - V_s}{V_t} \quad (12)$$

where Φ_t is the porosity at time t, V_t is the volume of the sample at time t, and V_c and V_s are the volume of clay and quartz respectively in the cell.

4. Results and Discussions

4.1 Compaction behaviour of clays

In this section results concerning the

- contribution of clay chemistry to compaction
 - effect of added electrolyte on the compaction profile and
 - porosity of mixed clay compacts,
- will be presented.

4.1.1 Contribution of clay chemistry to compaction profiles

From theory one would expect that the porosity of clays compacted under typical down hole pressures would depend on the charged nature of the clays. However data presented here will show that other factors such as initial particle size and dispersion history become important. During the compaction process the top platen was pushed into the compaction cell and the volume of the clay gel decreased and water drained away. A typical profile of top platen position *versus* time for a kaolinite-water gel at a constant pressure of 39 bar is presented in Figure 3.5. For consistency, equilibrium compaction was said to be reached when the stroke transducer changed by less than 0.03 mm in 5 minutes.

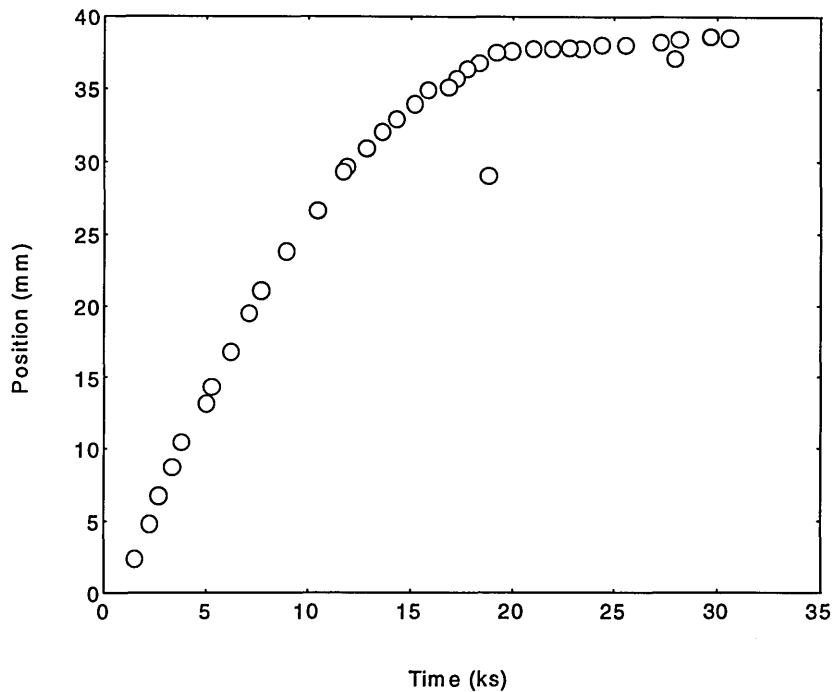


Figure 3.5: A compaction profile for kaolinite slurred in deionised water and compacted at 39 bar.

At pressures of 39 bar and greater for colloidal materials such as clays which are slightly compressible, the volume flow from the compacting slurry as a function of time is almost independent of the applied pressure [20]. According to Meeten and Sherwood's analysis [20], a pressure change from 500 to 600 bar would cause only a 0.044 % change in the volume of water extruded per unit time. Knowing the internal dimensions of the cell, the movement of the top platen was used to calculate the slurry volume V_t and then Equation 12 was used to calculate the change in compact porosity with compaction time. Porosity *versus* cell pressure data are presented in Figure 3.6 for Fullers Earth, Ca greenbond, Gelwhite, kaolinite and illite clays which had been slurred in deionised water.

The porosity of the Gelwhite-water slurry for a given compaction pressure was greater than that of Ca greenbond, kaolinite, Fullers Earth and illite. Gelwhite has the highest fraction of sodium present as an exchange ion than any of these clays and hence the clay is more likely to swell and form a gel than a calcium saturated clay such as Ca greenbond. It therefore requires a higher applied pressure to reduce the porosity of the compacting slurry. However it is also noted that the porosity of illite was less than that of kaolinite, in contrast to their relative layer charges. This is not what Chillingar and Knight [21] have found. Compaction profiles for clays slurred in water have been extracted from their paper and are presented in Figure 3.7.

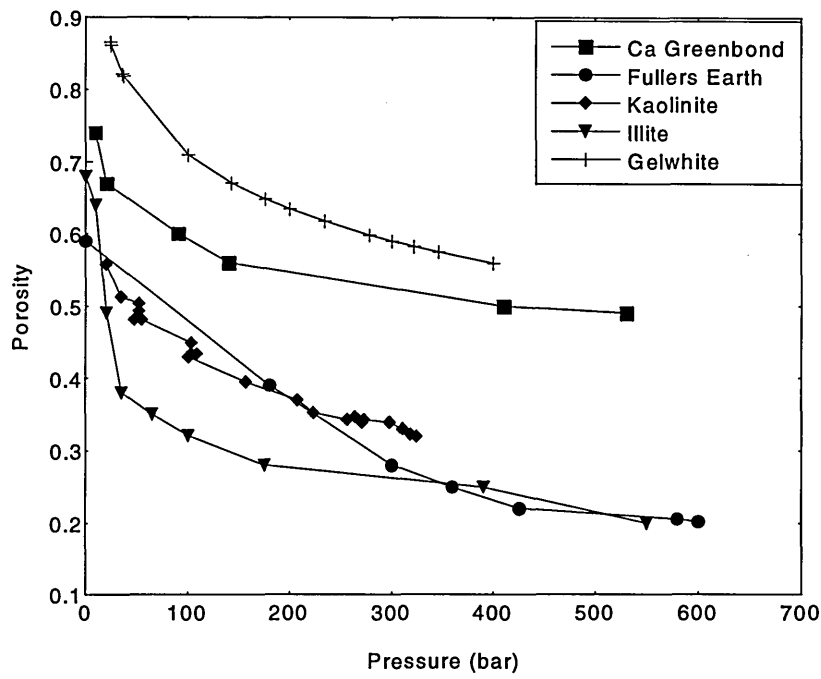


Figure 3.6: Volume porosity versus cell pressure for different clays slurried in deionised water.

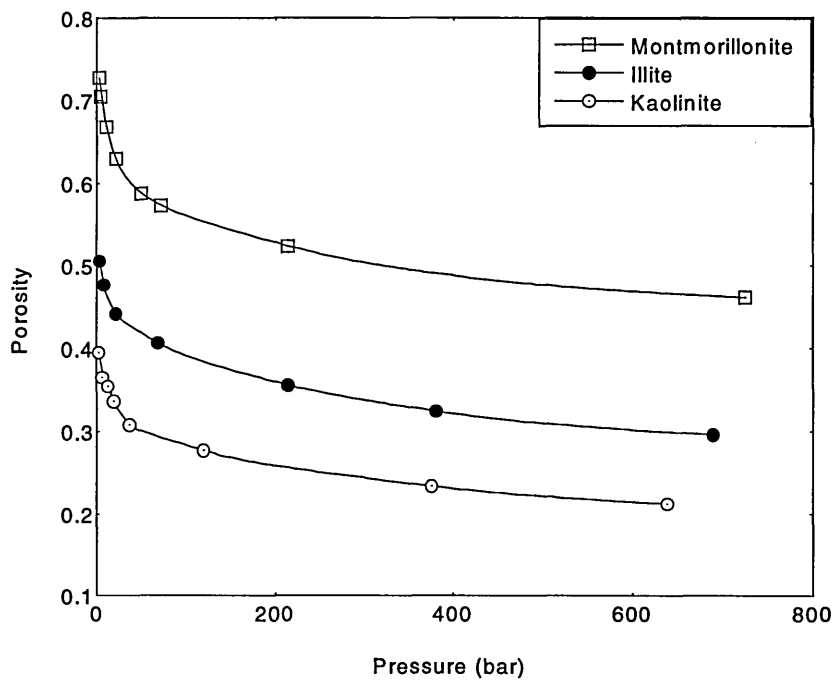


Figure 3.7: Volume porosity *versus* pressure data taken from Chillingar and Knight [21].

In the data set from Chillingar and Knight the volume porosity at any given compaction pressure goes in the order montmorillonite>illite>kaolinite. Very little information was given regarding the initial particle size of the clay and such a direct comparison of these types of clays could not be found elsewhere.

However research by Volzone and Hipedinger, [22] has shown that the particle size of the clay has a direct effect on the porosity of the final compact. Their data set was by no means complete in that montmorillonites (Arizona (SAz-1) and Wyoming (SWy-1)), with different particle size ranges were indeed compared, but, they often had different CEC values as well. However for two kaolinite samples with similar CEC values the one containing a higher fraction of particles 78 wt% < 2 μm as compared with 22 wt% < 2 μm had a higher porosity at 150 bar of 45.6 and 39.7 respectively. However Volzone and Hipedinger claimed (albeit again from a limited data set) that when comparing a kaolinite and a montmorillonite clay with similar particle size distributions the trends in mean pore radius *versus* CEC gave a straight line plot. The mean pore radius of another montmorillonite with a different CEC and particle size distribution fell on this straight line plot also. From this Volzone and Hipedinger concluded that relative CEC values gave the best correlation with the clay compact pore radius and cumulative pore volume.

However the SAz-1 and SWy-1 (Figure 3.8 and 3.9) montmorillonites give compacts that are reasonably layered and ordered with respect to the bedding plane.

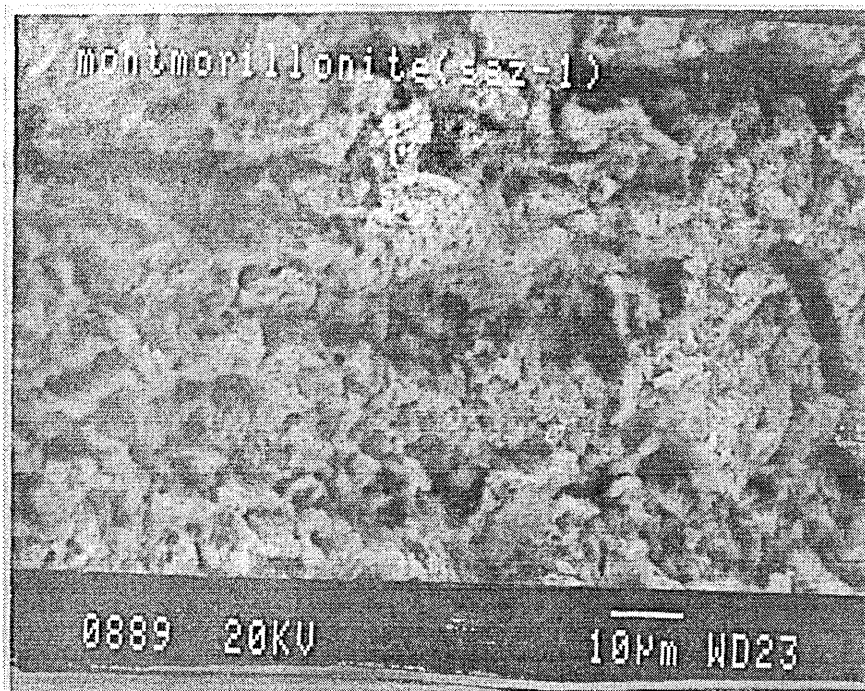


Figure 3.8: A micrograph of Ca montmorillonite (SAz-1)-water slurry compacted at 20 bar.

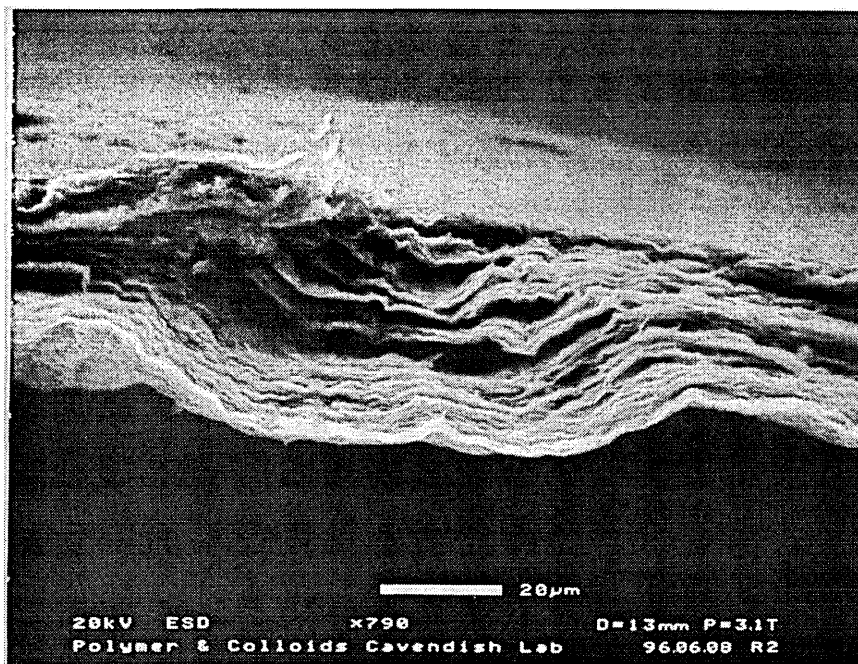


Figure 3.9: A micrograph of Na/Ca montmorillonite (SWy-1)-water slurry compacted at 2 bar.

Trying to explain the differences in the compaction profiles of Fullers Earth and Ca greenbond, i.e. why the porosity of Fullers Earth compacts are very much lower than those of Ca greenbond even though their CEC values and exchange chemistries are very similar is quite complicated. This complication arises because the microstructures of the compacts are different. For Ca greenbond the structure is nicely layered as expected while for Fullers Earth there are domains of clay that show no ordering with respect to the compaction direction. Micrographs of these compacts are presented in Figure 3.10 and 3.11.

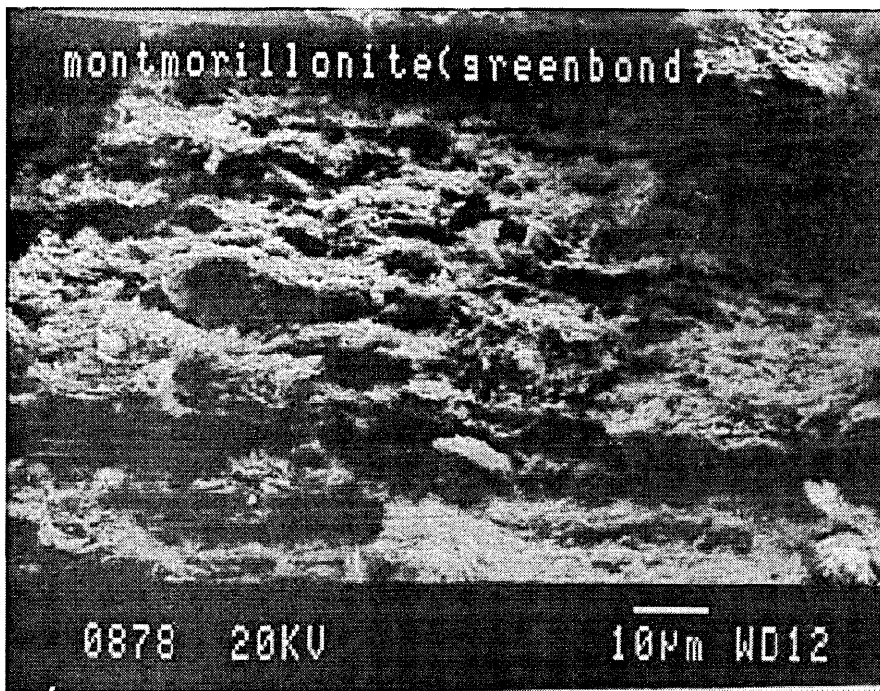


Figure 3.10: A micrograph of a Ca greenbond-deionised water compact formed under 20 bar.

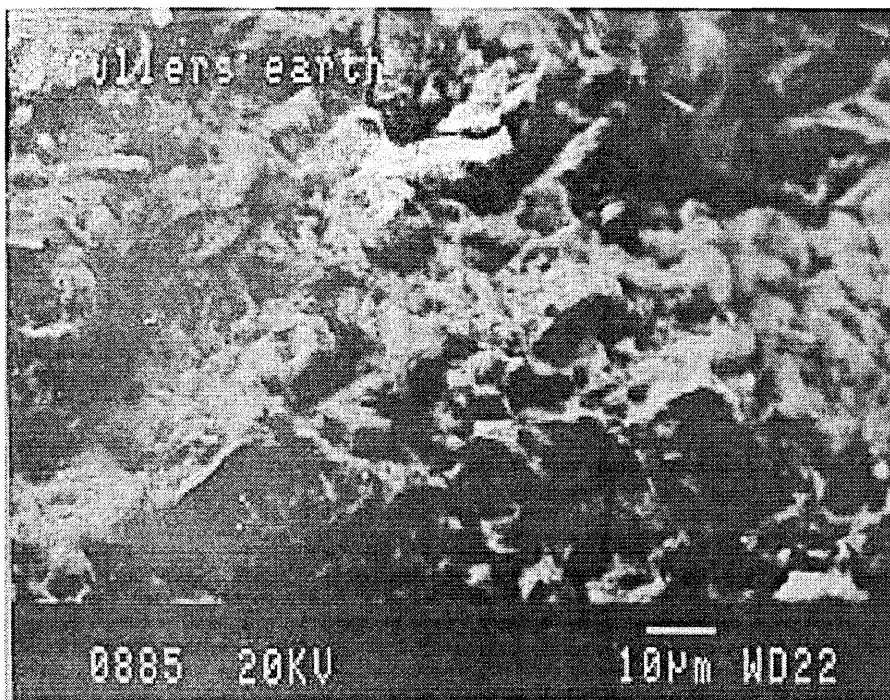


Figure 3.11: A micrograph of a Fullers Earth-deionised water compact formed under 20 bar.

Studies have been carried out on the microstructure of freshly quarried Fullers Earth which was subsequently freeze dried and imaged [23]. The micrographs received are similar to those shown in Figure 3.11 . The explanation given for the domain like microstructure is that the Fullers Earth is formed from volcanic ash and glassy type shards

remain in the Fullers Earth some of which alter to smectite clay over time. These shards contain a coverage of smectite flakes and have dimensions distributed between $290 \times 125 \mu\text{m}$ to $100 \times 20 \mu\text{m}$. These researchers found that Fullers Earth dispersed in a 0.1 M sodium hexametaphosphate solution dispersed only to a fine sand grading with no evidence of dispersed clay. In the work detailed in this thesis, the air dried-Fullers Earth was ground up in a ball mill and the fraction taken was less than $125 \mu\text{m}$. This solid was then slurried in deionised water which on the evidence of Robertson *et al.* [23] may not disperse the particles to $< 0.002 \text{ mm}$. If the domains are considered to act as single particles then one might expect from, the work of Volzone and Hipedinger [22], that the porosity would be lower than that of Ca greenbond.

A conventional treatment of the compaction curves was first used by Terzaghi and Peck, [24]. They showed that plotting the volume percent porosity as a function of the logarithm of the compaction pressure gives a straight line. The line can be described by an equation of the form

$$\Phi = a \ln(P/P_0) + b \quad (13)$$

where a and b are the slope and intercept of the plot respectively and P_0 is the reference pressure of 1 bar (0.1 MPa). This formula was applied here to the data for kaolinite as shown in Figure 3.12. It was used to generate an idealised compaction curve for kaolinite, which is presented in Figure 3.13 together with experimental porosity results for individual compacts formed under different pressures. The same curve fitting technique was used for the illite, Gelwhite and greenbond clays and the idealised curves compared with individual compaction experiments as for kaolinite. In all cases the agreement was reasonable with a maximum variation of $\pm 5\%$. However the Fullers Earth compaction curves could not be fitted using the logarithm type curve. The compaction curve fitting technique which generates a and b values is not based on any mechanical or chemical theory; but is purely an empirical fit.

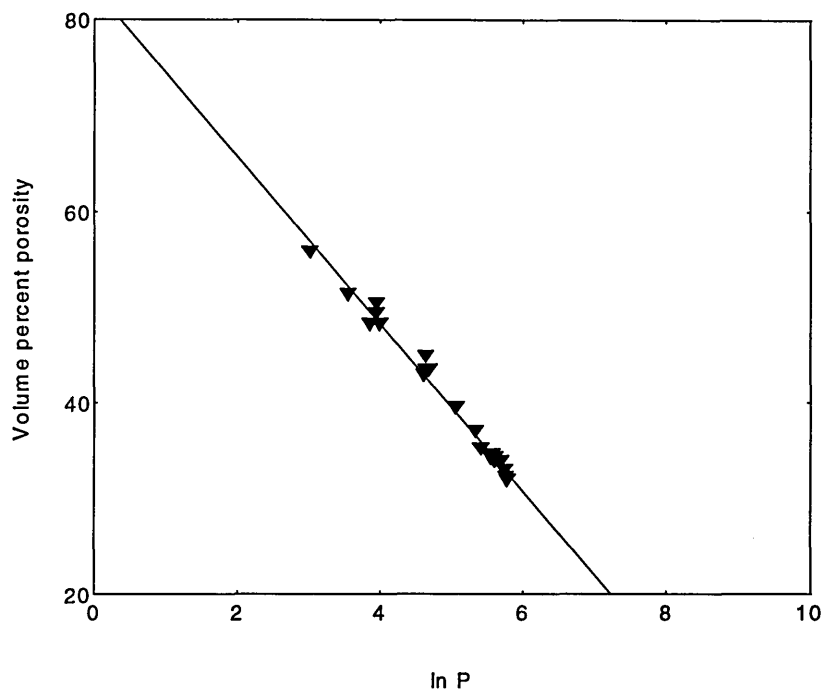


Figure 3.12: Volume percent porosity versus the \log_{10} of cell pressure for kaolinite-water slurries.

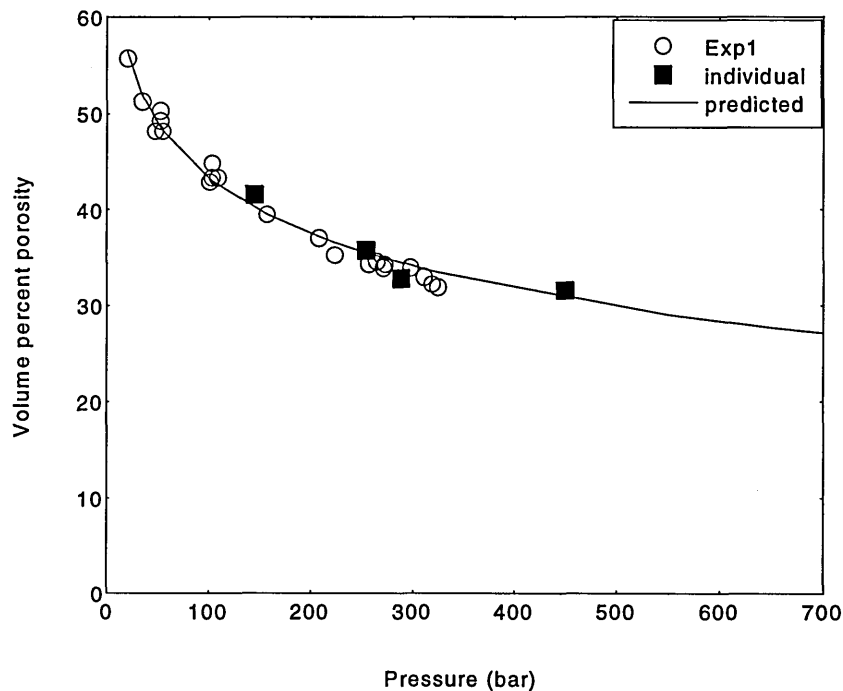


Figure 3.13: Plot showing the predicted, measured and independent checks on the porosity of kaolinite-water slurries.

The data in Table 3.3 could be used to predict the porosity of these clays under wellbore pressures.

In summary, the initial particle size of the clay coupled with the CEC affects the shape of the compaction curve. In the next section the change in compaction profile with added electrolyte will be examined.

Clay	<i>a</i>	<i>b</i>
Gelwhite	-10.9	121.2
Kaolinite	-8.3	81.4
Ca greenbond	-6.10	86.8
Illite	-5.9	63.5

Table 3.3: The *a* and *b* coefficients used in Equation 13 to determine the volume porosity as a function of pressure for listed clays.

4.1.2 Effect of added electrolyte on the compaction profiles

In this study the slurrying fluid used contained mainly the cation on the clay surface thus eliminating the complication of a time dependent ion exchange. The slurrying fluid was either deionised water or 0.5 M salt solution; in some cases 0.05 M salt solution was used.

Compaction profiles presented in Figures 3.14 to 3.16 show that the molarity of the slurrying fluid had little effect on the porosity *versus* pressure curve. Initial values at zero applied pressure are dependent on the weight of clay added to the slurrying fluid.

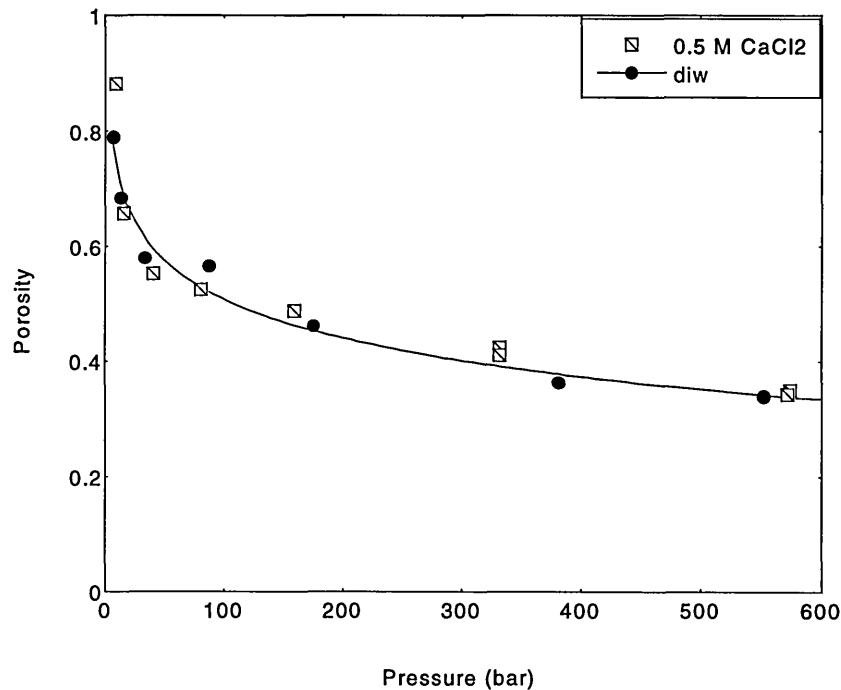


Figure 3.14: Volume porosity versus cell pressure for Ca greenbond compacted in de-ionised (diw) water and 0.5M calcium chloride

Clays slurried in water will be more dispersed than clays slurried in salt solution where the electrolyte shields the negative clay surfaces from each other allowing the clay

platelets to collapse together. However it is possible to prevent the swelling of the clays dispersed in water by applying an external pressure. Indeed that is what is being done here. Unfortunately the insensitivity of the pressure transducer does not allow the porosity of the clay to be examined at pressures intervals below 20 bar.

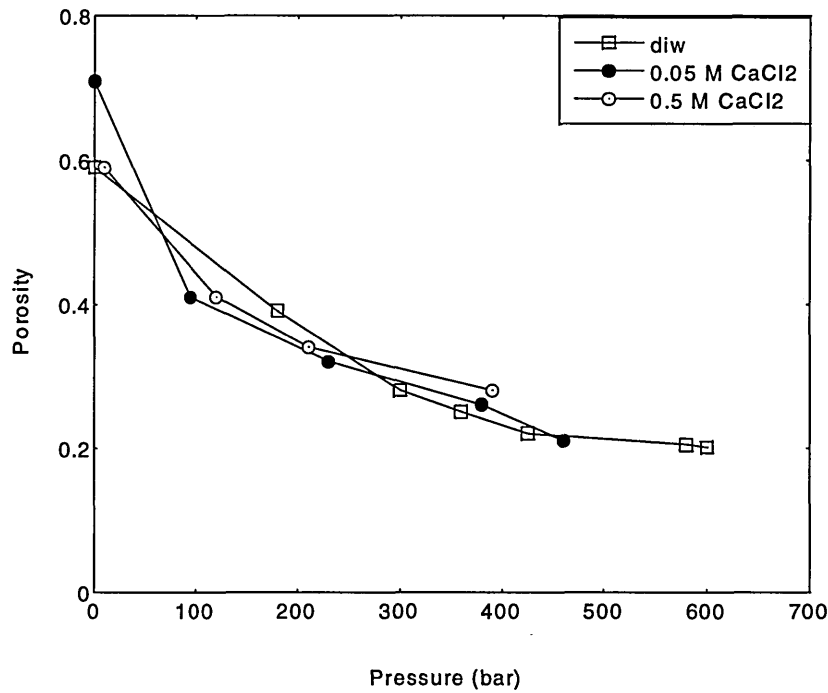


Figure 3.15: Volume porosity of Fullers Earth slurred in deionised water or calcium chloride.

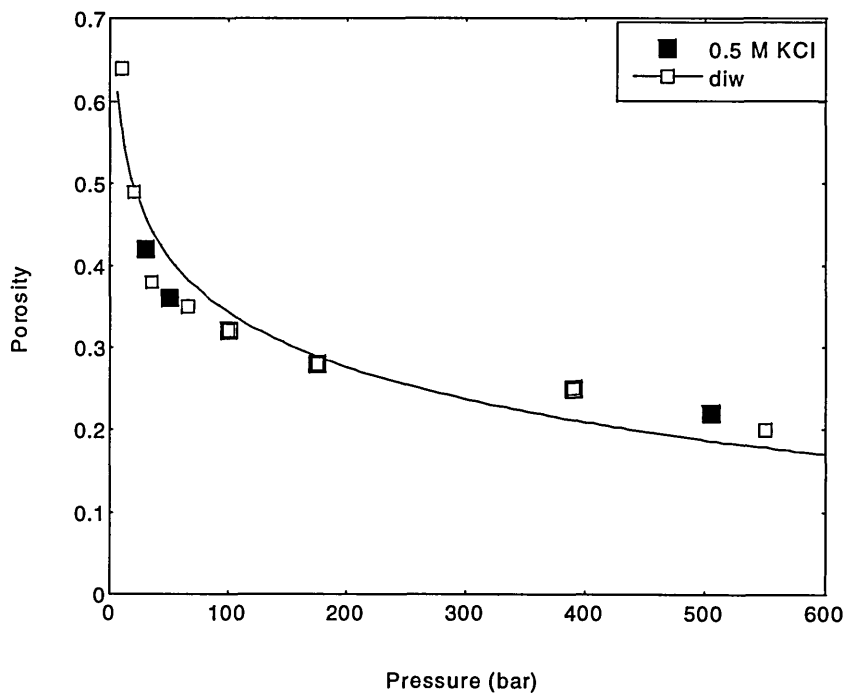


Figure 3.16: Volume porosity of illite slurred in deionised water or potassium chloride.

Even at pressures as low as 25 bar there are no apparent differences in the porosity of the compacts. Another way of examining this data is to determine if the swelling pressure of calcium montmorillonite in water due to repulsive interactions is less than the compaction pressure. A similar analysis has been carried out by Barclay and Ottewill [25] for the compression of sodium montmorillonite. In their work they measured the pressure developed in a montmorillonite dispersion as the clay plates were forced together. The experimental results were compared with pressure *versus* separation generated using DLVO theory (see Chapter 2 Section 3.3) for clay slurried in 10^{-4} and 10^{-1} M sodium chloride. After an initial compaction cycle the subsequent compaction and relaxation curves showed that at pressures of 10 bar or greater there was no discernible difference between the separation of the montmorillonite plates.

4.1.3 The porosity of mixed-clay compacts

A shale may contain a mixture of clays and it is not apparent how the overall porosity of the clay phase depends on the wt% of each clay type present.

The dependence of the porosity of kaolinite-water slurries compacted at 250 bar on the mass fraction of illite added is presented in Figure 3.17. The percentage volume porosity of the pure kaolinite compact was 36%, and as the fraction of illite was increased the porosity decreased linearly to 28% for pure illite. The line fit used in Figure 3.17 is best described by

$$\Phi_c = V_k \Phi_k + V_i \Phi_i \quad (13)$$

where Φ_c is the percentage porosity of the compact, V_k is the volume fraction of clay that is kaolinite, V_i is the volume fraction of illite, Φ_k the percentage porosity of pure kaolinite and Φ_i the porosity of pure illite.

The mass fraction of Gelwhite added to an equal mixture of illite and kaolinite was varied and the resulting change in porosity with Gelwhite mass fraction is presented in Figure 3.18. Increasing the fraction of Gelwhite, increased the porosity of the compact with a value of 53% for pure Gelwhite. The porosity of the compacts was predicted using an extended version of Equation 13,

$$\Phi_c = V_k \Phi_k + V_i \Phi_i + V_g \Phi_g \quad (14)$$

where Φ_g is the volume percent porosity of pure Gelwhite, and V_g is the volume fraction of Gelwhite in the compact. Equation 14 is used to generate the solid line in Figure 3.18.

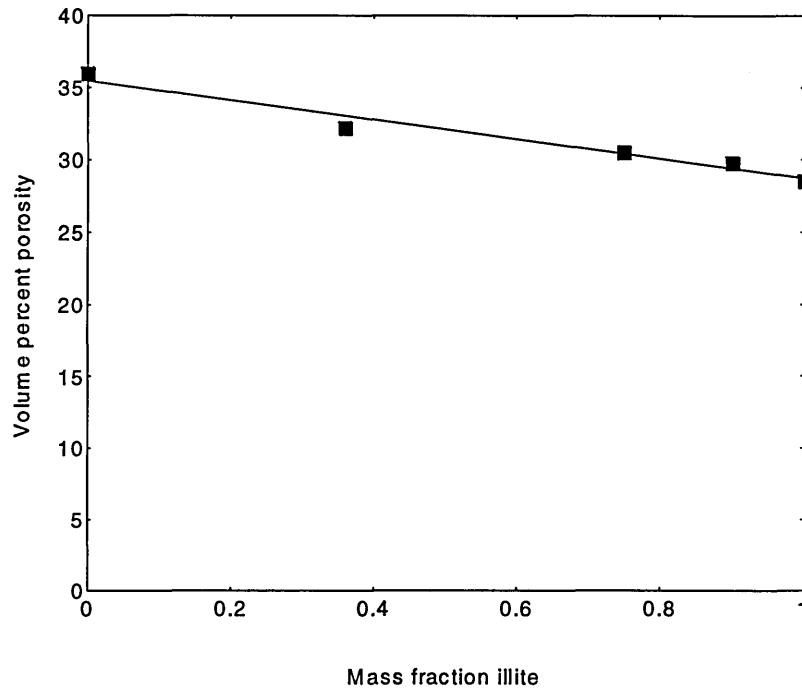


Figure 3.17: Porosity of water based slurries containing different mass fractions of illite and kaolinite and compacted at 250 bar.

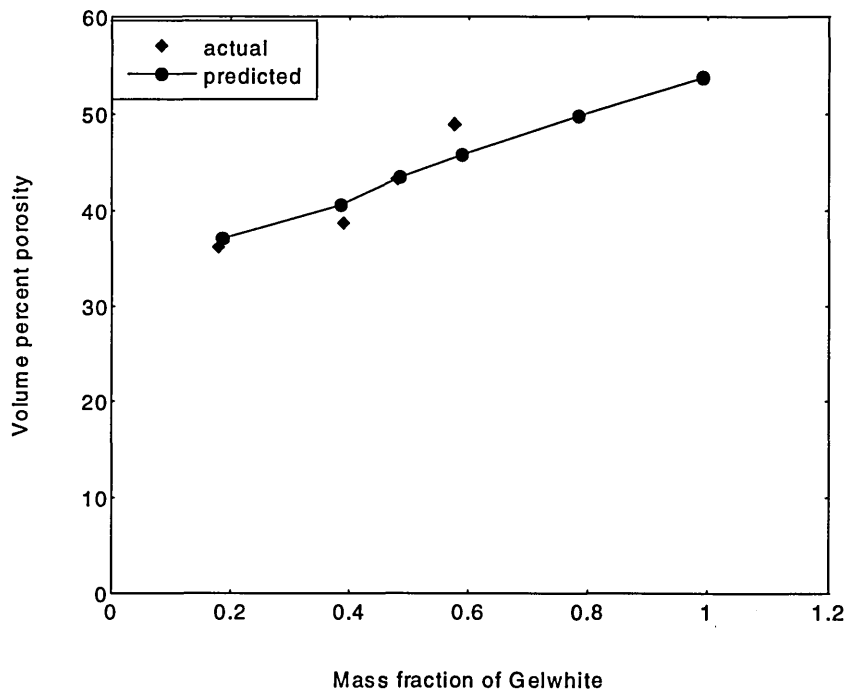


Figure 3.18: Porosity of water based slurries containing equal mass fraction of illite and kaolinite with varying amounts of Gelwhite and compacted at 250 bar.

The linear mixing law states that the volume porosity of a clay mixture compacted by radial drainage under 250 bar can be predicted from a combination of the volume fractions and porosities of the various components. This implies that the clays retain their respective pore space, which would happen if the clays were not properly mixed. To check this, a cross section of a compact containing illite, kaolinite and Gelwhite, was imaged by scanning electron microscopy (SEM) (Figure 3.19) and analysed semi-quantitatively using an energy dispersive X-ray analyser [26]. Several $10\ \mu\text{m}^2$ surface sections were analysed at different positions along the sample. Elements such as silicon, aluminium, potassium and calcium could be detected using the EDX [27]. The feature that distinguished kaolinite was the equal peak intensity from the silicon and aluminium representing the 1:1 layer of silica and alumina. For illite and Gelwhite the intensity was much higher for the silicon indicating a 2:1 layer. Illite could be distinguished from Gelwhite due to the detection of potassium in the former and calcium in the latter.

Illite, kaolinite and Gelwhite were found to be present, although the exact ratios could not be determined from the spectrum due to electron probe artifacts. This implies that the clays were mixed, but at high magnification the individual clay platelets could not be distinguished.

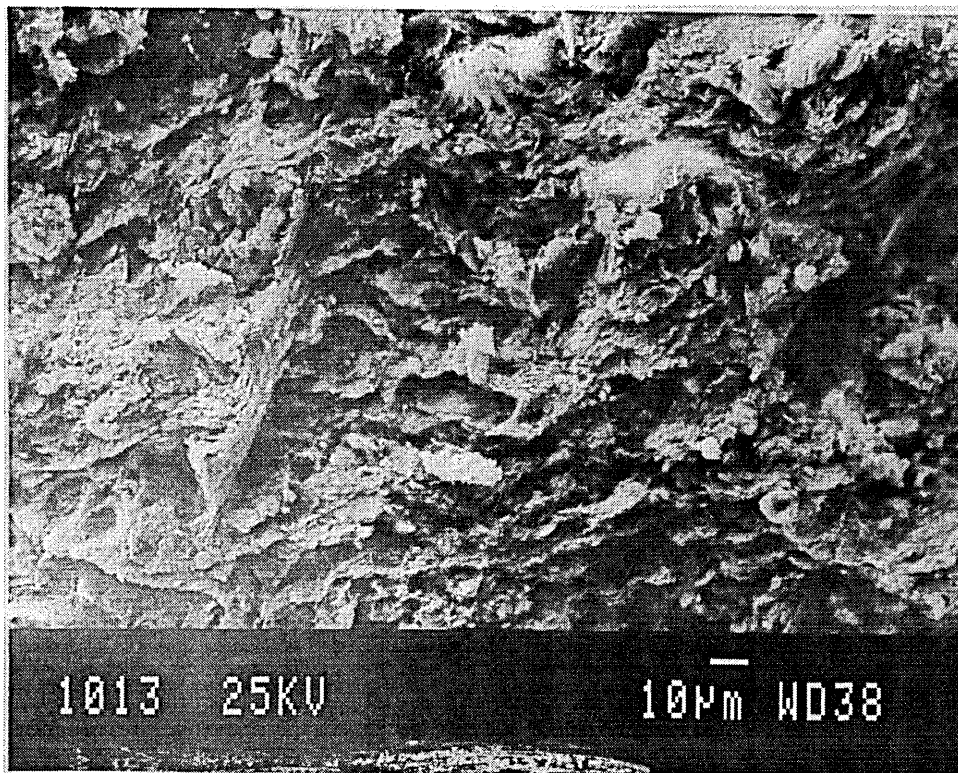


Figure 3.19: A section of a mixed clay compact containing 58% Gelwhite, 25% illite and 16% kaolinite compacted under 250 bar axial load.

SEM images of a compact containing an equal mixture of Gelwhite and kaolinite showed a layered structure (Figure 3.21) similar to pure Gelwhite, but different from the random structure of pure kaolinite (Figure 3.22). This suggests that kaolinite clay platelets slot into the pore space of the Gelwhite, however, this would lead to a porosity defined by:

$$\Phi_c = \Phi_g(1 - V_k) \quad (15)$$

where Φ_c is the clay compact porosity, Φ_g is the porosity of pure Gelwhite, and V_k is the volume fraction of kaolinite in the clay mixture. The porosity of the kaolinite and Gelwhite compact is not calculated by the above formula, but by Equation 14 which suggests that each clay retains its associated pore space when mixed with other clays. This could still allow a structuring shown in Figure 3.20 where the numbers of clay layers of kaolinite stack to a few mm. However the microstructure shown in Figure 3.20 was not evident under the electron microscope where a resolution of a micron could be achieved.

In shale systems it is possible to find mixed layered clays where the different mineral structures are mixed on an angstrom scale; in those situations it would be expected that Equation 15 would apply since the swelling clay (in this case Gelwhite) would dictate the maximum porosity value. Unfortunately no systematic study on shale samples could be found to show what the porosity was in situations where the clays remain as individual packets. But there is evidence to show the clays such as montmorillonite and kaolinite can exist in different mineralogical bands which lie only mm apart. Therefore one can suggest that the mixing method used is sufficient to represent some shale types.

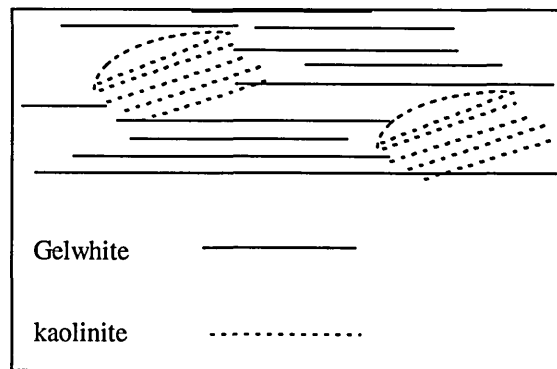


Figure 3.20: Kaolinite stacks in the pore space of Gelwhite

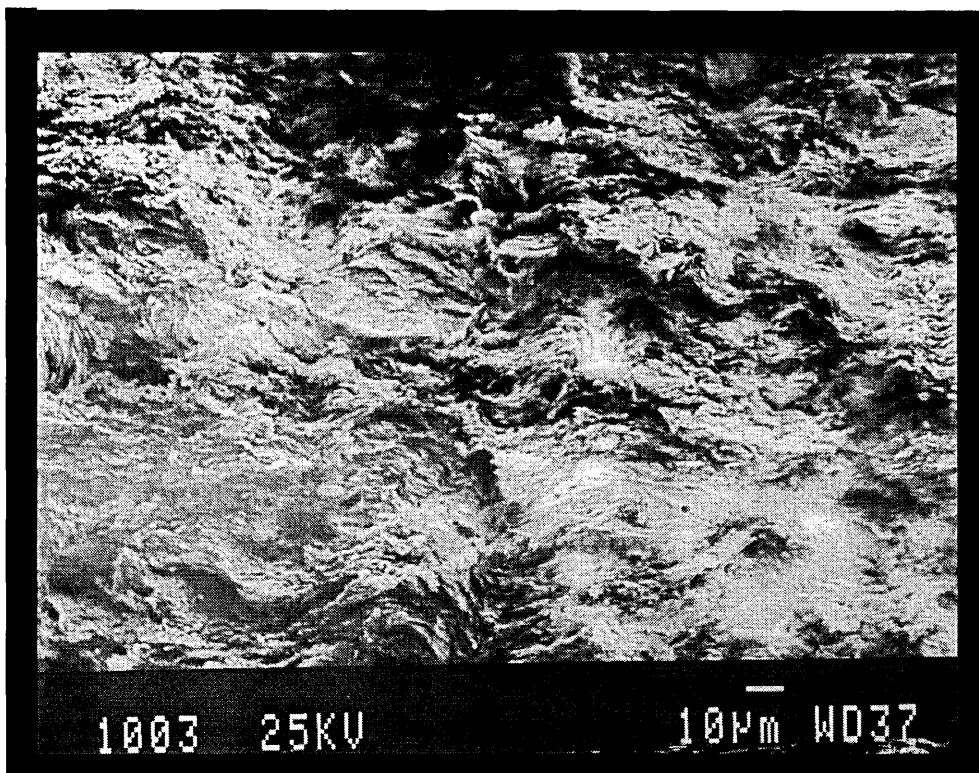


Figure 3.21: This micrograph shows the microstructure of a compact containing equal amounts of kaolinite and Gelwhite, compacted at 250 bar.

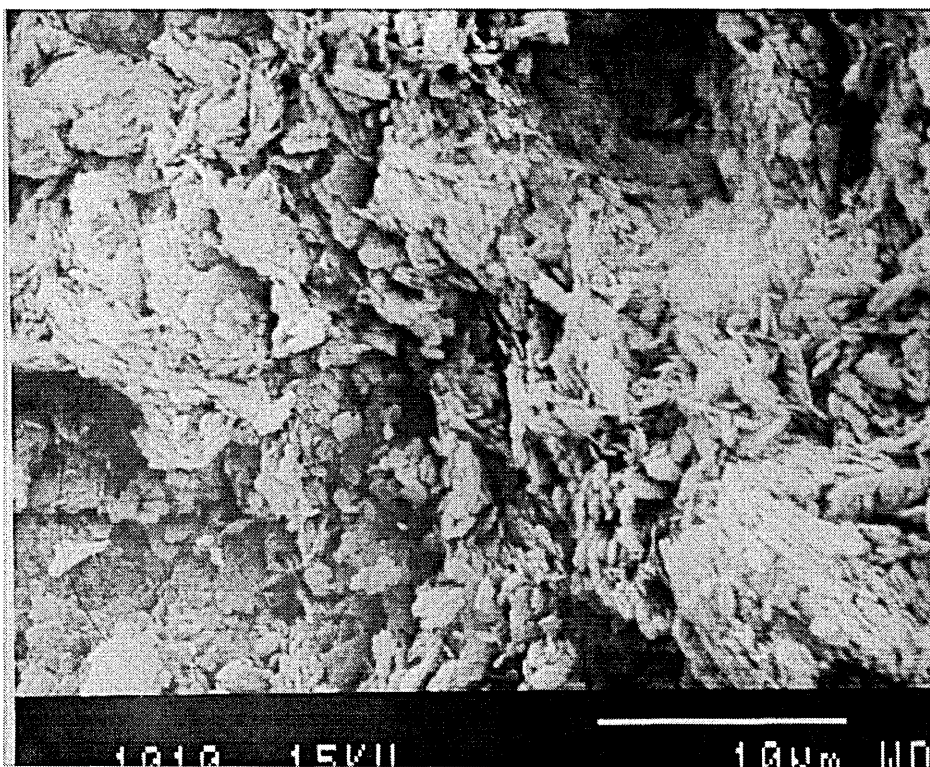


Figure 3.22: Kaolinite slurred in water and compacted under 250 bar pressure.

4.1.4 The porosity of compacts with quartz added

A comprehensive study of the compaction properties of synthetic shales requires the addition of granular materials in the form of quartz. Previous studies by Marion *et al.*, [17] have demonstrated the change in load bearing mechanism as the concentration of Kaolin (with a particle size range of 1 to 4 μm) is increased. However in their study the range of quartz particle sizes used was limited to that of an Ottawa sand composed of well rounded quartz grains of $280 \pm 60 \mu\text{m}$. This is larger than the quartz particles commonly found in shale. Thus the effect of particle size and shape on the transition from a shaly sand (quartz load bearing) to a sandy shale (clay load bearing) needs to be examined. As in the work presented here, Marion *et al.* obtained sand-clay mixture which appeared homogenous by shaking sand and clay particles in a sealed container. The slurring fluid used was 0.5 M NaCl and a confining pressures of 100, 200, 300, 400 and 500 bar and 10 bar pore pressure applied. The weight percentage of kaolinite was defined as the weight of room dry clay to the total mass of room dry kaolinite and sand.

Plots of porosity *versus* wt% kaolinite showed the porosity to decrease as the kaolinite content increased until a minimum value of porosity was reached. Adding more kaolinite after this minimum caused the porosity of the compact to increase again. For the sample compacted at 100 bar confining pressure (90 bar effective pressure) the minimum occurred at 20 wt% kaolinite with a porosity of 18 volume %. The pure kaolinite compacts had a porosity of 45 volume % compared with 36 volume % for compacts of pure Ottawa sands.

Data from a preliminary study carried out in the present research study are presented in Figure 3.23 for kaolinite slurried in water with quartz particles added. The shape of the curve obtained in [17] was similar to that shown in Figure 3.23 for the kaolinite with 10 μm inclusions. The transition from a shaly sand to a sandy shale (Figure 3.1) for the 10 μm particles is evident (Figure 3.23).

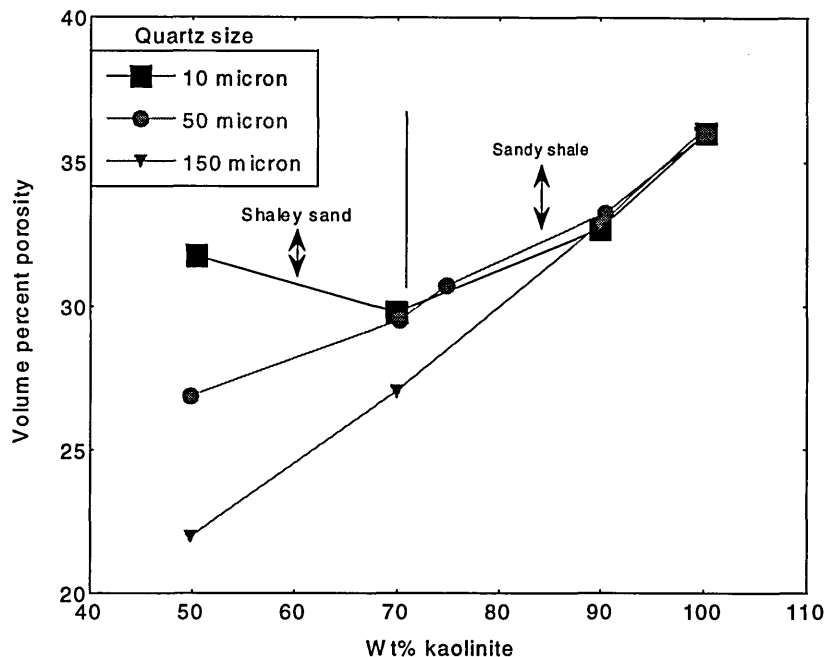


Figure 3.23: Volume porosity versus clay content for kaolinite compacts prepared at 100 bar and containing sized quartz.

For the systems profiles shown in Figure 3.23, it is the kaolinite with 10 μm inclusions that shows the transition from a shaly sand to a sandy shale similar to the behaviour documented by Marion *et al.*, [17].

In Chapter 5 glass beads are added to a montmorillonite film prepared for the Clay Membrane Cell in order to alter the porosity and ultimately the permeability. It was hoped to alter the levels of these inclusions to change the microstructure of the thin film from a sandy shale to a shaly sand.

4.1.5 Summary

Predicting the porosity of a wellbore shale (once the clay and silt content are known) from resistivity logs would be of use in detecting over pressured sections. In Section 4.0 variations in the porosity of clay compacts with clay type, electrolyte content and the addition of quartz have been noted and certain factors highlighted. These are listed here;

- The compaction behaviour of clays under near wellbore conditions is affected by the initial particle size. The final microstructure must depend on particle size and compaction process.
- Slurrying the clay in electrolyte prior to compaction has no apparent effect on the final porosity at pressures above 25 bar.

- A linear mixing law describes the dependence of mixed clay compact porosity on the fraction of each clay present.
- However the addition of granular material will affect the load bearing mechanism in the clays and ultimately the final porosity; the extent of the effect depends on the particle size of the quartz grains.

In trying to prepare “synthetic shales” in the laboratory several factors must be borne in mind. Shales have been compacted for millions of years during which diagenesis occurs resulting in mineral alteration and also soluble minerals precipitate out of solution causing cementation between the contact points. Also the presence of organics such as kerogen in shale can alter the interactions of clay particles during deposition resulting in altered microstructures. Finally some uncertainty exists as to the degree of mixing of different clays in non laminated shales [28].

Nevertheless the real influence of all these factors on the porosity of the clay phase in shale cannot be investigated until a complete understanding of the porosities obtained for clay silt mixtures in the laboratory has been studied.

4.2 Conductivity measurements-methods

4.2.1 Electrode evaluation

Before measuring the conductivity of clay compacts the electrode measurement system needed to be evaluated. Areas examined were the minimum sample length needed, the contribution of sample-surface conduction to the overall measured conductivities and comparison with conventional liquid electrode methods.

4.2.1.1 Surface conduction

The contribution of the liquid film on the shale surface (no allowances were made for surface roughness) to the measured resistance was investigated by measuring the resistivity of cores of different sizes. To model the results obtained the following assumptions were made.

The measured resistance of a shale core is the parallel combination of the bulk and surface resistance. The bulk resistance is given by

$$R_b = \frac{\rho_b l}{\pi r^2} \quad (16)$$

while the surface resistance is represented by

$$R_s = \frac{\rho_s l}{2\pi r \delta r + O(\delta r)^2} \quad (17)$$

The $O(\delta r)^2$ terms are so small that they can be ignored giving a total parallel resistance of.

$$R_t = \frac{l}{\pi r} \left(\frac{\rho_s \rho_b}{2\rho_b \delta r + r\rho_s} \right) \quad (18)$$

where R_b is the bulk resistance, R_s is the surface resistance R_t is the total resistance, l is the sample length, r is the sample radius, δr is the surface layer thickness, ρ_s is the surface resistivity, and ρ_b is the bulk resistivity.

The resistance was measured perpendicular to the bedding plane. It was therefore assumed that the sample was radially homogeneous and that variation of resistance was only due to variation of radius. The four-terminal electrodes were made of silver foil with the cross sectional area of the voltage terminals the same as for the brass electrodes. It was assumed that the results could be applied to any four terminal measurement which has electrodes of the same geometry. The liquid film had a uniform thickness δR over the total sample length l .

The resistivity of the liquid layer is approximately that of de-ionised water ($0.1 \Omega\text{m}$). No assumptions could be made about the thickness of the liquid layer. The term $r\rho_s \gg 2\delta r\rho_b$, therefore Equation 18 becomes

$$R_t = \frac{\rho_b l}{\pi r^2}. \quad (19)$$

If surface conduction is negligible, then from Equation 19, plotting R_t as a function of

$\frac{l}{\pi r^2}$ should give a line with a gradient of ρ_b and an intercept at zero.

Plotting sample resistance in Figure 3.24 as a function of sample dimensions gives a ρ_b of $133.6 \Omega\text{m}$ with an intercept at $-0.009 \text{ k}\Omega$. The linear regression coefficient is 0.999. This shows that in this experiment the contribution of the surface film to the conduction process is negligible.

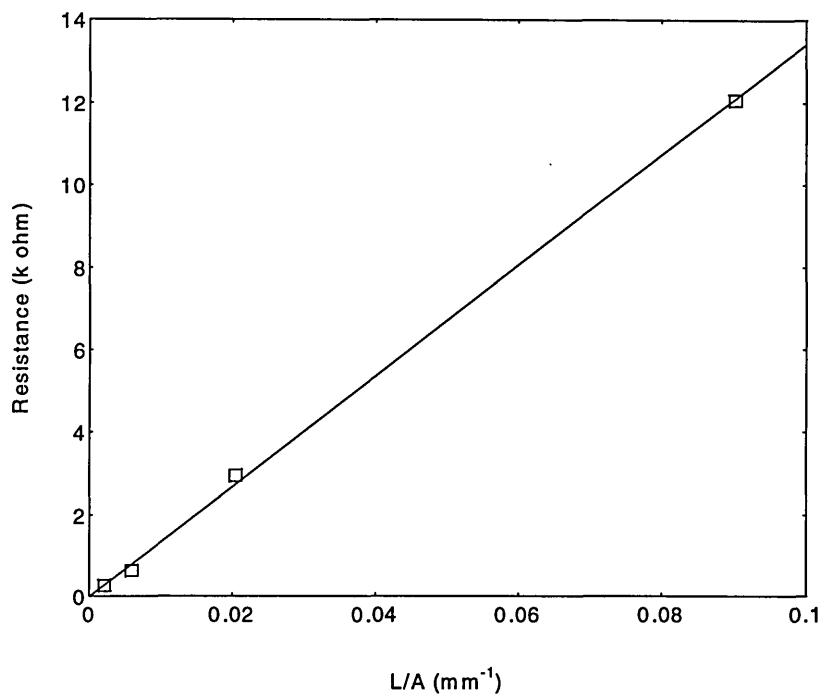


Figure 3.24: Measured resistance of shale cores (at 5 kHz) as a function of increasing radius.

4.2.2 Comparison of platen electrodes with liquid electrodes

Although the values obtained for Clashach cores from the liquid electrode and platen electrode methods (Table 3.4) are in agreement, the value obtained for the cementation factor m is low. The values quoted for m for a sandstone range from 1.8 to 2.2 [29] as measured using the conventional liquid electrode method. However, the conclusion is that the brass electrodes give a similar resistance value to that obtained using the more conventional liquid electrode method.

The following table lists the results from brass and liquid electrode measurement methods.

	Brass Electrodes	Liquid Electrodes
ρ_m (Ω m)	7.0	6.9
F	8.5	8.4
m	1.5	1.5

Table 3.4 Comparing measurement methods for determining the matrix resistivity (ρ_m) of a Clashach core with $\Phi = 0.24$

4.2.3 Electrode end effects

The effects of the water film close to the electrode surface and the finite dimensions of the voltage terminals on the uniformity of the electric field lines in the sample bulk were investigated. The variation of the resistance of Jurassic 2 shale and Clashach sandstone as a function of sample length is represented in Figures 3.26 and 3.27. The resistivity of Jurassic 2 shale cored parallel to bedding is less than that for the sample cored perpendicular to bedding orientation. In the parallel case, different mineralogical bands are available to the current and so it takes the least resistant path (Figure 3.25). In the perpendicular core, the current must pass through all the different mineralogical zones.

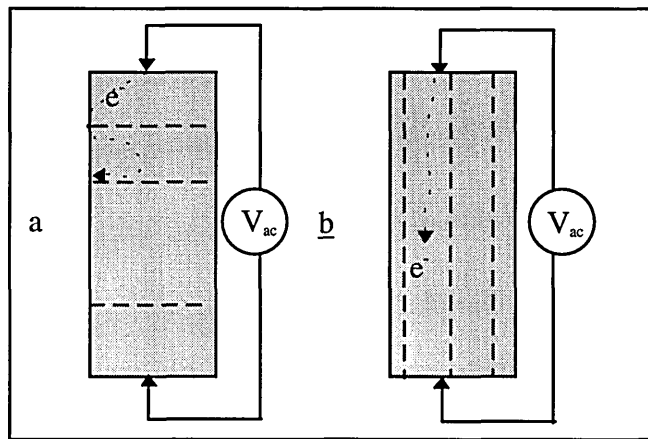


Figure 3.25 :Trajectory of an electron traveling perpendicular to the bedding planes (a) and parallel to the bedding planes (b).

The plots for the shale and Clashach cores are linear (constant resistivity) with negative intercepts. One physical explanation for this may be the finite size of the high impedance voltage terminal which causes the electric field lines to converge only at a certain distance from the electrode. Consequently near the voltage electrodes no current flows. The samples of Jurassic 2 less than 5 mm long were analysed using the Wayne Kerr component analyser (6425) in 2-terminal mode (Figures 3.28 and 3.29). This shows a non-linear behaviour which may explain the apparent negative intercepts on Figures 3.26 and 3.27. For samples longer than 5 mm, the resistance measurements were a linear function of sample length and therefore acceptable.

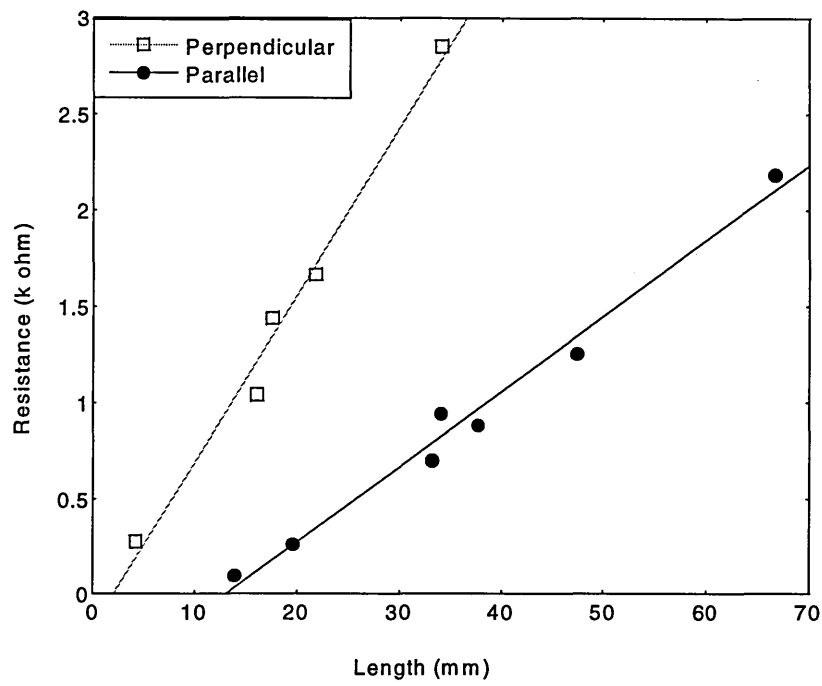


Figure 3.26: Resistance of the Jurassic 2 shale sample cored parallel and perpendicular to the bedding plane.

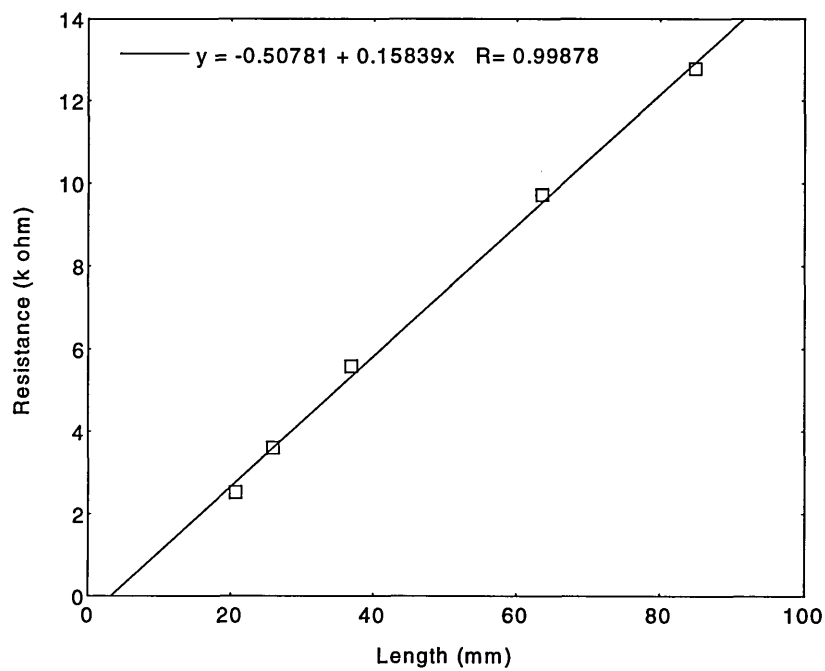


Figure 3.27: Resistance of the Clashach sandstone as a function of sample length

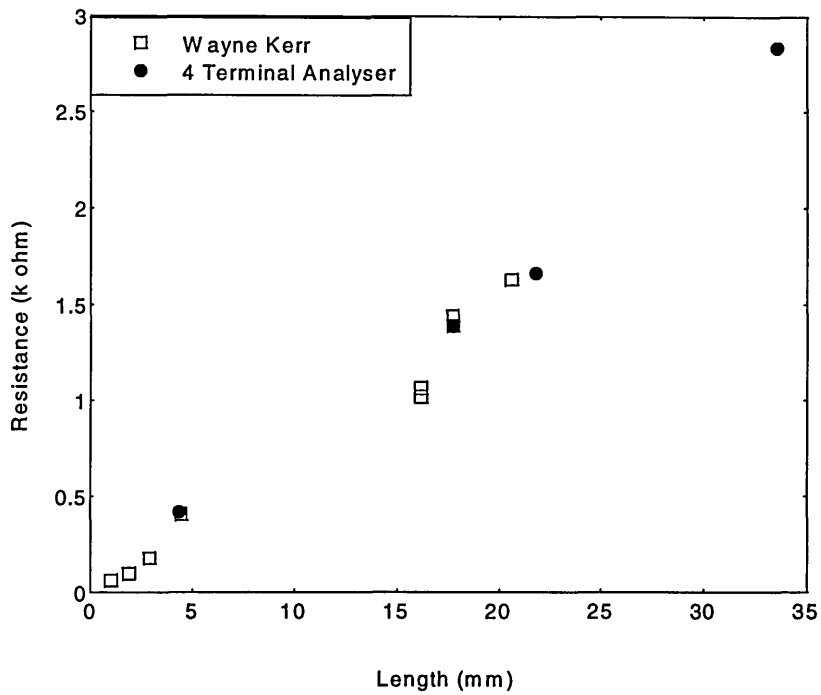


Figure 3.28: Comparing 4 terminal and 2 terminal resistance measurement methods for Jurassic shale.

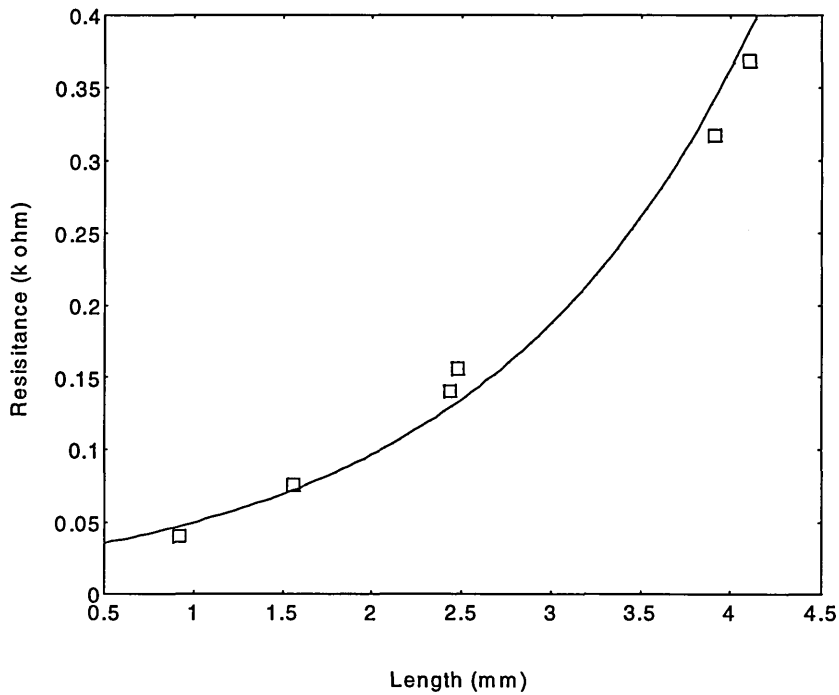


Figure 3.29: Measured resistance for a Jurassic 2 shale samples having a length less than 5 mm.

4.2.4 Summary

The brass platen electrodes are suitable for measuring the conductivity of clay compacts as long as the compact length is greater than 5 mm. This statement comes after showing that

- surface conduction is negligible
- measurements from platen electrodes are similar to conventional liquid electrodes, and
- below a sample length of 5 mm the electrode impedance affects the measurement.

4.3 Conductivity of clay compacts

The research carried out in this section is really a continuation of the work of Cremers, [15]. No more recent study can be found. Cremers measured the conductivity of sodium and calcium montmorillonites, and an illite clay as a function of clay content and added electrolyte. However the lowest volume porosity the clay gels reached in Cremers study was 0.5 compared with between 0.3 and 0.2 in data presented in this thesis. Cremers reduced the porosity by compaction under axial drainage with a maximum pressure of 15 bar compared with 600 bar in the study presented here. The possibility of reordering the clay at increased pressures must be born in mind when comparing the data from each study. Trends in data for Fullers Earth collected in this study will be compared with data from Cremers in this section.

Plots of conductivity *versus* porosity for Fullers Earth slurried in deionised water, 0.05 M CaCl₂, and 0.5 M CaCl₂ are presented in Figure 3.30.

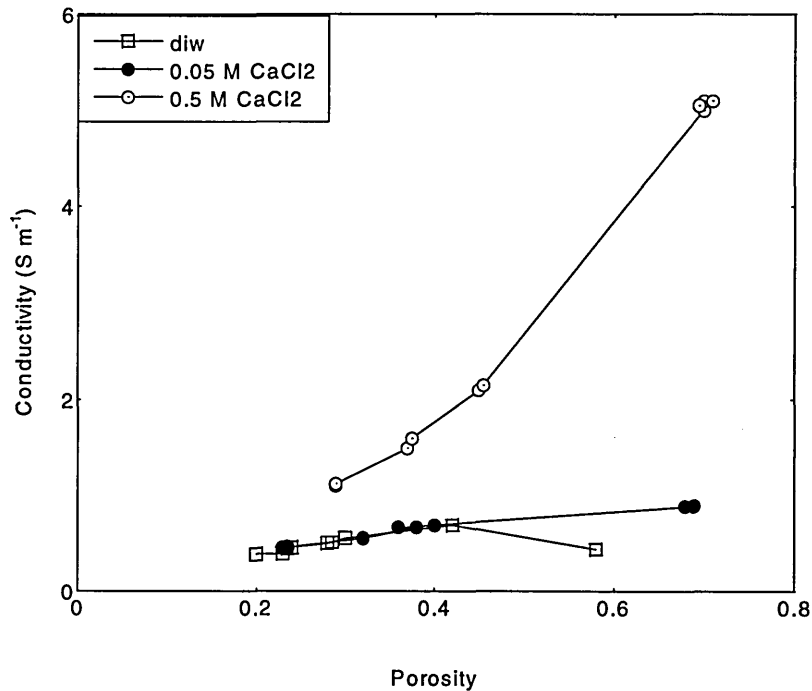


Figure 3.30: Conductivity (measured at 5 kHz) of Fuller's Earth in deionised water, 0.05 M CaCl₂ and 0.5 M CaCl₂ plotted against porosity.

The corresponding porosity *versus* compaction pressure for the Fullers Earth data are contained in Figure 3.15. The conductivity of the clay slurried in 0.5 M CaCl₂ is the

highest at the onset of compaction reducing to lower values as the salt is pushed out of the compacting slurry. A similar overall trend is seen for the Fullers Earth slurried in 0.05 M CaCl_2 although the overall conductivity values are lower. For the clay slurried in deionised water the curve of conductivity *versus* porosity rises to a peak and then falls as the porosity is reduced still further. In the experiment using deionised water the only source of mobile charge are the cations on the clay surface i.e. $\sigma_w \approx \text{zero}$. At high porosities the contribution of the mobile counterions to the conductivity of the pore fluid is shown by the $\frac{1 - \Phi_{\text{clay}}}{\Phi_{\text{clay}}}$ factor in Equation 3. As the porosity decreases the contribution of the clay surface to the pore fluid conductivity increases i.e. BQ_v increases. However the overall compact conductivity falls as the Φ^m term reduces faster. Physically this means that the conduction channels for ions between the tactoids are being reduced in size and the overall conductivity falls. Similar shaped curves were obtained for conductivity measurements of Ca greenbond slurried in deionised water and 0.5 M CaCl_2 (Figure 3.34) and illite in deionised water and 0.05 M KCl (Figure 3.35).

Cremers data for Ca montmorillonite is reproduced in Figure 3.31. The units of conductivity used in Figure 3.30 are mmhos cm^{-1} which equates to 0.1 S m^{-1} . Cremers measurements were carried out using a current oscillating at 1 kHz. Varying the frequency from 1 to 5 kHz had caused a 5 % increase in the measured values which is consistent with previously published work [30].

The data shown in Figure 3.30 for 0.5 M CaCl_2 is similar in trend but not identical to that shown by Cremers for calcium exchanged clay slurried in 0.8 M calcium chloride (Figure 3.31). For the slurries with 0.5 M calcium chloride the conductivity dropped as the porosity was reduced. However there is a difference between the two sets of data in that the porosity ranges over which the conductivity increases from 1 to 5 S m^{-1} are 0.6 to 1.0 in Cremers study and 0.3 to 0.7 in the data set presented here. This indicates that the measurements of the slurrying fluid conductivity (porosity equal to 1) is not in agreement, i.e. that the values measured for the 0.5 M CaCl_2 solutions are too high.

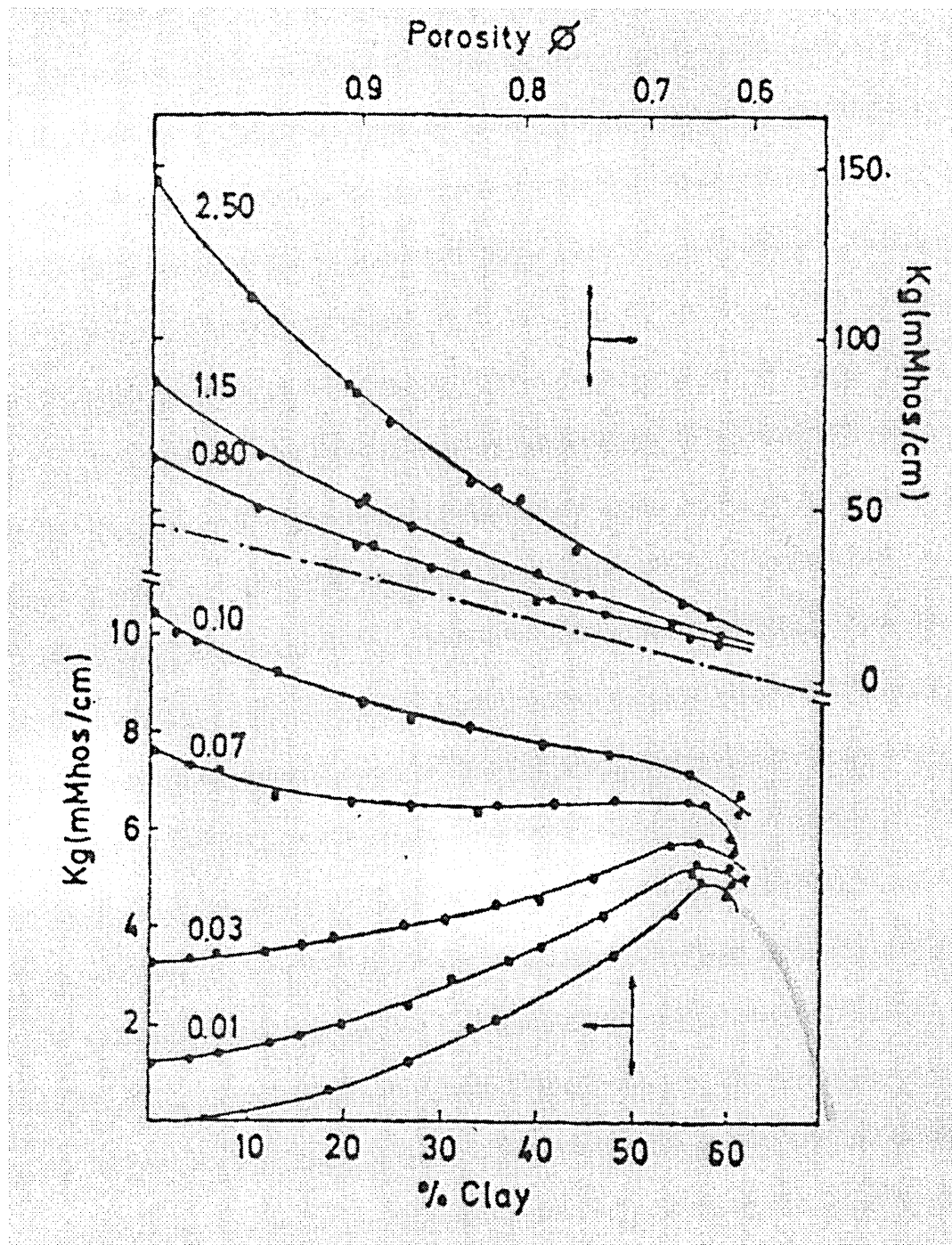


Figure 3.31: Data taken from Cremers, [15] showing the conductivity of Ca montmorillonite (1 kHz) slurried in calcium chloride. The numbers on the curves represent the calcium chloride concentration with the bottom curve being deionised water.

Unfortunately Cremers did not carry out an experiment in 0.05 M CaCl_2 but at salinities below 0.05 M the conductivity increase peaks at a porosity of 0.6 and falls again similar to the trend shown in Figure 3.30.

It is assumed that when the molarity of the slurring fluid is high as in the case of 0.5 M CaCl_2 , the contribution of the adsorbed cations on the clay surface to the overall

conductivity is negligible until the porosity approaches zero. This assumption is validated to a certain extent by the fact that a form of the Archie equation

$$\sigma_{\text{clay}} = \sigma_w \Phi_{\text{clay}}^m \quad (1)$$

normally applied to sandstone cores can be fitted to the 0.5 M data set by plotting log conductivity *versus* log porosity as shown in Figure 3.32.

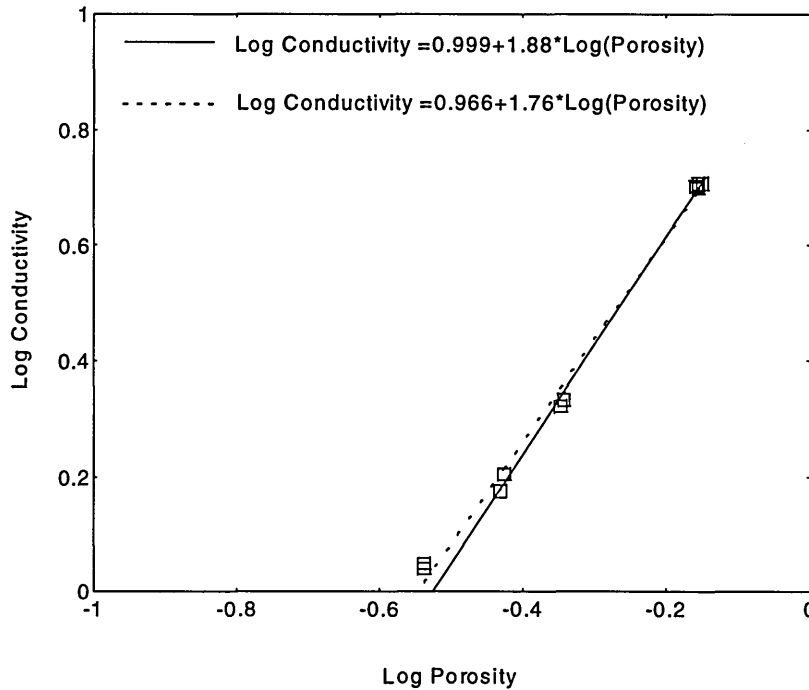


Figure 3.32: Log Conductivity (σ_m) *versus* Log Porosity (σ_m) for Fullers Earth slurried in 0.5 M calcium chloride. The slope of the line shows the cementation factor, m to have a value of 1.76.

The linear fit to the log data is represented in Figure 3.32 using a dashed line and yields 1.76 for the cementation factor m and 9.2 S m^{-1} for the pore fluid conductivity. However Kaleidagraph (a commercially available package) was used to fit the data for the other salinities that could not be fit with the Archie equation. It seemed reasonable at this point to determine what fit for the Archie equation would Kaleidagraph give when applied to the experimental data plotted in Figure 3.30 as conductivity *versus* porosity. The values for m and σ_w given were 1.88 and 9.9 S m^{-1} respectively with a requested error no greater than 0.001 %. This equation has been superimposed on Figure 3.32. Therefore one can

expect an error of 7% in the predicted values of m on the fitting procedure to the conductivity *versus* porosity plots.

It was expected that the surface cations on the clay would contribute a greater fraction to the conductivity of the slurries in 0.05 M CaCl₂ and deionised water. For these clays slurried in calcium chloride an engineering approach to the structure of the clay compact will be used. It will be assumed that the clay platelets are layered in stacks or tactoids in the compact. One could therefore assume that the main conduction path for ions is through the bulk pores around the tactoids-allowing the structure of the clay compact to become important. This would not discount the fact that there would be some charge hopping along the surfaces of the clay tactoids and some of the counterions may be expelled into the bulk pore fluid.

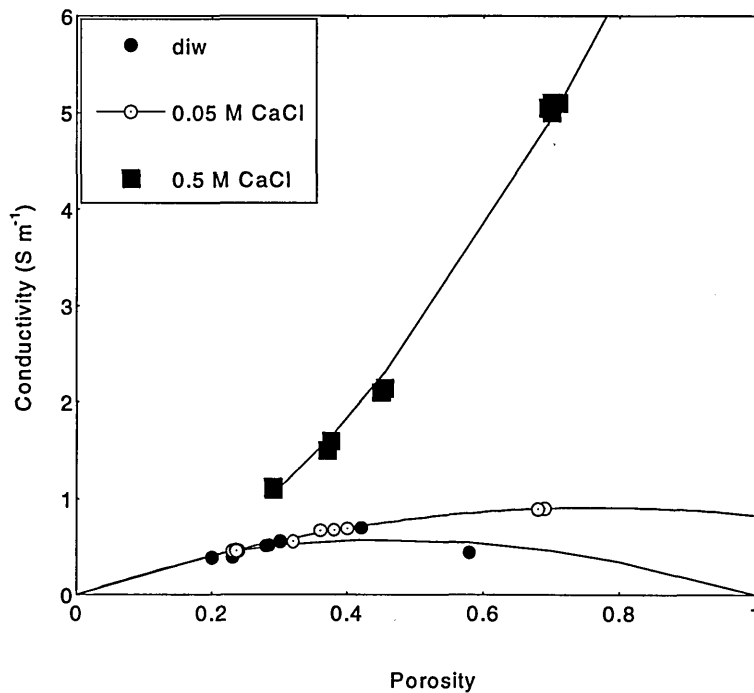


Figure 3.33: Conductivity data for Fullers Earth showing the model fit to the data.

A commercially available software package called Kaleidagraph was used to fit Equation 5

$$\sigma_{\text{clay}} = \left(A \Lambda C d_s \left(\frac{1 - \Phi_{\text{clay}}}{\Phi_{\text{clay}}} \right) + \sigma_w \right) \Phi_{\text{clay}}^m \quad (5)$$

to the data where the σ_w values for water and electrolytes were also predicted from the fitting routine (see Figure 3.33). The cementation factor m and the fraction of surface

cations, A, contributing to the conductivity of the pore fluid were determined. The same procedure was carried out for data for illite (Figure 3.34) and Ca greenbond (Figure 3.35).

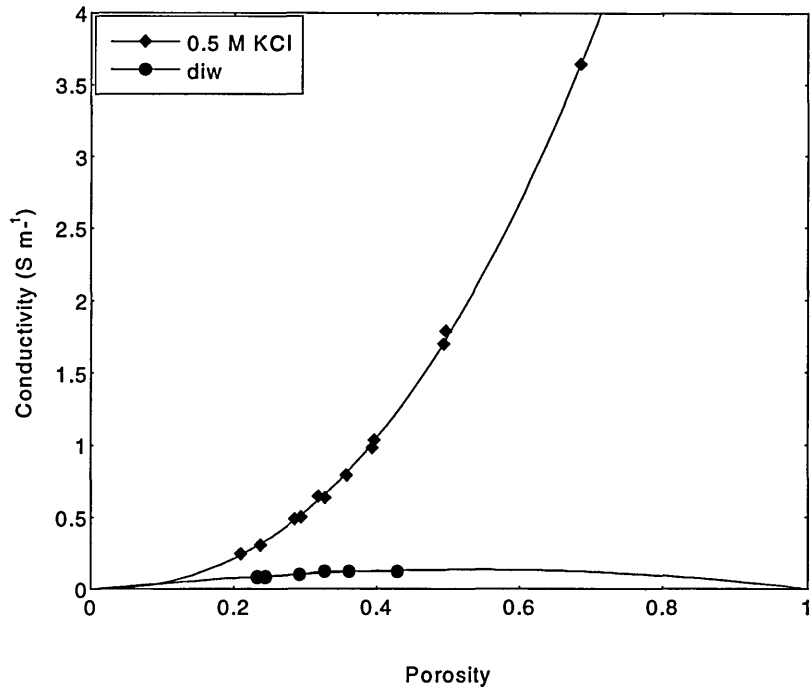


Figure 3.34: Conductivity (measured at 5 kHz) *versus* porosity for illite slurried in 0.5 M KCl deionised water. Model represented by solid lines.

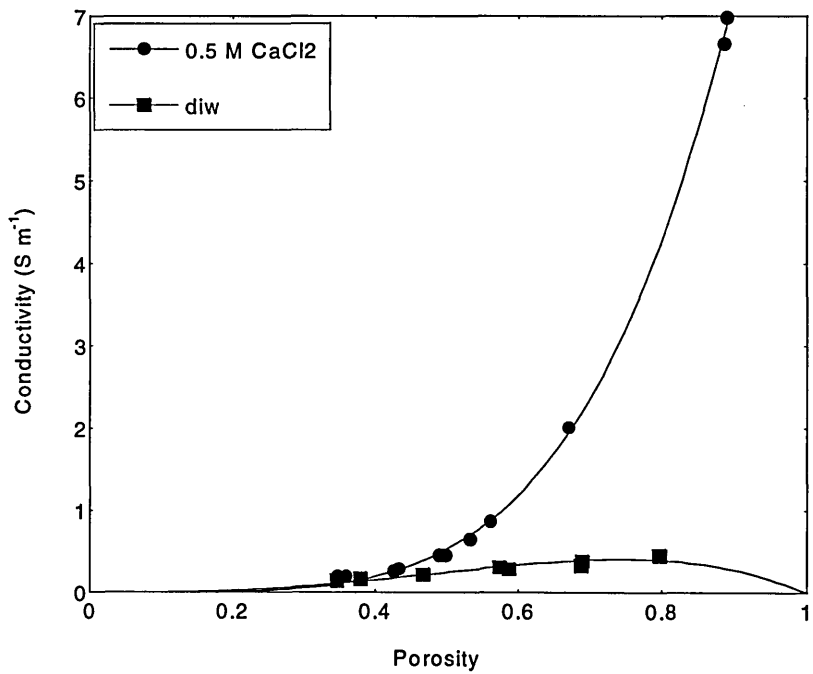


Figure 3.35: Conductivity (measured at 5 kHz) *versus* porosity for Ca greenbond slurried in 0.5 M CaCl₂ and deionised water. Model represented by solid lines.

Clay type	Slurrying fluid	σ_w (S m ⁻¹)	m	A
Fullers Earth	deionised water	0.0	1.86	0.2
Fullers Earth	CaCl ₂ (0.05 M)	0.8	1.88	0.2
Fullers Earth	CaCl ₂ (0.5 M)	9.9	1.88	NA
illite	deionised water	0.0	2.13	0.1
illite	KCl (0.5 M)	7.8	2.31	NA
Ca greenbond	deionised water	0.0	3.93	0.4
Ca greenbond	CaCl ₂ (0.5 M)	9.6	4.46	NA

Table 3.5: Some of the parameters calculated from the conductivity *versus* porosity profiles of clay slurries using a Kaleidagraph fitting routine. NA means not applicable.

The conductivities of the 0.5 M slurrying fluid (σ_w) presented in Table 3.5 are higher than values obtained from the Handbook of Chemistry and Physics [31]; namely 7.3 and 5.1 S m⁻¹ for calcium and potassium chloride respectively. These values were obtained from fitting Equation 1 and 5 to the conductivity *versus* porosity data. Similar results were obtained when the compaction cells were filled with electrolyte solution only. No explanation can be given for this discrepancy, however it is clearly an experimental artifact.

The variation in cementation factor (m) with ionic strength will not be examined here because of the limited data set. However it is certain that the variation in m with different clay types is real and not caused by experimental errors. Wyllie and Gregory [32] have shown that the cementation factor increases when changing from spherical glass particles to glass discs with an increased aspect ratio. However this area is still being investigated and research on ellipsoid packing by de Kuijper *et al.*, [7] has shown that in some cases the cementation factor can itself vary with porosity. Nevertheless the increase in cementation factor when using Ca greenbond compared with Fullers Earth can be explained in terms of the increased aspect ratio of the particles resulting in a greater number of grain contacts [9]. The difference in the aspect ratios of these two clay was evident in the micrographs presented in Figure 3.10 and 3.11 showing the ordered nature of single Ca greenbond particles compared with the lower aspect ratio of the domain-like

structure of Fullers Earth. Unfortunately the microstructure of this compacted clay cannot be compared with that of Ca Greenbond and Fullers Earth.

Using the Kaleidagraph fitting routine allowed the fraction of the surface exchange sites that contributed to conduction processes (A) to be calculated from the determined surface conductivities BQ_v . Values for the molar ionic conductivities were assumed to be those at infinite dilution. For calcium and potassium at 18 °C the values were 5.0 and 6.3 S m⁻¹ mol⁻¹ dm⁻³ respectively. The cation exchange capacities of Fullers Earth, Ca greenbond and illite were 0.90, 0.84 and 0.21 eq kg⁻¹. For Fuller's Earth, illite and Ca greenbond, A was found to be 0.2, 0.2 and 0.4 respectively. Cremers quoted a value of 0.52 for the Ca montmorillonite (Camp Berteau) slurried in CaCl₂. It is apparent in Figure 3.6 that the porosity of Fullers Earth and illite are less than that of Gelwhite when compacted in water at 250 bar. Therefore one would expect that the number of ions trapped in closed galleries is greater for Fullers Earth and illite leading to lower fractions of the surface cations contributing to conduction. No direct comparison can be found from the literature for such data. However a value of 2.6 S m⁻¹ at 0.6 porosity found for the surface conductivity of Fullers Earth (slurried in deionised water) at 5 kHz is of the same order of magnitude as values of 2.3 S m⁻¹ and 1.8 S m⁻¹ determined by Weiler and Chaussidon, [16] for the sodium and potassium exchanged forms of a Camp Berteau montmorillonite (slurried in deionised water). Measurements by Weiler and Chaussidon were carried out at 1 kHz.

4.3.1 Temperature effects

It was hoped that by examining the activation energy for electrical conduction as a function of compact porosity the switch over from bulk pore fluid to surface conduction at low porosities would be demonstrated. Applying Equation 9 to the conductivity *versus* temperature data in the range 21 °C to 50 °C gave constant values for the activation energy. An example of such a plot is given in Figure 3.36 for a Fullers Earth compact where the slope gives the activation energy. The activation energy for the electrical conduction is 20.5 kJ mol⁻¹ for the compact with a porosity of 0.49 (Figure 3.37). The activation energy for conduction for Fullers Earth and CaCl₂ increases as the porosity decreases. Activation energies were determined by Cremers for calcium montmorillonite slurried in different molarities of CaCl₂. These experiments were carried out under ambient pressure and in the temperature range 20 to 35 °C [15]. The data obtained in the present study also showed an increase in activation energy as the porosity decreased. All

of the data are presented in Figure 3.37, where they lie on an approximately straight line when plotted as activation energy *versus* volume percent porosity.

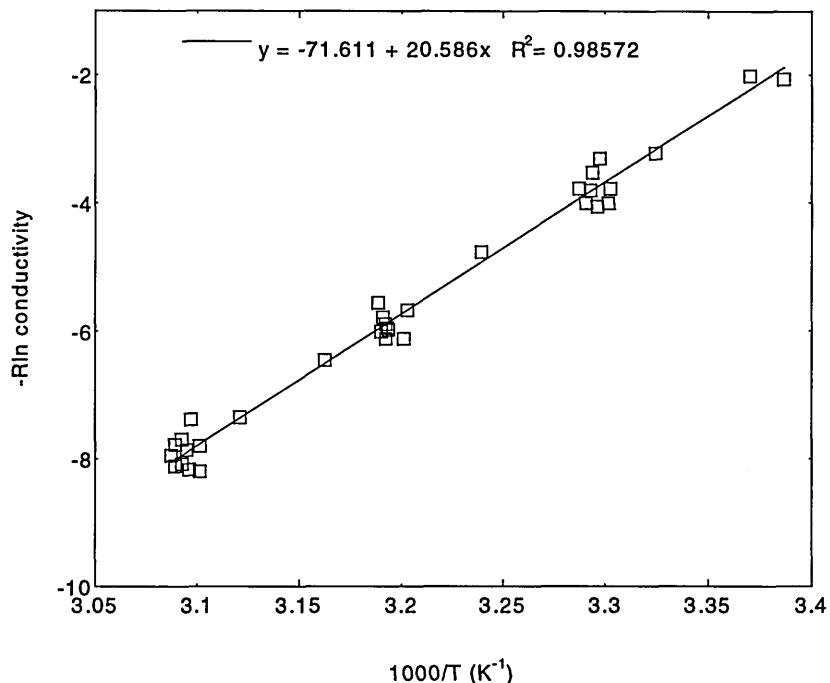


Figure 3.36: A plot of $-R \ln \text{conductivity}$ *versus* $1,000/T$ for Fullers Earth slurried in 0.5 M calcium chloride.

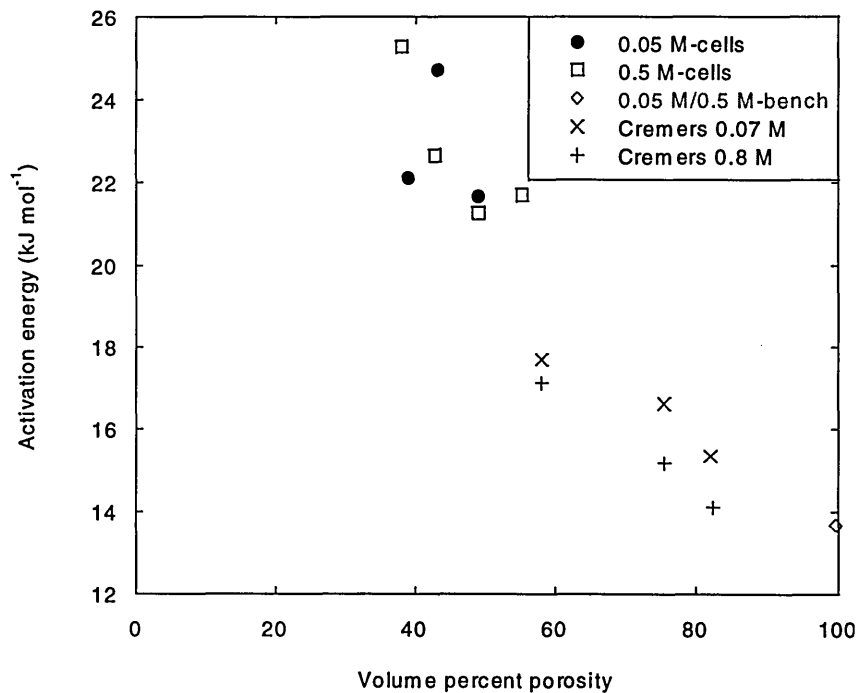


Figure 3.37: Activation energy *versus* porosity for Fullers Earth systems and smectite slurries. Data of Cremers [15] for the smectite slurries shown by + and x.

For the Fullers Earth data the activation energy increases from the pure solution value as the porosity decreases. A possible explanation for this is that the reduction in porosity forces the ions to move along the clay surface rather than in bulk pores. The activation energy for the former is expected to be greater than the latter [16], [6]. In Weiler *et al* [16] a value of 17.4 kJ mol^{-1} was quoted for a Na montmorillonite-water gel having a porosity of 60 % compared with 17.6 kJ mol^{-1} at 26 %. The changes noted in the work presented here are much higher which may be connected with the salt concentrations used and its effect on the structure of the clay tactoids.

5. Conclusions

The compaction behaviour of clays under near wellbore conditions is affected by the initial particle size and but not by the electrolyte concentration.

The porosity of clay mixtures can be accounted for in terms of a linear mixing law. It is possible to measure the conductivity of clay gels during compaction and results at high porosities compare well with previously published data. The activation energy for electrical conduction increases as the porosity reduces indicating the increased importance of surface conduction over bulk pore conduction.

6. Future work

Ideally one would like to be able to predict the porosity of the shale sections in the wellbore once the overburden stress and mineralogy were known. Therefore a more comprehensive study of the effect of clay particle size and shape on porosity is needed. In order to do such a study a systematic approach would be required to the preparation of clays prior to compaction.

The measurement of the conductivity of clay compacts at high pressures has been validated but the data set is limited. Results from experiments where montmorillonite was slurried in sodium chloride would be an interesting way to scope changes in the cementation factor. Moreover the effect of wellbore fluids such as potassium salts and glycol molecules on the conductivity of the native montmorillonites would also be of interest.

The model applied to the data is very simple and it is not really adequate to assume that the salinity of the pore fluid in a smectitic rock is the sum of the local sea water and the surface cations. Donnan exclusion should be incorporated into the model especially at high compaction pressures. This would necessitate the on line analysis of the pore fluid drained from the compacting clay.

7. References

- [1] Andika R., Rahman S., Richards B., and Tan, C.P. Effects of swelling and hydrational stress in shales on wellbore stability, SPE 38057, 1997.
- [2] Chenevert, M., Osisanya S. and Santarelli F., On the stability of shales and its consequences in terms of swelling and wellbore stability, SPE 23886, 1992.
- [3] Carminati, Stefano, Santarelli, F.J. Do shales swell? A critical review of available evidence, SPE 29421, 1995.
- [4] Aldred W., Bergt D., Rasmus J., and Voisin B. Real time overpressure detection. Schlumberger Oilfield Review Review, **1**, 17-27, 1989
- [5] Fernado M., Burau R. and Arulanandan K. A new approach to determination of cation exchange capacity, Soil Science Society, American Journal, **41** 818-820, 1977.
- [6] Waxman M. and Smits L. Electrical conductivities in oil bearing shaly sands, SPE 1863-A, 1967.
- [7] de Kuijper A., Sandar R., Hofman J. and de Waal J. Conductivity of two-component systems, Geophysics, **61**, 162-168, 1996.
- [8] The Technical Review (Schlumberger), Archie's Law: Electrical conduction in clean, water bearing rock, **36**, 3, 4-13, 1988.
- [9] Schwartz L. M. and Banavar J. R. Transport properties of disordered continuum systems: Physical Reviews B, **39**, 965-11, 1970.
- [10] Read H. and Watson J. Introduction to geology **1**, 1968.
- [11] Clavier C., Coates, G., and Dumanoir, J. The theoretical and experimental bases for the Dual Water model for the interpretation of shaly sands. SPE 6859, 1977.
- [12] Waxman M.H. and Thomas E.C. Electrical conductivities in oil bearing shaly sands, 2 the temperature effects of electrical conductivity, SPE Journal **14**, 213-225, 1974.
- [13] Pape H. and Worthington P.F. A surface-structure model for the electrical conductivity of reservoir rocks. Trans. SPWLA 8th European Formation Evaluation Symposium, London, Paper Z, 1983.
- [14] Revil A., Cathles L.M, Losh S. Electrical conductivity in shaly sands with geophysical applications. Journal of Geophysical Research, **103**, B10, 23,925-23,936, 1998.
- [15] Cremers A. Ionic movement in a colloidal environment, PhD thesis, Department of Chemistry, University of Louvain, 1968.

- [16] Weiler R. A. and Chaussidon J., Surface conductivity and dielectric properties of montmorillonite gels, *Clays and Clay Minerals*, **16**, 147-155, 1968.
- [17] Marion D., Nur A., Yin, H. and Han D. Compressional Velocity and porosity in sand-clay mixtures, *Geophysics*, **57**, 554-563, 1992
- [18] Data handbook of clay materials and other non-metallic minerals, Eds H. van Olphen and J.J. Fripiat, Pergamon Press, 1979.
- [19] Brindley G. and Brown G. Crystal structures of clay minerals and their identification, Mineralogical Society, London, 1984.
- [20] Meeten G.H. and Sherwood J.D. The hydraulic permeability of bentonite suspensions with granular inclusions, *Chemical Engineering Science*, **49**, (19), 3249-3256, 1994.
- [21] Chilingar G.V. and Knight L. Relationship between pressure and moisture content of kaolinite, illite and montmorillonite clays. *Bulletin of the American Association of Petroleum Geologists*, **44**, 101-106, 1960.
- [22] Volzone C. and Hipedinger N., Mercury porosimetry of compacted clay minerals, *Zeitschrift fur pflanzenernahrung und bodenkunde*, **160**, 357-360, 1997.
- [23] Robertson R.H.S., Tessier D. and White J.L., *Clay Minerals*, **17**, 255-258, 1982.
- [24] Terzaghi K. and Peck R. *Soil mechanics in engineering practice*, John Wiley and sons, 1948.
- [25] Barclay L. and Ottewill R., Measurement of forces between colloidal particles, *Discussions Faraday Society* **1** 138-171, 1970.
- [26] Smart B. Rowlands N., and Isaac A. Progress towards establishing relationships between the mineralogy and physical properties of coal measures rocks, *International Journal of Rock Mechanics, Mineral Science and Geomechanics, Abstracts*, **19**, 81-89, 1982.
- [27] Welton J.E. SEM petrology atlas. The American association of petroleum geologists, Tulsa, 50-72, 1984.
- [28] Pettijohn F.J. *Sedimentary rocks*, Harper and Row, New York, 260-299, 1975.
- [29] Carothers J.E. A statistical study of the formation factor relation. *The Log Analyst*, September-October, 1968.
- [30] Arulanandan K. Hydraulic and electrical flows in clays, *Clays and Clay Minerals*, **17**, 63-76, 1969.
- [31] *Handbook of Chemistry and Physics*, CRC Press Inc, Ed. 68th 1987-1988, D 225-D243.

[32] Wyllie M.R. and Gregory A. R. Formation factors of unconsolidated porous media: influence of particle shape and effect of cementation, Petroleum Transactions of the AIME **198**, 103-110, 1953.

CHAPTER 4

DESIGNING POLYGLYCOLS FOR SHALE STABILISATION

1. Introduction	84
2. Background	85
2.1 X-ray diffraction	85
2.2 Infrared spectroscopy	87
3. Experimental	87
3.1 Materials	87
3.1.1 Glycols	87
3.1.2 Polyglycol solutions	88
3.1.3 Mud preparation	88
3.1.4 Clay	89
3.1.5 Ion Exchange	89
3.1.6 Shale	90
3.1.7 Clay-polyglycol complexes	91
3.2 Adsorption studies	91
3.2.1 Glassware	91
3.2.2 Adsorption isotherms	91
3.2.3 GPC analysis	92
3.2.4 Infrared spectroscopy	93
3.2.5 X-ray diffraction	94
3.3 Molecular simulations	95
3.4 Shale dispersion tests	95
3.4.1 Closed-bottle test method for mechanistic studies	96
3.4.2 Slake Durability (Vole cage) tests	96
3.5 Bulk hardness tests	96
4. Results and discussion	97
4.1 Stabilisation of montmorillonite-glycol-water complexes	97
4.2 Adsorption Isotherms	100
4.3 Stabilisation of montmorillonite-glycol-salt complexes	108
4.3.1 Interactions with potassium exchanged clay	108
4.3.2 The addition of potassium chloride	109
4.3.3 The addition of calcium and sodium chloride	112
4.4 Summary	114
5. Testing the mechanism on shale	115
5.1 Cuttings dispersion tests with freshwater	116
5.2 Cuttings dispersion tests with salt added	119
5.3 Designing a new shale dispersion inhibitor	121
6. Conclusions	122
7. Future work	122
8. References	124

1. Introduction

Polyglycols have become established as cost-effective, environmentally friendly additives for water based muds (WBM) used to drill the reactive clay-rich rocks generally referred to as shales [1]. These compounds are typically added to WBM at concentrations between 3 and 10 wt% and are most commonly used in conjunction with a KCl/polymer base fluid, although they have also been added to freshwater muds and those containing sodium and calcium salts [2].

Compared with most other types of WBM, polyglycol systems give improved wellbore condition and produce firmer cuttings that do not readily disperse into the mud. These attributes generally result in faster drilling rates, fewer (or less severe) drilling problems and reduced mud volumes that, in turn, translate into reduced drilling and mud costs. Besides their improved cost-effectiveness, the combination of the ready biodegradation of most polyglycols and the low mud volumes leads to a smaller environmental footprint. Several theories have been put forward to explain how polyglycols inhibit shales:

- *Reduced water activity:* Polyglycols reduce the chemical activity of the mud filtrate and therefore could inhibit by an osmotic mechanism. However, the change in water activity due to the presence of only 3-5% polyglycol is not enough to make this theory tenable in the class of fluids discussed here. (Recently developed mud systems containing 30-60% methylglucoside [3] may provide some shale control by an imperfect osmotic mechanism)
- *Pore plugging by insoluble polyglycol droplets:* The cloud point property of some polyglycols has been proposed [4] as a key feature of the mechanism, in that insoluble polyglycol droplets (produced when the temperature of the mud or filtrate that has invaded the shale rises above the cloud point) can plug pores in the shale and thereby reduce invasion of the mud filtrate. While this theory may be valid in some situations, it does not explain the inhibitive properties of polyglycols that do not have cloud points, why those that have cloud points are also effective below the critical temperature or the strong synergy many glycols display with *specific* dissolved inorganic cations.
- *Adsorption of polyglycol on clay surfaces:* It is well known that polyglycols can adsorb on clays from aqueous solution [5] and this affinity has been

used to explain the inhibitive nature of the polyglycol muds. The proposal is that the polyglycol molecules compete with water molecules for adsorption sites on the clay minerals present in shales, and that this prevents water molecules from forming organised structures that would lead to swelling and dispersion.

- *Filtrate viscosity:* The increased viscosity of a WBM filtrate containing polyglycol has also been proposed as a contributing factor in their inhibitive properties [6] since viscous fluids will invade the rock more slowly and hence delay the onset of instability.

The assumption that polyglycol adsorption on shale minerals plays a role in inhibition was used as the starting point for this study. A number of glycols of different chemistries were chosen and their ability to stabilise swelling-montmorillonite examined. After an initial screening using mainly X-ray diffraction techniques, successful chemistries were tested on shale samples. The efficiency of the molecules at preventing water uptake by the shale was inferred from cutting dispersion tests and bulk hardness tests.

2. Background

2.1 X-ray diffraction

Since 1912 when von Laue examined the diffraction pattern from a copper sulphate crystal, X-rays have been used to determine the separation of crystallographic planes [7]. The theory of W. L. Bragg which deals with the reflection of X-rays by planes of atoms is used to extract the separation of clay layers from diffractograms. When monochromatic radiation is reflected from planes of crystals the path difference of the reflected rays vary. As shown in Figure 4.1 the extra distances traveled by ray BE over ray AD is given by (GY+YH) which in turn is equal to $2d\sin\theta$. When the path difference is equal to an integral number of wavelengths then the reflected rays interfere constructively giving a peak in the diffractogram. The Bragg condition is satisfied when $(GY+YH) = n\lambda = 2d \sin\theta$. Changing the incident angle while keeping the wavelength fixed (in this case Cu K_{α} radiation) allows different crystallographic planes to be examined. In experiments on montmorillonite the separation of planes with Miller indices 001 gives sufficient information on the hydration state of the clay.

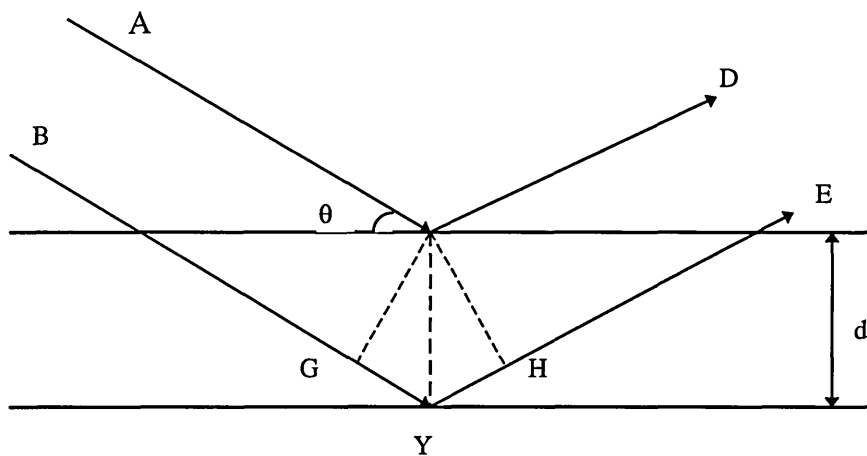


Figure 4.1: The path difference of reflected rays from crystallographic planes.

This distance is represented as d in Figure 4.2 and is often referred to as the basal spacing [8], where d corresponds to the basal spacing or can be represented by d_{001} .

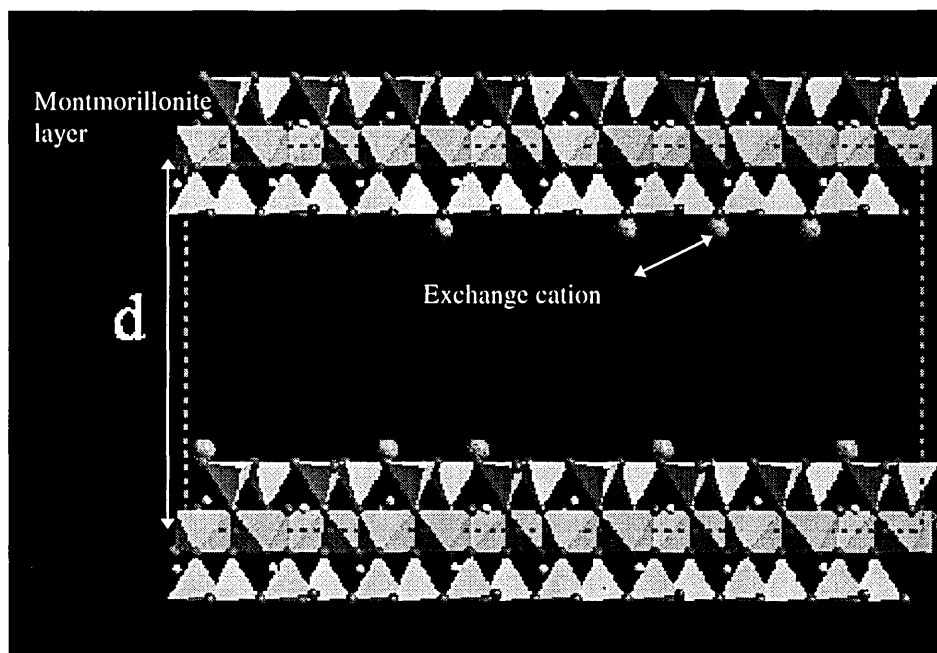


Figure 4.2: Physical interpretation of the basal spacing of montmorillonite represented here by d .

A lot of information exists in the literature on the examination of montmorillonite-glycol complexes using X-ray diffraction [9]. Primarily ethylene glycol was used to verify the presence of montmorillonite as the basal spacing expanded to 16.9 to 17.1 Å while for vermiculite (which has a higher layer charge) the spacings reached are typically no greater than 16.1 Å. Conventionally samples were mounted in powder form in the XRD however it is possible to examine solid pieces of material as long as the crystallographic planes are orientated. It is important to remember that 90% of the

diffracted radiation is collected from the first 4 microns of clay film when the basal spacing is 17 Å [10].

2.2 Infrared spectroscopy

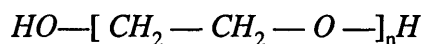
Infrared spectroscopy is perhaps best known as a technique to identify the presence of specific bonds in polymers. However Fourier transform infrared spectroscopy (FTIR) is also useful for examining the loading of a polymer on the clay but it does not distinguish between glycol adsorbed on the surface and that which is inserted between the clay layers. Spectra taken of glycol-montmorillonite mixtures are complicated in that the spectrum of the glycol alone is superimposed (with some peak shifts) on that of the untreated clay. Nevertheless peaks unique to the glycol and clay can be used to determine the polymer/clay ratio. Various infrared spectroscopic techniques have previously been used to determine the conformation of the polymer in the intergallery region and prove the existence of polymer-clay interactions. Characteristic peak shifts caused by such interactions have been exploited by others in clay studies [11] and also in examining the solution properties of surfactants in the micellar phase [12]. Using infrared spectroscopy Nguyen *et al.* [11] monitored the adsorption of ethylene glycol monoethyl ether (egme) on Ca montmorillonite. The interaction of the terminal OH group on the glycol with the clay surfaces was inferred from the peak shifts observed from monitoring the liquid egme compared with the adsorbed egme. Micelle formation of dodecylammonium propionate in chloroform was detected by studying the peak shifts of the COO⁻ band. Hydration of the surfactant headgroup on the addition of water could be detected using the same band [12].

3. Experimental

3.1 Materials

3.1.1 Glycols

The name polyglycol is used in this thesis to represent any mud additive which has polyethylene glycol as a segment. Polyethylene glycol consists of repeat units of:



where n in these studies can have an integer value between 5 and 24. A list of polyglycols with their formulae, source and molecular weight is given in Table 4.1.

Polymer	Source	Formula	M _w t(g mol ⁻¹)
peg	Aldrich	HO[CH ₂ CH ₂ O] _n H	400
C ₈ E ₇	MPC*	HO[CH ₂ CH ₂ O] ₇ C ₈ H ₁₇	410
C ₆ E ₇	MPC*	HO[CH ₂ CH ₂ O] ₇ C ₆ H ₁₃	
C ₄ E ₇	MPC*	HO[CH ₂ CH ₂ O] ₇ C ₄ H ₉	358
butyl-peg	**	HO[CH ₂ CH ₂ O] ₆ C ₄ H ₉	320
peg 400 DIM	Aldrich	CH ₃ O[CH ₂ CH ₂ O] _n CH ₃	400
pag	**	peg/PPG/random polymer	630
L31	ICI	peg ₂ PPG ₁₆ peg ₂	1100
50A50	**	peg/PPG/random polymer	≈1,000
50A140	**	peg/PPG/random polymer	≈1,400
B-NH ₂	Aldrich	CH ₃ CH(NH ₂)CH ₂ [PPG] _i [peg] _n [PPG] _m NH ₂	600
EO/BO 24%	MPC	peg/(OCH ₂ CH(CH ₂ CH ₃))/random polymer	600
EO/BO 45%	MPC	peg/(OCH ₂ CH(CH ₂ CH ₃))/random polymer	650
Sorbitol-po	**	Sorbitol + 9PO	720
Sorbitol	Aldrich	CH ₂ (OH)[CH(OH)] ₄ CH ₂ OH	200

Table 4.1: Polyglycols used in mechanistic studies.

*Manchester Polymer Centre, ** supplier can not be identified for confidential reasons.

Percentages cited after the EO/BO polymers represents the mol % of oxybutylene units in the polymer.

3.1.2 Polyglycol solutions

The polymers were used as received from the manufacturer. All the solutions were made up by weight on a three figure electronic balance. Polyglycol solutions in the concentration range of 5,000 to 110,000 ppm (0.5 to 11%) were used in adsorption studies. For experiments with salts present, molar solutions of potassium, calcium or sodium chlorides was used to dilute the neat polymer.

3.1.3 Mud preparation

All the polymers were used at concentrations required to give 5 wt% glycol in solution. Salts were added to give molar concentrations of each and the pH was not adjusted.

Fully formulated muds were prepared using 10 g of carboxymethylcellulose and 4 g of xanthan gum per liter of water. This mixture was allowed to hydrate and then used as a base for making the necessary salted fluids. The polyglycol was added some hours later and the mud rolled overnight to ensure good polymer mixing. Unless otherwise stated the systems were used at ambient temperature without hot rolling

3.1.4 Clay

The clay used for these adsorption experiments was a Wyoming montmorillonite obtained from the Source Clay Minerals Repository at the University of Missouri. The clay is known as SWy-1 [13] and contains calcium and sodium as the main exchange cations. In Table 4.2, the cation exchange chemistry of the clay is summarised. A procedure for replacing these cations with potassium is outlined in the next section.

Sodium	Calcium	Potassium	Magnesium	CEC (meq/100g)
23.5	38.7	2.0	15.7	79.9

Table 4.2: The cation distribution on the montmorillonite, SWy-1.

The clay sample contained some quartz which was removed by a sedimentation method described here. Approximately 2 g of SWy-1 was dispersed in 100 g of de-ionised water. No attempt was made to adjust the pH. The suspension was then poured into a graduated cylinder and left to sediment. After 4 hours the top 5 cm contained only particles of less than 2 μm equivalent spherical diameter [14]. This part of the suspension was carefully removed using a pipette and concentrated by centrifugation at 9,000 rpm for 30 minutes in a Europa 24M centrifuge. Then the clay gel was stored in a desiccator in the refrigerator to prevent bacterial formation.

Self supporting clay (SSC) films with a thickness $\approx 10 \mu\text{m}$ were prepared using samples of the SWy-1 gel. Some gel was smeared on polyethylene sheet using a glass rod and dried under ambient conditions until it could be removed from the plastic backing. These films were stored in sealed glass jars until required for experiments. This method of SSC film preparation was altered for use in the Clay Membrane Cell discussed in Chapter 5.

3.1.5 Ion Exchange

Approximately 700 ml of a 2 wt% SWy-1 dispersion was prepared by agitating some of the clay gel in de-ionised water overnight. To this dispersion 1400 ml of molar

potassium chloride was added and the mixture rolled for 16 hours. Then the clay fraction was separated by centrifugation and washed twice more with potassium chloride. The salt concentration was reduced by dialysis to a conductivity of $20 \mu\text{S cm}^{-1}$. After concentrating the SWy-1 clay by centrifugation, the gel was stored in the refrigerator. The extent of potassium ion exchange was determined by displacement with tetramethylammonium bromide and detected using ion chromatography. By this method of analysis, the exchange sites were found to be 90 % converted to the potassium form.

3.1.6 Shale

Pierre 2 is a cretaceous shale supplied by Terratek from an outcrop in South Dakota. This has a high montmorillonite content with sodium and calcium as the main exchangeable cations. Mineralogical analysis data are given in Table 4.3. The moisture content of the shale is approximately 20 wt%.

Mineral	wt %	Mineral	wt %
Quartz	32	Pyrite	2
Smectite	35	Illite	16
Kaolinite	2	Illite-smectite	9

Table 4.3: The mineralogy of Pierre 2 shale.

Oxford Clay is a Jurassic shale obtained from an open-cast mined quarry near Bedford, England. This shale has a water content around 22 wt% and its mineralogy is outlined in Table 4.4.

Mineral	wt %	Mineral	wt %
Quartz	32	K-Feldspar	7
Pyrite	5	Gypsum	1
Illite-smectite	17	Illite	30
Kaolinite	18	Chlorite	7

Table 4.4: The mineralogy of Oxford Clay.

3.1.7 Clay-polyglycol complexes

Clay-polyglycol pastes were prepared by mixing 6 g of a 5% polyglycol solution with 3 g of raw SWy-1. These mixtures were stored in glass jars and analysed by XRD after 1 and 16 hour intervals.

For some experiments, 50 g of a 2% clay-water dispersion (prepared from the gel) was mixed with 10 g of a polymer solution and 40 g of de-ionised water. These mixtures were rolled for 16 hours and the SWy-1 polyglycol mixture made into a SSC film.

In some experiments, ≈ 0.02 g of an untreated SWy-1 film was dipped into 10 g of a solution of the polyglycols in water or molar salt for a period of 16 hours. Then they were removed from the solution and dried at room temperature overnight before analysis.

3.2 Adsorption studies

3.2.1 Glassware

Borosilicate bottles were used in all the adsorption experiments. Care was taken that no polymer other than a polyglycol came into contact with the glassware. Between experiments the bottles were soaked in dilute nitric acid, washed several times with de-ionised water and dried in the oven at 105 °C. The surface tension of de-ionised water from some of these bottles was measured as a check for cleanliness, before they were used for adsorption studies.

3.2.2 Adsorption isotherms

Adsorption isotherms at 21 °C were obtained for some of the polyglycols on natural and potassium exchanged montmorillonite from deionised water and from 7% KCl solution. Two methods were used:

- Polyglycol solution was added to a 2 wt% suspension of clay and the mixture allowed to equilibrate with gentle agitation for 16 hours. Clear supernatant was then obtained by sedimentation or centrifugation and the equilibrium concentration of polyglycol measured by gel permeation chromatography and FTIR.
- Air-dry clay films were immersed in a test solution and the amount of adsorbed polyglycol measured directly by Fourier Transform Infrared Spectroscopy (FTIR).

3.2.3 GPC analysis

GPC analysis was carried out by the Manchester Polymer Centre using a chromatograph with a PLGel 30 cm, 50 nm mixed bed column and a Waters 410 Differential Refractometer detector. The mobile phase was tetrahydrofuran (THF) pumped at $1 \text{ cm}^3/\text{min}$ through the column operated at ambient temperature. The refractometer was thermostatted at $35 \text{ }^\circ\text{C}$.

Calibration of the system for quantitative analysis was done using neat polyglycols from SCR diluted with THF. The injection volume was $100 \text{ }\mu\text{l}$ and the peak area was calculated using computer software. An example of a calibration curve for peg 600 (a field glycol) is given in Figure 4.3.

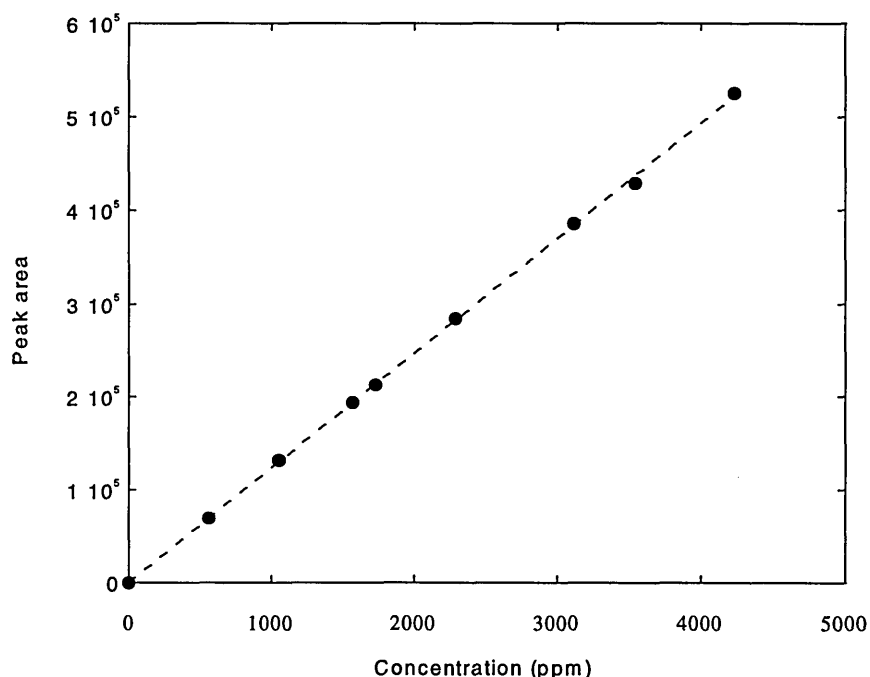


Figure 4.3: A calibration curve for peg 600.

For molecular weight determination, monodispersed polyethylene glycol molecules were used to calibrate the column. One problem with GPC analysis of polyglycol solutions containing potassium chloride is that both the polyglycol and the potassium chloride have the same retention time. To overcome this difficulty the salt was removed before analysis of the solutions by the following method: first a sample of the neat polyglycol was freeze-dried to measure the percentage of water present. Then a sample (5 to 10 g) of each polyglycol solution taken from adsorption experiments at SCR was freeze-fried overnight and the solid residue added to a known weight (10 g) of THF. The THF dissolved the polyglycol but left the

potassium chloride behind. These solutions were then injected on the column and the glycol concentrations determined.

Three separate analyses of one solution showed the variation to be ± 100 ppm. For the weight of clay used in the adsorption studies this error in the polymer concentration would cause a $\pm 1\%$ uncertainty in the final adsorbed amount.

3.2.4 Infrared spectroscopy

Transmission infrared spectra of clay films were obtained using a Nicolet 5DXC FTIR spectrometer. For quantitative analysis of polyglycols, calibration samples were made using mixtures containing known weights of clay, polyglycol and water. To construct the calibration curves and analyse the experimental samples, the area of a polyglycol absorption band at approximately 1450 cm^{-1} (asymmetric bending mode for-CH₃) was ratioed to the area of the montmorillonite lattice O-H stretch at 3630 cm^{-1} (see Figure 4.11) [15]. The calibration was approximately linear over the region of interest and ratioing the polyglycol band to the lattice absorption removed the need to know the thickness of the clay layer in the infrared beam. An example of a calibration curve is given in Figure 4.4. In cases where the SSC films soaked in solution no longer were self supporting, the films were floated onto a silicon wafer similar to one used in XRD. The silicon wafer was transparent to infrared radiation over the region of interest [16].

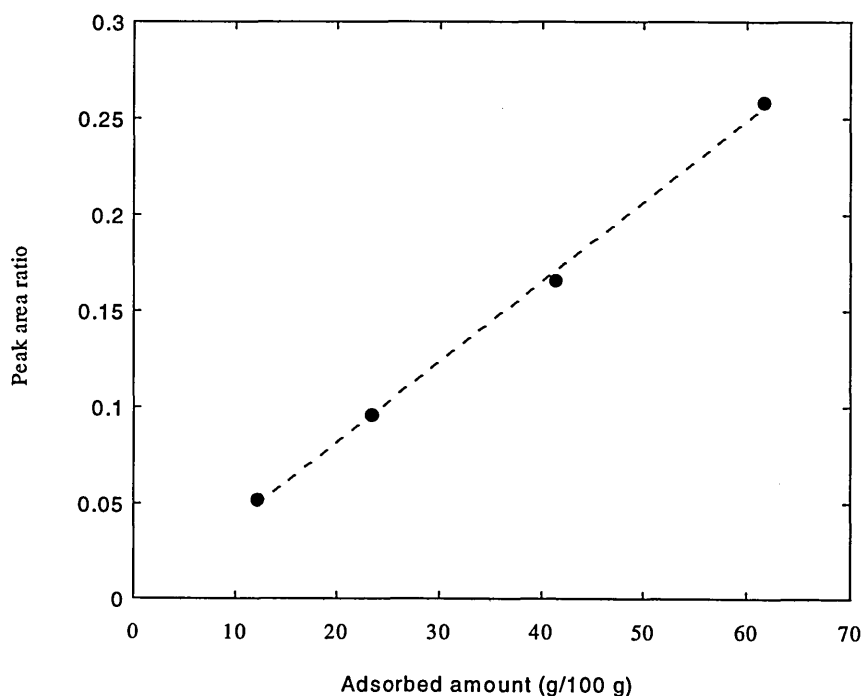


Figure 4.4: A calibration curve for peg 600

Transmission spectra of polymer solutions were collected by pouring the solution into a cylindrical cell with a fixed path length.

3.2.5 X-ray diffraction

A computer-controlled Siemens D500 X-ray diffractometer was used for these studies. The incident radiation was from a Cu $K_{\alpha 1}$ emission, with a nickel filter and had a wavelength of $\approx 1.54 \text{ \AA}$ [17]. The samples were scanned over the 2θ range of 2 to 12° , in steps of 0.01θ , which corresponds to a d spacing interval of 40 to 8 \AA .

A new sample holder was designed for the analysis of wet pastes. The clay-glycol paste was smeared on a silicon slide and covered with a piece of X-ray transparent-Melinex (ICI) having a thickness of $12 \mu\text{m}$. A cover containing a Melinex window represented in Figure 4.5 was then put on the sample holder to prevent the paste drying out. For XRD analysis, films were placed on a silicon slide and covered with Melinex which was taped to the sample holder. Securing the film like this prevented it deforming when water was used to hydrate it. During hydration water was dropped at the edges of the melinex and was drawn in by capillary forces to cover the clay film. Five minutes after adding the water the basal spacing had stabilised.

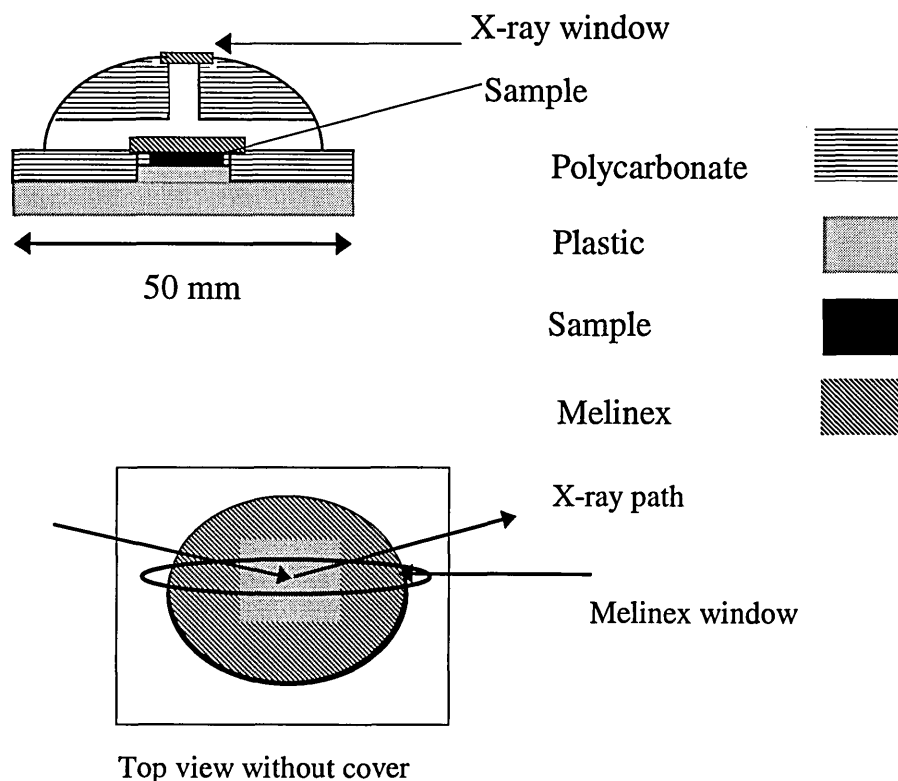


Figure 4.5: Sample holder designed for working with wet paste and hydrated clay films.

Tests showed that pastes prepared with calcium chloride solution and SWy-1 and water did not dry when mounted in the XRD sample holder during the fifteen minute scan time. When the pastes were scanned 16 hours after preparation, the peak positions had not changed and the intensities were only slightly higher. For all samples tested with polyglycols present, the measured positions varied $\pm 0.2 \text{ \AA}$ between consecutive tests.

In experiments where the water activity of the samples were controlled, a humidity cell [18] was attached to the sample holder. To verify the presence of the polyglycol the clay-polymer mixtures were dried for 24 hours over phosphorous pentoxide in the humidity cell and then analysed.

3.3 Molecular simulations

The simulations were performed by Dr Edo Boek, Schlumberger Cambridge Research, who used a commercially available molecular modelling package running on Silicon Graphics work stations. Monte Carlo, energy minimisation and molecular dynamics methods were usually carried out sequentially in that order. During the Monte Carlo simulations, the organic compounds and water are sorbed within the clay interlayers of a periodic three-dimensional simulation cell, whose cell dimensions are kept fixed. Following energy minimisation to remove any spurious strain, molecular dynamics was performed during which the dimensions of the simulation cell and in particular the clay layer spacing relax to their equilibrium values. This typically occurred within about 25 picoseconds (25,000 integration time steps) [20]. It is important to note at this stage that due to limitations in the computing code the adsorbed counter-ions were forced to remain close to the montmorillonite surface during the adsorption of glycol. Therefore no comment can be made on the position of these ions as the surface coverage increases. Also isomorphic substitutions were only present in the octahedral layers; resulting in uniform Coulombic forces at the surface.

3.4 Shale dispersion tests

Outer surfaces of a piece of the shale were scraped to remove any Hy-vis preserving fluid remaining from the storage tank. The shale was then crushed in a mechanical grinder and the 2-4 mm sized fraction selected by sieving. Sometimes two large pieces of shale were used to generate the cuttings. In this case these were not mixed and are referred to as Batch 1 and Batch 2 in the results section.

3.4.1 Closed-bottle test method for mechanistic studies

These experiments were carried out using 20 g of Oxford clay or Pierre shale cuttings, which had been sized 2 to 4 mm. This shale was placed in bottles containing 200 g of polymer solution, and then rolled at 30 rpm at ambient temperature. After the 4.5 hr or 7 hr test time, the remaining cuttings were recovered on 250 micron mesh sieves and dried for 24 hr at 105 °C.

3.4.2 Slake Durability (Vole cage) tests.

A known weight of approximately 30 g of sized shale cuttings were placed in the cages (1 mm mesh covering) and the container immersed in a 300 g sample of mud. Tests were run under ambient conditions for a period of 18 hr for Oxford shale clay. The cages were then washed gently and placed in an oven set at 105 °C for at least 12 hr. Dried shale weights were noted and recovery levels expressed as a percentage of the equivalent dried weights of cuttings added to each cage.

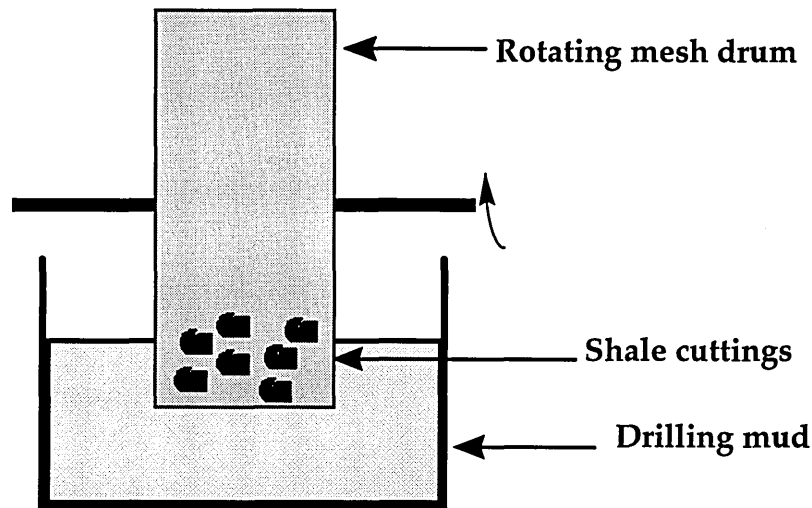


Figure 4.6: A schematic of the vol cage tests

3.5 Bulk hardness tests

The shale is treated for this test by soaking 30 g of sized cuttings in 300 g of mud for 10 minutes. All of the shale is then poured into the cuttings hardness tester [20] and the torque required to rotate the top platen measured as the cuttings are extruded.

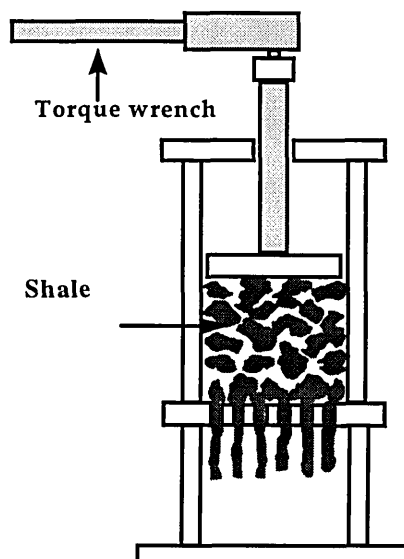


Figure 4.7: A schematic of the cuttings hardness tester.

4. Results and discussion

The purpose of this section is to present the data obtained from X-ray diffraction, Fourier transform infrared spectroscopy and molecular modelling activities. Many studies of the interaction of glycols with montmorillonite have been carried out by others and parallels with the present work will be drawn where possible. The ultimate aim is to provide an insight into the design of better glycol based shale inhibitors detailed in Section 5.3.

4.1 Stabilisation of montmorillonite-glycol-water complexes

As already outlined in Section 2.1 the separation of the clay layers depends on the ability of the clay to swell when in contact with water. The use of clay-water pastes in the examination of such expansion has been well documented in the work of Low [21]. In Figure 4.8 X-ray traces are presented for montmorillonite-water pastes with and without glycol added. The upper limit on the measured basal spacing is 40 Å representing approximately 10 layers of water in the interlamellar region. Such a build up of water would qualify as a system with osmotic swelling [22] and will be classed here as non-ordered. This does not discount the possibility of a large distribution of basal spacing values below 40 Å.

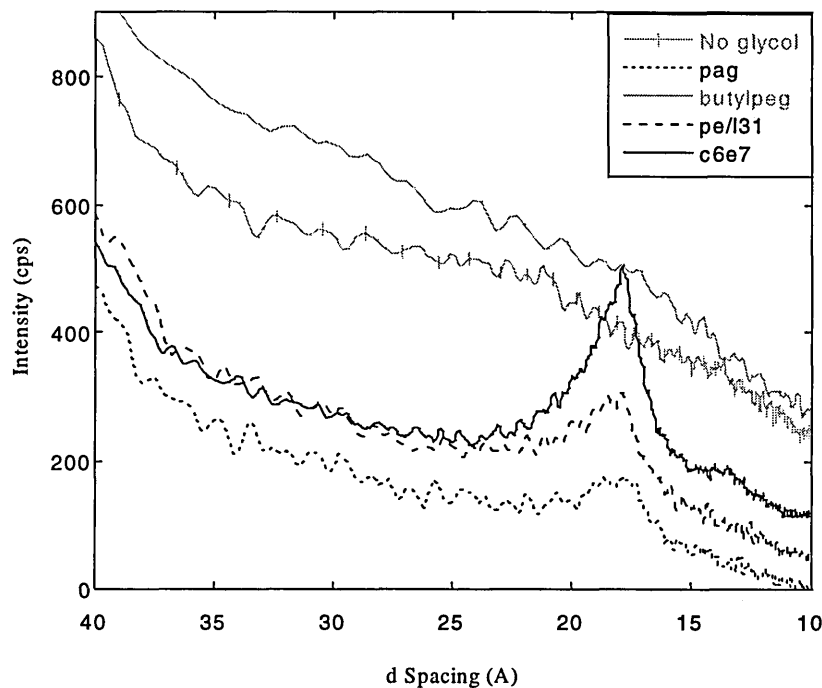


Figure 4.8: XRD traces for polyglycol-water-SWy-1 pastes

The traces for the non-glycolated paste and that with butyl-peg added are similar indicating a disordered system. For pastes with 5 wt% solutions of pag, L31 and C₆E₇ added, peaks are evident at $17.8 \pm 0.2 \text{ \AA}$. The formation of a 17.8 \AA montmorillonite-glycol complex was first shown by Bradley [23] to represent a bilayer of ethylene glycol ($\approx 8 \text{ \AA}$) in the interlamellar region; this is now an accepted view point. Despite changes in sample loading the peak formed for the pag complex remained broader than those formed with C₆E₇ and L31 indicating a wider distribution in basal spacing for the pag system. Further experiments with peg having molecular weights of 200, 600 and 1,000 g mol^{-1} gave similar non-ordered traces as observed for the butyl-peg systems.

One conclusion that can be made from this initial data is that glycols that contain hydrophobic segments are capable of ordering montmorillonite under these experimental conditions whereas completely hydrophilic glycols do not have this capacity.

This was an interesting discovery and it was decided to determine if there was an optimum concentration at which this ordering was induced in the glycol-clay complexes. Experiments were switched to self supporting clay films made from SWy-1 dispersions which had been treated with pag. The films were allowed to air dry and the basal spacing was measured before and after hydration. These X-ray traces are presented in Figure 4.9.

When no pag or 0.05 wt% pag was added to the SWy-1 dispersion the resulting air dried films had basal spacings of 14.8 Å. These films dispersed when water was added to their surface. Drying the non glycolated film in the humidity cell over phosphorous pentoxide for 16 hr reduced the basal spacing from 14.8 to 11.5 Å. No such reduction was observed for the film that was prepared using 0.05 wt% polymer confirming the presence of adsorbed glycol. Clay which had been treated with 0.2 wt% pag gave a broad peak which spanned the 14.8 and 17.8 Å spacings (Figure 4.9c). The appearance of distributions of interlayer spacings in glycol clay complexes is in agreement with work by Wu and Lerner, [24]. In their studies they exposed anhydrous Na-montmorillonite to polyethylene oxide of molecular weight 100,000 g mol⁻¹. At intermediate loadings (22.5 g/100g clay) their XRD traces showed broad peaks. On mixing composites with 13.6 Å and 17.7 Å basal spacings and annealing them at 100 °C a broad peak was observed in resulting the XRD trace. They concluded that the intercalates with intermediate loading contained a homogenous distribution of these expanded galleries rather than a uniform basal spacing. In the present study the broad peak switched to a sharp 17.8 Å (Figure 4.9 c(h)) on the addition of water. Either the material containing one layer of glycol had swollen osmotically producing the stable 17.8 Å complex or the pag had redistributed itself in the film.

The complex formed in the presence of 5.0 wt% pag remained stable at 17.8 Å on hydration. Aranda and Ruiz-Hitzky [25] proposed that the 17.8 Å complex contains a polyglycol molecule in a helical conformation which would be in keeping with its shape in concentrated salt solutions. Their interpretation relied on the increased electrical conductivity of clay films loaded with glycol leading them to propose that the cations (Na or Ca) were held centrally in the polymer helix allowing them to move more swiftly through the clay gallery. This suggestion is disputed here, since polymers having localised or distributed hydrophobicity, would be expected to have different helical sizes; in these studies they have been found to give the same basal spacing.

Once a bilayer of pag was present in the interlamellar region of the clay layer the clay films would not disperse when immersed in deionised water. Experiments were carried out in which the untreated SSC films were soaked in glycol solution. It is interesting to note that when untreated clay films were soaked in 5 wt% pag solutions they remained stable and gave a 17.8 Å spacing while films immersed in 0.05 wt% pag dispersed. The order of this second type of experiment is more in keeping with shale

dispersion tests in which the shale is exposed to the polymer and deionised water at the same time. Results from these shale tests will be presented in Section 5.1, Chapter 4.

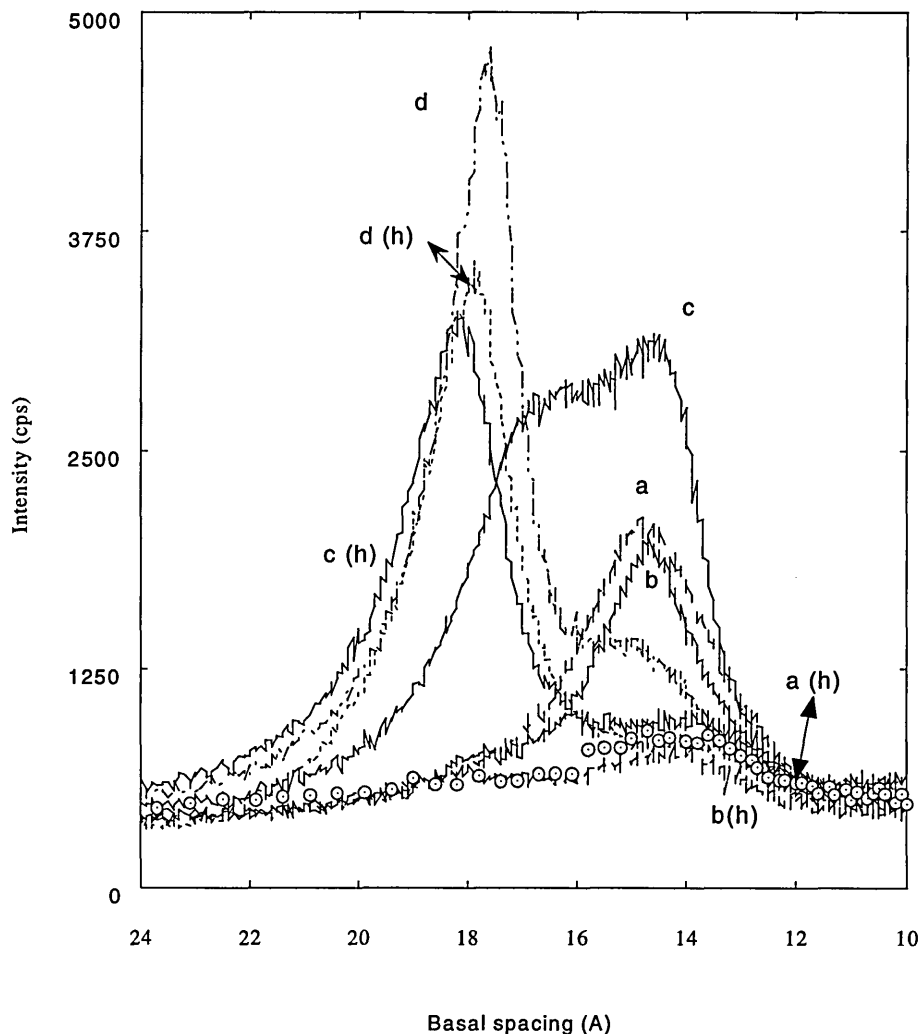


Figure 4.9: XRD traces of pag-SWy-1 films (a) non glycolated, (b) 0.05 wt%, (c) 0.2 wt%, (d) 5.0 wt%. The initial concentration of polymer added to the clay dispersion varies between 0.05% and 5.0 wt% and h indicates a film in contact with water.

The evolution of the basal spacing with the adsorbed amount up to oilfield concentrations was examined to check for differences in behaviour of hydrophilic and hydrophobic glycol. As a first step in this process the adsorbed amounts were measured and data are presented in the next section.

4.2 Adsorption Isotherms

Adsorbed amounts were determined by the solution depletion method using GPC, or by FTIR analysis of the clay-glycol mixtures

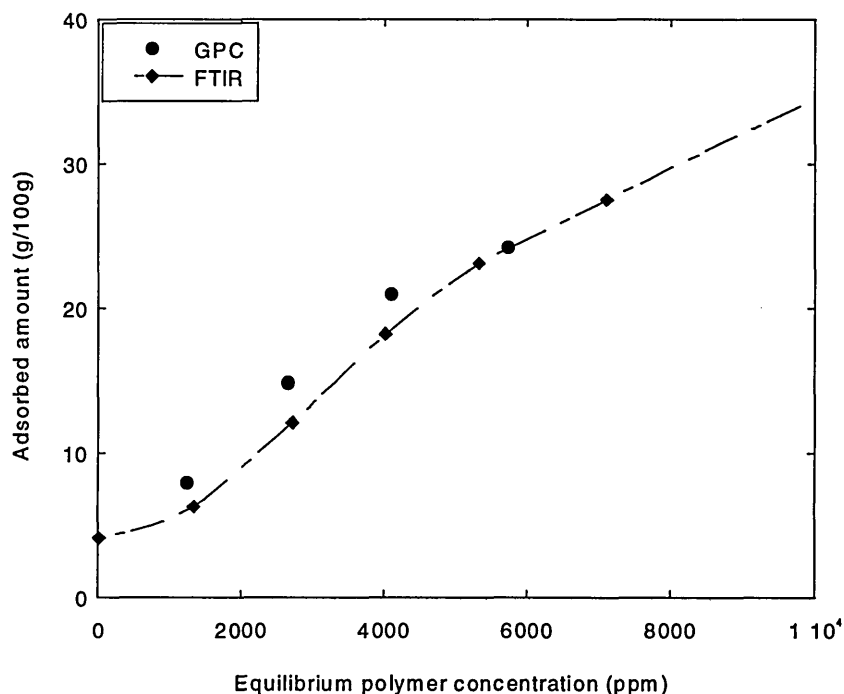


Figure 4.10: Adsorbed amounts determined for butyl-peg on SWy-1 from water by GPC and FTIR.

In most cases the data collected by solution depletion method followed by GPC of the solution gave higher values for the adsorbed amounts than those obtained by FTIR on the glycol loaded SSC films. This would suggest that the glycol is taken out of solution with the clay on centrifugation.. However this is not picked up by the analysis of the SSC films made from the treated clay in so far as the FTIR measurements give lower adsorbed amounts (see Figure 4.10). Nevertheless because of the expense incurred by the off site GPC analysis in house FTIR was relied upon for further studies.

In Figure 4.11 the transmission spectra of clay films with and without pag are presented. Important regions of the spectra are listed below;

- Montmorillonite lattice (octahedral layer) O-H stretch at 3630 cm^{-1} ,
- $\nu_s(\text{OH})$ of a hydrogen bonded glycol at $3418\text{-}3370\text{ cm}^{-1}$ overshadowed by water adsorbed on the clay surface,
- from the glycol $\nu_s(\text{CH}_3) + \nu_s(\text{CH}_2)$ at 2870 cm^{-1} . The sloping background in this region of the spectrum rendered this peak unsuitable for calibration purposes.

As the adsorbed amount increased the relative intensities of the glycol to clay peak increased as expected. The adsorption of polyglycols on montmorillonite has been studied by Parfitt and Greenland [26], Breen *et al* [27], and Zhao *et al* [28]. They have concluded that the energy of adsorption is similar to levels due to van der

Waals adsorption forces. As the molecular weight of the glycol increases the adsorption becomes more favourable as the net entropy due to water desorption increases. The ether oxygens in the polyethylene glycols are hydrogen bonded to the water on the clay surface and to the hydration shells of the cation.

The adsorption isotherm for the peg 600 is higher affinity in nature than those for pag, C₆E₇ and butyl-peg. The initial slope of the adsorption isotherms is affected by the affinity of the glycol for the clay surface as well as its conformation in solution. Indeed Parfitt and Greenland show a change in isotherm shape when changing from peg 400 to peg 600 similar to the one shown in Figure 4.12 going from pag to peg 600. Overall the adsorption levels are similar to those reported by Parfitt and Greenland, for pure calcium clay but almost twice the levels reported by Burchill *et al* [9] for sodium clay. The relative amounts of the sodium and calcium on the natural SWy-1 (Table 4.2) will affect the adsorption levels. Previous studies have shown that the adsorbed amount depends on the resident cation on the clay surface with the adsorption on the potassium exchanged clay reaching plateau values of 137 mg/g for potassium, and 154 mg/g for sodium (Kellomäki *et al.* [15]). The work by Parfitt and Greenland also backs up this trend [26].

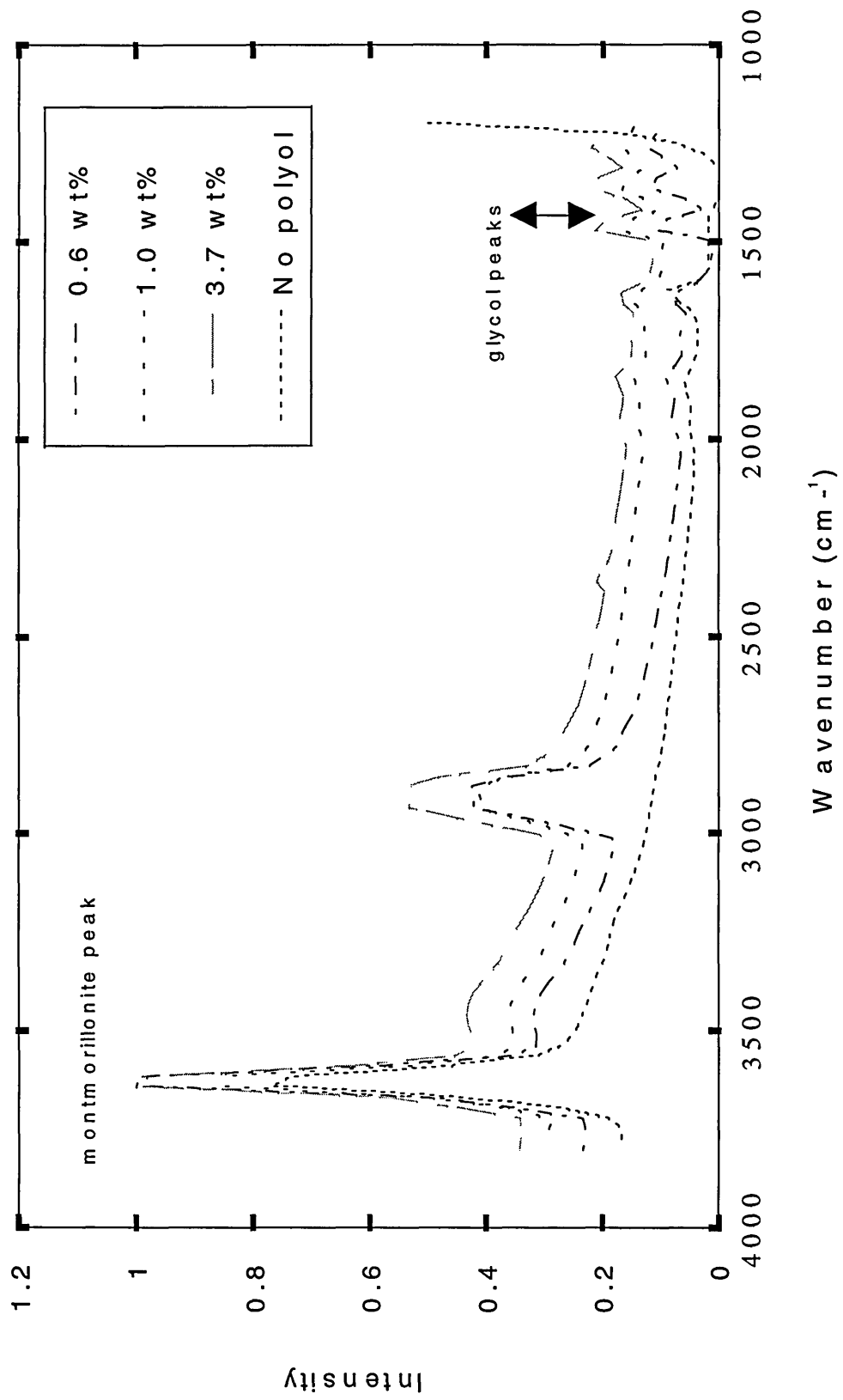


Figure 4.11: FTIR spectra showing untreated SWy-1 and SWy-1 loaded with pag

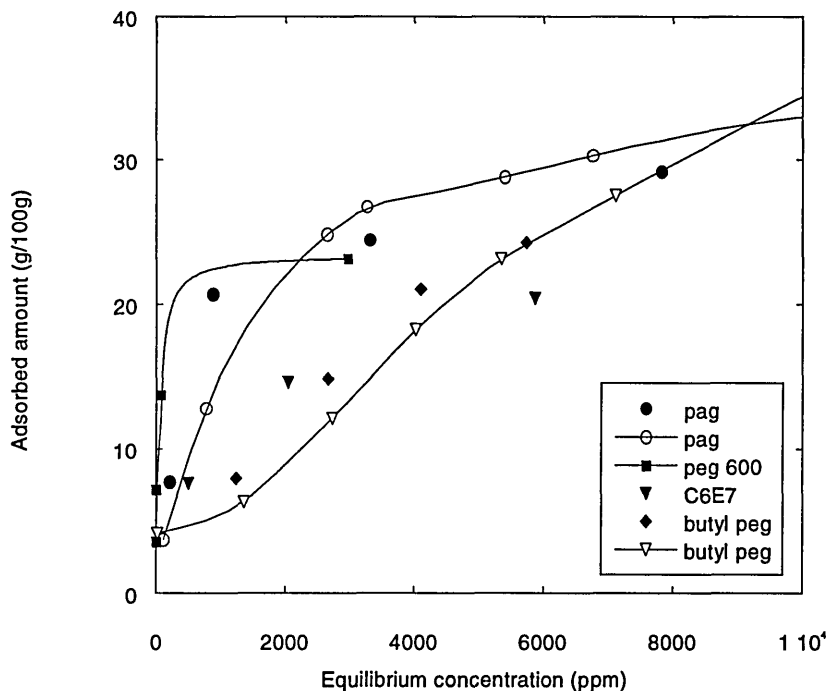


Figure 4.12: The adsorption behavior of some glycols on SWy-1 from water. All of the data was collected by GPC except for the pag and butyl-peg curves denoted by O and ∇ respectively. These were collected by FTIR.

The discrepancy could also be due to the experimental techniques. It had been noted by Parfitt and Greenland that 80 % of peg of molecular weight 300 g mol^{-1} could be removed from the clay surface by washing with deionised water. This washing procedure was not carried out in this study to remain consistent with shale experiments where washing of the shale in water would have affected the recovery results.

In oilfield applications one is limited to using higher concentrations as the glycol is depleted from the mud by adsorption onto the cuttings. Therefore it was necessary to extend the isotherms to added polymer concentrations around 50,000 ppm (5 wt%) (Figure 4.13).

Clearly the adsorbed amount increases rapidly above 25 g/100g. Following the variation in the basal spacing with adsorbed amount for pag and butyl-peg it can be seen that the basal spacing does not increase further. This data is presented in Figures 4.14 and 4.15. In Figure 4.14 the evolution of the basal spacing with adsorbed amount is shown for the pag/water solutions on SWy-1. As shown in Figure 4.9 the basal spacing increases from 14.8 to 17.8 Å with a broad transition peak. Once the 17.8 Å complex is formed the clay films are stable against hydration. They do not swell in contact with deionised water and remain intact albeit softer. Since the interlamellar region does not

continue to swell with the increasing adsorbed amount it must be assumed that there is condensation occurring on the tactoid surfaces.

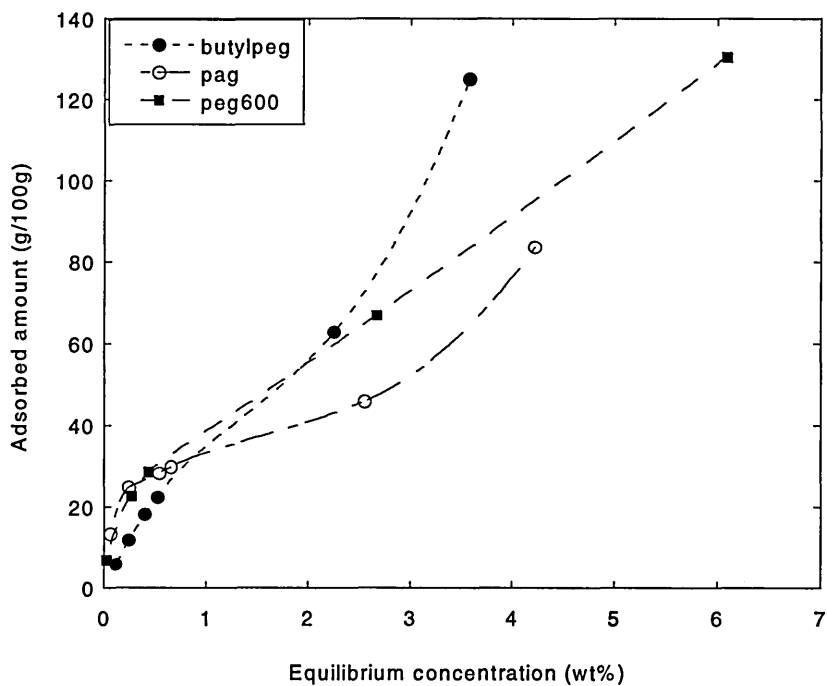


Figure 4.13: Adsorption isotherm showing the adsorption of glycol on SWy-1 from water.

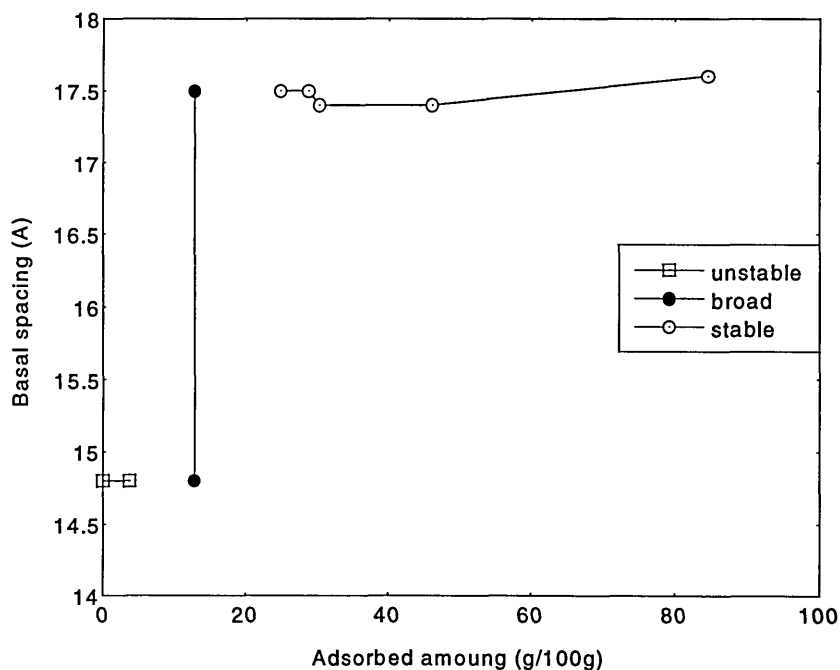


Figure 4.14: Basal spacing as a function of adsorbed amount for pag from water on SWy-1.

Similar experiments were carried out for butyl-peg and the change in basal spacing as a function of adsorbed amount is presented in Figure 4.15. When deionised water was

added to the surface of the montmorillonite-butyl-peg film, the films swelled until the film was no longer self supporting. The basal spacing of the hydrated mass was not detected in the 2 to 40 Å scan range of the XRD. The plot has a similar shape to the one for pag except for the initial reduction in basal spacing on the addition of butyl-peg.

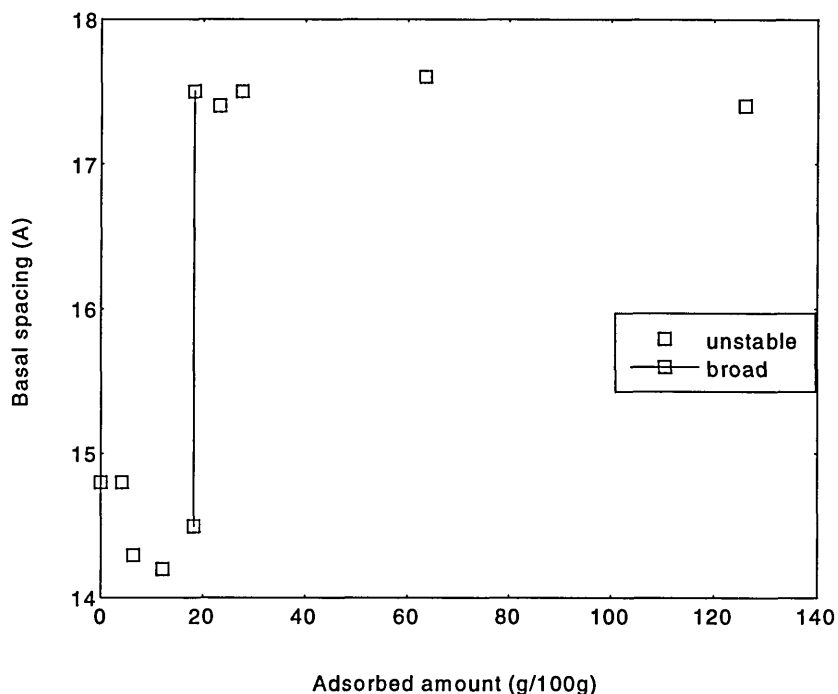


Figure 4.15: Change in basal spacing as a function of adsorbed amount for butyl-peg on SWy-1 from water.

This drop was reproducible and indicates a reduction in the amount of intercalated water and suggests the butyl-peg molecule is less bulky than the pag molecule. C₆E₇ stabilised the montmorillonite in a similar way to pag while peg 600 and butyl-peg allowed the clay film to disperse. Data for these polymers are presented in Table 4.5.

POLYMER	ADS. AMT (g/100g)	BASAL SPACING (Å)		
		AIR DRY	WET	DRIED (P ₂ O ₅)
peg 600	24	Broad	Dispersed	N/A
peg 600	85	17.8	Dispersed	17.7
C ₆ E ₇	0	14.6	Dispersed	N/A
C ₆ E ₇	55	17.5	18.2	17.0

Table 4.5: Basal spacings for peg 600 and C₆E₇ complexes with montmorillonite.

In order to improve on the stabilisation of montmorillonite with glycol it was necessary to understand why pag promoted stability over butyl-peg. Molecular simulations were used. A molecular simulation was carried out for the adsorption of pag on sodium exchanged-montmorillonite. A picture from one of these simulations is shown in Figure 4.16.

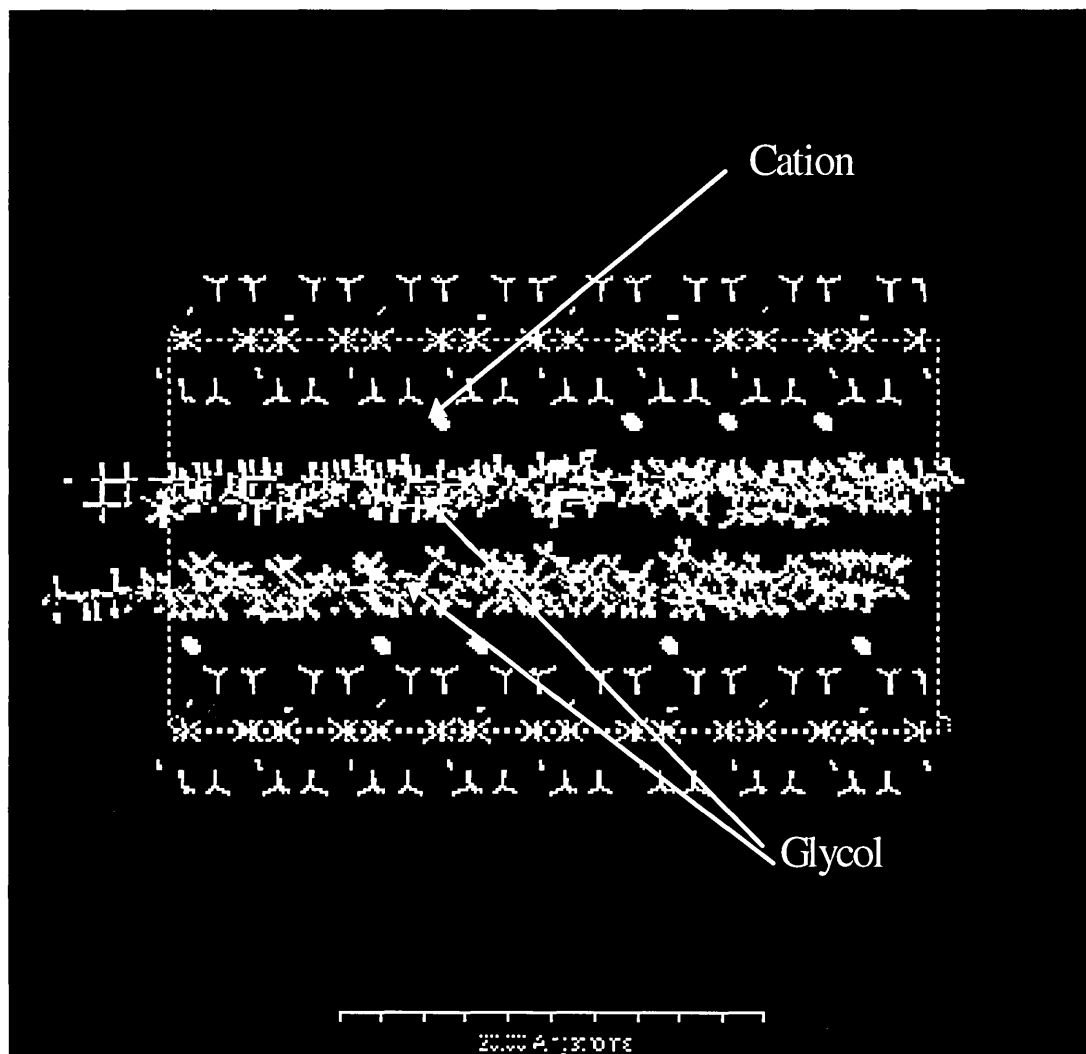


Figure 4.16: A snapshot of a simulation of the intercalation of pag into sodium montmorillonite. Simulation courtesy of Dr Boek, SCR.

The limitations of the simulation in terms of the restriction of the cation mobility together with the absence of water means that unreserved acceptance of their interpretation without the backup of experimental data such as that from XRD would not be wise. Nevertheless the simulations confirm that pag can intercalate into the interlamellar region and given the basal spacings measured by XRD it is possible to fit

a bilayer of pag in the space available. The molecules are arranged in such a way as to allow the methyl groups on opposite chains to interact.

4.3 Stabilisation of montmorillonite-glycol-salt complexes

Since salt is often added to drilling fluid it was considered appropriate to examine the effect of added salt on the ability of the glycols to stabilise montmorillonite.

4.3.1 Interactions with potassium exchanged clay

Butyl-peg was adsorbed from deionised water on potassium exchanged SWy-1 and the basal spacing monitored as a function of the adsorbed amount, (Figure 4.17).

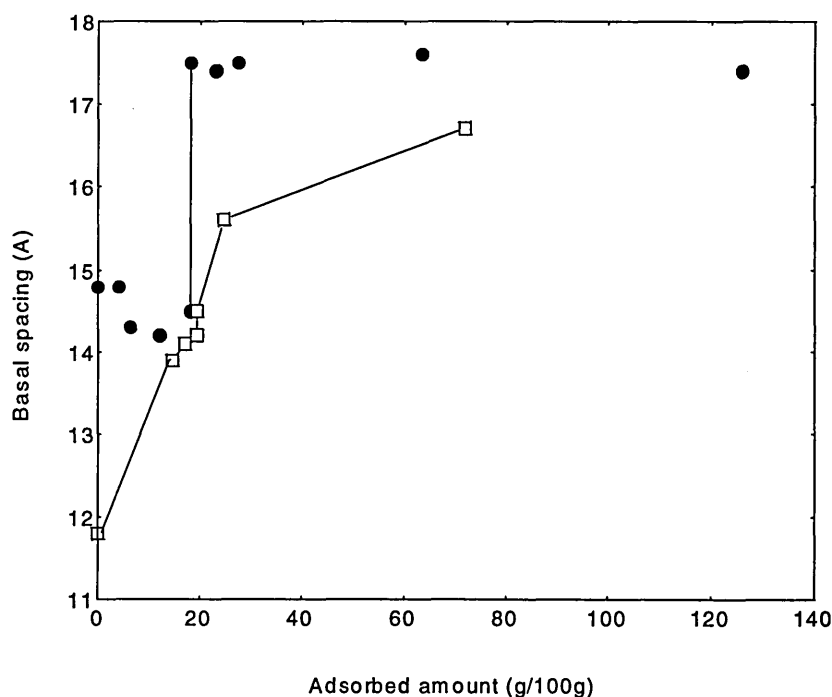


Figure 4.17 Basal spacing as a function of adsorbed amount of butyl-peg on SWy-1 ● and potassium exchanged SWy-1 □.

Potassium exchanged SWy-1 has less bound water than the mixed ion equivalent (SWy-1) and the basal spacing of the air dried clay films reflect this; 11.9 Å compared with 14.8 Å. The non-glycolated potassium exchanged SWy-1 film swelled and dispersed to a basal spacing greater than 40 Å. However once 18 g of butyl-peg had adsorbed per 100 g of potassium exchanged-SWy-1, the complex would not disperse when in contact with deionised water; it remained at the initial air dry spacing. This is in contrast to the natural SWy-1 films that dispersed regardless of the butyl-peg loading. The expansion of the interlamellar region with the adsorbed amount of butyl-peg is different for the natural and potassium exchanged clay (Figure 4.17). A broad peak

spanning 14.8 to 17.8 Å was present in the profile for the unexchanged clay separating the monolayer and bilayer spacings. In contrast this stepwise transition was absent for the potassium exchanged case and the basal spacing increased in a more gradual fashion albeit to a lower value of 16.6 Å. The conformation of the glycol molecule in the interlayer region of the potassium clay is currently unknown. A collection of basal spacing values obtained from studies on the adsorption of ethylene glycol and glycerol from vapour or neat liquid onto montmorillonites and vermiculites are presented by Bindley and Brown [14]. Generally as the charge on the unit layer increases giving a measured CEC of 0.9 to 1.19 meq/g of clay the basal spacing measured for the potassium exchanged complex is lower than that for the sodium; 14.2 *versus* 17.7. For smectites with higher layer charges and vermiculites with CEC values up to 1.90 meq/g of clay the measured basal spacings reduce, regardless of the exchange ion. These effects are more marked when glycerol is adsorbed rather than ethylene glycol. Kellomäki *et al.* [15] examined the adsorption of egme on Na, K, Mg or Ca Wyoming montmorillonite. They quoted a value of *ca.* 15.5 Å for all of the exchanged clays (previously dried at 110 °C) subjected to liquid egme or the vapour. From the studies of Burchill *et al.* [9] one can assume that the glycols interact with the hydration shells of the cation in the experiments where the clays are hydrated. However in work by Breen *et al.* [27] a pag was adsorbed onto potassium exchanged montmorillonite (Westone-L) with a CEC of 0.81 meq/g of clay. A basal spacing of 17.5 Å was recorded for the K-Westone-L. However it was easier to desorb a layer of pag to give a monolayer on heating the K-Westone-L than from the equivalent Na and Ca forms. This would suggest that the potassium bilayer complex was not as thermodynamically stable as those for the other exchange ions.

The most important observation that can be made from these experiments is that all of the ten glycols (some hydrophilic and some hydrophobic) tested on the potassium clay gave stability against hydration, when the basal spacing was approximately 14.8 Å or larger.

4.3.2 *The addition of potassium chloride*

The basal spacings of pastes prepared from mixing potassium chloride solution containing pag and SWy-1 are presented in Figure 4.18. It can be seen that the basal spacing increases as the concentration of pag in the solution increased.

However in the case of pastes the glycol loading is forced on the clay. In the wellbore situation the glycol solutions would be allowed to absorb through the shale

surface and travel into the clay interlayers. With this in mind SWy-1 films were soaked in KCl-glycol solutions; none of the montmorillonite films dispersed. After allowing them to air dry the films were analysed using XRD and FTIR for basal spacing and adsorbed amount determination. Data from for these parameters are presented in Figure 4.19 and 4.20.

In Figure 4.19 the adsorption levels of glycol onto SSC films dipped in glycol /KCl solutions are shown. The adsorption levels are similar for all the glycols but lower than those for similar experiments without salt as shown in Figure 4.13. The flocculation of clay in the presence of salt has been shown elsewhere to alter the tactoid structure and decreases the effective surface area of the clay available to polymer condensation.

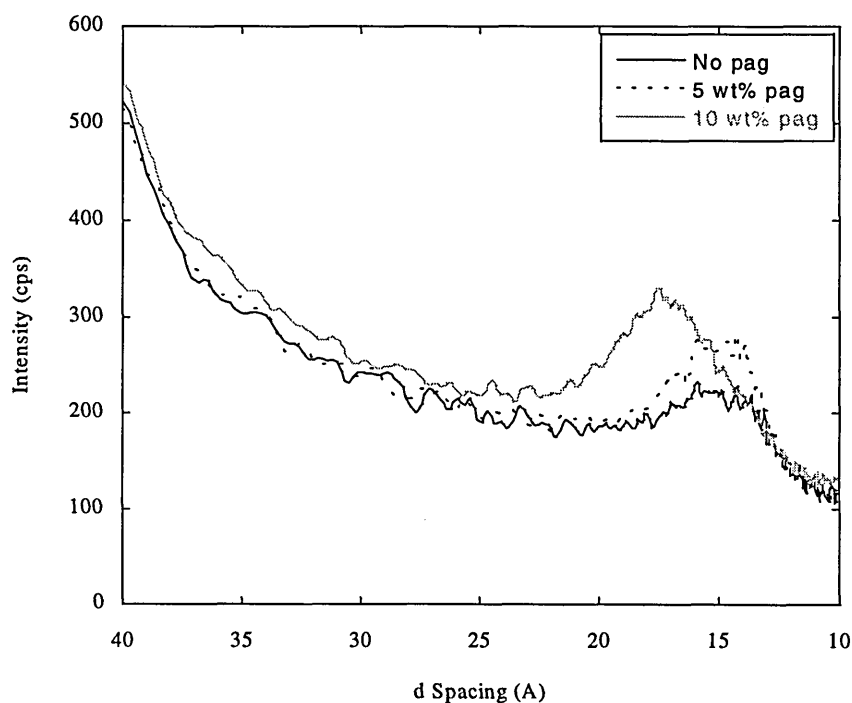


Figure 4.18: XRD traces for pag-potassium chloride-SWy-1 pastes. In all cases [KCl] was 1M.

For films treated with peg 600, pag and butyl-peg the basal spacing did not exceed 15.5 Å. Data for the pag system is presented in Figure 4.20. Once again no distinctive switch to bilayer formation (seen for the films without potassium) was noted. The profile shown in Figure 4.20 is similar to that presented in Figure 4.17 for films formed from K montmorillonite-butyl-peg dispersion. The clay films required a low loading of pag (less than that required for bilayer formation) to prevent them dispersing in deionised water. This was also true for the peg 600 and butyl-peg in this experiment and also

when adsorbed on pre-exchanged potassium montmorillonite from deionised water (Section 4.3.1).

The presence of molar potassium chloride limits the adsorption of the glycol but the stability towards redispersion of the film is awarded to any glycol-clay complex. Similarly the presence of potassium on the clay before introducing the glycol-water gave the same trend. This suggests that the resident ion on the clay exchanges in the presence of the glycol. Breen *et al.* [27] demonstrated using NMR measurements that potassium ions could displace cesium from the cesium-pag complex when a low level of pag was present. As the level of pag increased or in the complete absence of pag the displacement was not so efficient.

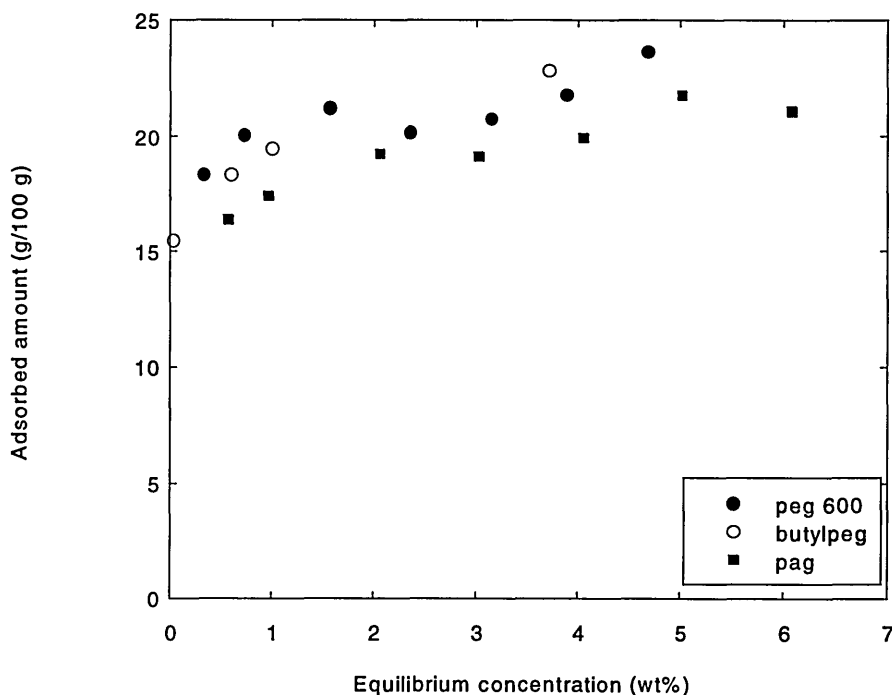


Figure 4.19: Adsorbed amounts *versus* equilibrium concentration for glycols from potassium chloride onto SWy-1. Potassium chloride was 1M.

The cesium ion is held more strongly on the clay surface than the potassium ion (Chapter 2, Section 3.1) and one could therefore postulate that the potassium ion would displace the sodium ion more readily than the cesium ion as the former is the more hydrated and less tightly held. However this is pure conjecture and no real evidence exists. In fact to the contrary, Grandjean and Laszlo [29] suggested from NMR studies of C_8E_4 adsorbed on sodium montmorillonite that the mobility of the sodium ion on the clay surface was reduced in the presence of the glycol. Reduced mobility of the cation on the clay surface would lead to reduced chances for ion exchange. In Chapter 5

Section 6.2.2 results from synchrotron experiments are presented. The basal spacing of an SWy-1 film (previously treated with peg 600-sodium chloride) was monitored after pipetting potassium chloride solution on the surface. Within minutes a peak at *ca.* 15 Å started to develop. Either a layer of peg 600 was washed from the film or some potassium was adsorbed on the SWy-1-peg 600 complex leading to reduced basal spacings.

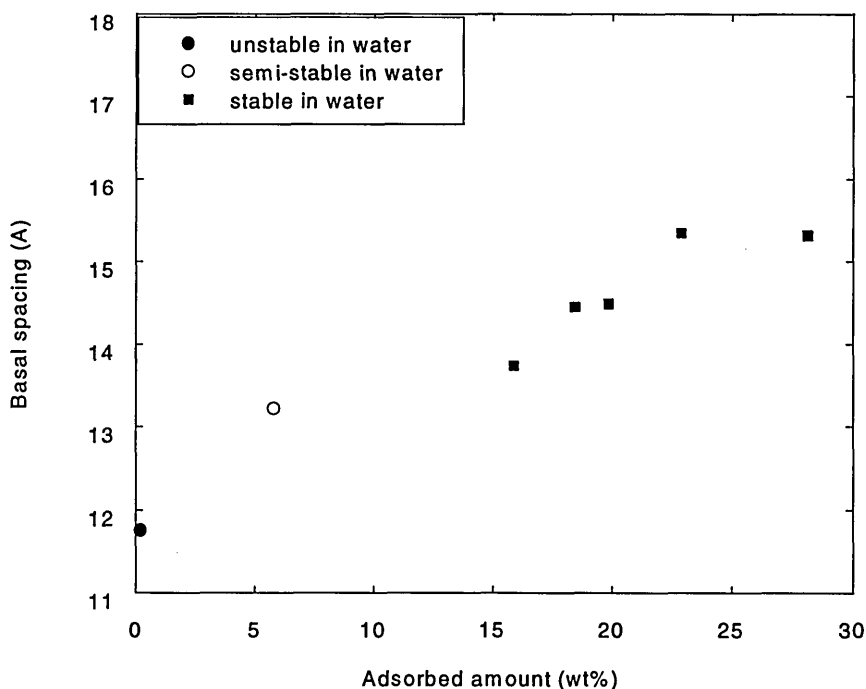


Figure 4.20: Evolution of basal spacing *versus* adsorbed amount for clay films of SWy-1 dipped in pag-KCl solutions. Potassium chloride was 1M.

4.3.3 The addition of calcium and sodium chloride

To investigate ion exchange in the presence of glycol, pastes were prepared with and without glycol. Salts added to the natural Na/Ca SWy-1 were either molar potassium chloride, sodium chloride or calcium chloride and the glycol was added at 5 wt%.

When such concentrated salt solution is added to a montmorillonite clay ion exchange takes place, the clay layers become structured and the double layers are collapsed [30]. Faisandier *et al.* [31] used small angle X-ray scattering (SAXS) to determine the separation of Na-montmorillonite layers in the suspensions slurried with 0.1, 0.5 and 1.0 M NaCl or KCl. At salt concentrations of 0.1 M NaCl or KCl there was no noticeable difference between the two systems when scanned between 5 and 500 Å. However once the molarity was increased to 0.5 M or 1 M differences in the structures of the pastes were noted. The clay slurried in NaCl was now not so homogenous with

layer spacings of *ca.* 20 Å and an estimated 20-30 layers per tactoid. These spacings were in agreement with those proposed by Slade *et al.* [32] for Wyoming montmorillonite slurried in sodium chloride. However in the study of Slade *et al.* [32] the basal spacing was found to reduce to 15.5 Å between 1 and 2.0 M salt solution. The slurries containing KCl were visually inhomogenous, had layer spacings of *ca.* 15 Å and between 70 and 80 layers per tactoid. In the present study the basal spacings for the NaCl system was 19.0 Å whereas the peak in the presence of KCl was broad spanning 11.7 to 17.2 Å. Although the molarity of the CaCl₂ solution was 1 the ionic strength was higher than that of the NaCl and KCl making it difficult to comment on the effect of the exchange ion. In oilfield applications the salt concentration used is typically 0.5 to 1.0 M. One could comment that the cation in the slurring solution has a greater effect than changing the concentration at least in this regime.

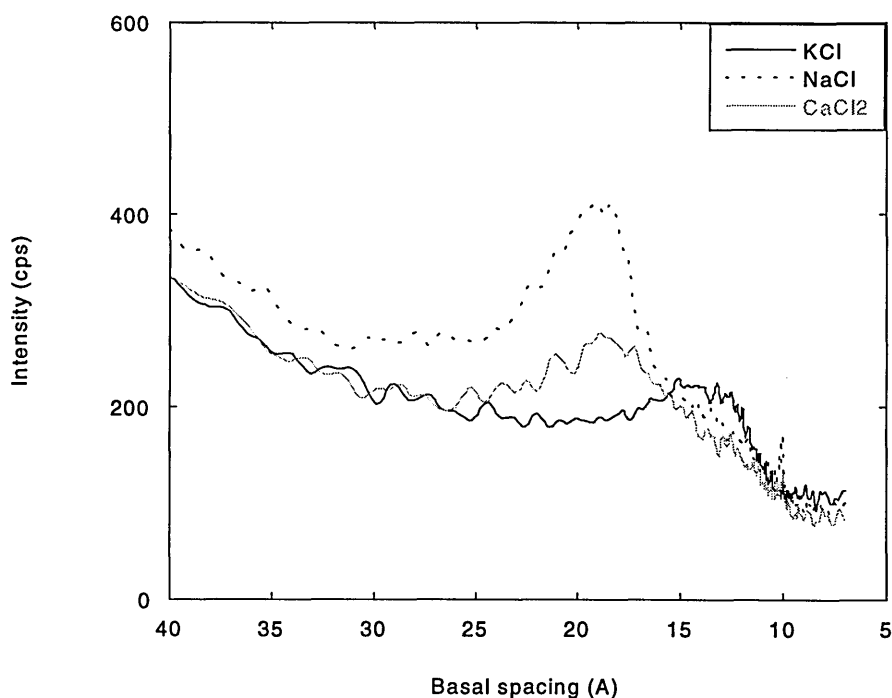


Figure 4.21: XRD traces of SWy-1-salt pastes.

Generally the diffraction peaks were sharper when glycol was added but the peaks were in similar positions to the non-glycolated equivalent (refer to Figure 4.21 and 4.22).

This suggests that when the salt solution was placed in contact with SWy-1 at the same time as the glycol the counter ion was changed.

On dilution of a paste with deionised water by a factor of 2, those containing sodium chloride and calcium chloride glycolated with butyl-peg swelled osmotically dispersing

to a basal spacing greater than 40 Å while the potassium chloride-butyl-peg pastes remained stable.

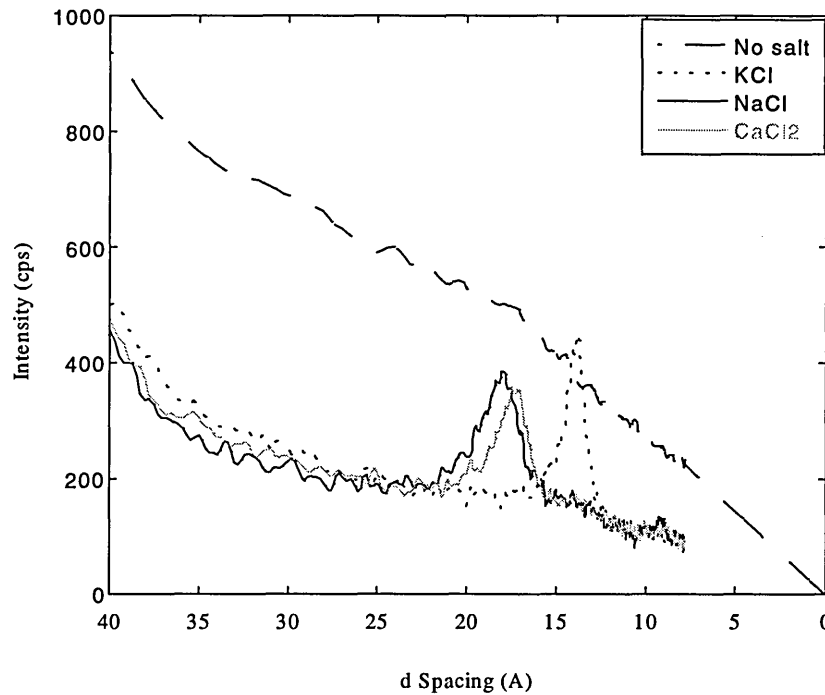


Figure 4.22: XRD traces for butyl-peg -salt-SWy-1 pastes

4.4 Summary

In this section the mechanism of stabilisation of swelling montmorillonite will be summarised with a view to its application to shale.

In the wellbore glycols can be introduced to the shale sections in waterbased muds containing freshwater or with molar NaCl, CaCl₂ or KCl present. Ultimately the purpose of these muds is to prevent the hydration and swelling of shales which leads to reduced diameter wellbores and wall erosion. The approach during the initial stages of this study has been to investigate the interaction of glycols with a research montmorillonite SWy-1. This clay was taken to represent the swelling clay in down hole shales. A range of glycols were chosen with different degrees of hydrophobicity and the following studies were carried out:

- the adsorption of glycols on mixed Na/Ca montmorillonite to determine the loading on the clay surface. X-ray diffraction was used to measure the number of layers of glycol in the interlamellar region,
- the same study carried out for the potassium exchanged form of SWy-1,
- the hydration of self supporting films containing intercalated glycol,

- the addition of calcium, sodium and potassium chlorides to SWy-1-glycol pastes and measurement of the basal spacing using X-ray diffraction.

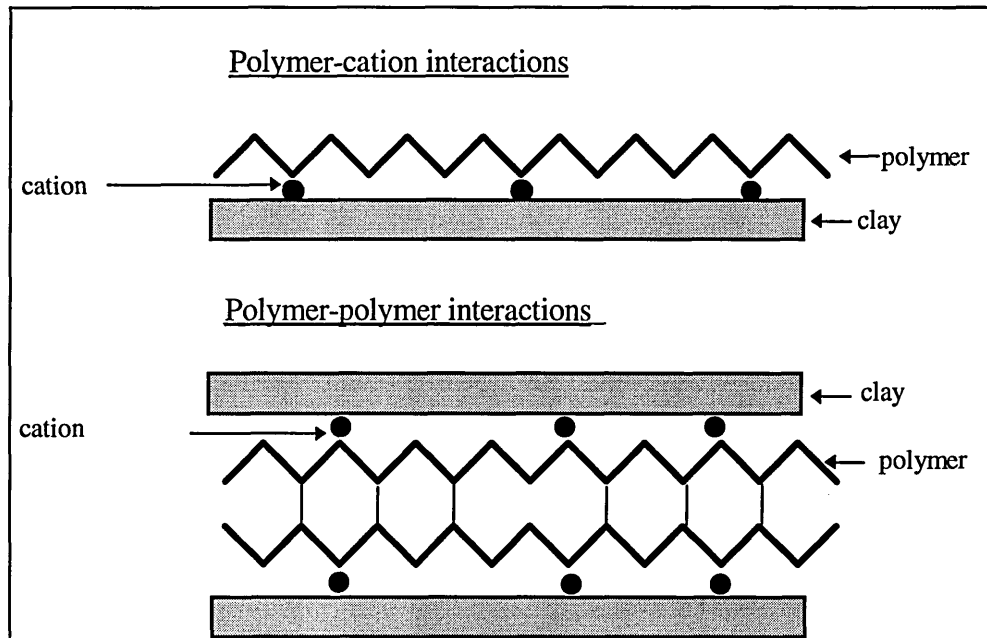


Figure 4.23: Schematic representation of the 2 possible modes of montmorillonite stabilisation by glycols.

From these experiments enough of an understanding of the hydration and swelling of montmorillonite was obtained to attempt to design shale swelling inhibitors. In summary the pertinent points are that:

- a bilayer of adsorbed glycol containing, an alky chain longer than C_4 (butyl) or pendant methyl groups, prevents the ingress of water into the interlamellar region of Na/Ca montmorillonite and the subsequent hydration of the counter ions,
- once the clay is exchanged to the potassium form a monolayer of intercalated glycol such as polyethylene glycol prevents the swelling of the clay when in contact with water,
- clay slurried in salt solutions gives distinctive basal spacings which remain unchanged when glycol is added i.e. the glycol replaces the adsorbed water

A schematic representing these findings is presented in Figure 4.23.

5. Testing the mechanism on shale

The real goal of this work was to design polyglycols as mud additives which prevented shale swelling. In Section 5 this work will be outlined. For confidentiality reasons some of the chemistries tried will not be mentioned.

5.1 Cuttings dispersion tests with freshwater

The use of shale cuttings dispersion tests to evaluate the inhibitive nature of a new chemical is not a new procedure. Results from this type of test correlate well with data obtained from shale swelling tests and shale hardness tests [33]. This test has been used previously to examine the inhibitive properties of additives other than glycols. Bailey *et al.* [34] used cuttings erosion to evaluate the inhibitive properties of polyacrylamides with different degrees of ionicity.

The test allows one to quickly screen new additives on a range of substrates. However this test should be run in conjunction with bulk hardness tests which assesses the hardness of the shale pieces after soaking them in glycol solutions.

Using data from three cuttings dispersion tests for the recovery of pag from deionised water the reproducibility of this test method was found to be ± 0.6 wt%. However when different batches of Pierre 2 shale were used, results varied by as much as 11 wt% between batches. One explanation for this could be differences in the mineralogy of individual pieces of Pierre 2 shale; to which the polyglycol/water solutions are very sensitive. Due to this sample problem only trends can be compared between sets of results obtained between different batches of shale.

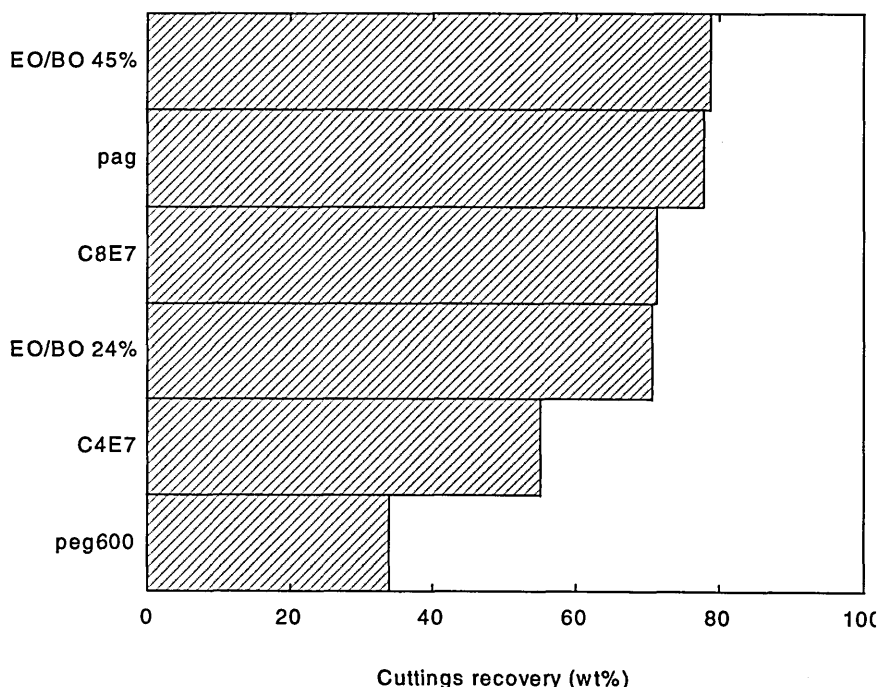


Figure 4.24 Cuttings recovery of Pierre 2 shale (Batch 2), from polyglycol/water solutions. The roll time was 4.5 hr.

The data in Figure 4.24 shows that cuttings inhibition improves when hydrophobic groups are present on the glycol chain. This suggests that shale dispersion is reduced when pag is present in the test solution, compared to just water or peg 600; this trend is in keeping with data obtained on pure Wyoming montmorillonite in this study. Increasing the length of the alkyl chain from C₄ to C₈ and increasing the butylene oxide content of the EO/BO polymer improved the recovery levels. Note here that C₄E₇ is not butyl-peg.

Cuttings recovery results from 4 hour rolling tests showed a decrease of only a few percentage points compared with the 1 hour test in the case of PAG or EO/BO (24% BO: butylene oxide) solutions, while the recovery from water or peg 600 was reduced by 40% by extending the test time. This suggests that the mechanical agitation of the cuttings has no effect on the shale treated with hydrophobic polymer after a certain time interval, while new shale surface is continuously exposed when using water or peg.

This improvement in shale recovery with the addition of an alkyl group is probably due to the formation of a bilayer of glycol in which hydrophobic groups prevent cation hydration; as suggested by XRD studies for the alkyl ethoxylate C₆E₇ (Figure 4.8). In Table 4.6, results for a range of alkyl ethoxylates are presented. These polymers form micelles when used at concentrations of 5% in water [35]. Nevertheless they would be expected to intercalate as individual entities in the interlamellar region of the clay [36].

Polyglycol	Recovery wt %
C ₄ E ₆ (butyl-peg)	20.6
C ₈ E ₇	67.1
C ₁₂ E ₉	58.0
C ₁₂ E ₁₀	62.2
C ₁₂ E ₂₃	73.3
C ₁₃ E ₁₀	60.6

Table 4.6: Cuttings recovery of Pierre 2 shale (Batch 1) from polyglycol/water solutions. Roll time was 4.5 hr. Error on the test method was ± 0.6 wt%.

Increasing the number of ethylene oxide units generally improves the inhibitive properties of the polyglycols. When increasing the alkyl chain length from dodecyl to tridecyl on E₁₀ the percentage recovery drops, which, on first analysis, conflicts with the relative performance of C₄E₇ and C₈E₇ shown in Figure 4.24.

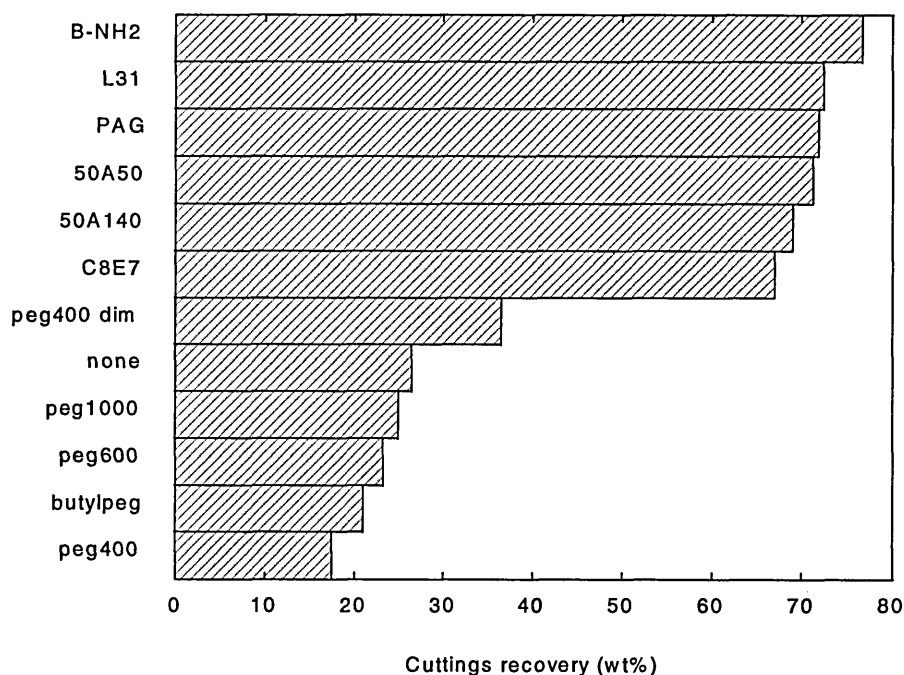


Figure 4.25 Cuttings recovery of Pierre 2 shale (Batch 1) from polyglycol/water solutions. Roll time of 4.5 hr.

No explanation for the relative performance of the polyglycols containing hydrophobic groups such as B-NH₂ and PAG is offered at present, although there appears to be an improvement in shale retention when methyl groups are attached on either end and when the alkyl chain is increased in length. Small increases in shale recovery are seen with increasing molecular weight of the peg chains.

Some of these molecules which are known to form bilayer complexes such as peg 600 actually reduce the recovery levels compared to those obtained when water only is present. Either the expansion of the clay layers causes the shale matrix to become stressed and crack or the hydrophylic glycol aids the hydration of the clay and cation surface.

The addition of 1 or 2 wt % of low molecular weight polyhydroxyalkanes to peg 600 and pag solutions, increased the shale recovery levels by a small but significant amount. Using peg 600/water solutions, the cuttings recovery increased from 34 to 41% with the addition of 2 wt% 1,2 propandiol. It is interesting that some of these additives

are good inhibitors in their own right; for example 5 wt % sorbitol in water (without polyglycol) gives a shale recovery of 52% which is greater than the value for peg 600. These polyhydroxyalkanes or alditols have a greater potential to combine with the clay because of their numerous hydroxyl groups and should diffuse into the interlayer faster because of their size. The sorption of water by polyhydroxyalkanes and polyalkylene glycols has been studied by Cohen *et al.* [37]. It was shown that in concentrated solutions polyhydroxyalkanes were associated with fewer water molecules than polyethylene glycols. In fact the steric arrangement of the adjacent hydroxyl groups could be manipulated to reduce the adsorbed water. One could therefore postulate that polyhydroxyalkanes would have less associated water than polyethylene glycols in the spacing between two clay layers.

The performance of polymers in the presence of potassium chloride and other salts was examined and considered in the next section.

5.2 Cuttings dispersion tests with salt added

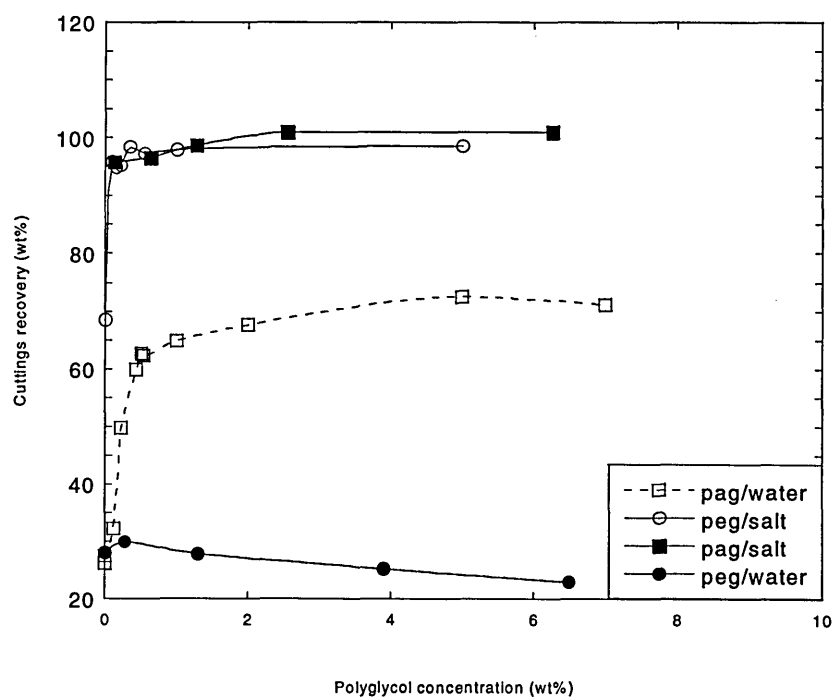


Figure 4.26: A plot of the recovery of Pierre 2 shale (Batch 1) as a function of polyglycol concentration. When molar potassium chloride is present in the test solution the shale retention is increased. 4.5 hr roll time. Error on the measurement (± 0.06 wt%).

Also noted in Figure 4.26 is the fact that shale recovery from *peg/water* solutions is seen to reduce as the concentration of *peg 600* increases. This slightly dispersive action in glycol/ de-ionised water has also been observed for other polyglycols and

glycerols of low hydrophobicity during the course of this study. The lack of inhibition in de-ionised water was examined further and confirmed by reducing the concentration of peg 600 in the test solution and monitoring the shale recovery as shown in Figure 4.26. As the peg 600 concentration was reduced, the shale retention values increased (22.9 to 29.9 ± 0.6 wt%) to reach that of water. In experiments with PAG, once a critical concentration of polymer was reached in the test solution, the cuttings recovery values remained constant around 70%. Both these concentration profiles indicate an adsorption process but, while this has a positive effect on controlling dispersion with PAG, it is detrimental in the case of peg 600.

Adding molar potassium chloride to the peg 600 and pag solutions increased the cuttings recovery to values near 100 wt%, as shown in Figure 4.26. Even at polyglycol concentrations as low as 0.1 % there was only a slight decrease in cuttings recovery values compared with those at 5 %. This indicates that, regardless of the hydrophobicity of the polymer, the potassium chloride plays the dominant role when present with any glycol.

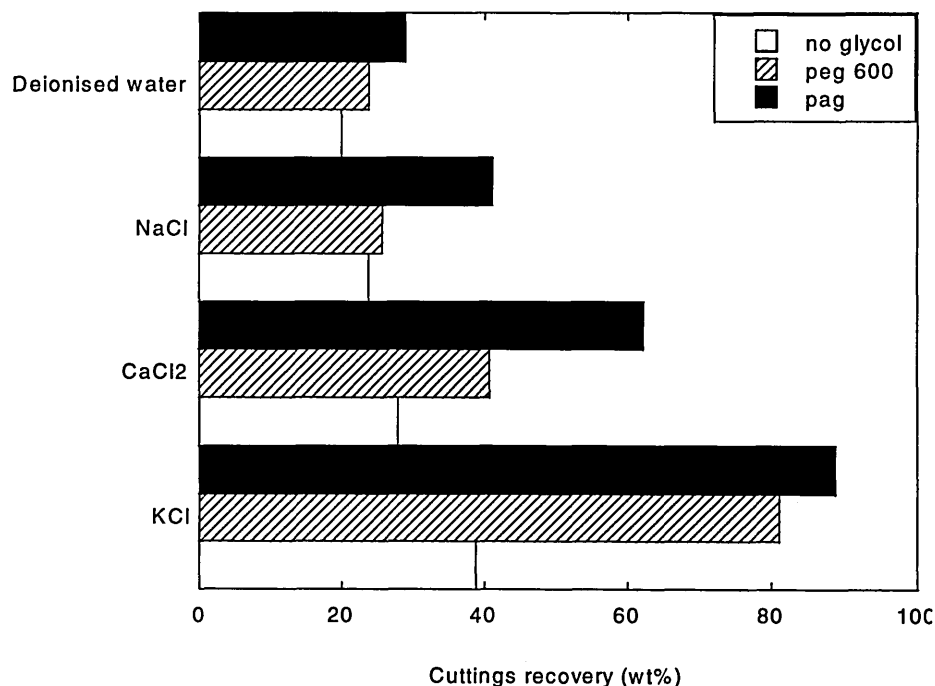


Figure 4.27: Recovery of Oxford Clay cuttings (>1 mm) from polyglycol/salt solutions.

Figure 4.27 shows that as with potassium chloride, salts such as sodium and calcium chloride alter the recovery levels in much the same order as the measured basal spacing, *i.e.* potassium chloride gives increased recovery over sodium chloride. This trend in the cuttings levels with cation type has been found by Aston and Elliott [2].

5.3 Designing a new shale dispersion inhibitor

The strategy was to combine increased interaction with the clay surface together with enhanced intermolecular interactions. It was important that the polymer remained soluble in the mud was relatively cheap and non toxic. The alditol family was chosen as the central portion for the oligomer and it was end capped with propylene oxide.

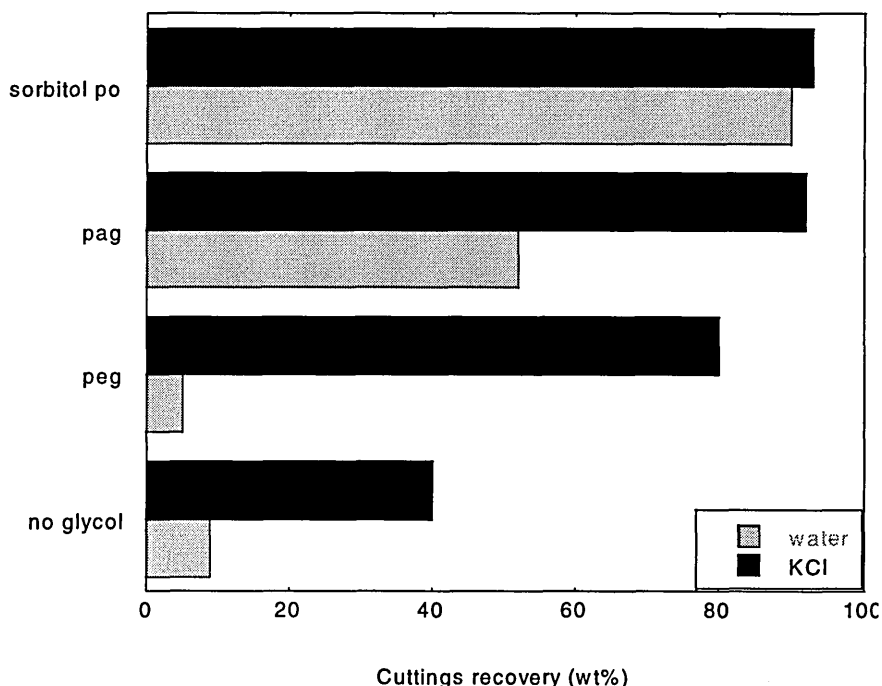


Figure 4.28: Recovery of Oxford Clay after exposure to drilling fluids.

In Figure 4.28 the performance of one of these designer molecules (sorbitol-po) can be seen to be better than pag and peg 600 in freshwater. This was also also true when sodium chloride was added. However on the addition of potassium chloride the recovery levels from all of the glycols were similar. Incidentally in keeping with the shale recovery levels from different salts the basal spacings of SWy-1 films dipped in 5 wt % solutions of sorbitol-po (with and without salt) were always 16.5 Å regardless of the cation present.

It is possible to get high levels of recovery for dispersion tests where the shale cuttings are soft. To check for such anomalies the hardness of the treated cuttings can be measured using a standard oilfield test [20]. The torque required to compact the cuttings and force the material through numerous holes in a steel plate is measured as the top platen rotates. The greater the torque values achieved the harder the cuttings. The hardness of shale soaked in glycol-freshwater muds was measured (see Figure 4.29) and the result correlated well with those from the cutting dispersion tests.

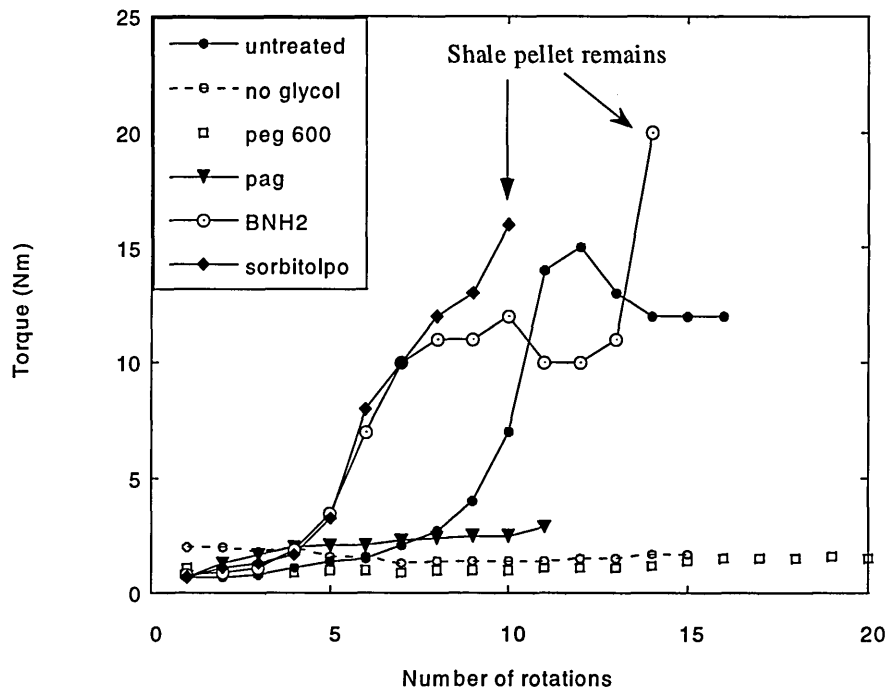


Figure 4.29: Bulk hardness of Oxford shale cuttings treated with glycol-freshwater muds.

For BNH₂ and sorbitol-po some of the cuttings were too hard to extrude and a pellet of shale remained in the bottom of the tester. This pellet of shale was found to have a water content of 22 wt% which is the value obtained for the untreated Oxford Clay.

6. Conclusions

The performance of polyglycols in the recovery of shale depends on the hydrophobic nature of the polymer, as was found in studies on pure montmorillonite substrates. The interactions between the hydrophobic portions of the polyglycols appears to be responsible for the higher levels of inhibition [38], [39] obtained with these materials in the absence of potassium chloride. When potassium chloride is present in the test solution the shale recovery is maximised even at low polymer concentrations, and the contribution from hydrophobic interactions is small compared with that from the interaction of any polyglycol with the potassium ion.

7. Future work

The performance of the new polyglycols as shale erosion inhibitors is better than that of peg 600 or pag. However more research is needed to understand the true role of the potassium ion in the presence of glycol. FTIR could be combined with neutron scattering studies to determine the hydration state of the potassium ion in the presence

and absence of glycol, and the interaction of the glycol with the hydration shell of the cation.

Comprehensive studies of the effect of molecular weight and hydrophilic-lypophilic balance on the performance of the glycol as shale inhibitors is also needed. Detecting the occurrence of ion exchange processes using Nuclear Magnetic Resonance spectroscopy would allow one to determine the true role of the salt added to the mud system. It has been documented previously that [14], [27] that glycol desorbs from the interlamellar region when the montmorillonite-glycol complexes are heated. In the wellbore temperatures can rise to greater than 100 °C and so tests should be carried out in which the shale cuttings are soaked in glycol solutions held at temperatures between 80 and 100°C.

8. References

- [1] Reid P. I., Elliott G. P., Minton R. C., Chambers B. D. and Hurt D. A.. Reduced environmental impact and improved drilling performance with water based muds containing glycols, SPE 25989, 453-463 1993.
- [2] Aston M. S. and Elliott G. P. Water based glycol drilling muds-shale inhibition mechanisms, SPE, 28818, Europec London, 1994.
- [3] Simpson J. Environmentally acceptable water-based mud can prevent shale hydration and maintain borehole stability, IADC/SPE 27496, Drilling Conference, Dallas, 1994.
- [4] Bland R., Pariseau D., Jones T. and Jachnik R. Polyglycol technology update, American Association of Drilling Engineers, Drilling Fluids Technology Conference, Houston, 1996.
- [5] Theng B. Clay polymer interactions: summary and perspectives, *Clays and Clay Minerals*, **30**, 1-10, 1982
- [6] Bland R., Smith G., Eagark P., and Van Oort E. Low salinity polyglycol water-based drilling fluids as alternatives to oil based muds, SPE/IADC 29378, Drilling Conference, Amsterdam, 1995.
- [7] Whiston C. X-ray methods, Wiley, New York, 1987.
- [8] Van Olphen H. An introduction to clay colloid chemistry, Wiley, New York, 1977.
- [9] Burchill S., Hall P. L., Harrison R., Hayes M., Langford J., Livingston W., Smedley R, Ross D. and Tuck, J. Smectite-polymer interactions in aqueous systems, *Clay Minerals*, **18**, 373-397, 1983.
- [10] Rich C.I. Determination of the amount of clay needed for X-ray diffraction analysis. *Proc. Soil Sci. Soc. Am.* **39**, 161-162, 1975.
- [11] Nguyen T.T, Raupach M. and Janik L.J. Fourier transform infrared study of ethylene glycol monoethyl ether adsorbed on montmorillonite: implications for surface area measurements of clays, *Clays and Clay Minerals* **35**, 1, 60-67, 1987.
- [12] Scheuing D. Fourier transform infrared spectroscopy in colloid and interface science, ACS Symposium Series 447, 1-23, 1990.
- [13] Van Olphen H. and Fripiat J.J. (Editors). Data handbook for clay materials and other non-metallic minerals, Pergamon Press, 1979.
- [14] Bindley G.W. and Brown G., Crystal structures of clay minerals and their identification, Mineralogical Society, London, 1984.

- [15] Kellomäki A., Nieminen P., and Ritamäki L.. Sorption of ethylene glycol monoethyl ether (egme) on homoionic montmorillonites, *Clay Minerals*, **22**, 297-303, 1987.
- [16] Infrared spectroscopy, Ed: George B., and McIntyre P., *Analytical chemistry by open learning*, John Wiley and Sons, 1987.
- [17] *Handbook of Chemistry and Physics*, CRC Press Inc, Ed. 68th 1987-1988, D 225-D243.
- [18] Denis J. H, Keall M. J, Hall P. L. and Meeten G. M. Influence of potassium concentration on the swelling and compaction of mixed (Na, K) ion exchanged montmorillonite, *Clay Minerals*, **26**, 255-276, 1991.
- [19] Boek E. S., Coveney P. V. and Skipper N. T., Monte Carlo molecular modeling studies of hydrated Li, Na, and K smectites: Understanding the role of potassium as a clay swelling inhibitor, *Journal of the American Chemical Society*, **117**, 12608-12617, 1995.
- [20] Aston M. S. Portable tester measures cuttings hardness at the rig, *World Oil*, September 1993.
- [21] Low P.F. Nature and properties of water in montmorillonite-water systems, *Soil Science. American Journal*, **43**, 651-658, 1979.
- [22] Sposito G. and Prost R. Structure of water adsorbed on smectites, *Chemical Reviews*, **82**, 554-572, 1982.
- [23] Bradley W.F. Molecular associations between montmorillonite and some polyfunctional organic liquids, *J. American Chemical Society*, **67**, 975-981, 1945.
- [24] Wu J., and Lerner M., Structural, thermal and electrical characterization of layered nanocomposites derived from Na-Montmorillonite and polyethers, *Chemical. Material*, **5**, 835-838, 1993.
- [25] Aranda P. and Ruiz-Hitzky E. Poly(ethylene oxide)-silicate intercalation materials, *Chemical. Material*, **4**, 1395-1403, 1992.
- [26] Parfitt R. L and Greenland D. J. The adsorption of poly(ethylene glycols) on clay minerals, *Clay Minerals*, **8**, 1970.
- [27] Breen C., Rawson J., Mann B. E. and Aston, M. In situ ¹³³Cs and ¹H solution-phase NMR, thermoanalytical and X-ray diffraction studies of the adsorption of polyalkyleneglycol on Texas benonite, *Colloids and Surfaces A: Physicochemical and Engineering Aspects*, **132**, 17-30, 1998.

- [28] Zhao X., Urano K. and Ogasawara S. Adsorption of polyethylene glycol from aqueous solution on montmorillonite clays, *Colloid and Polymer Science*, **267**, 899-906, 1989.
- [29] Grandjean J. and Laszlo P. Interaction of nonionic polymers at a clay interface, *Magnetic Resonance Imaging*, **14**, 983-984, 1996.
- [30] Swartzen-Allen S. and Matijevic' E., Surface and colloid chemistry of clays, *Chemical Reviews*, **74**, 385-400, 1974.
- [31] Faisandier K., Pons C.H., Tchoubar D. and Thomas F. Structural organisation of Na- and K-montmorillonite suspensions in response to osmotic and thermal stresses, *Clays and Clay Minerals*, **46**, 636-648, 1998.
- [32] Slade P. G., Quirk J.P. and Norrish K. Crystalline swelling of smectite samples in concentrated NaCl solutions in relation to layer charge, *Clays and Clay Minerals*, 234-238, 1991.
- [33] Reid P., Harrington P. and Minton R. Shale tests help develop inhibitive water based muds, *Ocean Industry*, October, 19-25, 1991
- [34] Bailey, I., Keall M., Audibert A. and Lecourtier J. Effect of clay/polymer interactions on shale stabilisation during drilling, *Langmuir*, **10**, 1544-1549, 1994.
- [35] Almgren M., Brown W. and Hvidt S. Self aggregation and phase behaviour of polyethylene oxide-polypropylene oxide polyethylene oxide block copolymers in aqueous solution, *Colloid and Polymer Science*, **273**, 2-15, 1995.
- [36] Platikanov D., Weiss A. and Lagaly G. Orientation of nonionic surfactants on solid surfaces: n-alkyl polyglycol ethers on montmorillonite, *Colloid and Polymer Science*, **255**, 907-915, 1977.
- [37] Cohen S., Marcus Y., Migron Y., Dikstein S. and Shafran A. Water sorption and binding and solubility of polyols, *Journal Chemical Society, Faraday Transactions*, **89**, 3271-275, 1993.
- [38] Boek E. S., Coveney P. V., Craster B. and Reid P. I. Mechanisms of shale inhibition by polyglycol water based muds and the development of improved additives through combined use of experimental and molecular modelling techniques, *Proceedings of the Sixth International Symposium on Chemistry in the Oil Industry*, April 1997, Royal Society of Chemistry, 58-70, 1998.
- [39] Brady M. E., Craster B., Getliff J.M. and Reid P. I.. Highly inhibitive, low salinity glycol water-based drilling fluid for shale drilling in environmentally sensitive locations, *SPE 46618*, 1998.

CHAPTER 5

DESIGN AND RECOMMENDED USE OF A CLAY MEMBRANE CELL TO
INVESTIGATE BARRIER FORMATION BY POLYMERS.

1. Introduction	127
2. Background theories.....	127
2.1 Pertinent literature.....	127
2.2 Diffusion, Osmosis and Permeability	129
2.3 Model for ion and water movement through films	132
3. Designing the Clay Membrane Cell	136
4. Experimental	142
4.1 Clay Membrane Cell	142
4.2 Clay film preparation	144
4.3 Mounting the film in the cell.....	144
4.4 Solution preparation.....	145
4.5 Ion transfer analysis	145
4.6 Cuttings dispersion tests.....	146
4.7 Synchrotron radiation experiments	146
5. Results and discussion.....	146
5.1 Clay films supported by coarse discs	147
5.1.1 <i>Comparing silicates with glycols</i>	147
5.1.2 <i>Silicates</i>	150
5.1.3 <i>Summary</i>	153
5.2 Clay films supported by fine discs	154
5.2.1 <i>Osmotic tests</i>	154
5.2.2 <i>Clay film examination through synchrotron experiments</i>	157
5.2.3 <i>Pathways for diffusion</i>	160
5.2.4 <i>Application of the Sherwood model</i>	164
5.2.5 <i>Hydrostatic tests</i>	169
6. Conclusions	173
7. Future work	174
8. References	175

1. Introduction

It is well established that the overall movement of water into a shale formation can be reduced by adding hydrophobically modified glycol to a water based drilling mud [1]. However, when salt is present in solution the cation tends to alter the polymer's performance, because it exchanges onto the clay surface and influences the shale swelling levels. This aspect has been shown in Chapter 4 where the application of glycol muds as shale inhibitors in the presence of salt has been studied. Ideally an adsorbed polymer layer would prevent the movement of ions into the shale (as well as reducing water flow), allowing the direction of water movement to be finely tuned by balancing the mud and pore fluid activities [2].

In order to evaluate the level of ion and water movement in shale when treated with mud additives, a Clay-Membrane Cell has been designed and developed at SCR. This cell, described in detail in this chapter, allows the transport of salt and water across a treated montmorillonite film with glass beads to be monitored.

A literature review of research in related areas will be given. Firstly the design path of the Clay Membrane Cell will be outlined along with some preliminary results and the current status of the clay cell in terms of possible type of tests run will be discussed. A model previously developed by Dr John Sherwood, Schlumberger [3] will be applied to a set of data to extract values for clay film permeability to water and salt diffusivity. The limitations of the model will also be discussed. Finally attempts to determine the permeability independently using hydrostatic tests will be outlined.

2. Background theories

2.1 Pertinent literature

Membrane preparation processes have many industrial uses, for example salt extraction from food products, the production of vaccines for the pharmaceutical industry, and the purification of chemicals. In addition cell membranes perform vital tasks in biological systems. In each application the efficiency of the separation process relies on membrane properties such as pore size, net surface charge and permeant solubility.

During some of these processes, the chemical potential of a species may differ on either side of the membrane. This would dictate the direction of fluxes of materials if the system was allowed to equilibrate.

The first report of such osmotic effects date back to Abbe Nollet (1748) and later to Pfeffer in 1877 [4]. Pfeffer carried out experiments to show that a membrane impermeable to sugar, but permeable to water allowed a flux of water into the sugar rich reservoir. To combat this flow, a pressure equal to the osmotic pressure was applied. This pressure was later related to the ideal gas law by van't Hoff. Some of the analysis that followed their work could only be applied to systems where the membrane had constant properties and was perm selective. In reality membranes are usually leaky to all species (albeit to differing extents) and in some cases the barrier properties are affected by the solution chemistry under investigation. Good examples of such membranes are those prepared from clay bearing materials.

It is not new to suggest that clay membranes can give rise to chemical osmosis. In fact the subject has been discussed by many researchers such as Young and Low [5]; Kemper and Rollins [6] and Fritz [7]. The salt-exclusionary nature of the clay is due to the net negative charge on the clay surfaces that repels the anions as they enter the pore spaces. This exclusion is largest when the double layers of adjacent clay platelets overlap, thereby leading to a net negative potential in the pore space. The cations remain coupled with the anions in the "free water" contained in the bulk pores, or external fluid reservoirs, and only water itself moves freely. Obviously, the efficiency of the clay at rejecting the salt depends in some way on the charge on the clay, the salt concentration, the applied pressure or matrix porosity, and the presence of adsorbed organics.

Many experiments have been designed to determine the anion reflection coefficients of clay under different conditions for geological studies, landfill sites and wellbore stability. Some of these previous studies have used elaborate experimental devices. The clay is held under a known confining pressure (sometimes tens of MPa), and then fluid is pushed through the clay under a pressure and the retention of ions on the clay surface determined by analysis of the eluent. In many of these experiments the clay film varies in thickness from one to several millimeters. The pressure changes evolve over a long time scale and the experiments require careful pressure control which is expensive. These experiments are similar in principle to those carried out at SCR on shale cores using the Hassler cell first reported by Hassler *et al.* [8]. In this test a core is placed under a confining pressure and synthetic pore fluid is pumped through the centre.

Alternative experiments are designed to look at the self diffusion coefficients of the ions through clay dispersed in a dilute salt solution using tracer experiments (Robin *et al.* [9] and Mokady and Low [10]).

There seems to be a need for a simple experimental set-up that involves thin clay films, allowing more rapid pressure changes to be observed. Ideally the experimental system would be cheap and simple to use allowing considerably more chemical systems to be analysed. Some related work involving thin clay membranes (Sujata De and Saroj Kumur Sanyal [11]) was found after the design of the Clay Membrane Cell at SCR. However they heated treat their clay films at 500 °C for several hours. The authors deemed this necessary to ensure stability during the osmotic test time and to allow them to epoxy the film between two reservoirs. Clearly this heat treatment may physically alter the pore space and affect the swelling properties of the mineral.

2.2 Diffusion, Osmosis and Permeability

The model developed by Dr John Sherwood, Schlumberger for the movement of water and salt incorporates the principles of diffusion, osmosis and permeability. This model is described in Section 3.2 of Chapter 5 but the principles behind these phenomena will be outlined here in order.

Diffusion

The kinetic energy of an atom or molecule (E) is given by $E = 1.5kT$ and enables the species to move as long as the temperature is greater than 0 K [12]. The molecule or ion is said to take a “random walk”. Therefore if two unstirred solutions containing a salt at different concentrations are placed either side of a permeable membrane then after some time the solutions will have the same salt concentration. This process by which mixing is brought about is called diffusion. The random movement of atoms or particles can be confirmed by the observation of Brownian motion. This phenomenon was first observed by Brown when he examined the movement of pollen seeds on a water surface. It was thought to be due to the water molecules knocking against the pollen grains and Brownian motion today is linked to that hindered diffusion. The coefficient of diffusion D_s is defined by Fick’s Law

$$\frac{\partial c}{\partial t} = D_s \frac{\partial^2 c}{\partial x^2} \quad (1)$$

where c is the concentration, x is distance measured at right angles to a solution plane having a constant density and t is time. When the solution contains one species only then D_s becomes the coefficient of self diffusion. In monovalent salt systems D_s can be expressed as

$$= \left(\frac{2uv}{u+v} \right) RT \quad (2)$$

where u and v are the velocities of the cations and anions when subject to an electric field of 1 volt per cm.

Osmosis

A standard undergraduate experiment which helps to demonstrate the process of osmosis is described here. A sugar solution is poured into a bag the walls of which are impermeable to sugar but permeable to water. Differences in chemical potential of the water and sugar on either side of the walls means that the species want to equilibrate. However the walls only allow the water through and so there is an influx of water into the sugar solution and the pressure in the bag builds up. Eventually the pressure reaches a steady state and there is equal flux of water in either direction across the membrane. If this pressure had been applied to the concentrated sugar solution in the form of a hydrostatic pressure then no flow of water would have occurred. The maximum value the pressure could have would be the osmotic pressure if the bag walls were truly perm selective, permeable to water and they did not burst under the pressure.

For simplicity if one considers zero applied pressure difference, then the pure solvent has higher free energy than that of the solvent in the salt solution, hence the solvent flows into the salt solution until equilibrium is reached [13]. The pressure difference is the osmotic pressure difference and gives us a measure of the concentration difference. The standard interpretation is to utilise the chemical potential of the solvent, μ_s ; which is given by

$$\mu_w = pV_w + RT \ln x_w . \quad (3)$$

In Equation 3, μ_w is the chemical potential of solvent, R is the gas constant, T the temperature, V_s the partial molar volume of the solute and p the thermodynamic

pressure. The mole fraction of solvent is x_s . Correspondingly the equation for the chemical potential of the solute is given by

$$\mu_s = pV_s + RT \ln x_s. \quad (4)$$

Manipulating these equations can give the osmotic pressure differential ($\Delta\pi$) across a membrane as

$$\Delta\pi = \frac{RT}{V_w} \ln \left[\frac{a_w^1}{a_w^2} \right] \quad (5)$$

where a_w^1 and a_w^2 are the activity of the solvent on side 1 and side 2 of the membrane at temperature T . These activities can be measured in a thermostatted and calibrated humidity meter

The flux of solute per unit area across the membrane (j_s) is

$$j_s = \omega \Delta\pi \quad (6)$$

where ω is the solute permeability of the membrane.

An applied pressure difference leads to fluid flow across the membrane. This flow is directly proportional to the applied pressure difference, and introduces a hydraulic permeability [14]. In the absence of chemical effects (*i.e.* a salt gradient) the total flux of fluid per unit area, j_v , is given by

$$j_v = L_p \Delta p \quad (7)$$

where L_p is the hydraulic permeability and Δp is, the pressure difference across the membrane.

Using Equations 6 and 7 the total flux across the membrane per unit area is

$$j_v = L_p (\Delta p - \sigma \Delta\pi). \quad (8)$$

This states that the total flux is that caused by the applied pressure difference minus the flux caused by the osmotic pressure, where σ is the reflection coefficient that

characterises the efficiency of the membrane. There are alternative, equivalent, flux equations written as

$$j_s = \omega \Delta \pi + (1 - \sigma) c_s j_v \quad (9)$$

This relates the solute flux to the total flux, and c_s is the solute concentration.

Permeability

In 1856, Henry Darcy [15] studied the flow of water in sand filters. From his study on horizontal flow through a gravel pack he concluded that

$$Q = \frac{k_D A (\Delta p)}{\nu l} \quad (11)$$

where, the driving force for flow is the hydrostatic pressure differential Δp , Q is the volume flow per unit time, k_D is a permeability, A the cross sectional area of the sample, l the sample thickness, and ν the fluid viscosity.

2.3 Model for ion and water movement through films

The treatment of the membrane fluxes shown in Equation 8 allows parameter such as the hydraulic permeability and the reflection coefficient to be determined if the flux is zero and the pressure differential and osmotic pressure are known. A model which allows these parameters to be determined when the pressure differential and the osmotic pressures are varying with time has been developed by Sherwood [3].

This model of hindered solute transport across a membrane published by Sherwood [3] has subsequently been expanded on by Sherwood to apply to the Clay Membrane Cell which had been originated by the author as part of this PhD program. This model will be referred to as the Sherwood Model throughout this chapter. The Sherwood model assumes that the ions move in one direction across the clay film and the water in the opposite direction. It is also assumed that the ions or water do not change the permeability of the clay film during the test time. The example given [3] is of a sodium chloride solution moving through a sodium exchanged clay. No allowances are made for a third species (such as glycols) and the solutions are assumed to be dilute enough to be ideal. The Sherwood model is similar to one developed by Laidler and Shuler [16] for flow of uncharged species through polymer film except that the

Sherwood model acknowledges Onsager's reciprocal relations and there are 3 transport coefficients rather than 2. The transport coefficients that can be determined are the permeability, diffusion coefficient, and membrane selectivity. The exact details of the model are given extensively elsewhere [3] and so only a brief overview will be given here.

The basis for the model are the flux equations for the salt (j_s) and the water (j_w) of the form

$$j_w = \lambda_{ww} \Delta\mu_w + \lambda_{ws} \Delta\mu_s \quad (11)$$

$$j_s = \lambda_{sw} \Delta\mu_w + \lambda_{ss} \Delta\mu_s \quad (12)$$

Rewriting the chemical potentials ($\Delta\mu$) and transport coefficients (λ_{ij}) gives

$$j_w = (1 - x_s^0) k \Delta p - V_w^{-1} [(1 - \lambda) RTk + \lambda V_s D] \Delta x_s \quad (13)$$

$$j_s = \lambda x_s^0 \Delta p + \lambda D \Delta x_s \quad (14)$$

where,

Δp is the jump in pressure across the membrane, Δx_s is the jump in salt mole fraction from x_s^0 , k is the Darcy transmission coefficient, D is a diffusivity and λ is a transmission coefficient for ion movement.

Details of the development of the Clay Membrane Cell along with the current version are given in Section 3.0 of Chapter 5. Some pertinent points will be highlighted here to help with understanding the application of the Sherwood Model to the experiment. In the Clay Membrane Cell the hydrostatic pressure differential across the montmorillonite film can be calculated from measurements of the fluid heights in the capillary tubes. Also the change in salt concentration on the low salinity side of the clay film is measured using a conductivity probe. This conductivity data can be manipulated to give the mole fraction differential of the salt across the film. Equations 15 and 16 show the variation of the pressure differential and the salt mole fraction respectively with time.

$$\Delta p = \Delta p_0 \frac{(\lambda_2 e^{-k_1 t} - \lambda_1 e^{-k_2 t})}{\lambda_2 - \lambda_1} + \lambda_1 \lambda_2 \Delta x_s^0 \frac{(e^{-k_1 t} - e^{-k_2 t})}{\lambda_2 - \lambda_1} \quad (15)$$

$$\Delta x_s = \Delta p_0 \frac{(e^{-k_1 t} - e^{-k_2 t})}{\lambda_1 - \lambda_2} + \Delta x_s^0 \frac{(\lambda_1 e^{-k_1 t} - \lambda_2 e^{-k_2 t})}{\lambda_1 - \lambda_2} \quad (16)$$

For experiments using the Clay Membrane Cell the hydrostatic pressure differential at the start of the test (Δp_0) was set to zero thus eliminating the first terms in Equations 15 and 16. These equations have been solved by Sherwood [3] to give solutions shown in Equation 17 and 22 (see Figure 5.1);

$$\Delta p = a_1 \exp(a_2 t) - a_3 \exp(a_4 t) \quad (17)$$

where a_2 depends on the permeability of the clay film to water and a_4 depends on the salt diffusivity. For these experiments a_1 is usually equal to a_3 and gives the transmission coefficient for salt λ i.e. $\lambda=0$ corresponds to a perfect ion exclusion membrane and $\lambda=1$ corresponds to unimpeded salt flow.

In Figure 5.1 the shape of curve b before the peak is governed by the decay in the osmotic pressure. As the salinity differential approaches zero (curve c approaches zero) the fluid flows back across the membrane and the flow rate is mainly controlled by curve a.

On further analysis,

$$-a_2 = \frac{2Sg\rho^0 kV_w}{A_c} \quad (18)$$

where S is the surface area of the membrane, g is the acceleration due to gravity, k is a permeability, V_w is the molar volume of water and A_c is the cross sectional area of the capillary tube. The Darcy permeability (k_d) can be extracted using

$$k_d = \nu V_w h k \quad (19)$$

where ν is the fluid viscosity and h is taken as the measured film thickness.

Since $1-\lambda \ll 1$ in Equation 13, one can ignore the second term on the left had side giving

$$\lambda D_s = \frac{-n_w^0 a_4}{2S} \quad (20)$$

where n_w^0 is the number of moles of water on one side of the film. Sherwood showed that,

$$D_s = hV_w D \quad (21)$$

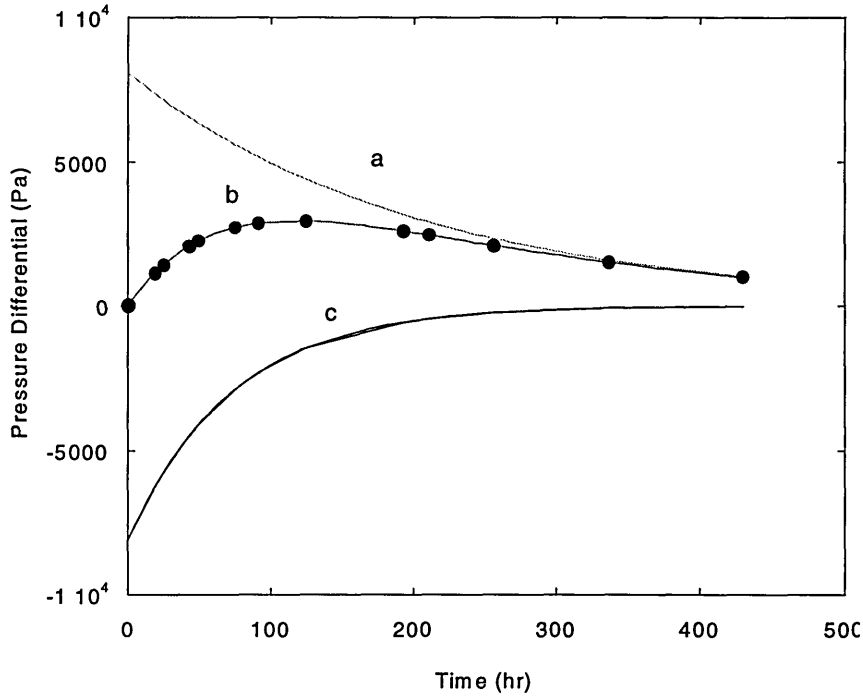


Figure 5.1: A typical experimental profile of pressure differential *versus* time (b) fitted using Equation 17 to analyse each section of the graph. Curve (c) represents the contribution from the salt diffusivity, and curve (a) the permeability of the clay film to water.

Correspondingly curves of mole fraction differential of salt *versus* time can be analysed;

$$\Delta x_s = b_1 \exp(b_2 t) + b_3 \exp(b_4 t) \quad (22)$$

In an osmotic test where initially a salinity gradient exists across the clay film both the developed hydrostatic pressure (Δp) and the changes in salinity differences (Δx_s) can be inferred from capillary hydrostatic head and conductivity readings. For the second type of test the salinity on both sides of the membrane is the same. the membrane. The

hydrostatic pressure Δp is allowed to fall to zero. Obviously Δx_s^0 is set to zero and since $|\lambda_1| \gg |\lambda_2|$ the pressure difference across the membrane becomes

$$\Delta p = \Delta p_0 \exp(-a_2 t). \quad (23)$$

Plotting $\ln \Delta p$ versus t gives a slope of $-a_2$ which can be related to the Darcy permeability using Equation 18.

3. Designing the Clay Membrane Cell

In this section the design path of the Clay Membrane Cell presently in use will be outlined under the following stages:

1. Unsupported clay film clamped between two perspex reservoirs
2. Optimising the preparation method of the montmorillonite film to improve homogeneity.
3. Addition of capillary tubes for measurement of volume change. Amendment of cell clamping method to prevent spurious volume readings.
4. Addition of porous discs to prevent film deformation and free swelling of the montmorillonite film.

Exact details of the cell in use today will be described in Section 4.1 of Chapter 5 and results given in Section 5.0 of Chapter 5.

Self supporting montmorillonite films had been used at Schlumberger Cambridge Research for studies on glycol-montmorillonite interactions, a full description of which was given in Chapter 4. These studies did not provide any kinetic information and the permeability of the film to water or ions after treatment with the polymer additives was not examined.

In initial versions of the cell, the clay film was formed by spreading gel on a plastic sheet and removing the film once it had air dried. This film was then clamped between two perspex reservoirs (shown in Figure 5.2). The cell was open to the atmosphere and a conductivity probe inserted on the low salinity side (B). The contents of the cell were stirred by motors placed on either side of the membrane.

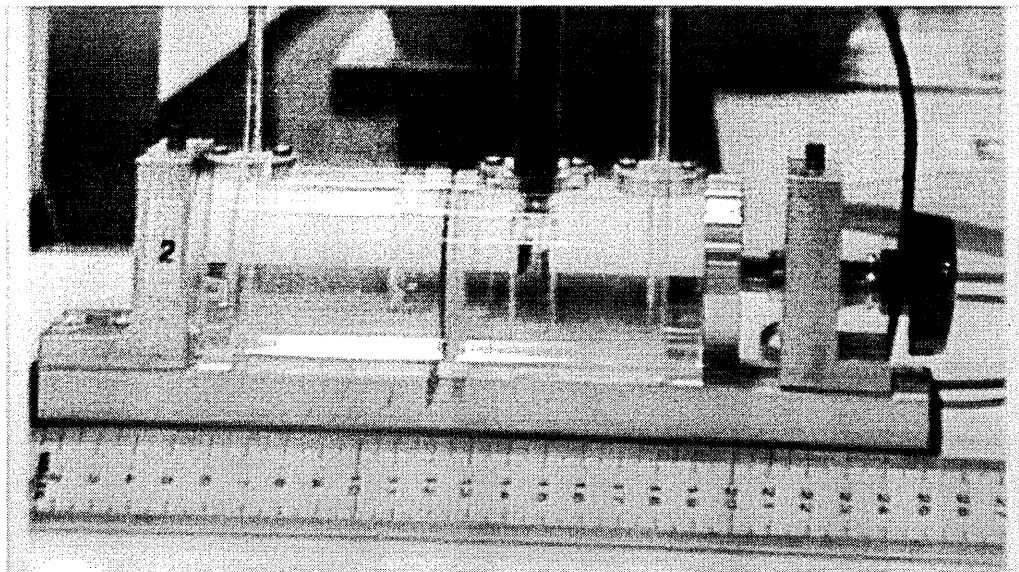


Figure 5.2. An early version of the Clay Membrane Cell. In initial experiments the capillary tubes were replaced by stirrers. Side A is on the left and side B on the right. Ruler dimensions are in cm.

Initially 10 wt % potassium chloride was used on side A and 2 wt % potassium chloride on side B. The conductivity was monitored as a function of time and the profiles for filter paper alone and a clay film are shown in Figure 5.3.

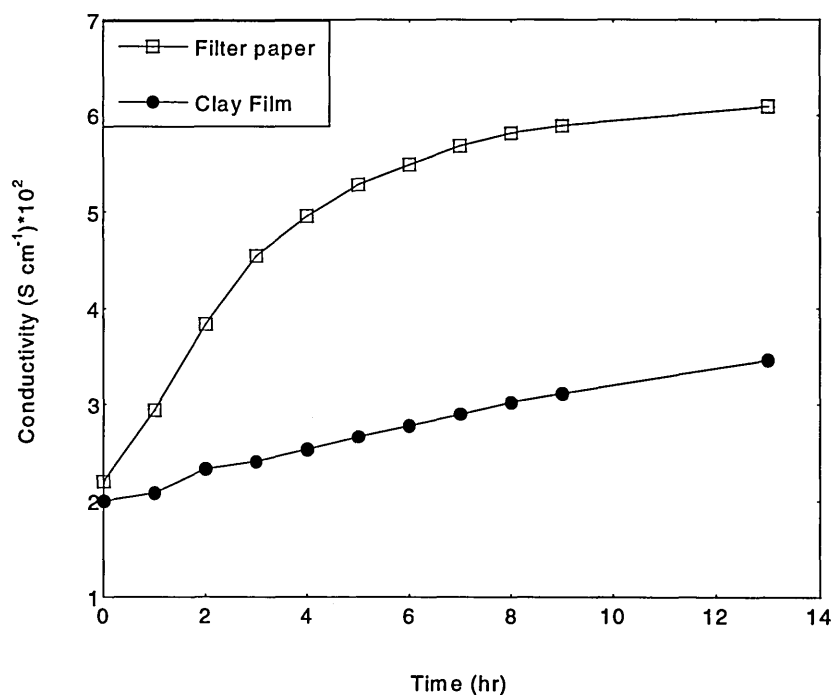


Figure 5.3: Conductivity *versus* time for solution in side B with either filter paper or an air dried montmorillonite film separating the reservoirs.

Basically it takes the potassium chloride solutions longer to equilibrate through the air dried montmorillonite film than through the filterpaper . This suggests that the clay film is less permeable to ions than the filterpaper which is expected since the clay carries more charge. These experiments were repeated with 5 wt% of mud additives listed in Table 4.1 Chapter 4 added to the 10 wt% potassium chloride solutions on side A. The effect of glycols used in Chapter 4 and sodium silicate on the conductivity change on side B was monitored (Figure 5.4).

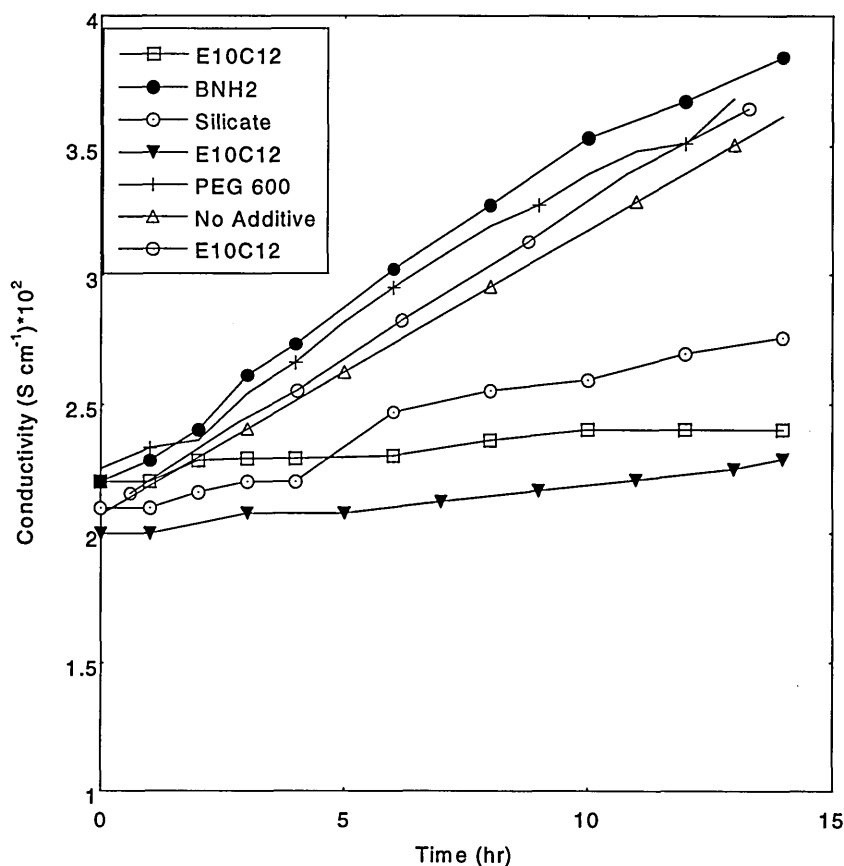


Figure 5.4: Variation in conductivity as a function of time on side B of the clay film.

At the time these experiments were carried out the exact effect of the glycol additives on transport of salt through the film was not fully understood. However the ability of silicates to set up osmotic barriers preventing ion movement is well documented [17] and in line with this the conductivity change in the presence of silicate is slow compared with an untreated clay.

Initially adding 5 wt% of the polyhydroxy alkane $E_{10}C_{12}$ to the 10 wt% KCl appeared to slow down the equilibration of the salt. However when a new batch of the

clay film was prepared this glycol was seen to have little effect on the salt diffusion rate; this third set of data has been represented by O in Figure 5.4.

In fact many problems existed with the method for preparing the clay films in that the results obtained varied between batches of films which was not surprising since the thickness of the film alone could vary between 15 and 22 μm when air dry. Variation in the microstructure of the film could also be detected by SEM and the surface of the clay film formed close to the plastic was noticeably smoother than the surface formed closer to the air. Consequently a new method of preparing the clay film was sought which led to the method of preparing filtercakes used at Schlumberger [18] being modified slightly. Basically a clay dispersion was poured onto filter-paper in a filtration cell and the solids concentrated under a pressure of 2 bar. A complete description of the method will be given in Section 5.2 Chapter 5. It was a surprise to find that the response of this film to potassium chloride movement was very similar to that of the clay film formed by the previous method (Figure 5.5).

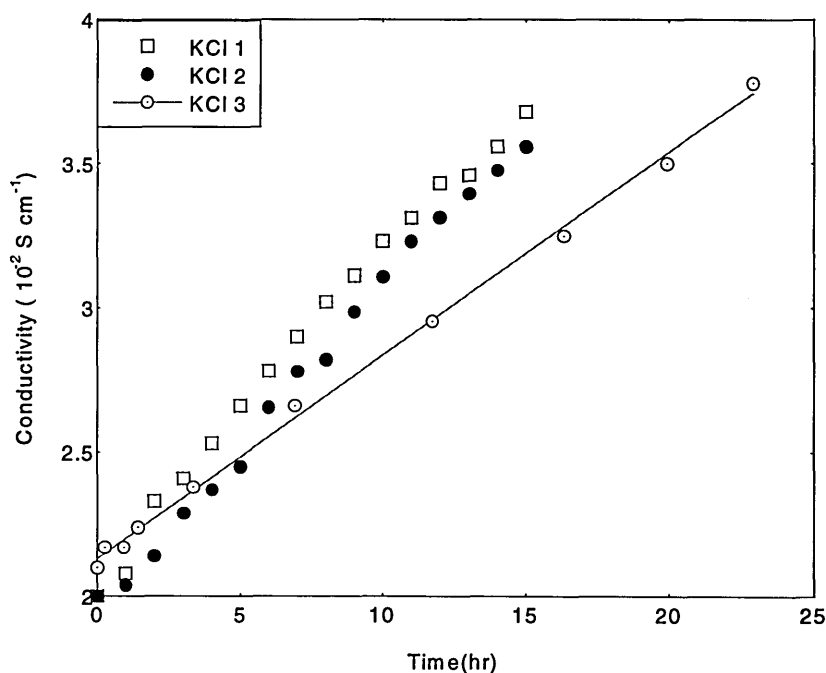


Figure 5.5: Variation in the conductivity of the solution on side B with time for films formed by gel deposition (KCl 1, KCl 2) and the new filtration method (KCl 3). In all cases the films were air dried.

There was some concern that conditions of drying the clay film would alter its permeability to ions and water. The films formed by filtration were subsequently dried over magnesium chloride in a desiccator. The drying time appeared to cause variations in

the conductivity profiles especially when glycols were present. The significance of these variations on future data interpretation could not be properly evaluated at this stage but it was considered better to eliminate potential problems caused by the drying process, (Figure 5.6).

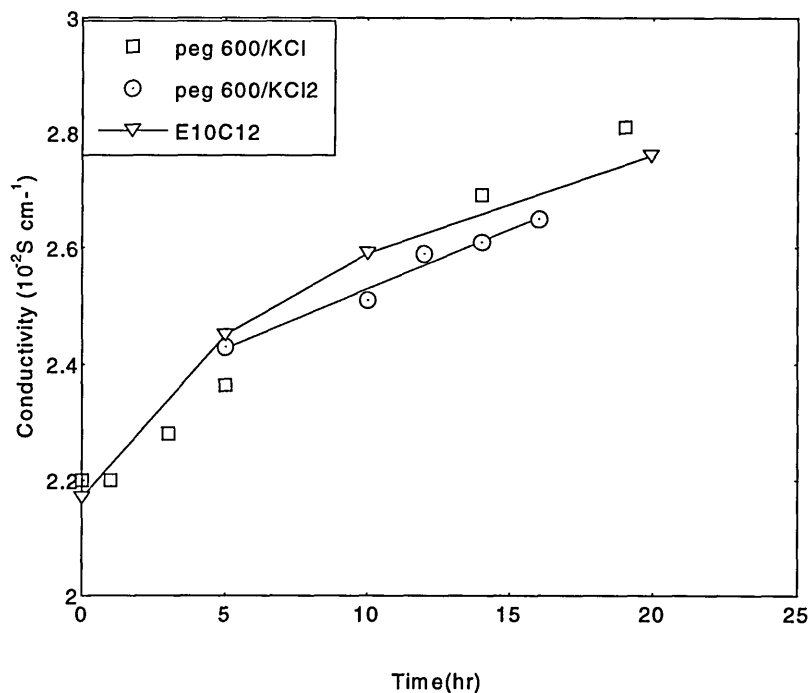


Figure 5.6: Conductivity of reservoir B as a function of time. Montmorillonite films were formed by the filtration method. For the film labeled peg 600/KCl2 the clay film had been dried for 4 hr as opposed to 12 hr for the other films.

Therefore it was decided to insert the film in the osmotic cell directly from the filtration cell. However phenothalein blue indicator was seen to leak at the contact between the film and the O-ring. It was realised that the film needed to be hardened by salt treatment in the filterpress before moving it to the Clay Membrane Cell. This ensured that the film would be sealed on the O-ring in the cell.

During this test the clay film could distort in the cell under the osmotic pressure. This reduced the accuracy of the volume measurements, and the clay film was also prone to rupture. A system of discs were put in the cell to support the film from gross distortion. On closer examination of the swelling of the clay film in contact with different additives (Figure 5.7) it was decided that the clay film should be confined in the Clay Membrane Cell.

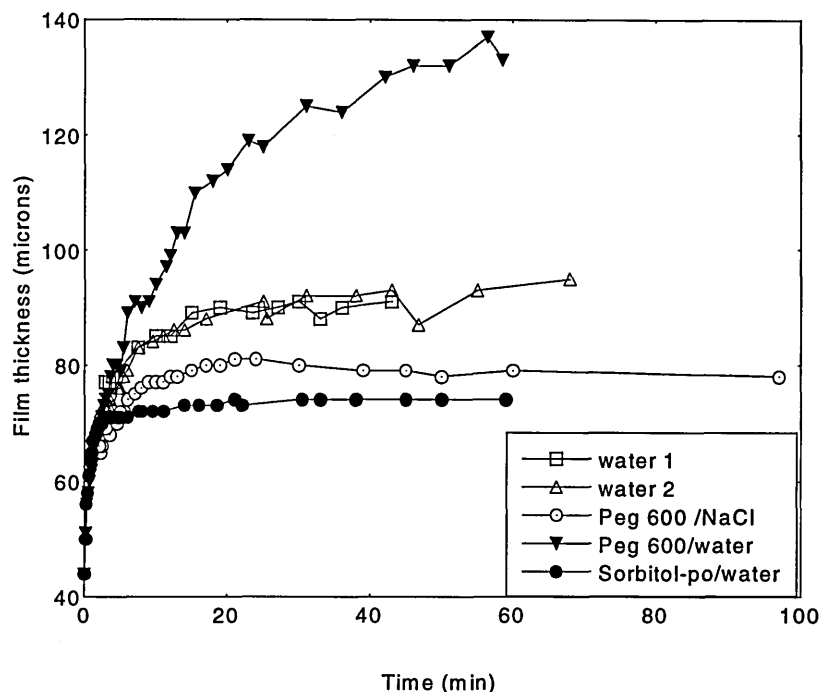


Figure 5.7: The swelling of clay films (treated with 0.5 M CaCl_2) placed in contact with solutions from the Clay Membrane Cell.

In Figure 5.7 the swelling curves of a montmorillonite film sandwiched between two filter papers soaked with the test solution are shown. The salts were molar and the glycol was added at 5 wt%. Measurements were made using a digital micrometer which exerted a force of approximately 20 N on the film during measurements. The reproducibility of these results were acceptable as shown by the similarity in the profiles for the films with water only added. Interpretation of the data is complicated due to the presence of multiple salts but general trends are as expected from research presented in Chapter 4. The glycols containing hydrophobic portions such as Sorbitol-po prevent the swelling of the montmorillonite film compared with the hydrophilic peg 600. For the clay treated with peg 600/water, data collection stopped when the increased compressibility of the swollen film affected the micrometer reading.

The clamping arrangement of the cell was adjusted in order to prevent O ring relaxation during the test. Holding the cell halves together using 6 bolts prevented spurious changes in the fluid heights in the capillary tubes. The final version of the clay cell is shown in Figure 5.8.

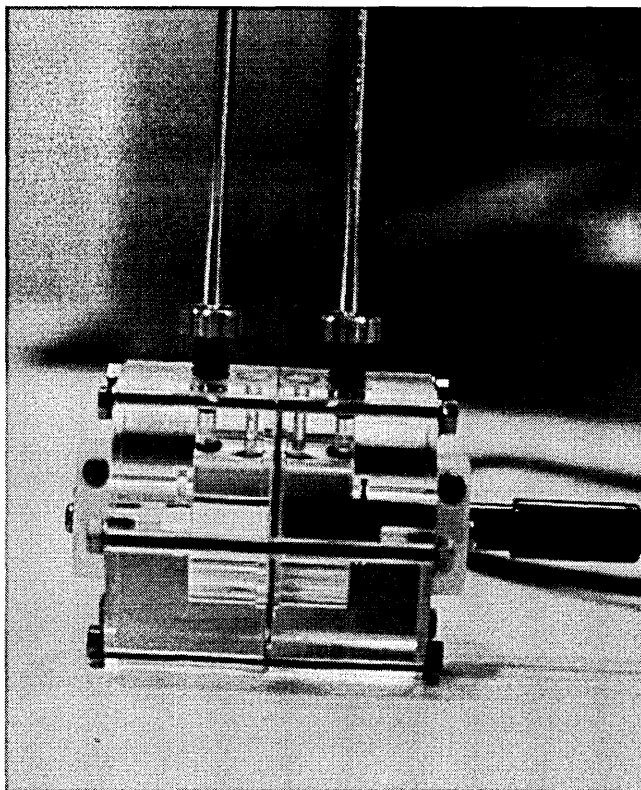


Figure 5.8: The latest version of the Clay Membrane Cell with capillary tubes either side of the film and a conductivity probe inserted horizontally in side B.

4. Experimental

Details of the optimised Clay Membrane Cell setup and solution and clay film preparation are given in this section.

4.1 Clay Membrane Cell

A schematic of the clay-membrane cell is given in Figure 5.9 and a Photo supplied in Figure 5.10. It was machined from Perspex to a tolerance of ± 0.02 mm at SCR and comes in two identical sections except for the O-ring grooves in the face of side A. Glass filters were purchased from Robu Glass. A coarse disc has a pore size of 100 to 250 μm while for the fine discs the pore size was 1.0 to 1.5 μm . The discs with a diameter of 31 mm are placed at the openings of each cell-half to support the clay films. The clay film does not cover the outer O-ring, thus fluid leakage is prevented. The cell halves are clamped together using six threaded screws placed through the outside walls. There is no direct control on the applied load taken by the clay film. Solutions are then added to each side of the film and changes in liquid levels on either side of the film can be monitored using capillary tubes with internal diameters ranging from 3.2 mm to 0.6 mm. These glass tubes are connected to the clay-membrane cell using brass and polycarbonate fittings.

Both the discs and tubes are cheap enough to be disposable or can be cleaned in an ultrasonic bath with solvent before reuse. Housings are also in position for septa through which samples of fluid can be taken for ion analysis or polymer addition made as the test progresses.

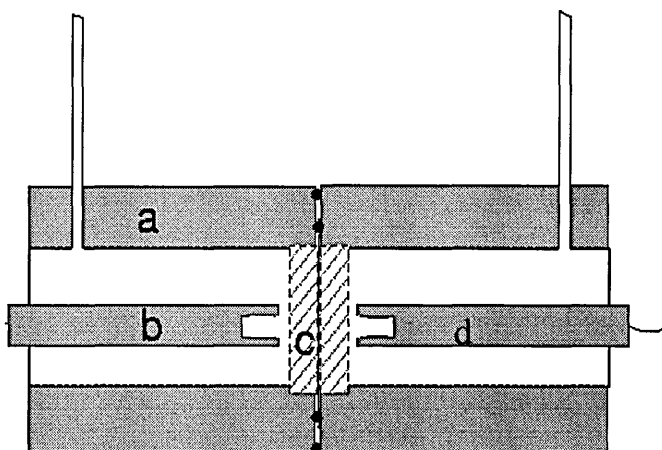


Figure 5.9: A schematic of the Clay Membrane Cell. The cell parts highlighted are labeled (a) representing the cell body, (b) a perspex insert, (c) the porous disc and (d) a conductivity probe. The clay film is shown as a fine line between the two discs.

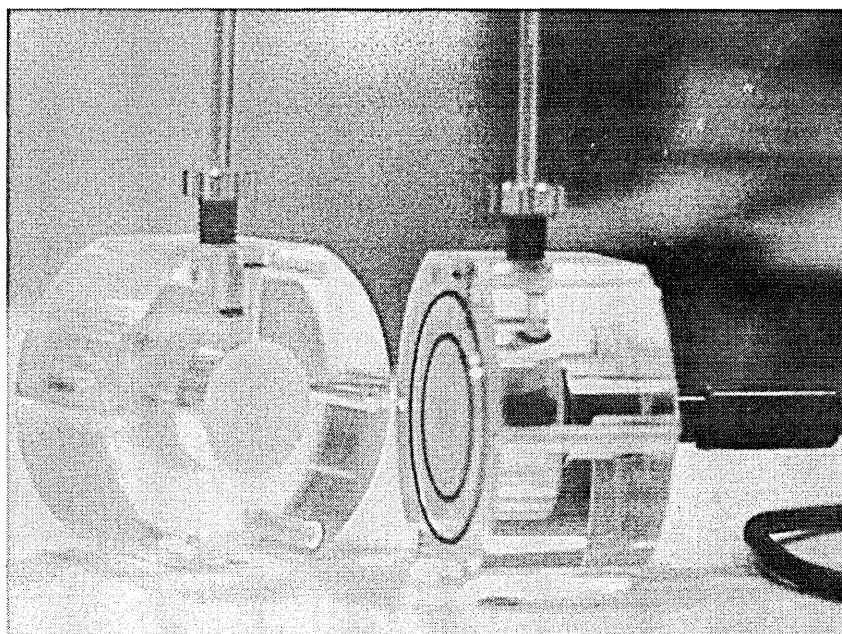


Figure 5.10: The inside of the Clay Membrane Cell showing the glass discs at the entrance to each cell half. For this picture the conductivity probe was inserted in side A.

For ease of reference during this report, side A of the assembled cell will be designated as that containing the polymer additive and the highest salinity. Side B will contain the lower

salinity solution without polymer. Conductivity probes containing carbon electrodes were designed especially by Sentek. These had specified volumes and dimensions which allowed them to be interchanged for perspex inserts normally placed through the end of side A. Conductivity and phase angle measurements were made using a current oscillating at 50 kHz and supplied by a component analyser manufactured by Wayne Kerr. Tests were run at a temperature of $25 \pm 1^\circ\text{C}$. by placing the cell in a plastic bag and partially immersing it in a temperature controlled water bath.

4.2 Clay film preparation

The $< 2 \mu\text{m}$ fraction of the montmorillonite standard SWy-1 [19] was selected by sedimentation [20] and the clay washed and dialysed with de-ionised water until the native salt was removed. This sized montmorillonite was then concentrated by centrifugation and the gel stored below 5°C . The solids content of the homogenised gel was checked by drying a sample at 105°C overnight. Then an appropriate weight of gel was added to the deionised water to prepare a 1.36 wt% dispersion and the solids fraction was checked by drying multiple samples for at least 12 hr at 105°C .

A 0.9 wt% dispersion of glass beads with a mean spherical diameter of $2 \mu\text{m}$ was added to the montmorillonite until the mass fraction of beads was 0.3. This was done with the intention of modifying the porosity and permeability of the final compacted film in an attempt to mimic variations in real shales. The resultant dispersion was allowed to stand for at least 24 hr at temperatures less than 5°C . Exactly $40.0 \pm 0.1 \text{ g}$ of this dispersion was weighed into an API filtration cell containing a filter-paper with an average pore diameter of $0.45 \mu\text{m}$. This filter paper was made by Durapore from polyvinylidene flouride. After compaction at a pressure of $2.0 \pm 0.2 \text{ bar}$ for 2 hr only a solid film remained and then $20.0 \pm 0.1 \text{ g}$ of a 0.5 M salt solution (remaining solution was used for side B of the Clay Membrane Cell) was poured into the filtration cell taking care not to disturb the clay surface. The salt solution was pushed through the clay film under pressure of 2 bar for one hour by which time the film was hardened and ready for placement in the Clay Membrane Cell.

4.3 Mounting the film in the cell

The clay film with the filter paper backing was cut to a diameter of 40 mm. When coarse discs were used the film with the backing was placed in the Clay Membrane Cell with the filter-paper towards the low salinity side. As the cell halves were clamped together the film was pushed into the porous disc on the high salinity or wellbore side called A.

When fine discs were used, a filter-paper disc of diameter 31 mm was placed over the center of the clay film assembly. This layered filter-paper-clay-filter-paper assembly was then placed in the cell with the filter-paper disc covering the fine disc only on the high salinity side of the cell. As for the test with coarse discs the filter-paper sheet used in the compaction cell touched the fine disc on the low salinity reservoir. As the cell was closed the clay film was shaped by the filter-paper.

4.4 Solution preparation

All salts were Analar grade and were supplied by Aldrich. De-ionised water was used for making solutions. In all cases, solution contamination was prevented by using new glassware when required and sample weights were noted to three decimal places. The pH was adjusted using the appropriate hydroxide and checked using a pre-calibrated Radiometer pH meter. Glycols were used as received from Aldrich and are listed in Table 5.1. Formulations for the silicate solutions were as listed below. Sodium silicate 14.006 g of silicate solution from Aldrich which contains (~ 27 wt% solids), 83.838g of 3.5 M sodium chloride and sodium hydroxide weighed in to raise the pH. Potassium silicate 14.06 g of potassium silicate supplied by Prolabo which contained (~ 27 wt%) of silicate 84.002 g of 3.5 M potassium chloride and potassium hydroxide was added to adjust the pH.

Polymer name	Polymer formula
peg 600	$\text{HO}[\text{C}(\text{H})_2\text{C}(\text{H})_2\text{O}]_n\text{H}$
sorbitol-po	sorbitol+9po
eda-po	eda+4po

Table 5.1: Lists of glycols with their chemical formulae used in this study. Eda represents ethylene diamine and po represents propylene oxide.

4.5 Ion transfer analysis

Ion analysis was carried out using a Dionex Ion Chromatogram (IC). In order to minimise the risk of blocking the IC column with silicate precipitate, only solutions from side B were analysed. Multiple dilutions were carried out on the sample and stock solutions to maximise the accuracy of the measurement.

Conductivity measurements were made continuously on later experiments. The probe containing the carbon electrodes was positioned horizontally in the cell. The probe leads were attached to a Wayne Kerr component analyser and the conductance measured

at 50 kHz. The phase angle was also checked as any change from 0° indicated polymer adsorption on the electrode surfaces. The probes were calibrated using salt solutions that had been equilibrated at 25°C . A third order polynomial fit to the data was used to convert the conductivity *versus* time profiles to concentration *versus* time.

4.6 Cuttings dispersion tests

Oxford clay cuttings sized between 2 and 4 mm were added to glass bottles containing silicate solutions prepared using the same recipe as for the cell experiments. The closed bottles were rolled at 60 rpm under ambient conditions for 2 or 16 hr. Recovery levels are expressed as a percentage of the original dry weight of cuttings added.

4.7 Synchrotron radiation experiments

These experiments were carried out at the UK laboratory in Daresbury. Electrons circulating within the synchrotron radiate energy continuously over a wide range of wavelengths. Radiation is diverted to individual stations located on the ring. Experiments were carried out on Stations 16.4 or 9.7. The beam of basically white radiation passes through the sample and the received diffracted intensity at a given wavelength can be related to the interplanar spacing using the Bragg equation. Several SWy-1 clay films mounted and conditioned in SCR osmotic cells were examined using in-situ synchrotron X-ray diffraction. The X-ray optics (2θ angle and alignments) were optimised for determining the montmorillonite 001 d-spacing. The 2θ angle of the bottom detector was 0.974° . The incident beam was defined by parallel slits; the opening was set at $35\ \mu\text{m}$ for optimal definition of the film thickness. The data acquisition time for diffraction patterns at each step of the traverse was 10 s. A typical measurement time for a full traverse (say 30 steps) was therefore about 6 min. As such the equipment was conditioned by a team from Birkbeck college to reduce the incident angle to 1.5° and the beam width to $35\ \mu\text{m}$ to allow examination of the thin film in-situ in the clay membrane. During the experiments the Clay Membrane Cells were taken from the water-bath and placed without any modification in the beam path. It was placed on one end perpendicular to the normal mode of use so that the diffracted radiation could be sampled by the detector.

5. Results and discussion

In this section results from tests in which the clay film was supported using coarse and fine discs will be presented. The results will be discussed with a view to validating the

experiment. Where possible preliminary results will be compared with expected values from the literature.

5.1 Clay films supported by coarse discs

These were the first experiments carried out in the Clay Membrane Cell in which the film was supported during the test using porous discs with a pore size *ca.* 100-250 μm . As such the aim was to determine if the test was useful in comparing the potential of different drilling fluid additives in setting up osmotic membranes. In Section 5.1.1 of Chapter 5 the ability of silicate and glycols to create osmotic barriers will be compared. In Section 5.1.2 of Chapter 5 the dependence of the osmotic membrane efficiency formed from silicates on pH and salt type will be presented.

In tests side A denotes the wellbore and side B the porefluid in the shale. Draining Oxford shale cores under pressure gives an eluent with 0.1 M NaCl, 0.01 M KCl, 0.04 M MgCl_2 and 0.04 M CaCl_2 [17]. This combination of salts would have caused a massive increase in the number of experiments required for interpretation of the results from the osmotic experiments. Keeping the concentration of homoionic salt on side B at 0.5 M ensured the montmorillonite film formed a seal against the cell edges.

5.1.1 Comparing silicates with glycols

The interactions of glycol molecules with both clays and shale had been studied (see Chapter 4). Research had also been carried out on silicate systems at SCR by Bailey *et al.* [17] which showed that the mechanism of operation of glycols and silicates at shale surfaces were very different. In the case of glycol systems the molecules intercalate preventing clay swelling while for silicates osmotic membranes were set up on or in the clay surface. In this section experiments are carried out to see how these very different mechanisms manifest themselves in the Clay Membrane Cell.

In Figure 5.11 the fluid movement from the 0.5 M calcium chloride solution into the 3 M sodium chloride solution with and without additives is presented. The test had started with 5 cm of fluid in the capillary tubes on both sides of the clay film. As the test progressed the fluid levels increased on side A and decreased on side B. After some time no liquid was present in the capillary tube on side B and the meniscus dropped through the cell walls. However the walls were so thick that the solution always covered the montmorillonite film, but this means that the hydrostatic pressure

exerted on side B was smaller or non existent compared with the pressure developed on side A.

During the first couple of hours the water movement profiles are the same for all the systems. Once the tests have been running for 10 hr then the systems start to show different behavior. The volume of fluid pumped across the clay film to side A increases rapidly for the silicate formulations. Data given for the sodium silicate system are for two independent tests carried out using the same solution formulation but different batches of clay, filter-paper and glass discs. Eventually the silicate experiments are terminated as the fluid height on side B drops into the cell.

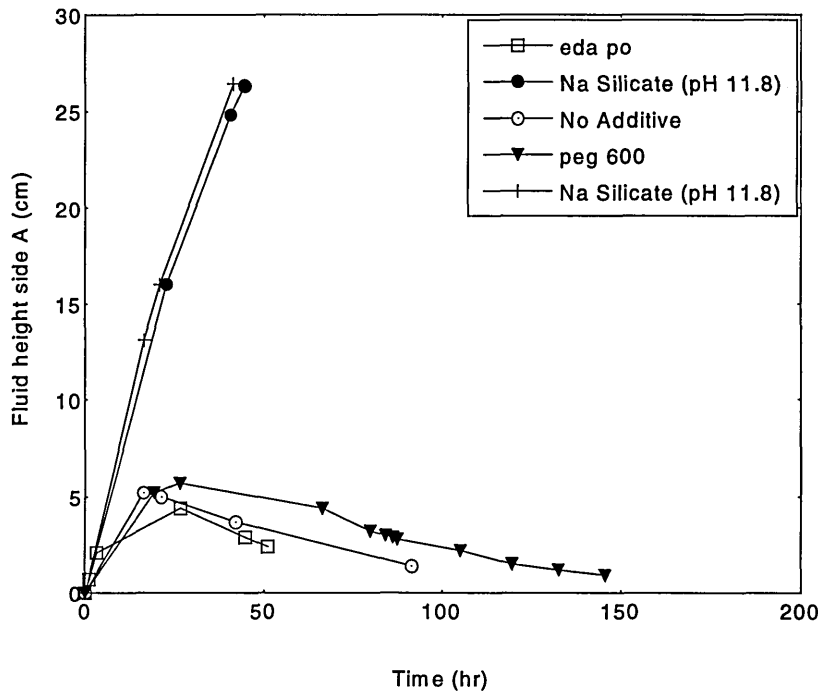


Figure 5.11: Fluid flow across the clay film into the high salinity side

In the profiles for non silicate systems in Figure 5.11 there is evidence of coupled osmotic flow; *i.e.* simultaneous movement of water and ions. Initially fluid flows from side B to A but after a time the fluid returns to side B. Repeats of these tests were performed in which the solutions from side B were stored and analysed using ion chromatography. This data is presented in Table 5.2. In Table 5.2, f_t is the fraction of sodium or calcium ions that have passed through the clay film. At equilibrium the expected value is 0.5 and the systems with no additive and glycol added can be seen to allow movement of sodium and calcium across the clay film over a 20 hr period. Indeed by the time these tests have run for 36 hr the equilibration was almost completed as can be shown for the glycol test analysed after 150 hr. Examination of the data for systems

without silicate shows that the movement of ions continues after the maximum in the water transport profiles. Having done this analysis there is no apparent difference (under this testing regime) in the water or salt movement for systems with and without glycol.

From the data presented in Table 5.2 it can be seen that there is no transference of ions across the clay film in the silicate experiments. It is nothing new to suggest that the precipitation of silicate in contact with calcium can be used to form an osmotic membrane [21]. However these experiments verify that this phenomena can be detected on a thin montmorillonite clay film in the Clay Membrane Cell. Also of importance to Schlumberger is the speed at which the presence of an osmotic barrier can be verified. A similar experiment in the Hassler cell would take several weeks.

Polymer system	Height change side A (+/- 0.2 cm)	% Volume increase on side A	f _i of Sodium	f _i of Calcium	Test Time (hr)
No additive	4.7	3	0.2	0.3	20
No additive	2.9*	2	0.4	0.4	40
peg 600	5.2	4	0.3	0.4	19
peg 600	5.5	4	0.3/0.2	0.3/0.3	19
peg 600	5.2	4	-	-	19
peg 600	1.0	1	0.5	0.5	150
eda-po	3.5	2	0.4	0.4	36
Na Silicate	15.3	10	0.0	0.0	22
Na Silicate	15.6	10	0.0	0.0	22

* was 4.4 at 20 hr

Table 5.2: Listings of fluid transfer volumes and fraction (f_i) of available ions transported across the clay film.

When the cells were dismantled it was found that the clay film had been pushed part way into the porous disc on the high salinity side (see Section 5.3 Chapter 5) and the disc on the low salinity side along with the filter paper could be peeled off the embedded film. When viewed under an optical microscope no holes on the surface of the clay film could be detected. However the film could not be removed from the disc thus eliminating the chance of postmortem analysis

At this stage in the research it was known that the glycol had an effect on the free swelling of montmorillonite when added to salt solutions. It was therefore decided

to modify the clamping procedure for the film in the clay cell in order to “expand” the lower region of the graph shown in Figure 5.11. Data from these experiments will be presented and discussed in Section 5.1.2 of Chapter 5.

5.1.2 Silicates

The precipitation and gelation of the silicate with a drop in pH and with divalent ions respectively is of interest to Schlumberger for the improvement of silicate based drilling fluids. Selecting sodium or potassium silicate for a drilling fluid is sometimes a complex decision and it was decided to carry out experiments to compare the performance of potassium and sodium silicates. From initial experiments in which the pH of the sodium silicate solution was varied the difference in the response of the osmotic cell was apparent.

Different experiments were performed to define a testing program that would allow silicate systems to be screened quickly. One of the first decisions to be made was which salt solution should be used on side B. Potassium silicate in potassium chloride was run *versus* seawater, calcium chloride and sodium chloride (Figure 5.12).

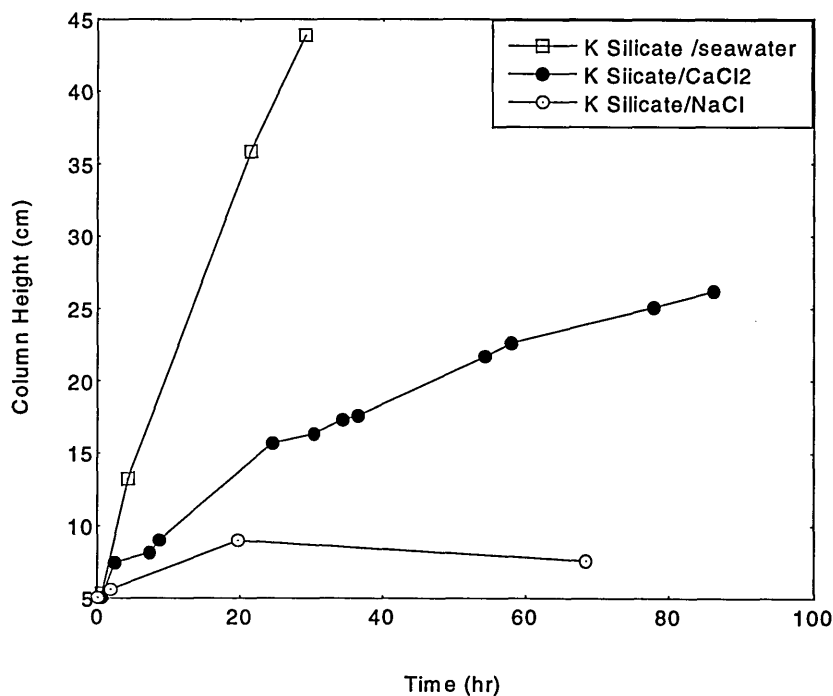


Figure 5.12: Fluid flow profiles for a homoionic potassium silicate (pH 13.3) run against different salts on side B.

The fluid transfer levels are greatest when seawater is used but the time required to analyse all the components of the seawater by ion chromatography made this option

unrealistic for bulk screening. In the case of sodium chloride coupled osmotic flow is apparent during the time scale of the test. Initially water flows into side A to dilute the salt solution however as the ions leak through the clay film into side B the driving force for water flow or simply the osmotic pressure differential is reduced and water flows back to side B. When calcium chloride was present on side B no net reversal of water flow was detected as the divalent ion facilitates osmotic barrier formation.

Therefore it was decided to use calcium chloride on side B in future tests with silicates. From the data in Figure 5.13 and Table 5.3 it can be seen that changing the pH of the silicate solution alters the level of fluid movement and that the response is different for different silicate systems. In fact there is a marked difference between the fluid movement levels for the Na silicate and K silicate levels at pH 12.4. This difference of 5.8 and 19.4 cm of movement for the sodium and potassium systems respectively cannot be explained in terms of the osmotic pressure differences alone; since the water activity of the solutions was 0.84 and 0.88 respectively. In Table 5.3 the fluid movement levels (B to A) and ion concentrations on side B are presented.

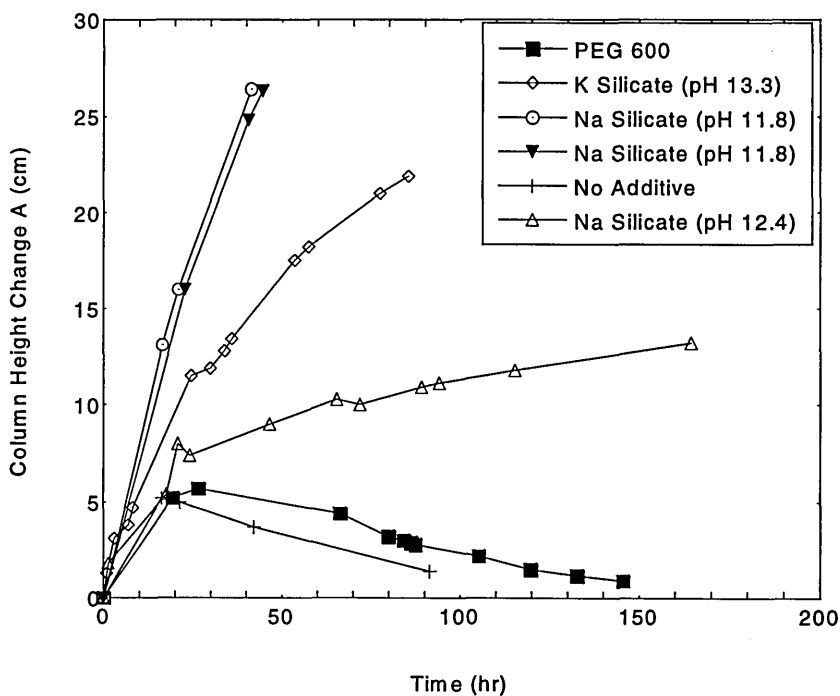


Figure 5.13: Fluid transfer levels in the Clay Membrane Cell in the presence of silicates. The systems are homo-ionic with 3 M sodium or potassium chloride on side A and 0.5 M calcium chloride on side B initially.

Repeat runs using the same test conditions can be seen to give good reproducibility in terms of fluid movement. The salts used were 20.5 mg/g Ca on side B or on side A 78.6

mg/g of Na or 122.2 mg/g of K. In most cases there is no evidence of depletion of Ca from side B and not much leakage of sodium or calcium across the clay film. The error in the measurement is such that it would be improper to compare the values for sodium and potassium and use them to comment on the quality of the osmotic membrane. It is clear that there is some uncertainty as to the nature of the silicate anions present in solution. Nuclear Magnetic Resonance studies have been carried out by Knight [22] to show that as many as 16 anions can be identified in a potassium silicate solution. One could therefore postulate that the structure or porosity of the silicate precipitate would vary with pH as the solution species vary. Unfortunately no direct study on membrane quality could be found in the literature.

pH of solution side A (+/- 0.1)	Height change (A) (+/-0.2cm)	% vol. change	Ca (B) mg/g ± 0.5	Na (B) mg/g ± 0.5	Test Time (+/- 0.5 hr)
11.8	15.3	10	21.4	0.4	22
11.8	15.6	10	21.3	0.3	22
12.4	5.8	4	19.5	1.0	18
12.4	5.8	4	20.6	0.3	18

pH of side A (+/-0.1)	Height change (A) (+/- 0.2cm)	% vol. change	Ca(B) mg/g ± 0.5	K(B) mg/g ± 0.5	Test Time (+/-0.5 hr)
11.8	12.7	8	21.5	N/A	17
11.8	14.3	9	20.5	1.1	24
12.4	19.4	12	23.4	1.0/0.9	23
12.4	17.9	11	23.9	1.2/1.3	17
13.3	14.7	9	21.7	1.6	20
13.3	13.1	8	22.0	1.6	21

Table 5.3: Fluid transfer to side A and ion concentrations on side B for sodium silicate and potassium silicate *versus* calcium chloride at different test times.

The formulations prepared for the Clay Membrane Cell experiments were used in cuttings dispersion tests. Data from these tests are presented in Table 5.4.

System	pH	% rec. (2 hr)	% rec. (16 hr)
sodium	11.8	99	99
	12.4	80	57
potassium	11.8	100	100
	12.4	100	100
	13.3	100	100

Table 5.4: Recovery levels for Oxford shale cuttings from silicate solutions.

Data are tabulated from two independent shale dispersion tests one which was run for 2 hr and the other was allowed to continue for 16 hr. From the levels of shale recovered in Table 5.4 it is apparent that the poorest formulation is sodium silicate at pH 12.4. The shale remaining after the soak time for this sodium formulation was softer than that recovered from the other systems. It can be seen in Table 5.3 that the volume of water drawn from the calcium chloride solution into the silicate side is lowest in the case of sodium silicate at pH 12.4. In all other cases the shale has been hardened by the silicate fluid

The exact location of the membrane setup by the silicate interaction with the calcium ion or the drop in pH has not been verified by the Clay Membrane Cell experiments. Experiments carried out with the Hassler cell in which the silicate system was pushed through an Oxford shale core for a number of weeks showed that the flow rate through the core was reduced [17]. However the presence of silicate precipitate was not tracked along the core length but alterations to the shale texture on the inlet side a few mm in from the external surface was noted. .

5.1.3 Summary

The work outlined in this section has shown the following;

- fluid transfer measurements are adequately reproducible from the Clay Membrane Cell
- it is possible to compare data obtained from the Clay Membrane Cell with values obtained from shale dispersion experiments.

At the time this research was carried out the establishment of osmotic barriers on the clay surface was perceived as the route to finding a water based mud with oil based mud performance as a shale stabiliser. The Clay Membrane Cell containing a montmorillonite film and one sheet of filterpaper was adequate for these purposes at Schlumberger. However to help in understanding the movement of ions on the clay surface in the

presence of glycol additives it was decided to develop the cell further. Details of these experiments are outlined in the next section.

5.2 Clay films supported by fine discs

An experiment to examine the effect of glycol on the transfer of water and salt through a thin clay film was sought.

In these tests the coarse discs used in the work with silicates were replaced by discs with finer pores (*ca* 1.5 μm) and filter-paper was added on the high salinity side of the film. The fluid levels were monitored on both sides of the clay film for the duration of the test. In some cases the movement of salt ions was inferred from conductivity measurements. This complete set of data allowed the Sherwood model to be applied to help with interpretation. Attempts at independent checks on some of the parameters determined from this model were carried out using direct permeability measurements. Data from these tests are presented in this section.

5.2.1 Osmotic tests

As a first step in this work it was checked that the fluid flow in the cell was detected properly. In Figure 5.14 the fluid flow out of side B is symmetrical with the fluid flow into side A. However trivial this may seem it justifies the modifications to the clamping arrangements of the cell during the design as described in Section 3.0 and 4.1.

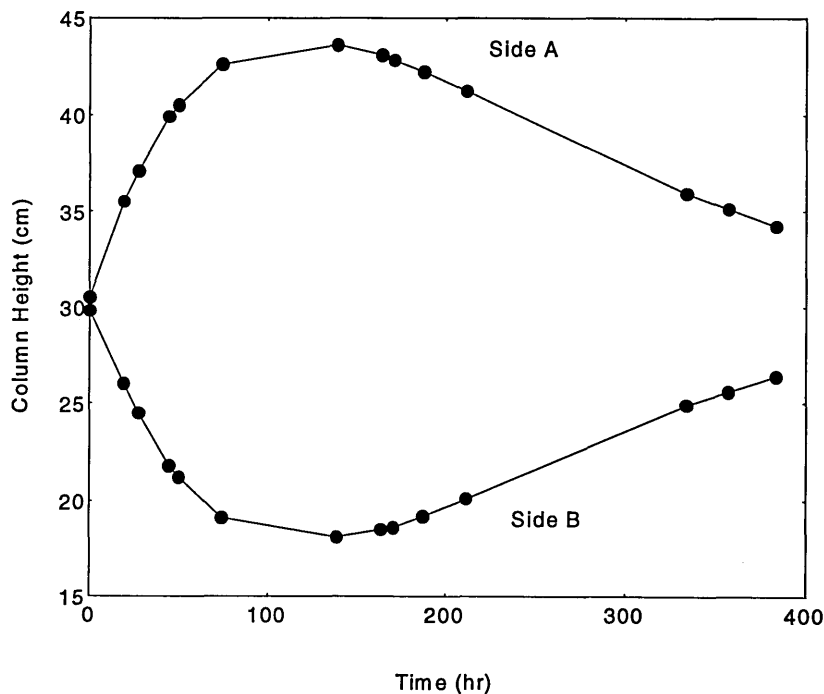


Figure 5.14: Fluid flow between 0.5 M CaCl_2 and 3.0 M NaCl .

When the Clay Membrane Cell was dismantled after this test the filter-paper-clay film-filter-paper sandwich could be lifted out of the cell. The thickness could be measured using a digital micrometer. The filter-paper is incompressible and the measurements showed that the clay film was 10 μm thicker in the centre than around the edges. This suggests that there is a bending moment on the clay cell when the edges are bolted together. From an average of 10 measurements diagonally across the film taken immediately after removal from the cell a thickness of $110 \pm 10 \mu\text{m}$ was calculated. Measurements on the film taken directly from the filterpress gave a value of $120 \pm 3 \mu\text{m}$ for the thickness. This simple analysis shows that the film was confined during the test in the osmotic cell but not necessarily compacted. When the assembly had been allowed to dry in air the clay film could be removed from the filter-paper backing for analysis by XRD and FTIR.

The fluid heights developed were now substantially more (Figure 5.15) than had been measured when the clay film was allowed to swell into one of the porous discs.

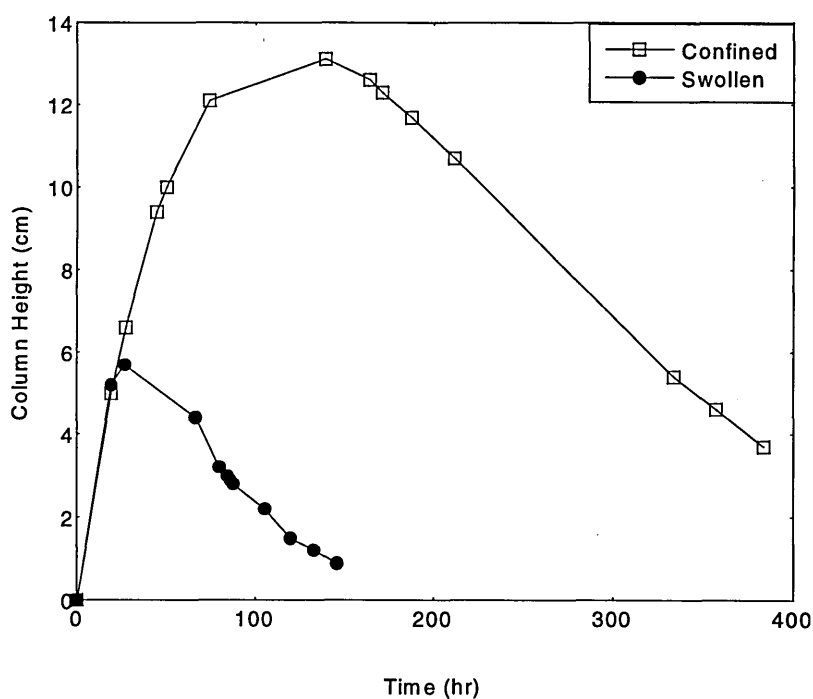


Figure 5.15: Comparison of fluid flow profiles for clay films held between different disc types in the clay cells. Solutions were 3.0 M sodium chloride and 0.5 M calcium chloride.

One could postulate that the clay film confined between two fine discs was less porous than one allowed to swell into the more porous disc. Reducing the porosity of the clay matrix could increase the ability of the montmorillonite to reject the salt. Alternatively

the permeability of the film to water flow would be higher in the case of the swollen film. The osmotic pressure differential across the clay film at the start of the tests can be calculated using Equation 5. It is then interesting to note that the hydrostatic pressures developed are of the order of kPa while the osmotic pressure in the cell at time zero was 38 MPa. This immediately suggested that the clay films were permeable to ions, *i.e.* had a low reflection coefficient otherwise the fluid would continue to pump into side A.

The aim of this work was to determine the possibility of developing a water based mud additive which would form an osmotic membrane. The first step was to add 5 wt% of a polyol to side A of the cell and monitor the change in the fluid flow profile. Data from such an experiment on a sodium chloride-(glycol) / sodium chloride system is given in Figure 5.16.

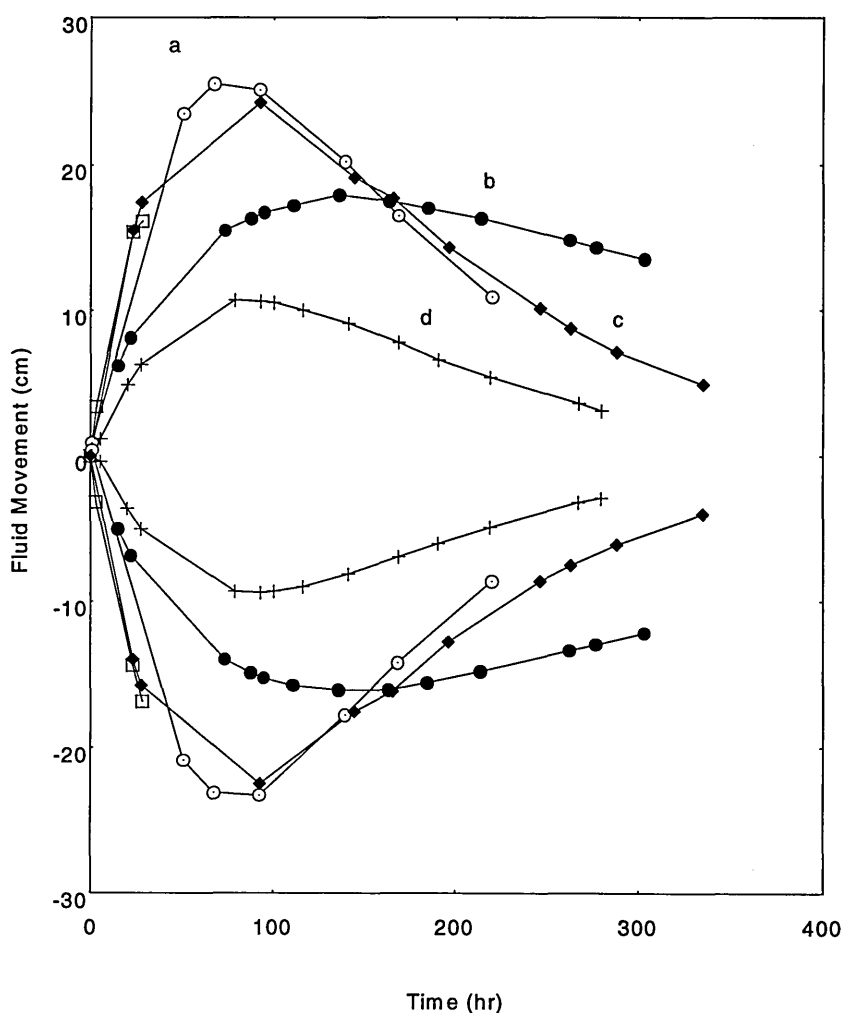


Figure 5.16. Fluid flow profiles across a clay film for sodium chloride systems with and without polyol added. a is NaCl, c is NaCl, b is NaCl and eda-po, d is NaCl and peg 600.

It can be seen from Figure 5.16 that the 2 experiments (15a&c) run for solutions without glycol appear to give similar trends in fluid movement *versus* time. These

experiments were carried out in parallel using the same batch of clay, glass beads and filter paper but different cells. In all cases the curves show a maximum indicating coupled osmotic flow although for these experiments the leakage of ions was not monitored. Adding peg 600 and eda-po to the 3 M sodium chloride solution changes the shape of the curves lowering the maximum in the curves and altering the shape of the return profile. No data could be found in the literature for similar experiments of clay treated with polyol. XRD studies of clay films treated with eda-po and films treated with peg 600 in the presence of 1M NaCl had equal basal spacings of 18.4 Å. This means that changes in the bulk pore size caused by the interlamellar region alone cannot be used to explain the differences in the shapes of the curves for the two glycols. It was deemed necessary to attempt to determine the condition of the clay film during the test time in terms of the thickness and basal spacing. With this purpose in mind access to the synchrotron source at Daresbury was gained in collaboration with Dr Chris Hall, Schlumberger, Cambridge and Dr Sally Colston, Birkbeck College, London.

5.2.2 Clay film examination through synchrotron experiments

Others such as Huang *et al.* [23] have used synchrotron sources to examine the mineralogy, hydration and dehydration of clays at high pressures and temperatures. A powerful X-ray source allows one to examine bulk samples at high pressures and temperatures. This was the first time an experiment on such a thin clay film (inside or outside the clay cell) had been attempted and there was a total of 6 days of research time available throughout the 2 year period. The specific aims of the work were to

- measure the basal spacing of the clay film in-situ in the clay cell,
- detect any bulk swelling of the clay film by measuring the in-situ thickness,
- confirm the intercalation of the glycol throughout the clay film
- check if the glycol reduces the volume of the bulk pores in the film or forces the film to expand.

A special cell base was designed to allow the Clay Membrane Cell to be placed in the synchrotron beam while the osmotic test was running; other experimental details were given in Section 4.7 Chapter 5. The capillary tubes were left in the cell and except for slight changes in temperature during the 20 minute test time, the X-ray monitoring was essentially non destructive. Initial experiments were carried out on air dried films placed outside the Clay Membrane Cell. Then the beam widths were adjusted to 35 µm and a clay film scanned in the Clay Membrane Cell with solutions present. Examples of the profiles obtained are given in Figure 5.17.

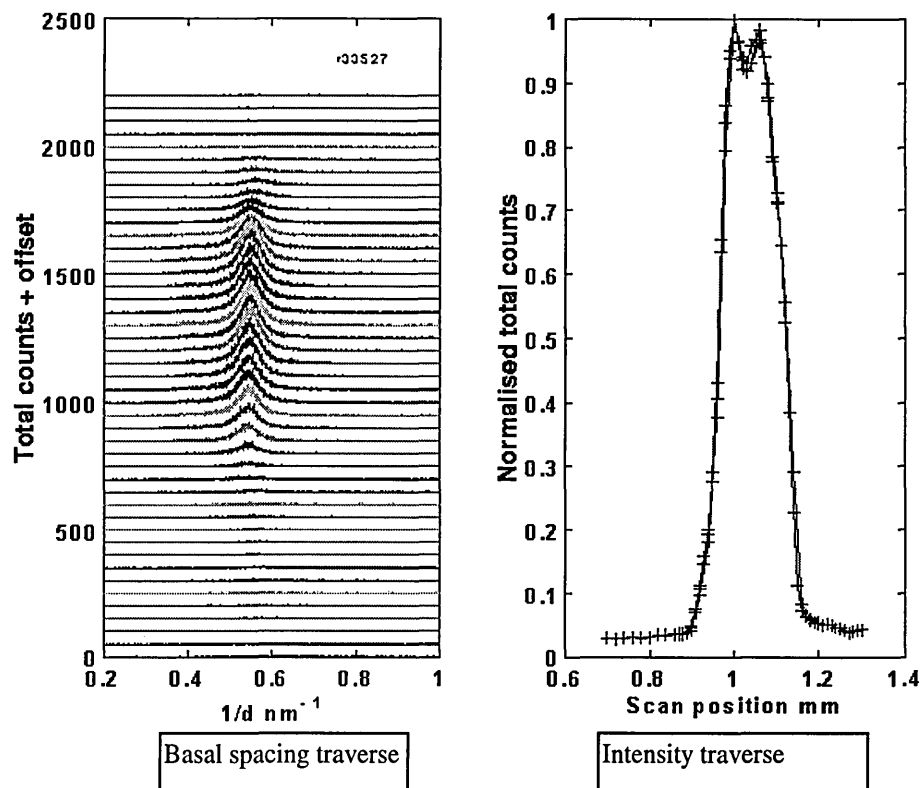


Figure 5.17: Profiles from the synchrotron experiments showing the variation in basal spacing and diffracted intensity as the beam passes from solution through the clay film and back into the solution. The film had been placed in a 3 M KCl-(eda-po)/0.5 M NaCl system and allowed to reach equilibrium before scanning.

On the left (of Figure 5.17) in the basal spacing traverse the beam moves from side B (initial low salinity) to side A (initial high salinity side). No diffracted radiation is detected in the solution and once the X-rays interact with the clay film the basal spacing at 18.4 Å can be detected. This peak can be tracked until the beam is only incident on the solution showing that the glycol eda-po is intercalated throughout the 120 µm film.

On the right hand side of Figure 5.17 the integrated diffracted intensity at different beam positions in steps of 10 µm is shown. The full width at half maximum reads as 160 µm which is greater than expected. In fact placing an air dried film in the clay cell without solutions gave a peak width at half height of 135 µm when the hand held micrometer read 73 µm. Close examination of the Intensity traverses showed that the slope of the leading and trailing edges of the peak were different. This anti-symmetry could be accentuated by placing objects under the base at one side of the cell thus making the films appear thicker. Simply rotating the cell gave a spread of values of 128, 130, 195 and 200 µm. Ideally the clay cell would be suspended from the ceiling to

avoid any misalignment in the stage but the number of days assigned to the project had finished by then.

Preliminary experiments showed that the basal spacing measured for the tests listed above (Figure 5.16) that had been running for at least 200 hr agreed with values measured for unconfined montmorillonite pastes as documented in Chapter 4. This suggests that the confinement of the clay film does not prevent the intercalation of the glycol. Unfortunately the synchrotron analysis came after the maximum in the fluid flow profiles. The significance of which was not understood at the time the Synchrotron experiments were carried out. However it is known that from that time period on the clay film in the cell always had the same basal spacings. The intercalation of glycol was verified by XRD at SCR after the films had been removed from the cell and dried over phosphorous pentoxide.

One attempt was made at setting a test up in the Daresbury laboratory to evaluate the early time behaviour when the glycol comes into contact with the clay and some evidence of ordering of the clay film was seen. The aim had been to detect changes in d-spacing as the cell chemistry was altered, in this case by adding potassium chloride. This cell had previously been equilibrated with 3 M sodium chloride/0.5 M sodium chloride for one day and a basal spacing of 18.5 Å was noted. The solution on side A was then replaced with a 3 M NaCl-peg 600 solution and an intensity change in the diffracted peak in the centre of the clay film was noted after an 8 hr period as shown in Figure 5.18. This increase in intensity of the basal reflection signifies glycolation. No change in the basal spacing was detected which is in keeping with data collected in Chapter 4.

Because of the limited beam time the top half of the cell was removed with the porous disc and a 1 M potassium chloride solution pipetted directly onto the filterpaper over the clay film. The cell was then resealed and the basal spacing measured. The cell was scanned every minute and the development of a second peak at 15.4 Å was noted. Data from this experiment are presented in Figure 5.18. A basal spacing of 15.4 Å has been noted before in Chapter 4 for montmorillonite films treated with peg 600 in 1 M KCl. It either signifies that a layer of glycol is washed from the interlamellar region or the clay part ion exchanges to the potassium form which favours monolayer intercalation. When the cell was returned to SCR the glycolation of the clay film was verified by drying the film over P₂O₅.

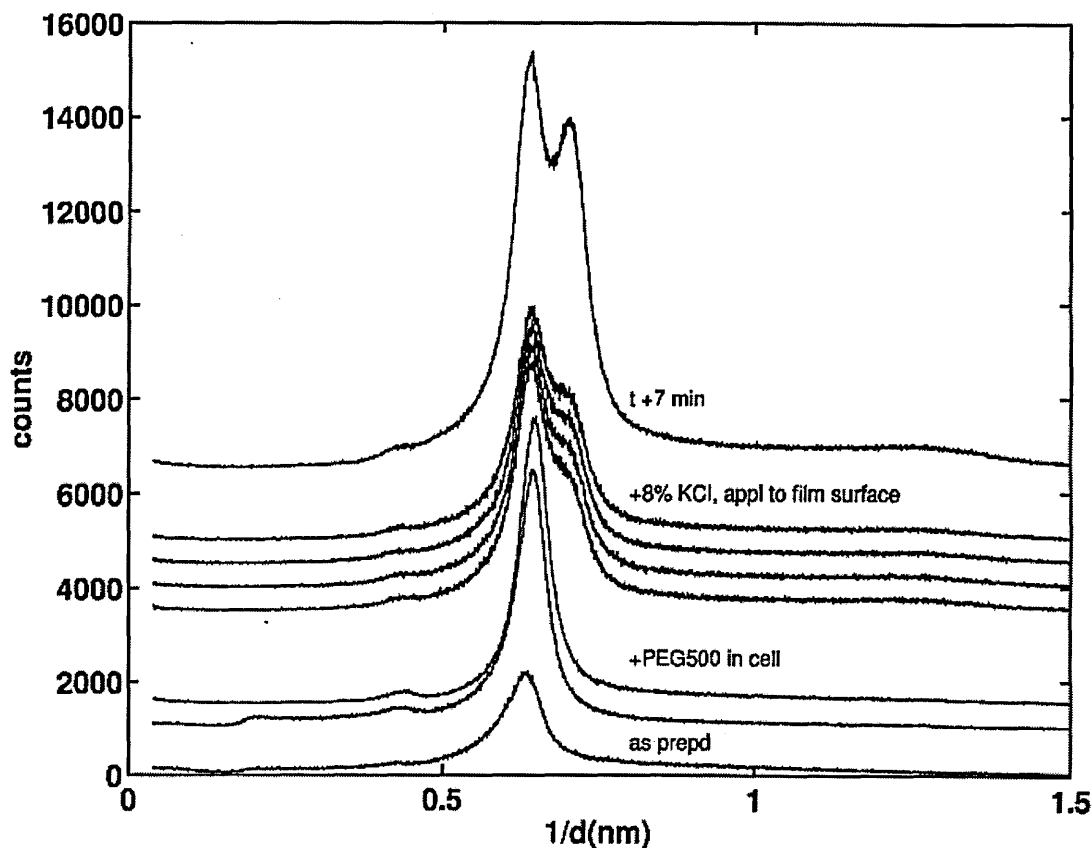


Figure 5.18: Diffraction profiles showing the change in peak intensity with the addition of peg 500 and subsequent peak shift on the addition of potassium chloride in the centre of the clay film.

Although much progress was made in examining the condition of the clay film in-situ in the cell more work has yet to be done. The chance to complete this program was hindered by the limited beam time allowed for a private company such as Schlumberger.

Nevertheless the following conclusions could be drawn,

- it is possible to locate a thin clay film in-situ in the Clay Membrane Cell,
- without stage misalignment it would be possible to monitor the swelling of the film,
- the glycols intercalate thoroughly into all the available interlamellar regions,
- confining the clay film does not prevent glycol intercalation,
- it would be possible to examine the equilibration of salinity across the film using basal spacings as a marker.

5.2.3 Pathways for diffusion

Although a lot of research has been carried out on diffusion through clay gels and nano-composites there is not a clear picture as to the exact structure of a clay gel or film.

Tactoid formation in concentrated dispersions (of montmorillonites bearing calcium ions) would be expected to manifest itself in the final film. However this would suggest

potassium chloride on side A and sodium chloride on side B. Potassium chloride was chosen as eda-po gives bilayer complexes with potassium chloride whereas peg 600 displays monolayer intercalation.

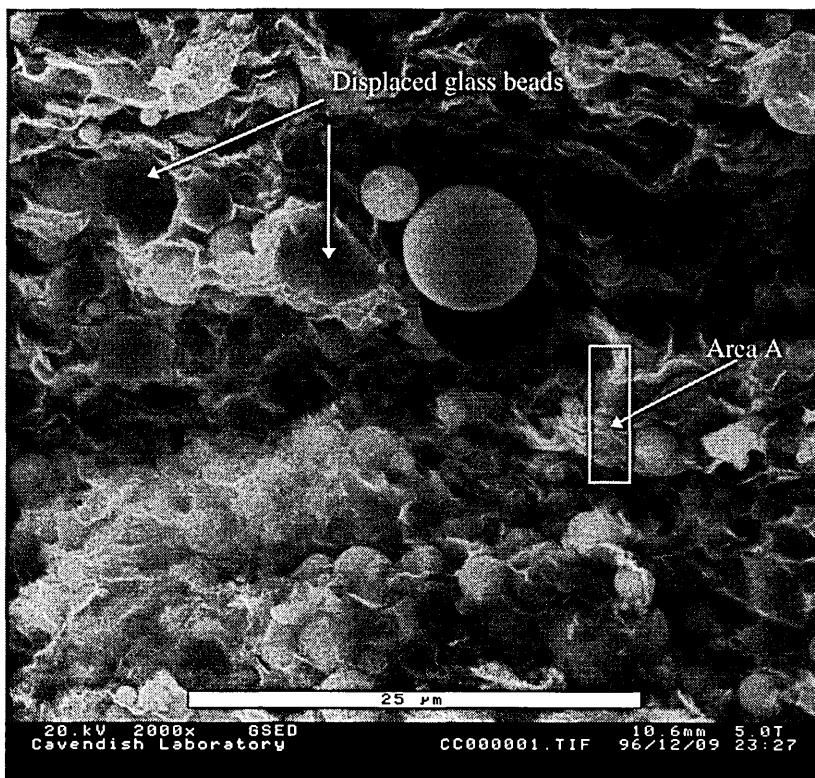


Figure 5.20: Micrograph taken on the Esem of an SWy-1/glass bead film without prior salt treatment and under ambient humidity conditions. The bar on the micrograph represents 25 μm .

Data from these experiments are presented in Figure 5.21 again showing the drop in peak fluid flow with the addition of glycol. The basal spacing of the clay film treated with salt only is 14.5 \AA , for eda-po is 18.4 \AA compared with 14.8 \AA for peg 600.

As shown in Figure 5.16 the presence of the glycol in tests presented in Figure 5.20 causes the maxima in the fluid flow profiles to drop. For the films treated with salt only and treated with peg 600 the basal spacings are the same but the difference in the fluid height profiles suggest that the permeability of the film to water or ions is affected by the presence of the peg 600. To get the response shown the permeability of the film to water would need to be reduced or the permeability to ions increased.

Any change in the leakage of ions is still under debate. As mentioned in Chapter 4. Aranda and Ruiz-Hitzky [26] suggest that the conductivity of clay composites in the presence of intercalated polyethylene oxide is increased as the ions move through the

middle of the intercalated glycol, where they are somewhat shielded from the negative charge on the clay layers.

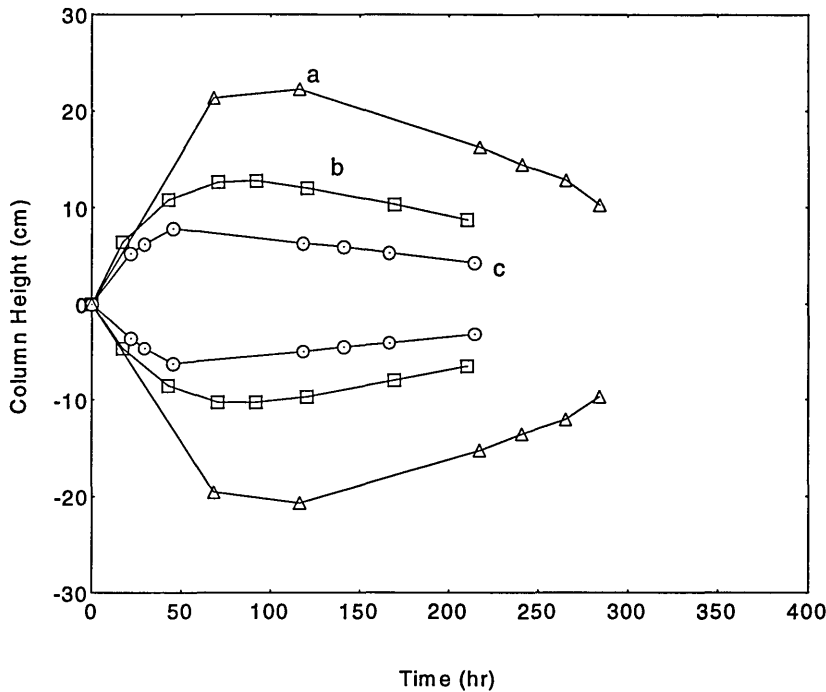


Figure 5.21: Fluid flow profiles across a clay film for potassium chloride (3 M) *versus* sodium chloride (0,5 M) systems with and without polyol added; a is salt only, b is KCl/eda-po, c is KCl/peg 600.

However this line of argument is complicated by the fact that in a 1.75 M, 1:1 electrolyte the diffuse double layer thickness is *ca.* 2.3 Å. This number has been estimated using Equation 24 from the Debye Huckel theory [27].

$$\kappa^2 = \frac{2n_0e^2z^2}{\epsilon_r\epsilon_0KT} \quad (24)$$

where κ^{-1} is the diffuse layer thickness, n_0 is the number of ions pairs per unit volume (m^3), e is the charge on an electron (1.6×10^{-19} C), z is the valency of the ions, and the product $\epsilon_r\epsilon_0$ is the permittivity of water (7.1×10^{-10} J C⁻² m⁻¹), K is the Boltzmann constant (1.4×10^{-23} J K⁻¹), and finally T the absolute temperature. Assuming a separation of the clay layers of $(14.8-9.5)=5.3$ Å this suggests that an ion moving through the middle of the non-glycolated interlamellar region would be traveling under the same potential as an ion in bulk solution. Could the experiment then detect the difference in the rates for an interlamellar region glycolated or non glycolated? This question has yet to be answered. However applying the model of Sherwood to the data

collected in the Clay Membrane Cell would allow the permeability and diffusion rates of the salt to be determined.

5.2.4 Application of the Sherwood model

The solutions of the Sherwood model have been presented in Section 6.3.0 Chapter 5. Before applying the model to the data of the type shown in Figure 5.22 the issue of reproducibility needed to be addressed.

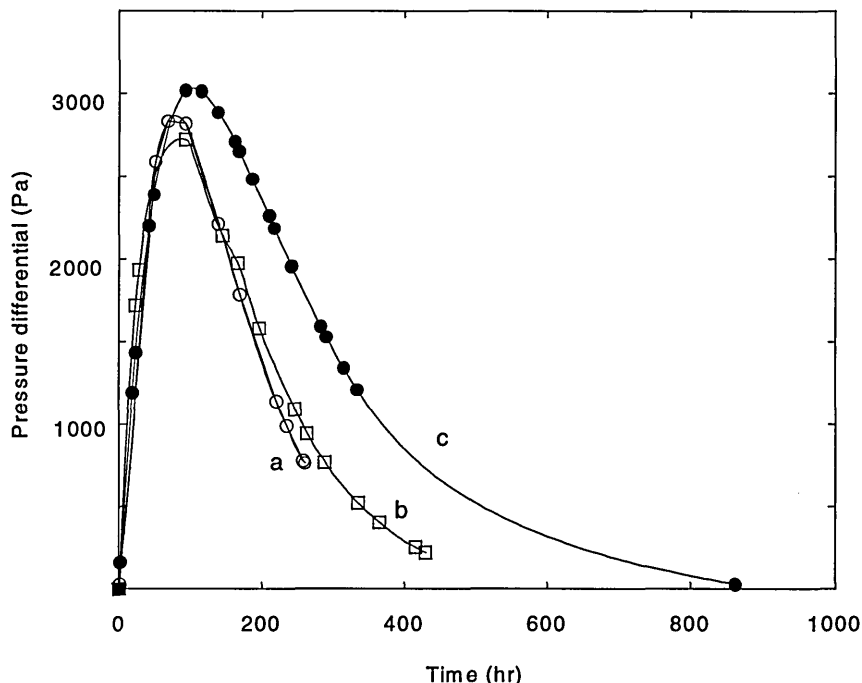


Figure 5.22: Repeatability of the membrane cell experiments where sodium chloride was used on either side of the film. a and b are experiments that were started on consecutive days. c was started a month later with a different batch of filterpaper.

As mentioned in Section 5.1.1, Chapter 5 the reproducibility of the fluid flow profiles in the assessment of the silicate formulations was very good. From Section 5.2 onwards the clay films were confined between the two sheets of filterpaper and the finer discs. Profiles collected under this testing regime were not always so reproducible. It could be that the floc structure in the clay dispersion (see Section 5.2) changes with time thus altering the structure of the final film. Alternatively the surface of the clay film could be remolded depending on the topography of the filterpaper. Technical information would not be released by Millipore on likely variations in the structures of the filterpaper. But since the paper were formed by spin coating, the possibility of different distribution in pore sizes between batches of filterpaper was possible. Using the same batch of filterpaper and starting experiments on consecutive days gave reproducible results as shown in Figure 5.22, a and b.

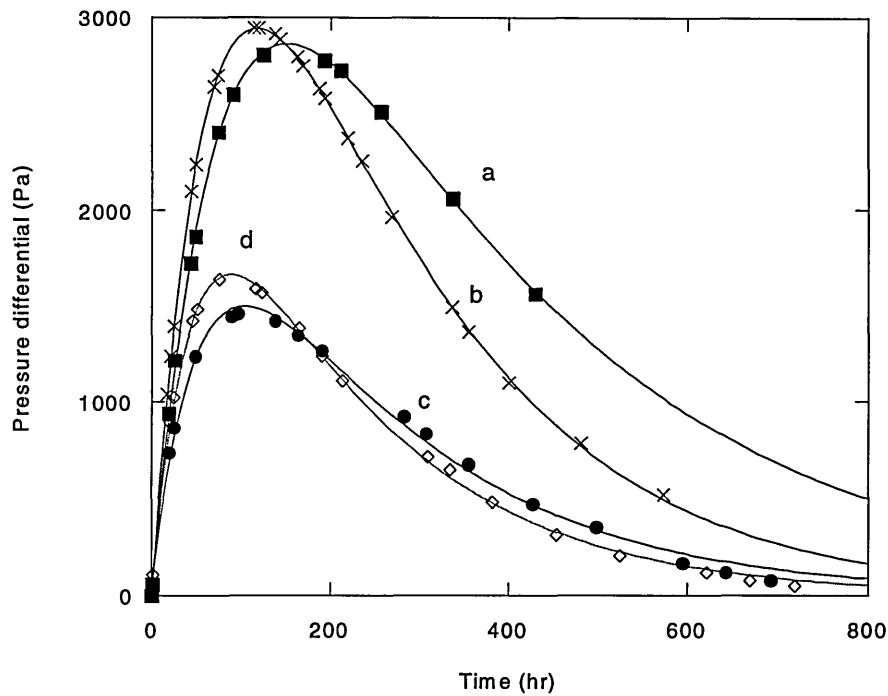


Figure 5.23: Pressure profiles as a function of time for homo-ionic systems with and without glycol. a is sodium chloride, b is potassium chloride, c is NaCl/eda-po and d is KCl/eda-po

Pressure differential and mole fraction differential *versus* time for experiments run with the same cation on each side are presented in Figure 5.23 and 5.24. The shape of the pressure profiles are similar to those obtained previously and displayed in Figure 5.21. It is interesting to note that at the peak in the pressure profile the salt concentration has not equilibrated on each side of the membrane (Figure 5.24) , *i.e.* further leakage of salt occurs from side A to B when the water is flowing back from side A to B.

The homoionic sodium chloride experiment will be fit as an example and then the same fitting procedure carried out for the other 3 experiments but for brevity just the results from this routine will be supplied.

In the experiment with sodium chloride on either side 3.0 M salt and 0.5 M salt was used on either side of the clay film. The values for Δp using a density of 1069.6 kg m^{-3} intermediary between the 1020.7 kg m^{-3} and 1118.2 kg m^{-3} Applying Equation 15 to the differential pressure *versus* time profile the following values were obtained

$$a_1 = 6.14 \times 10^3 \text{ Pa}, a_3 = 6.22 \times 10^3 \text{ Pa}, a_2 = -3.12 \times 10^{-3} \text{ h}^{-1} \text{ and } a_4 = -1.22 \times 10^{-2} \text{ h}^{-1}$$

The rapid process corresponds to the decay rate a_4 and the slow process to a_2 ; these rates can be used as obtained from the pressure data alone. Using Equation 18 and 19 the membrane permeability can be calculated as follows;

$$-a_2 = \frac{2Sg\rho^0 kV_w}{A_c} \quad (18)$$

Values of $S = 7.55 \times 10^{-4} \text{ m}^2$, $A_c \cong 9.1 \times 10^{-6} \text{ m}^2$, $g = 9.81 \text{ m s}^{-2}$, $\rho^0 = 1069 \text{ kg m}^{-3}$ and $V_w = 1.8 \times 10^{-5} \text{ m}^3 \text{ mole}^{-1}$ were used. This gave $k = 3.4 \times 10^{-8} \text{ moles m}^{-2} \text{ Pa}^{-1} \text{ s}^{-1}$. If one now assumes that the film thickness $h = 120 \text{ }\mu\text{m}$ and that the viscosity of the solution is close to that of water $\nu = 10^{-3} \text{ Pa s}$, then by

$$k_d = \nu V_w h k \quad (19)$$

$$k_d = 7.3 \times 10^{-20} \text{ m}^2 \text{ or } 7.3 \times 10^{-8} \text{ Darcy}$$

The total volume of water on any one side of the clay film excluding solution in the capillaries is approximately $V_d V_w n_w^0 = 1.4 \times 10^{-5} \text{ m}^3$, so that $n_w^0 = 0.78$

$$\text{Using Equations 21, } \lambda D = \frac{-n_w^0 a_4}{2S} \text{ and 22, } D_s = h V_w D$$

the diffusion coefficient of the salt can be calculated. $D = 1.5 \times 10^{-3} \text{ moles m}^{-2} \text{ s}^{-1}$ and $D_s = 3.2 \times 10^{-12} \text{ m}^2 \text{ s}^{-1}$.

Corresponding plots for the mole fraction differential *versus* time are presented in Figure 5.24.

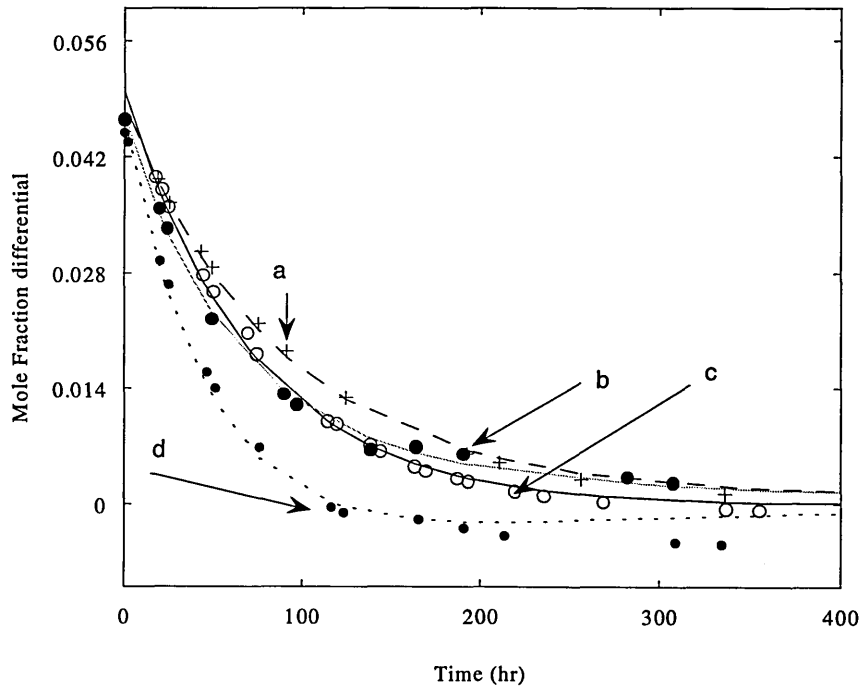


Figure 5.24: Mole fraction differential of salt as a function of time for homo-ionic systems with and without glycol. a is sodium chloride, b is NaCl/eda-po, c is KCl/KCl and d is KCl/eda-po

The error on the measurement is apparent since the mole fraction differential drops below zero into the negative in some cases. The model is difficult to fit to the curves and tends to give a single rate constant since a high percentage of the salt diffuses through the film in early time (before the peak in the hydrostatic pressure curve). Analysis of the fit to the hydrostatic pressure differential *versus* time clearly allows the permeability and diffusion coefficients to be extracted from data presented in Figure 5.23. The use of the profiles in Figure 5.24 extracted from the conductivity data is not necessary for determining these two transport coefficients.

Parameters determined from the fitting routine are compiled in Table 5.5.

System	Permeability (k_d) $\times 10^{-20}(\text{m}^2)$	Diffusion coefficient (D_s) $\times 10^{-12}(\text{m}^2 \text{s}^{-1})$
NaCl	7.3	3.2
KCl	9.7	4.0
NaCl/eda-po	10.0	4.4
KCl/eda-po	9.3	7.1

Table 5.5: Parameters determined from fitting the Sherwood model to the pressure differential *versus* time profiles displayed in Figure 5.22.

Data presented in Table 5.5 are from the analysis of one complete set of experimental results and given the small increase in permeability detected on the addition of the glycol eda-po it would be dangerous to assume that there is a real increase in the permeability once KCl or glycol is added to the cell. In order to compare the values tabulated here with some of those in the literature an estimate of the volume porosity of the clay film was required.

The porosity of the montmorillonite-glass beads film was calculated after its removal from the API filtration cell (Section 4.2 Chapter 5). The thickness of the wet film was measured with a micrometer and the total volume of the film estimated using the diameter of the film also. From the weight of dispersion added to the filtration cell the volume of montmorillonite and glass beads was calculated. From an average of three calculations a volume porosity of 0.7 ± 0.1 was obtained.

Many studies on the hydraulic conductivity of clays and shales exist in the literature but much care is required when converting from units such as cm/sec to m^2 . Also there is usually some uncertainty when comparing results due to the sized fraction of

clay taken to form the compacts under study, the compaction pressures used and the salt concentration. One study is presented by Kharaka and Berry [28] in which the permeability of a Wyoming bentonite (92 % < 2 μm) to seawater was determined. The sample was 3.2 mm thick and compacted under a pressure of 133 bar. A permeability of $3.3 \times 10^{-21} \text{ m}^2$ was determined. Unfortunately 133 bar was the lowest pressure used in the study by Kharaka and Berry but they found that doubling the compaction pressures halved the measured permeability. This would lead one to postulate that the permeability of a film compacted at say 17 bar would be of the order of $1.9 \times 10^{-20} \text{ m}^2$ at least the same order of magnitude as the values obtained in this study. Banin and Low [29] determined the hydraulic conductivity of sodium exchanged Wyoming bentonite to sodium chloride with a maximum concentration of 0.05 M. The lowest porosity of clay gel used was 0.8 and the permeability was estimated as $98 \times 10^{-20} \text{ m}^2$. Direct measurement of the permeability of the clay film used in the osmotic tests will be discussed in the next section.

The diffusion coefficients presented in Table 5.5 are for the combined anion and cation. The diffusion coefficients for NaCl and KCl at infinite dilution and 25 °C are 1.6 and $1.9 \times 10^{-9} \text{ m}^2 \text{ s}^{-1}$ respectively [30]. Generally it is expected that diffusion rates in compacted clays are less than those in reduced solution because of the reduced cross sectional areas of flow, the tortuous nature of the flow paths and the exchange of some salt species with the surface [30]. The general procedure followed in this work is to measure the diffusion rate of the anion through the structured clay and then calculate the tortuosity factor and assume it remains unchanged for the cation. Such diffusion coefficient are called effective diffusion coefficients and Shackelford and Daniel [30] quote values in the range of 4 to $10 \times 10^{-10} \text{ m}^2 \text{ s}^{-1}$ for the diffusion of anions through kaolinite. Mokady and Low [10] quoted values in the range of 2 to $6 \times 10^{-10} \text{ m}^2 \text{ s}^{-1}$ for the diffusion coefficient of NaCl through sodium exchanged Wyoming montmorillonite gels with a volume porosity varying from 0.7 to 0.9. In Equation 22 $D_s = hV_w D$ the value used for h was the thickness of the film (120 μm). In reality the salt flow will not be direct from one side of the film to the other. Oscarson *et al.* [31] measured the diffusion rate of iodide through compacted Avonlea bentonite. They defined a tortuosity factor τ as being equal to $(h/h_e)^2$ where h_e is the effective diffusion distance of the ion from one side of the film to the other. Values of h_e vary from $2h$ to $4h$ as the volume porosity of the compacted

clay changed from 0.6 to 0.43 respectively. Using values for h_e in Equation 22 would only increase the salt diffusion coefficient given in Table 5.5 by less than a factor of 10.

5.2.5 Hydrostatic tests

Darcy [15] established that it was possible to determine the permeability of a material by measuring the flux of water under a known differential pressure. Therefore it was decided to try such tests using the montmorillonite film in the Clay Membrane Cell. In these tests there was no osmotic pressure difference and the tests were started with a difference in hydrostatic pressure on side A and B of the clay cell. The rate of fluid flow varied exponentially with the pressure differential and Equation 23 was used to analyse the data. A plot of $\ln \Delta P$ versus test time for a film with 1.75 M sodium chloride either side is given in Figure 5.25. The slope of the plot is related to the permeability through Equations 18 and 19.

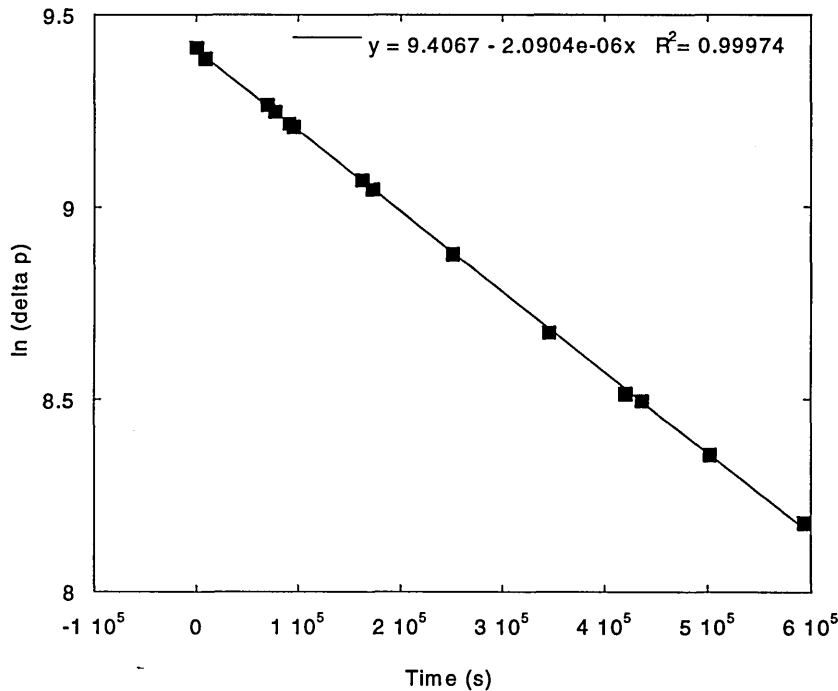


Figure 5.25: Plot of $\ln \Delta p$ versus test time for 1.75 M sodium chloride. The slope is used to calculate the permeability.

In this case the clay film had been treated with 1.75 M sodium chloride in the filterpress before insertion into the Clay Membrane Cell. Initially these tests were carried out to determine the permeability of the clay film to water directly. These results were then compared with those obtained by fitting the Sherwood model to data from the equivalent osmotic test; a test in which the 3.0 M and 0.5 M NaCl had been used. It is

not clear that a clay film equilibrated in 3.0 M and 0.5 M salt will have the same structure as a film that was always conditioned in 1.75 M salt. The term “history effect” is often used to describe the reluctance of clays to be reconditioned under certain circumstances. This experiment was repeated for clay films conditioned with 0.5 M and 1.75 M sodium chloride. The results for the two 1.75 M tests varied by a factor of 1.5 with the first result of $1.4 \times 10^{-19} \text{ m}^2$ and a repeat test giving $0.9 \times 10^{-19} \text{ m}^2$. Note here that the permeability of the film to water calculated from the Sherwood fit on the osmotic test was $0.7 \times 10^{-19} \text{ m}^2$ as shown in Table 5.5.

On examination of the surface of the clay film containing glass beads it was found that the top surface of the film contained some glass beads which protruded through the surface not covered by filter paper. This is shown in Figure 5.26 where the film is upside down.

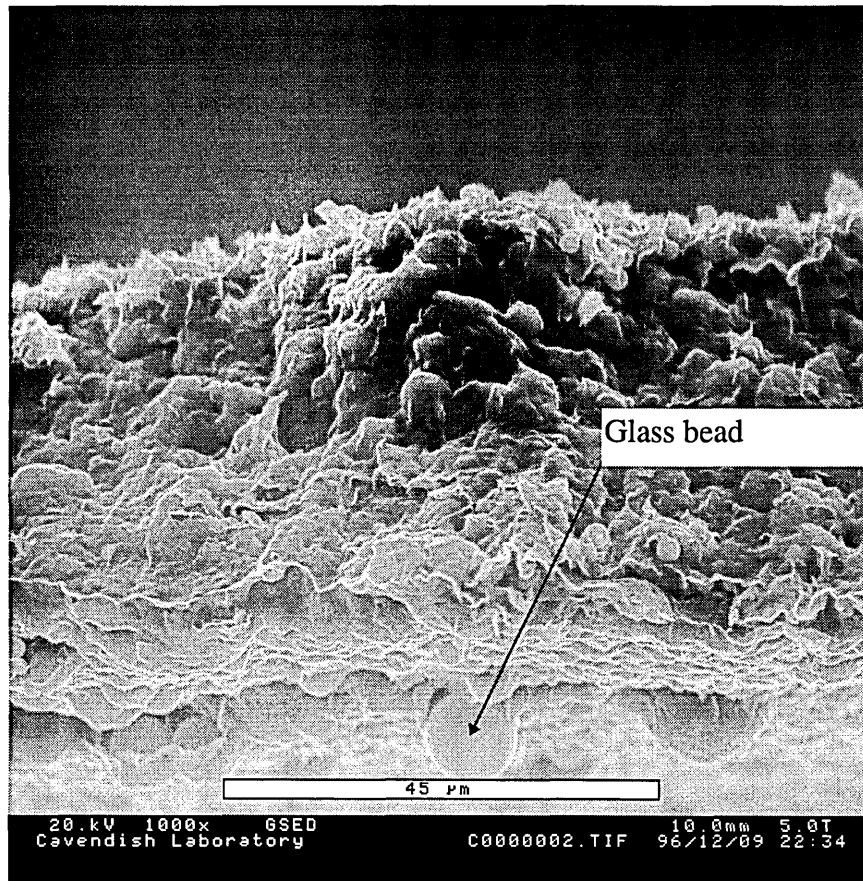


Figure 5.26: A micrograph of a clay film containing glass treated with 0.5 M CaCl_2 . The film had been air dried before insertion into the esem.

It was suggested that the protrusion of the beads would cause some randomness in the permeability of the film surface and consequently the surface of a film without glass beads was examined under the esem and is shown in Figure 5.27.

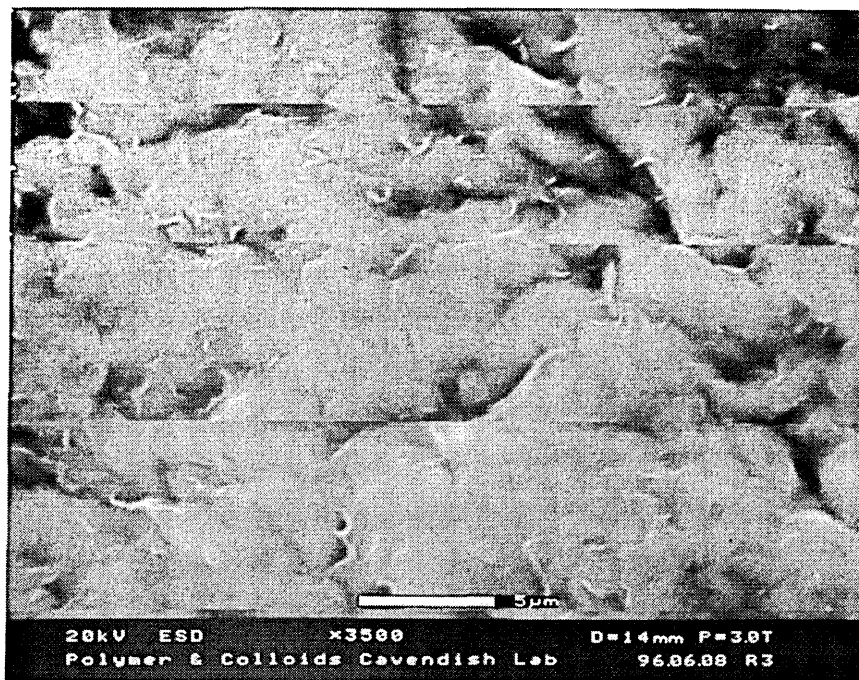


Figure 5.27: Surface of montmorillonite film exposed to the fluid and without glass inclusions. This micrograph was taken in an esem and jumps in the picture are due to vapour pressure affecting the rastoring.

However experiments run on beadless films gave similar variations. This was consistent with variations in permeabilities obtained from repeat runs with 0.1 M CaCl_2 . This data is presented in Figure 5.28.

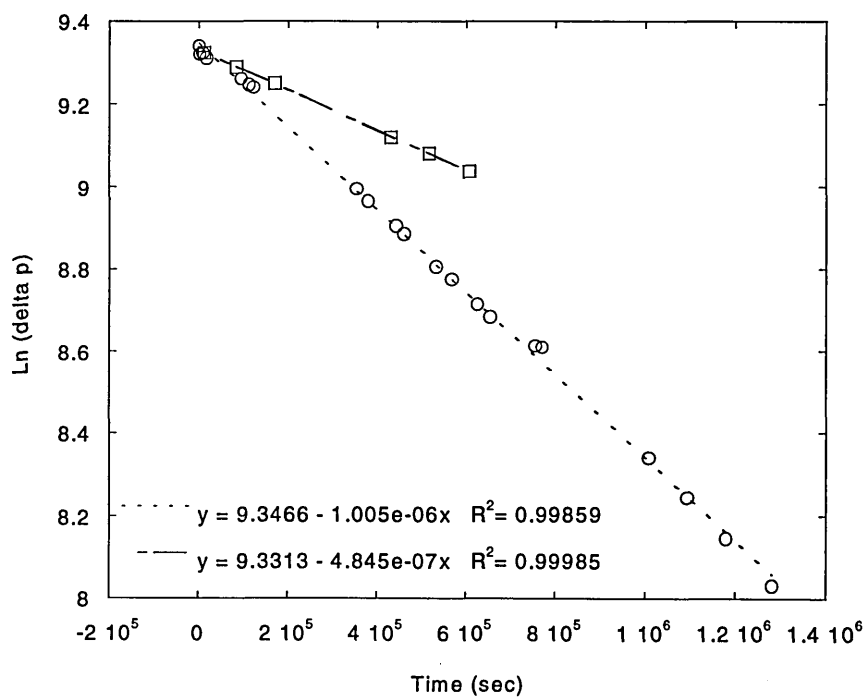


Figure 5.28: $\ln \Delta p$ versus time for repeat tests on the permeability of a clay film to 0.1 M CaCl_2

It was suggested to other users of the test at Schlumberger Cambridge Research that they should condition the clay film with salt and then add the additive through the ports provided. The change in permeability would then be detected. An example of such a change in permeability is shown in Figure 5.29. For 4 repeat runs of this test the results gave values of a reduction in permeability of 55 wt% with a maximum variation of ± 5 wt% between runs. Incidentally the reduction in permeability of a shale core conditioned using the same chemistry on a shale core in a Hassler cell for 5 weeks was 61 % as shown in Figure 5.30.

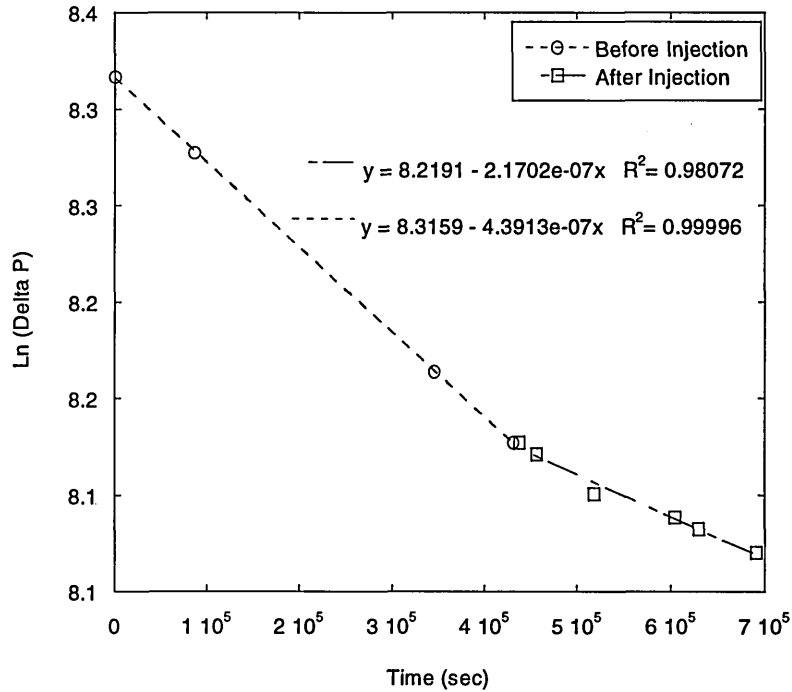


Figure 5.29: A reduction in permeability after the injection of an additive into the clay cell. Data courtesy of Dr John Crawshaw, Schlumberger.

This comparison is encouraging since the test time for the Clay Membrane Cell was 1 week compared with at least 5 weeks for the Hassler cell test. The experimental equipment required for the Hassler cell costs several thousand pounds compared with approximately 100 pounds for a Clay Cell. Where mass screening of additives is required the Clay Membrane Cell has obvious benefits.

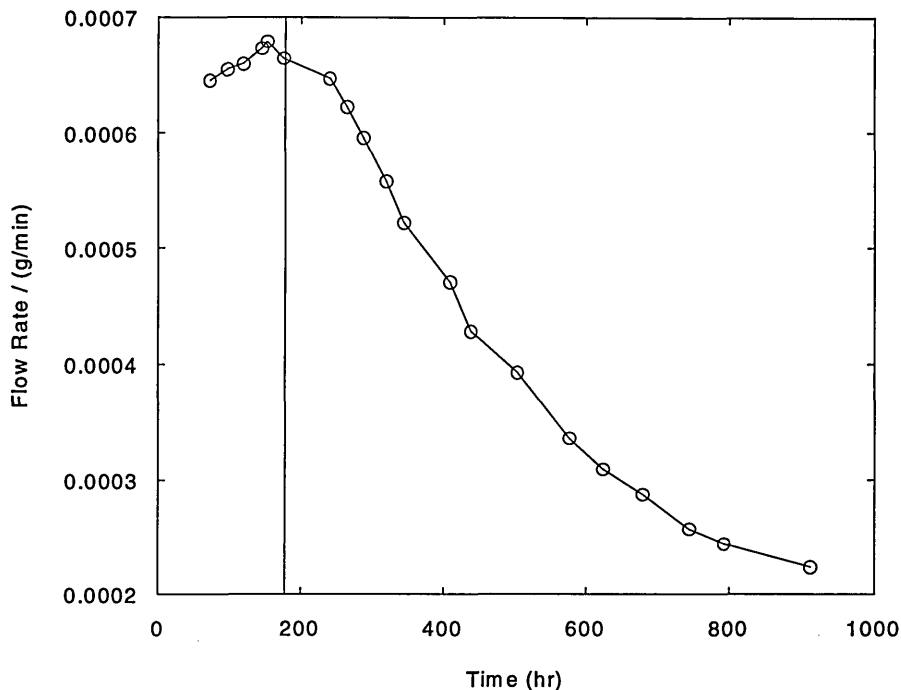


Figure 5.30: Drop in flow rate through the shale core on the injection (190 hr) of the additive. Data courtesy of Dr John Crawshaw.

6. Conclusions

A new test method has been designed to allow bulk screening of polymers for their performance in osmotic membranes. The Clay Membrane Cell is easy to use and gives results that can be compared with those obtained for similar work on shale. It is ideal for bulk screening as it is cheap to manufacture and maintain.

In cases where the clay films are confined between finer discs the intercalation of glycol can be monitored *via* changes in the pressure *versus* time profiles. Using synchrotron sources the basal spacing of the montmorillonite film can be measured insitu in the clay cell. For this configuration of experiment using fine discs, repeat experiments give different results for the permeability of the film to water. However this can be overcome by injecting the mud additive after the montmorillonite-beads film has been conditioned

The application of the Sherwood model to determine some characteristics of the film is useful in that it helps in understanding the flow process happening across the membrane.

7. Future work

There is still some uncertainty as to the position of the osmotic barrier produced by the presence of silicates. If it is setup on the outer surface of the montmorillonite film then it could be accidentally removed in the wellbore under certain flow regimes or by the action of the drill string. Monitoring the flow of silicate through the film as well as the ability of the silicate formulations to block porous glass discs of different pore size would give more information on the physical characteristics and location of the barrier.

Examination of the effect of intercalating species on the transport properties of the montmorillonite film was made possible by the modification of the clamping method for the film. It has not been verified yet by the application of the Sherwood model to the data from osmotic tests or the direct measurement of permeability that the glycol additives change the permeability substantially. This could be because the porosity of the montmorillonite-glass beads film is too high and changes in the pore size due to alterations of the basal spacings are not detected. Also the salt concentration used is very high and the salt is allowed to diffuse through the film past the charged clay surface unhindered. Reducing the salt concentration and reducing the porosity of the montmorillonite-beads film (by compaction or increased weighting of beads) could help emphasize more the effect of the additives.

Finally the Sherwood model needs to be extended to allow for the presence of the glycol and any deviation from ideality in the salt solutions.

8. References

- [1] Reid P. I., Dolan B. and Cliffe S. Mechanisms of shale inhibition by polyols in water based drilling muds, SPE 28960, SPE International Symposium on Oilfield Chemistry, San Antonio, 1995.
- [2] van Oort, E., Hale A.H., Mody F.K. and Roy S. Critical parameters in modeling the chemical aspects of borehole stability in shales and in designing improved water-based shale drilling fluids, SPE 28309, 171-186, 1994.
- [3] Sherwood J.D. A model of hindered solute transport in a poroelastic shale., Proceedings Royal Society London, A **445**, 679-692, 1994.
- [4] Santus G. and Baker R., Osmotic drug delivery: a review of the patent literature., Journal of Controlled Release, **35**, 1-21, 1995.
- [5] Young A. and Low P.F. Osmosis in Argillaceous rocks, Bulletin American Association Petroleum Geologists **49**, 1004, 1965.
- [6] Kemper W.D. and Rollins J.B. Osmotic efficiency coefficients across compacted clays, Soil Science Society American Proceedings, **30**, 529, 1966.
- [7] Fritz S. Ideality of clay membranes in osmotic processes: A review, Clays and Clay Minerals, **34**, 214-223, 1986.
- [8] Hassler G. L., Rice R. R., and Leeman E.H., Aime Trans., **118**,116-120, 1936.
- [9] Robin M.J., Gillham, R.W. and Oscarson, D.W. Diffusion of strontium and chloride in compacted clay-based materials, Soil Science Society American Journal, **51**, 1102-1108, 1987.
- [10] Mokady R. S and Low P. Simultaneous transport of water and salt through clays :1 transport mechanisms, Soil Science, **105**,112-418, 1968.
- [11] Sujata D. and Daroj Kumar S. Isothermal coupled transport process across clay membranes, Journal Indian Chemical Society, **68**, 331-333, 1991.
- [12] Newman F.H. and Searle V.H.L The general properties of matter, Arnold, London, 323-325, 1961.
- [13] Cussler E.L. Diffusion, mass transfer in fluid systems, Cambridge University Press, 1984.
- [14] Van Oort E., Hale A.H. and Mody F.K. Critical parameters in modeling the chemical aspects of borehole stability in shales and in designing improved water-based shale drilling fluids', SPE 28309, 1994.
- [15] Bear J. The dynamics of fluids in porous media, Elsevier Press, 106, 1972.

- [16] Laidler K. J. and Shuler K. E. The kinetics of membrane processes. I. The Mechanism and the kinetic laws for diffusion through membranes; *Journal of Chemical Physics*, **17**, 851-855, 1948.
- [17] Bailey L., Craster B., Sawdon C., Brady M. and Cliffe, S. New insight into the mechanisms of shale inhibition using water based silicate drilling fluids, IADC/SPE 39401, Dallas Texas, 1998
- [18] Meeten G.H. and Sherwood J.D. The hydraulic permeability of bentonite suspensions with granular inclusions, *Chemical Engineering Science*, **49**, 3249-3256, 1994
- [19] Van Olphen H. and Fripiat J.J. (Editors). Data handbook for clay materials and other non-metallic minerals, Pergamon Press, 1979.
- [20] Bindley G.W. and Brown G., Crystal structures of clay minerals and their identification, Mineralogical Society, London, 1984.
- [21] Iler R.K, The Chemistry of silica; Wiley-interscience, New York, 1978.
- [22] Knight C. T. A two-dimensional silicon-29 nuclear magnetic resonance spectroscopic study of the structure of the silicate anions present in aqueous potassium silicate solution, *Journal Chemical Society Dalton Transactions*, 1457-1460, 1988
- [23] Huang W., Bassett W. and Wu T. Dehydration and hydration of montmorillonite at elevated temperatures and pressures monitored using synchrotron radiation, *American Mineralogist* **79**, 683-691, 1994.
- [24] Sherwood J.D. Ionic motion in a compacting filtercake, *Proceedings Royal Society London A* **437** 607-627, 1992.
- [25] Subrammanlan P. and Fitch, A., Diffusional transport of solutes through clay: use of clay modified electrodes, *Environmental Science Technology*, **26**, 1175-1178, 1992.
- [26] Aranda P. and Ruiz-Hitzky E. Poly(ethylene oxide)-silicate intercalation materials, *Chemical Materials*, **4**, 1395-1403, 1992.
- [27] Everett D. H. Basic principles of colloid science, Royal Society of Chemistry, **42**, 1988.
- [28] Kharaka Y.K. and Berry F.A. Simultaneous flow of water and solutes through geological membranes I. Experimental investigation, *Geochimica et Cosmochimica Acta*, **37**, 2577-2602, 1973.
- [29] Banin A. and Low P.F. Simultaneous transport of water and salt through clays: 2. Steady-state distribution of pressure and applicability of irreversible thermodynamics, *Soil Science*, **112**, 69-88, 1971.

[30] Shackelford C.D. and Daniel D. E. Diffusion in saturated soil 1 and 2, *Journal of Geotechnical Engineering*, **117**, 467-507, 1991.

[31] Oscarson D.W., Hume H.B., Sawatsky N.G. and Cheung S.C.H. Diffusion of iodide in a compacted bentonite, *Soil Science Society American Journal*, **56**, 1400-1406, 1992.

1. Summary and Conclusions

This thesis is called “Studies of the Modification of Ion and Water Movement through Clays and Shales”. The main strength of the research project has been in the design of new experimental methods to use while examining the movement of water or ions through clays subjected to different experimental conditions. Studies were carried out on compacting clays and thin montmorillonite films treated with mud additives. Also the use of X-ray diffraction methods to examine how glycols prevent montmorillonite swelling in parallel with shale erosion tests is a new approach to the design of shale inhibitors.

Methods for compacting clays described in Chapter 3 were applied when preparing orientated films for the Clay Membrane Cell in Chapter 5. The use of self supporting clay films to investigate the interaction of glycols with montmorillonite in Chapter 4 established the need to monitor the intercalation of glycol in the film insitu in the cell. It also helped in planning an experimental matrix. Overall the result of the experimental design has been to allow the bulk screening of systems over short time scales but with controlled reproducible conditions.

The porosity of the kaolinite, illite, Ca greenbond and Fullers Earth compacted in this study at high pressures is affected by the initial particle size of the clays and the volume fraction of each clay present but not by the concentration of electrolyte. Knowing the composition of a compact would allow one to predict the porosity of the matrix at least over the pressure range below 600 bar. However from this study the shape and volume of each individual pore in the hydrated compact under pressure cannot be commented on. It is still a goal to determine the tortuosity of the internal pore structure to help in the design of polymer systems providing maximum permeability reductions to water and ions.

In setting up an experiment to measure the conductivity of the compacting clay slurries the brass platen electrodes were shown to give linear readings for clay compacts longer than 5 mm. One can be confident that the measured clay-compact conductivity is reasonable as the trends obtained are in keeping with those expected from Cremers work. Attempts to determine the fraction of the surface cations contributing to the conductivity show that the results are coupled to the microstructure of the compacts. This is most evident from the comparison between Ca greenbond and Fullers Earth where the former has an orientated structure and the latter a domain type

of ordering. Such structure differences manifest themselves in the cementation factor m . Results from experiments where montmorillonite was slurried in sodium chloride would be an interesting way to scope changes in the value of m caused by the structuring of the clay layers into tactoids or domains. Moreover the effect of wellbore fluids such as potassium salts and glycol molecules on the conductivity of the native montmorillonites would also be of interest. However it is not obvious how accurate the Waxman and Smits model is at determining the CEC of the clay phase of shale from resistivity logs without a larger data set on both clays and shales. In fact the conductivity model applied to the data is very simple and it is not really adequate to assume that the salinity of the pore fluid in a smectitic rock is the sum of the local sea water and the surface cations. Donnan exclusion should be incorporated into the model especially at high compaction pressures. This would necessitate the on line analysis of the pore fluid drained from the compacting clay.

The activation energy for electrical conduction was determined for Fullers Earth slurried in different concentrations of calcium chloride as a function of compact porosity. The switch over from bulk pore fluid to surface conduction at low porosities was demonstrated.

The mechanism of prevention of swelling montmorillonite was investigated with a view to its application to shale. In the wellbore glycols can be introduced to the shale sections in waterbased muds containing freshwater or with molar NaCl, CaCl₂ or KCl present. Ultimately the purpose of these muds is to prevent the hydration and swelling of shales which leads to reduced diameter wellbores and wall erosion. The approach during the initial stages of this study has been to investigate the interaction of glycols with a research montmorillonite SWy-1. This clay was taken to represent the swelling clay in down hole shales. A range of glycols were chosen with different degrees of hydrophobicity and the adsorption and intercalation monitored using GPC/FTIR and XRD respectively. The following conclusions were made from the mechanistic study:

- a bilayer of adsorbed glycol containing, an alky chain longer than C₄ (butyl) or pendant methyl groups, prevents the ingress of water into the interlamellar region of Na/Ca montmorillonite and the subsequent hydration of the counter ions,
- once the clay is exchanged to the potassium form a monolayer of intercalated glycol such as polyethylene glycol prevents the swelling of the clay when in contact with water,

- clay slurried in salt solutions gives distinctive basal spacings which remain unchanged when glycol is added *i.e.* the glycol replaces the adsorbed water

The performance of polyglycols in the recovery of shale depends on the hydrophobic nature of the polymer, as was found in studies on pure montmorillonite substrates. The interactions between the hydrophobic portions of the polyglycols appears to be responsible for the higher levels of inhibition obtained with these materials in the absence of potassium chloride. When potassium chloride is present in the test solution the shale recovery is maximised even at low polymer concentrations, and the contribution from hydrophobic interactions is small compared with that from the interaction of any polyglycol with the potassium ion.

The performance of the new polyglycols as shale erosion inhibitors is better than that of peg 600 or pag. However more research is needed to understand the true role of the potassium ion in the presence of glycol. FTIR could be combined with neutron scattering studies to determine the hydration state of the potassium ion in the presence and absence of glycol. The interaction of the glycol with the hydration shell of the cation could also be examined.

Comprehensive studies of the effect of molecular weight and hydrophilic-lypophilic balance on the performance of the glycol as shale inhibitors is also needed. Detecting the occurrence of ion exchange processes using Nuclear Magnetic Resonance spectroscopy would allow one to determine the true role of the salt added to the mud system.

A new test method has been designed to allow bulk screening of polymers for their performance in osmotic membranes. The Clay Membrane Cell is easy to use and gives results that can be compared with those obtained for similar work on shale. It is ideal for bulk screening as it is cheap to manufacture and maintain.

The Clay Membrane Cell has been very useful for examining the osmotic barriers set up by silicates. Test time is reduced by weeks compared to collecting data on shale samples in the Hassler cell. There is still some uncertainty as to the position of the osmotic barrier produced by the presence of silicates. If it is setup on the outer surface of the montmorillonite film then it could be accidentally removed in the wellbore under certain flow regimes or by the action of the drill string. Monitoring the flow of silicate through the film as well as the ability of the silicate formulations to block porous glass discs of different pore size would give more information on the physical characteristics and location of the barrier. The Clay Membrane Cell containing

a montmorillonite film and one sheet of filter paper was adequate for these purposes at Schlumberger. At the time this research was carried out the establishment of osmotic barriers on the clay surface was perceived as the route to finding a water based mud with oil based mud performance as a shale stabiliser. However to help in understanding the movement of ions on the clay surface in the presence of glycol additives it was decided to develop the cell further.

Several attempts at blocking off certain diffusion paths and then determining the permeability to water and ions of a montmorillonite film was made using the Clay Membrane Cell. The flux of water across the membrane is certainly altered by the presence of the glycol. However the hydrostatic pressures developed are generally low (even for salt only systems); of the order of kPa compared with MPa osmotic pressure differential. This is in part due to the high salt concentrations used which lower the ability of the negative clay layers to reject anions, and also the fact that the porosity of the thin films of montmorillonite-containing glass beads is high. Further osmotic experiments using lower salinities and more compacted films might enhance the affect of the glycol on the transport through the film.

From the study on the stabilisation of montmorillonite and shale by glycols it is clear that some glycols do prevent the development of multiple water layers in the interlamellar region but not the movement of salt. These results have been confirmed by synchrotron experiments on clay films insitu in the osmotic cell. However results from Clay Membrane Cell tests show that the glycol inhibitors do not set up osmotic membranes and therefore work by a different mechanism to oil based muds and silicates.

The application of the Sherwood model to determine some characteristics of the film is useful in that it helps in understanding the flow processes happening across the membrane. In the osmotic tests the water flows to the high salinity side as the salt leaks in the opposite direction. From these profiles the permeability of the film to water and the diffusion coefficient of the salt across the film can be determined. Changes to these parameters when glycol is added to the test solutions cannot be commented on due to the limited data set and leave scope for further work. However the possibility of independently checking the permeability of the film by means of a hydrostatic tests was investigated and shown to be viable.

Ideally one would design an experiment to combine the techniques used in the compaction of clays and the Clay Membrane Cell. A carefully sized clay would be

compacted to equilibrium and the conductivity monitored during the compaction phase. From this data the cementation factor of the clay film could be determined allowing a better understanding of the structure of the clay film. Keeping the film thickness constant then the movement of water and ions through the clay film could be detected as in the Clay Membrane Cell. If the cell was machined from perspex then the synchrotron source could be used to monitor the changes in the basal spacing throughout these experiments.